

Titan II Hybrid Rocket Engine Documentation

Rice Eclipse Technical Propulsion System Report to the 2022 IREC

John Perez¹ and Michael Riccardi²
Rice University, Houston, Texas 77005

Daniel Cohen³, Bryn Gerwin⁴, Jonathan Lloyd⁵, Jeffrey Michel⁶, Alejandro Toscano Rodriguez⁷, Joshua Stelling⁸,
Loren Young⁹, and Steven Zhao¹⁰
Rice University, Houston, Texas 77005

and

Katie DeSpain¹¹, Nicholas Ess¹², Justin Guilak¹³, John Keogh¹⁴, Caroline Koester¹⁵, Eduardo Landin¹⁶, Rafe Neathery¹³,
Clayton Ramsey¹³, Anastasiya Romanova¹⁷, Prithve Shekar¹³, Jonas Weissberg¹³, Clyde Xu¹³, and Eric Yang¹³
Rice University, Houston, Texas 77005

The Titan II engine is Rice Eclipse’s design for a flight-optimized hybrid rocket engine. The engine will be used as the propulsion system for Eclipse’s rocket that will compete in the 2022 Spaceport America Cup 30,000 ft student-researched-and-developed hybrid and liquid engine category. Titan II is based on the design of the team’s Titan hybrid engine, which was a prototype engine of the same impulse class as Titan II, but was not optimized for flight. Titan II increases the total impulse from the original Titan engine and significantly decreases the total engine mass from 145 lbs to 102.3 lbs, so the engine can realistically propel a rocket to the 30,000 ft target altitude. Titan II is designed to produce 1,200 lbf of average thrust over an 7.67 second burn, producing a total impulse of 9,200 lbf-sec, using an HTPB mixture as its solid fuel and liquid nitrous oxide as its oxidizer. The oxidizer feed system is pressure-fed, using the high vapor pressure of nitrous oxide as a self-pressurizing system for the Oxidizer Tank. The Titan II engine is designed to be housed within a 6 in inner diameter airframe, whereas the original Titan engine was designed for a 8 in inner diameter airframe. This change in airframe diameter enables the use of commercial-off-the-shelf components which greatly simplifies the airframe design. This smaller airframe size also greatly decreases the overall drag on the rocket, increasing the achievable altitude for a given total impulse and rocket mass.

¹ Rice Eclipse Propulsion Lead (Former Design Lead), Mechanical Engineering ('21)

² Rice Eclipse Vice President/Design Lead, Mechanical Engineering ('22)

³ Titan II Subteam Co-Lead, Mechanical Engineering ('23)

⁴ Titan II Subteam Co-Lead, Mechanical Engineering ('23)

⁵ Nozzle Subteam Lead, Mechanical Engineering ('23)

⁶ Rice Eclipse President (Former Titan II Subteam Co-Lead), Mechanical Engineering and German Studies ('21)

⁷ Former Titan II Subteam Co-Lead, Mechanical Engineering ('20)

⁸ Chemicals Subteam Lead (Former Propulsion Lead), Mechanical Engineering ('21)

⁹ Fluid Flow Subteam Lead, Mechanical Engineering ('21)

¹⁰ Ground Systems Subteam Lead, Mechanical Engineering ('23)

¹¹ Former Rice Eclipse President, Civil and Environmental Engineering ('21)

¹² Luna Subteam Co-Lead, Mechanical Engineering ('23)

¹³ Titan II Team Members ('21 - '24)

¹⁴ Former Aerodynamics Lead, Mechanical Engineering ('21)

¹⁵ Former Chemicals Subteam Lead, Chemistry ('22)

¹⁶ Former Fluid Flow Subteam Lead, Computer Science and Statistics ('22)

¹⁷ Luna Subteam Co-Lead, Computational & Applied Mathematics and Visual & Dramatic Arts ('22)

Table of Contents

Table of Contents	2
Revision Log	6
I. Introduction	7
A. Project Motivation	7
B. Design Overview	7
II. Engine Propellant Selections	10
A. Hydroxyl Terminated Polybutadiene (HTPB) Solid Fuel	10
B. Nitrous Oxide Liquid Oxidizer	10
III. Engine Performance Requirements Definition	12
A. Chamber Pressure	12
B. Oxidizer-to-Fuel Ratio	12
C. Total Impulse	14
D. Mass and Flow Rate of Propellants	16
IV. Oxidizer Storage and Feed	17
A. Oxidizer Tank	17
1. General Pressure Vessel Design Methodology	18
2. Body Cylinder	19
3. Forward Bulkhead	20
B. Injection Assembly	23
1. Injection Bulkhead	24
1.1 Aft Dome	26
1.2 Pre-Injection Chamber and Injector Plate Section	27
1.3 Wall Stress Considerations	27
1.4 Pressure Ports	28
1.5 O-Ring Grooves and Seals	29
2. Oxidizer Feed Conduit	30
3. Injector Plate	31
3.1 Injector Holes	32
3.2 Data Collection	35
3.3 Plate Material Selection	35
3.4 Injector Plate Retention	35
C. Oxidizer Tank Vent and Relief System	36
1. Vent Valve	38
2. Relief Valve	40
D. Oxidizer Tank and Bulkhead Retention	41
1. Orbital Welding	41
2. Fasteners	42
2.1 Forward Bulkhead Fasteners	42
2.2 Injection Bulkhead Fasteners	43
V. Thrust Chamber Assembly	45

A. Combustion Chamber Assembly	46
1. Fuel Grain	47
1.1 Grain Geometry	48
1.2 Fuel Regression Characterization	49
1.3 Thermal Protection and Properties	51
1.4 Grain Manufacture and Pre-Test Manual Inspection	51
2. Combustion Chamber	51
3. Pre- and Post-Combustion Chambers	55
3.1 Pre-Combustion Chamber	56
3.2 Post-Combustion Chamber	57
4. Fuel Grain Liner	58
5. Combustion Chamber Spacers	59
B. Nozzle Assembly	60
1. Nozzle Insert	62
2. Nozzle Casing	64
3. Nozzle Casing Fasteners	65
VI. Ground Support Equipment	66
A. Ground Oxidizer Fill System Plumbing Assembly	66
B. Oxidizer Fill Assembly	69
C. Fill Process	70
D. Ignition System	71
E. Instrumentation	72
1. Load Cell (LC)	72
2. Pressure Transducers (PTs)	72
3. Thermocouple (TC)	74
4. In-Flight Instrumentation	74
F. Static Test Stand	74
VII. Propulsion System Testing and Results	76
A. Oxidizer Tank Pressure Testing	76
B. Thrust Chamber Assembly Pressure Testing	76
C. Engine Tanking and De-Tanking	76
D. Static Hot Fire Testing	76
E. Planned Engine Optimization after Testing	77
F. Planned Engine Optimization after Flight	77
VIII. Appendix - Detailed Calculations	78
A. Engine Performance Requirements Definition Calculations	78
1. Oxidizer to Fuel Ratio as a function of HTPB Mass Calculations	78
2. Total Mass and Required Mass Flow Rate of both the Fuel and Oxidizer Calculations	78
B. Oxidizer Storage and Feed Assembly Calculations	80
1. Hoop stress and axial stress calculations to determine Oxidizer Tank Body Cylinder wall thickness	80
2. Injection Bulkhead Assembly Calculations	81
2.1 Injection Bulkhead Wall Stress Calculations	81
2.2 Oxidizer Feed Conduit Calculations	82

2.2.1 Oxidizer Feed Conduit Radius Calculation	82
2.2.2 Oxidizer Feed Conduit Pressure Drop Calculations	83
2.3 Injector Plate Retention	87
3. Tank Vent/Relief System Calculations	88
3.1 Clark Cooper EH30-042-D012-OXCY Vent Valve Flow Capacity Calculations	88
3.2 Dip Tube Length Calculations	89
3.3 Generant HPRV-500 SS-T-915 Relief Valve Flow Capacity Calculations	90
4. Oxidizer Tank and Bulkhead Retention	91
4.1 Orbital Welding Geometry	91
4.2 Forward Bulkhead Fasteners	91
4.2.1 Bearing stress calculations on the fastener holes within the Forward Bulkhead	92
4.2.2 Tearout stress calculations on the fastener holes within the Forward Bulkhead	92
4.2.3 Shear stress calculations on the Forward Bulkhead fasteners	93
4.2.4 Maximum preload calculations for Forward Bulkhead fasteners	93
4.3 Injection Bulkhead Fasteners	94
4.3.1 Bearing stress calculations on the fastener holes within the Injection Bulkhead	95
4.3.2 Tearout stress calculations on the fastener holes within the Injection Bulkhead	95
4.3.3 Shear stress on the Injection Bulkhead fasteners	95
4.3.4 Maximum preload calculations for Injection Bulkhead fasteners	96
C. Thrust Chamber Assembly Calculations	97
1. Fuel Grain Calculations	97
1.1. Fuel Grain Initial Radius	97
1.2. Optimal Fuel Grain Length	97
1.3. Fuel Grain Penetration Length	98
2. Combustion Chamber Calculations	98
2.1. Combustion Chamber Hoop Stress Calculations	98
2.2. Combustion Chamber Holes Bearing Stress Calculations	99
2.3 Combustion Chamber Tearout Stress Calculations	99
3. Nozzle Assembly	101
3.1 Nozzle Insert Radii Calculations	101
3.2 Nozzle Casing Fasteners	102
3.2.1 Bearing stress calculations on the fastener holes within the Nozzle Casing	102
3.2.2 Tearout stress calculations on the fastener holes within the Nozzle Casing	103
3.2.3. Shear stress on the Nozzle Casing fasteners	103
3.2.4 Maximum preload calculations for Nozzle Casing fasteners	104
D. Propulsion System Testing	104
1. Dip Tube Length Calculations for Static Testing	104
1.1 Four second burn	104
1.2 Six second burn	104
1.3 Full burn	105
IX. Appendix - Detailed Simulations	106
A. Engine Performance with the Chosen Oxidizer to Fuel Ratio Affected by Oxidizer Contamination	106
B. Oxidizer Feed and Storage Assembly Simulations	106
1. Oxidizer Tank FEA Static Simulation	112

2. Injection Bulkhead FEA Static Simulation	112
3. Injector Plate FEA Static Simulation	112
C. Thrust Chamber Assembly Simulations	121
1. Combustion Chamber Stress Simulations	121
2. Nozzle Assembly Simulations	124
X. Appendix - MATLAB Scripts	129
A. Titan II Engine Parameters	129
B. Conduit Calculations	130
C. Injector Hole Diameter	130
D. Titan II Regression	132
XI. Appendix - System Parts and Weights	133
XII. Appendix - Engineering Drawings	136
XIII. Appendix - Detailed Testing Logs	137
XIV. References	138
XV. Acknowledgments	140

Revision Log

Revision Number	Date	Change Summary
1	12/9/19	First full version of Titan II engine documentation
2	06/29/20	Titan II complete engine documentation revision two <ul style="list-style-type: none">• Decreased mass by 10 lbs• Integrated Oxidizer Aft Bulkhead, Feed Line, and Injection Bulkhead• Shrank combustion chamber diameter• Improved fuel regression rate analysis• Improved engine retention with shoulder screws• Improved injector plate retention• Improved engineering drawings
3	10/31/20	Titan II complete engine documentation revision three <ul style="list-style-type: none">• Increase in engine's average thrust to 1200 lb

I. Introduction

A. Project Motivation

Rice University's Rice Eclipse rocket team was founded with the goal of designing, building, testing, and successfully flying a rocket powered by a student-developed propulsion system. The team has spent the past six years developing its knowledge base and design experience in hybrid rocket propulsion and collegiate competition rocketry to achieve this goal. Eclipse's *Noctua* series of rockets have competed in the COTS solid motor categories of the Spaceport America Cup for the past three years, each providing valuable lessons on rocket design and flight performance. Eclipse has developed a total of three hybrid rocket engines, beginning with the 50 lbf - thrust Mk 1.0 hybrid engine and its second iteration named Luna, which is currently operated by the team. The third engine, named Titan, was initially designed to produce 800 lbf of thrust over 10 seconds. This engine was the team's first attempt at designing and test-firing a hybrid rocket engine of this scale. The Titan engine design was not optimized for flight, and served as the base-case large-scale hybrid rocket engine for the team to improve on in a future engine design. After two hot fires of the original Titan engine, the team decided that the only way it would be able to achieve its long term goal of flying a student-developed rocket equipped with its own hybrid propulsion system would be to completely redesign the engine. Additionally, a flight-optimized engine redesign was chosen as a project because it would be an incomparable learning experience for members and, for the first time, would incorporate every single Eclipse team (Propulsion, Avionics, and Aerodynamics) into one unifying project. The Titan II hybrid rocket engine detailed in this report is Eclipse's second iteration of the Titan engine. Titan II is a flight-optimized version of its predecessor, designed to power a rocket to compete in the 30,000 ft student researched and developed (SRAD) liquid and hybrid rocket category of the Spaceport America Cup.

B. Design Overview

Titan II is designed to produce 1200 lbf of average thrust over an 7.67 second burn for a total impulse of 9,200 lbf·sec. The engine uses a hydroxyl-terminated polybutadiene (HTPB) fuel mixture as its solid fuel and nitrous oxide as its liquid oxidizer, building off Eclipse's experience with this propellant combination in its previous hybrid engines. The oxidizer system is pressure fed; the nitrous oxide stored in the engine's Oxidizer Tank is a saturated liquid, so it self-regulates its pressure to nitrous oxide's vapor pressure at a given temperature (roughly 750 psi at 70°F¹). The engine's maximum outer diameter is 6.25 in, and is 108.5 in (9 ft, 0.5 in) long. The engine's geometry allows it to integrate with a 6 in inner diameter airframe as its flight vehicle, as the Oxidizer Tank (OD of 6.25 in) is an integrated component of the airframe. The small diameter minimizes the drag on the flight vehicle and simplifies the vehicle design due to the availability of commercial rocket components for 6 in inner diameter airframes. Eclipse also has past experience with designing and fabricating 6 in diameter airframes, which will be leveraged for the flight vehicle design for Titan II. Due to the fact that Rice Eclipse is a student-run organization, and especially due to the fact that this is the first engine that the team has designed for flight, the engine design uses a minimum factor of safety to yield of 2.0. Table 1 below summarizes the key engine characteristics of Titan II.

Table 1. Titan II Key Engine Characteristics	
Average Thrust	1200 lbf
Burn Time	7.67 sec
Total Impulse	9200 lbf · sec
Chamber Pressure	500 psi
Fuel	Solid HTPB Mixture
Oxidizer	Liquid Nitrous Oxide
Oxidizer-to-Fuel (O/F) Ratio	5.62
Combustion Temperature	5627 °F
Liftoff Thrust-to-Weight Ratio - Optimal	11.7
Theoretical Specific Impulse	202.47 sec
Empirical Specific Impulse	TBD
Minimum Safety Factor to Yield	2.0

As presented in this report, the engine's total mass is 105.5 lb, with a total length of 115.2 in (9 ft, 7.2 in). As the exact regression rate model of the engine's fuel grain cannot be determined until experimental data is taken from hot fires, the engine currently has a longer-than-optimal Combustion Chamber Assembly which can contain a longer fuel grain if the fuel's regression rate is lower than expected. Once experimental data is taken, the Combustion Chamber Assembly will be cut down to its optimal length. Assuming the optimal length of the fuel grain is the same as the most accurate model the team currently has, the final mass of the Titan II engine will be 102.3 lb, with a total length of 108.2 in (9 ft 0.2 in). Table 2 below summarizes fuel mass specifications:

Table 2. Titan II Mass Specifications	
Fuel Mass - Optimal	11.24 lb
Oxidizer Mass	39.35 lb
Engine Dry Mass (Optimal)	59.1 lb (55.9 lb)
Engine Wet Mass (Optimal)	105.5 lb (102.3 lb)

A full CAD image of the engine is shown below in Figure 1. The engine is broken down into two key assemblies: the Oxidizer Storage and Feed Assembly and the Thrust Chamber Assembly. Each assembly is further detailed and subdivided in its respective section of this report.

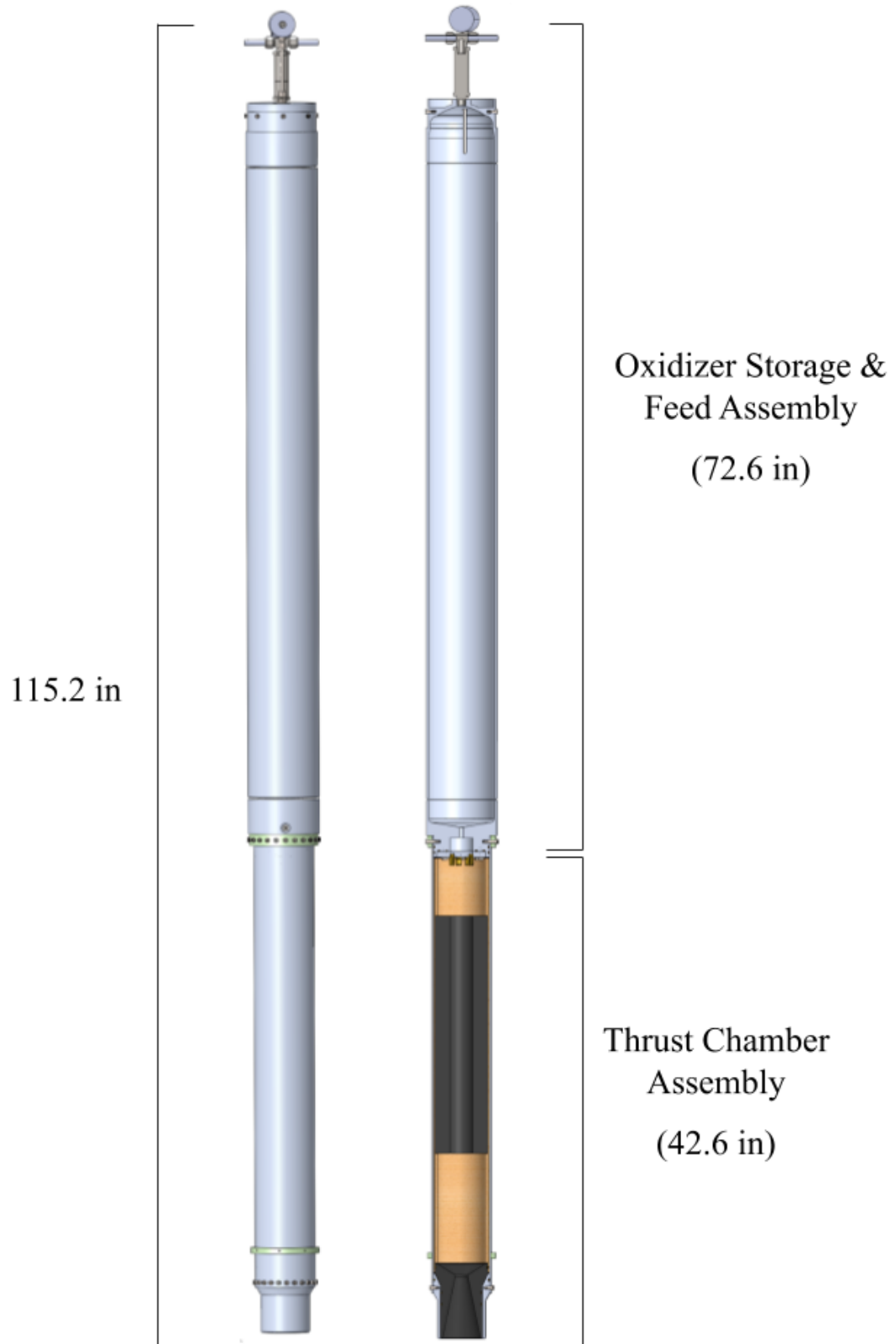


Figure 1. Titan II full engine assembly

II. Engine Propellant Selections

The Titan II engine is a hybrid rocket engine, which combusts a solid fuel and a liquid oxidizer. Eclipse’s experience with SRAD rocket engines has focused on hybrid engines rather than liquid engines or solid motors. Hybrid engines are simpler, safer, and less expensive to manufacture than liquid engines due to the lack of a liquid fuel system, but they retain some of a liquid engine’s system complexity versus a solid motor, which makes them a valuable educational experience in learning rocket propulsion fundamentals. Designing Titan II as a hybrid rocket engine gives Rice Eclipse a complex design challenge that will build its team members’ knowledge of rocket propulsion while staying within Eclipse’s operating budget and allows the team to leverage its past design experience and experimental data from ground tests of its other hybrid engines.

There are many different combinations of propellants that can be used in a hybrid rocket engine. Titan II uses a mixture of hydroxyl-terminated polybutadiene (HTPB) rubber, isocyanate curative, and carbon black as its solid fuel. The selected oxidizer is liquid nitrous oxide (N₂O). HTPB and nitrous oxide is a common hybrid rocket propellant combination. Both propellants are safe, easily storable, and easy to procure. All of Eclipse’s past hybrid engines have used this propellant combination, which allows the team to draw on the designs and experimental data from the team’s past engines in designing Titan II.

A. Hydroxyl Terminated Polybutadiene (HTPB) Solid Fuel

The engine’s fuel grain includes three components: hydroxyl-terminated polybutadiene (HTPB), modified MDI isocyanate curative, and carbon black. HTPB was selected for use as fuel because it is very safe and relatively easy to store and handle (it is non-toxic and presents no decomposition or compatibility hazards at room temperature or in standard lab conditions), is commonly produced, and produces a large amount of energy while burning generally steadily. HTPB fuel grains are easier to handle and manufacture than fuel grains made from paraffin wax, another fuel that the team considered, because HTPB starts as a room temperature liquid. It can be poured into a mold of the desired shape and then cured to solid, rather than requiring grating to reduce it from a slab to workable material, being melted, and then cast into shape. Additionally, if a combination of HTPB and paraffin wax was to be used, mixing these two together would require large effort to prevent uneven distribution and consistency, both of which are detrimental to an even, consistent burn and could potentially produce dangerous combustion instabilities.

Modified MDI isocyanate curative is used to cure the HTPB from liquid to solid, and was selected because it is relatively inexpensive and easy to procure and was designed and synthesized specifically to react efficiently with HTPB to cure it to a safe consistency (firm, not gummy, and without large bubbles). Carbon black is used to ensure combustion stability, as well as to assist in quick ignition, by increasing the absorptivity of the fuel grain to the radiative heat of the igniter. The mass fractions of components for the Fuel Grain are based on past experiences with experimentation with Fuel Grain scheduling -- pouring small samples of a potential composition and testing it for hardness and consistency. The composition of the Fuel Grain is broken down by component in Table 3. The process for design and manufacture of Titan II’s fuel grain is covered more thoroughly in *Section V.A.1.4*.

Table 3. Titan II Solid Fuel Grain Component Mass Fractions		
Component	Component Purpose	Mass Fraction
Hydroxyl-Terminated Polybutadiene (HTPB)	Solid fuel for combustion	83%
Modified MDI Isocyanate Curative	Cures liquid HTPB into a solid to be cast into fuel grain	17%
Carbon Black	Increases fuel grain’s absorptivity to radiative heat of combustion	3% of combined HTPB and curative mass

B. Nitrous Oxide Liquid Oxidizer

The choice of oxidizers that could be used for this engine is more restricted than the choice of fuels. Common liquid oxidizers used for aerospace applications are often either cryogenic liquids or hypergolic liquids. Cryogenic liquids require extensive ground support equipment to condition the oxidizer, and hypergolic liquids are highly toxic

and highly reactive. Nitrous oxide is an alternative oxidizer that is commonly used in hybrid rocket engines due to its wide availability, safety compared to other oxidizers, and high vapor pressure, which enables nitrous oxide to be stored as a saturated liquid at the ambient temperatures expected for this engine. As a result, while oxidizer is drawn from the engine's Oxidizer Tank during a burn, the nitrous oxide self-pressurizes, which allows for more efficient blowdown operation of the engine. At room temperature the self-pressurization pressure of nitrous oxide is roughly 750 psi, so this was set as the targeted pressure for the nitrous oxide in the Oxidizer Tank¹. Nitrous oxide's self-pressure-regulation is limited by the temperature of the nitrous oxide in the tank, which is affected by both the ambient conditions around the tank and vaporization of the nitrous oxide as oxidizer is drawn from the tank. Vaporization is an endothermic process, so the temperature and by extension vapor pressure of the liquid nitrous oxide in the tank decreases over the course of a burn. This variation in tank pressure when using nitrous oxide prevents consistent control of the oxidizer's mass flow rate through the injector, which could be improved by pressurizing the nitrous oxide with an inert gas to maintain constant tank pressure. However, adding a pressurization system adds cost, mass, and complexity to the engine design, so it was not included in the design of Titan II in the interest of keeping the engine design as simple as possible for the first flight-ready hybrid engine built by the team. A nitrous oxide tank pressurization system using nitrogen as a pressurant has been successfully deployed on Eclipse's smaller Luna hybrid engine, and the team plans to integrate an oxidizer pressurization system in the next hybrid engine it designs in this impulse class.

III. Engine Performance Requirements Definition

With propellants selected, the team had to determine key high-level performance requirements for the engine in order to proceed further with the engine design.

A. Chamber Pressure

The first parameter considered is the engine's chamber pressure. In general, increasing chamber pressure increases the theoretical efficiency of an engine, but higher chamber pressures also increase the engine's mass because more material is required to safely withstand the stresses induced by the higher pressure load. The chamber pressure must also be low enough to maintain positive pressure in the engine's propellant feed system and prevent backflow of combustion gases into the feed system. Titan II's feed system relies on nitrous oxide's self-pressurization behavior, so the selected chamber pressure must be below the expected oxidizer vapor pressure at liftoff and termination. All of Eclipse's previous hybrid engines have used a chamber pressure of 500 psi, based on research conducted into previous HTPB-nitrous oxide hybrid engine designs from other university research teams.^{2,3} 500 psi is a middle-ground value that produces acceptable theoretical engine efficiency without requiring excess material to withstand pressure-induced stresses. 500 psi also provides sufficient pressure drop between the Oxidizer Tank and the Thrust Chamber to achieve the required oxidizer mass flow rate without requiring exotic injector geometries.

B. Oxidizer-to-Fuel Ratio

The second key parameter is the optimal oxidizer-to-fuel (O/F) ratio for combustion between the HTPB fuel mixture and nitrous oxide oxidizer. Each combination of propellants has a unique oxidizer-to-fuel ratio that produces the maximum theoretical specific impulse for a given chamber pressure and nozzle expansion ratio, based on the chemical thermodynamics of the combustion reaction and the properties of the resulting exhaust product mixture. To determine this value for nitrous oxide and the HTPB fuel mixture described above in Table 3, the team performed a parametric sweep of mixture ratios between the two propellants using the ProPEP 3 Propellant Characterization software tool, which performs combustion chemical equilibrium analysis to characterize different propellant combinations. The total propellant mass was held constant at 44 lbs (20 kg) as an estimate of the total propellant mass required for the engine, which was still to be determined based on the results of this analysis. The ratio of nitrous oxide mass to the HTPB fuel mixture mass (i.e. the combined mass of all three fuel components) was then varied to determine the O/F ratio that produces the highest theoretical specific impulse. All three fuel components were included in the mixture ratio analysis because the combustion temperatures of HTPB, isocyanate curative, and carbon black are all below the expected chamber temperature of 5627 °F. To keep the total propellant mass at a constant 44 lbs, the parameter varied in the analysis was the mass of HTPB, which was coupled to the masses of each other propellant component per the equations shown below:

$$O/F = \frac{m_{ox}}{m_f}$$
$$O/F = \frac{20 \text{ kg} - (1.3378m_{HTPB})}{1.3378m_{HTPB}}$$

The complete calculations are detailed in *Appendix VIII, Calculation A.1*. A sample ProPEP input using the final propellant mass fractions is shown in Figure 2 below. The propellant components were selected from the ProPEP database to most closely match the properties of the HTPB, curative, and carbon black used in the fuel grain mixture. The chamber pressure input was set to 500 psi and the propellant temperature was set to 303 K, corresponding to 30°C, which is the average midmorning temperature at Spaceport America in mid-June. The nozzle exit pressure is set to 10.9 psi, an approximation of the altitude of the rocket halfway through the burn.

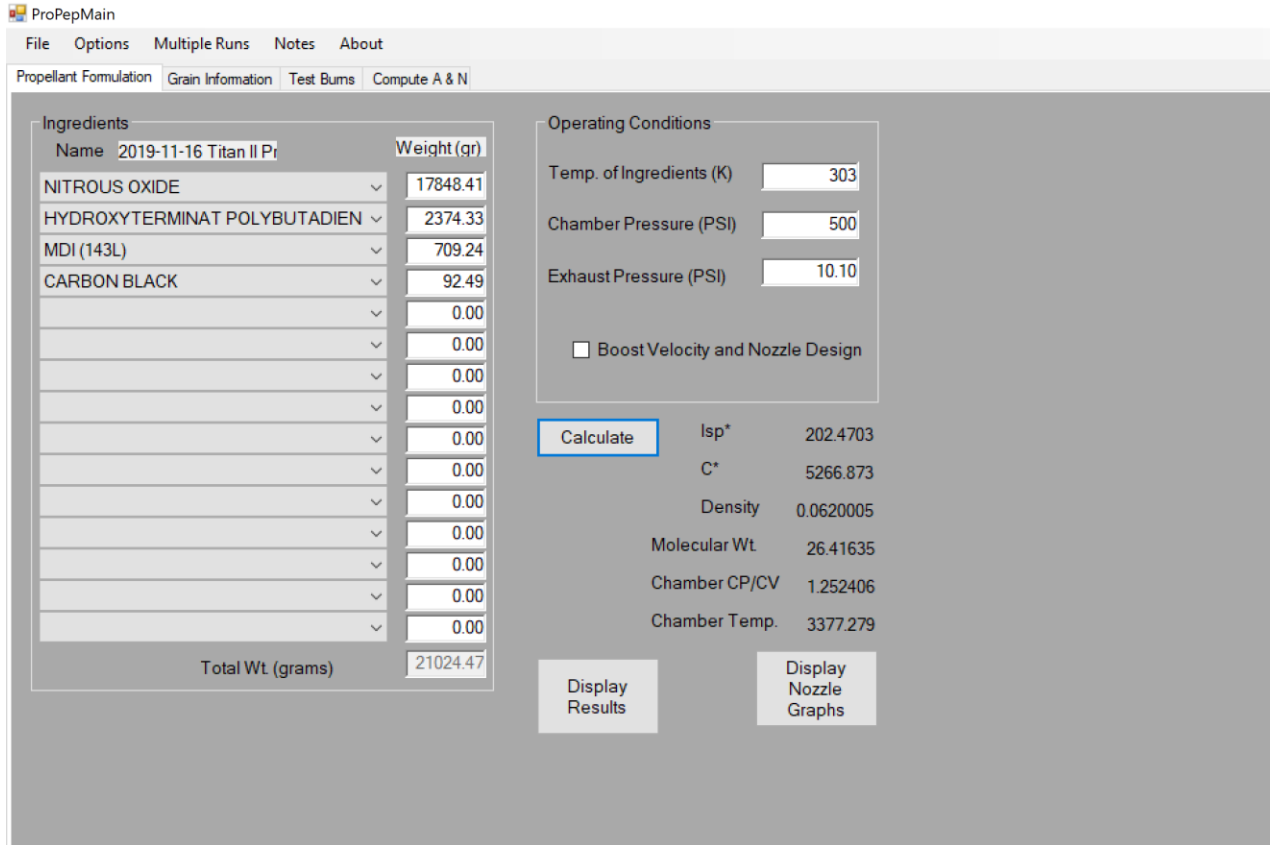


Figure 2. ProPEP 3 Propellant Characterization tool sample iteration input

For each iteration, the mixture ratio and the six ProPEP outputs for specific impulse (I_{sp}), characteristic velocity (C^*), exhaust gas density, exhaust gas molecular weight, exhaust gas specific heat ratio assuming frozen nozzle flow, and chamber temperature were recorded. The mixture ratio and specific impulse values were then plotted, shown in Figure 3 below:

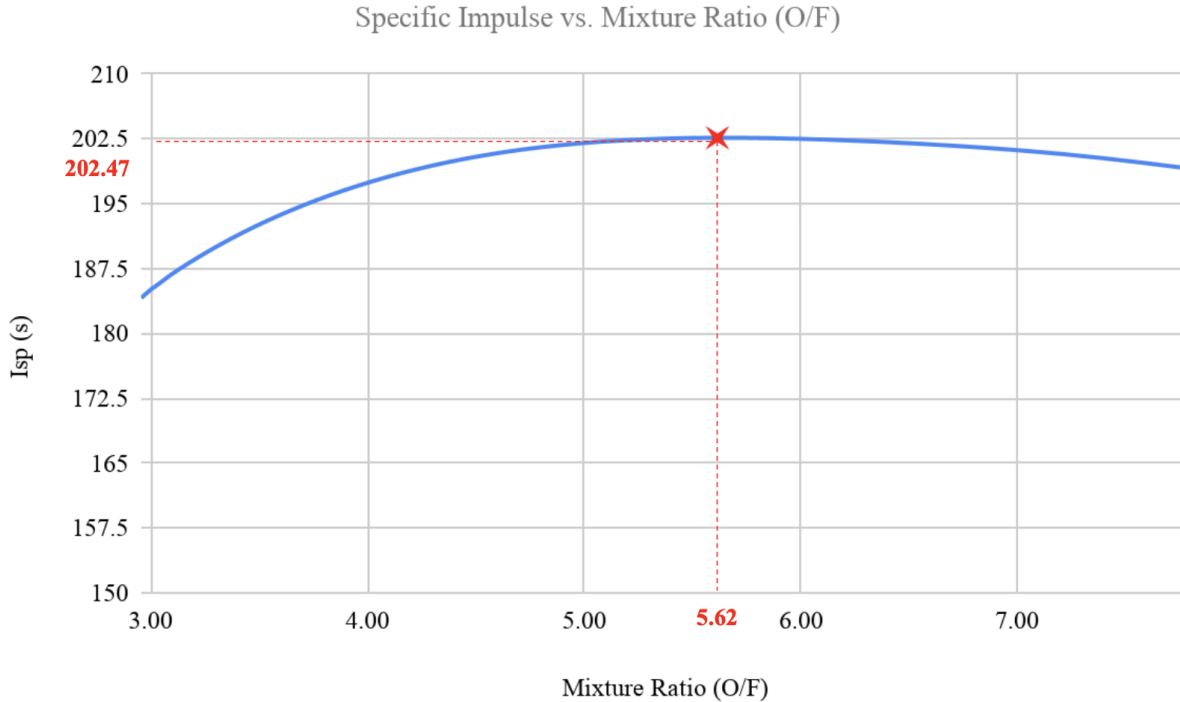


Figure 3. Titan II propellant mixture ratio optimization study results

The maximum theoretical specific impulse found from the parametric sweep was 202.47 seconds, produced at an O/F ratio of 5.62. This ratio is consistent with the standards present in literature, which typically depict O/F ratios for the combination of HTPB and nitrous oxide being between 4 and 10.⁴

A common contaminant found in purchased nitrous oxide is sulfur dioxide, due to the manufacturing process of the gas. To verify that contamination will not affect the performance of the engine, calculations for the chosen O/F ratio were performed again while taking sulfur dioxide contamination into account. 2% of the combined propellant mass was chosen as a conservative estimate for how much sulfur dioxide might be present in the oxidizer tanks. This alteration resulted in a negligible performance difference of around or under 1%. ProPEP inputs and outputs for this simulation can be found in *Appendix IX, Simulation A*.

C. Total Impulse

The third key parameter is the engine’s total impulse, which is further broken down into the engine’s average thrust and its total burn time. The total impulse of the engine is determined with the equation:

$$I_{total} = F_{t,avg} \cdot t_{burn}$$

The previous iteration of the Titan engine was designed to produce an average thrust of 800 lbf. As a result, Eclipse’s current mobile test stand for hybrid engines was designed for a thrust of 800 lbf with a factor of safety of 2. A higher thrust-to-weight ratio would increase the rocket’s stability off the launch rail due to the higher net acceleration -- permitting a shorter launch rail for the rocket to reach its critical speed for a stable flight. On the other hand, increased thrust would increase in-flight energy dissipation due to greater aerodynamic drag at higher velocities. To balance these competing parameters, the team conducted a series of simulations using the OpenRocket flight simulation program to gauge the effect of different thrust and burn time combinations, as well as different airframe outer diameters, on the expected altitude of a flight vehicle powered by Titan II. The team simultaneously used the “TitanIIEngineParameters” MATLAB script found in *Appendix X* of this report to determine the propellant mass required given a thrust and burn time, and to determine the volume of the Oxidizer Tank needed to carry the required oxidizer mass. The diameter of the Oxidizer Tank was the driver of the airframe diameter. The OpenRocket simulation iterations quickly showed that the airframe must be kept to an outer diameter of 6.5 in or below in order to reduce drag on the airframe enough to reach 30,000 ft, even if using the maximum allowed 9208 lbf·s engine total impulse

mandated by FAA regulations and the Spaceport America Cup rules. This 6.5 in outer diameter limit removed the possibility of using a commercially-available Oxidizer Tank for the engine, due to their high masses and large diameters for the internal volumes required. The remaining Oxidizer Tank options were either a custom Composite Overwrapped Pressure Vessel (COPV) fabricated by a contractor, or a custom aluminum tank made in-house. The tradeoffs between these two options are discussed further in *Section IV.A* of this report.

Reaching 30,000 ft in the OpenRocket flight simulations required significant mass reductions of both the engine and the rocket airframe, so the team decided it would be best to design an engine that produces as close to the 9208 lbf·s maximum impulse as possible. This minimizes the mass reduction required to achieve 30,000 ft, and any mass reduction beyond the critical value to achieve the altitude would serve as a performance margin that could be easily reduced later on. After completing several simulations, the team initially decided that 800 lbf of average thrust over an 11.5 second burn time (9200 lbf·s total impulse) with an engine wet mass of 105 lbm was a realistic set of requirements that would achieve the 30,000 ft altitude. However, while performing additional simulations when designing Titan II's airframe, it was determined that 800 lbf of average thrust would not be sufficient to reach the critical speed for a stable flight with a reasonable length launch rail. To address this issue, the thrust of Titan II was increased to 1200 lbf of average thrust over an 7.67 second burn, keeping the same total impulse of 9200 lbf·s total impulse. Before finalizing this thrust increase, rigorous stress analysis was performed on the mobile test stand, proving that it could withstand the 1200 lbf thrust with a factor of safety of greater than 2.0, with minimal modifications. This analysis and the required modifications are discussed in detail in the *Ground Systems Documentation*.

The full set of OpenRocket simulations conducted during this initial study are not included in this report, but the final OpenRocket flight simulation of the engine as it is documented in this report with a minimalist 60 lbm airframe is shown below in Figure 4. This estimate puts the flight vehicle at an apogee of 29,335 ft.

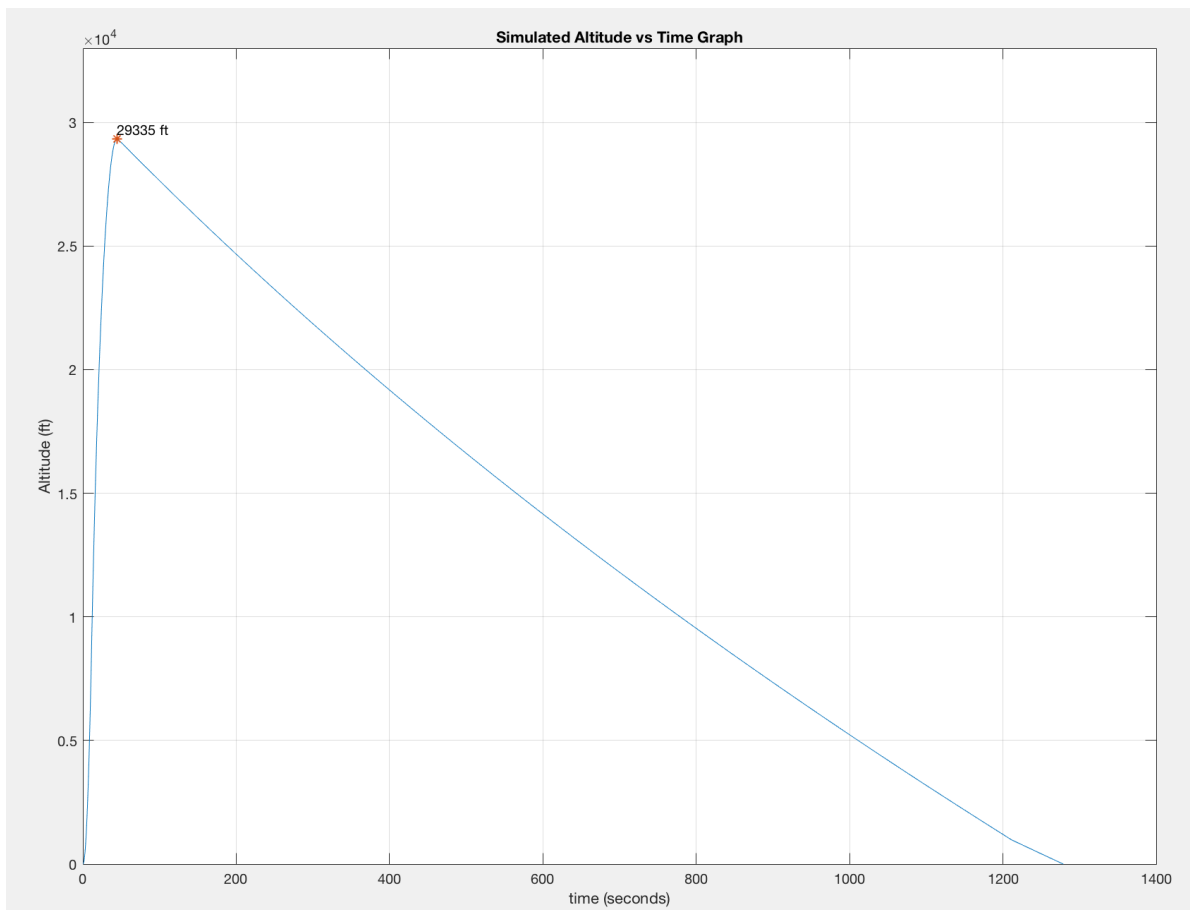


Figure 4. Titan II flight vehicle preliminary altitude estimate

D. Mass and Flow Rate of Propellants

The final key parameters are the total mass and required mass flow rate of both the fuel and oxidizer. These values were calculated using the previously-defined theoretical specific impulse, O/F ratio, average thrust, and burn time specifications. The specific impulse equation below was used to calculate the mass flow rate of propellant required for the 7.67 second burn at 1200 lbf average thrust:

$$I_{sp} \cdot g = \frac{F_{t,avg}}{m'_{prop}}$$

These calculations resulted in a fuel mass of 7.00 lbm and an oxidizer mass of 39.35 lbm. The complete calculations can be found in *Appendix VIII, Calculation A.2*. Note that the masses of fuel and oxidizer are only the masses required to complete an ideal burn and include no performance margins. The performance margin for this engine is built into an excess fuel margin, which is detailed in the Fuel Grain section (*Section V.A.1*) of the report.

IV. Oxidizer Storage and Feed

The Titan II Oxidizer Storage and Feed System consists of three systems that work together to collect, contain, and release the oxidizer while mitigating any pressurization risks that may arise. The Oxidizer Tank is designed to house the desired 39.35 lbm of nitrous oxide. The Injection Assembly permits oxidizer to flow out of the storage tank at the required rate into the Thrust Chamber. The Vent/Relief System allows oxidizer to safely flow out of the Oxidizer Tank; a vent valve is used for controllable venting and a relief valve is used for rapid automatic venting should the pressure inside the tank become too high.

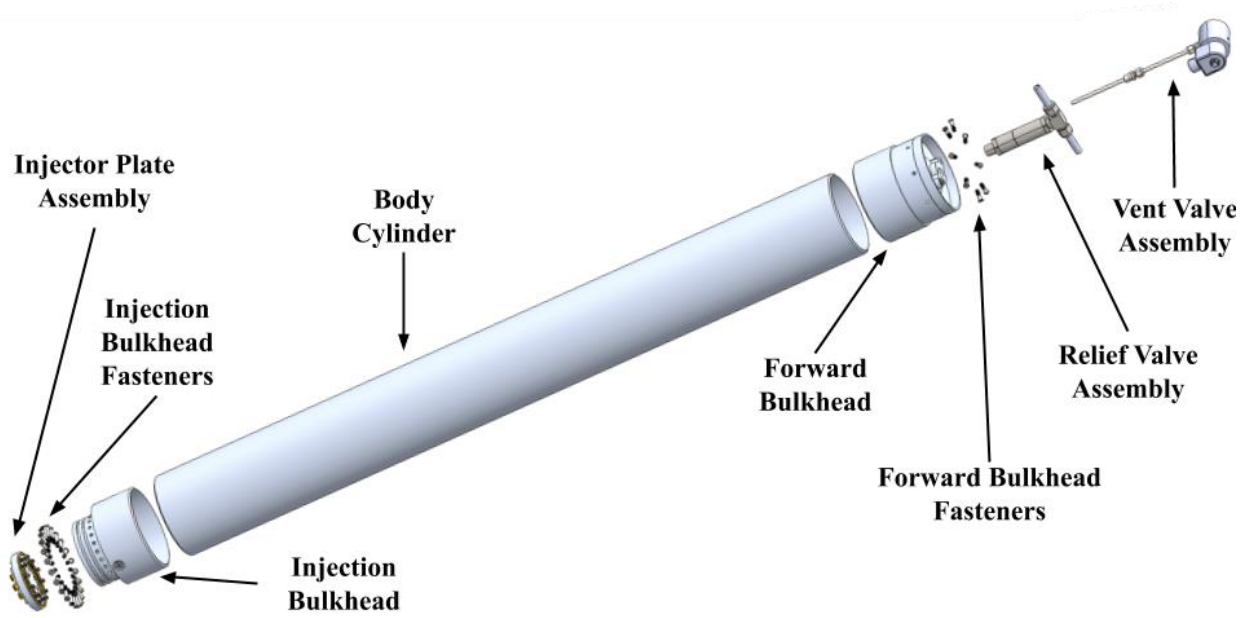


Figure 5. Oxidizer Storage and Feed System (exploded view)

A. Oxidizer Tank

The Oxidizer Tank is the main pressure vessel for the engine's oxidizer, housing all necessary nitrous oxide. The aft-end bulkhead, which will be referred to as the "Injection Bulkhead", is shared with the Thrust Chamber, providing a direct route of oxidizer flow into the Thrust Chamber. The Oxidizer Tank will be exposed to the air, and have no composite airframe around it. Because of this, the Oxidizer Tank outer diameter will match the outer diameter of the airframe, which is 6.25 in. Both the Forward Bulkhead and the Injection Bulkhead will be welded onto the Oxidizer Tank. The forward and aft sides of the Oxidizer Tank will be fastened to separate components of the airframe. All of these design aspects are detailed below.

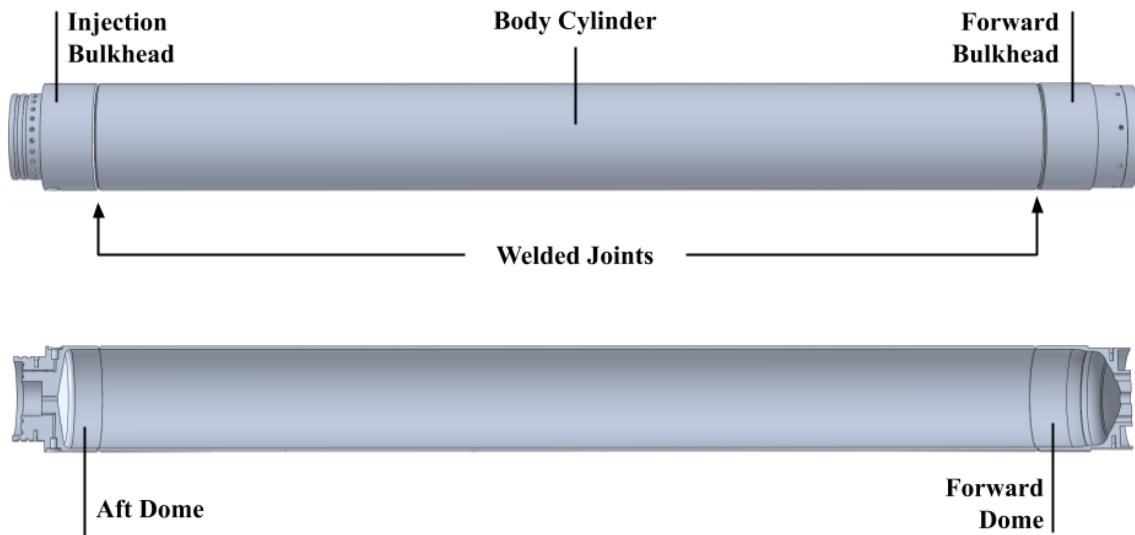


Figure 6. Oxidizer tank

Table 4. Oxidizer Tank & Bulkheads Design Specifications	
Material	Aluminum 6061-T6
Available Volume	1663 in ³
Total Mass*	28.60 lb
Total Length*	65.73 in
Outer Diameter	6.25 in
Minimum Wall Thickness	3/16 in

* Mass and length given are for the assembly including the Injection Bulkhead, Body Cylinder, and Forward Bulkhead, but not fasteners

1. General Pressure Vessel Design Methodology

The team initially considered two varieties of tanks: a Composite Overwrapped Pressure Vessel (COPV) tank and a custom-made aluminum tank. These two options were identified as the most weight-efficient tank options that the team could pursue. After contacting multiple COPV tank manufacturers, it was determined that COPV tanks are optimal for pressure vessels whose internal pressure ratings are far higher than what the Titan II engine requires. Purchasing a COPV tank would result in an overdesigned and expensive pressure vessel. On the other hand, designing and manufacturing a custom tank proved to have many benefits. Some of these include a lower cost, better control of manufacturing, the ability to integrate the tank into the airframe (which in turn reduces the rocket's mass), the ability to customize its forward and aft bulkheads to enable incorporation of plumbing, and the potential to teach newer members how to design and manufacture a large assembly. Because of this, the team decided to pursue the design of a custom aluminum tank.

In order to properly size the Oxidizer Tank, the necessary oxidizer volume must first be determined. For this to be accomplished, a density value was determined for the expected vapor pressure and temperature of the nitrous oxide. The density of the liquid nitrous oxide changes depending on the temperature of the nitrous oxide tank, because the high pressure causes the fluid to exist as a saturated liquid. This means that any change in temperature results in a

change in the vapor pressure of the tank, resulting in this shift in density. Since determining the exact real-time density value of nitrous oxide is beyond the capabilities of the team, it was decided that a constant density value needed to be agreed upon in order to continue with the design of the overall engine. This value depends on temperature, so a study was conducted to best define the likely temperature that the Oxidizer Tank would experience during the Spaceport America Cup competition day. The average weather conditions in Las Cruces, New Mexico in mid-June during the competition dates showed a low temperature of 68°F and a high temperature of 95°F. The team selected the mid-morning temperature value of approximately 86°F, or 30°C, because this represents the likely time that the Titan II engine will fire. The engine is optimized at this temperature, but the team is planning to test at a range of temperatures -- venting the tank if the ambient temperature is above 86°F and using heating tape if it is below. Furthermore, the oxidizer tank components were designed with a fixed density even though the team acknowledges that the density is not constant. Knowing this temperature, and using a reference document presenting the thermophysical properties of saturated nitrous oxide, a value of 688 kg/m³ was chosen.⁵

When matched with the total oxidizer mass needed for the 1200 lbf of thrust, as well as the 7.67 seconds of burn time, the total oxidizer volume needed was determined to be 1583 in³. However, although this value is the exact amount of nitrous oxide necessary for the full engine burn, the Oxidizer Tank was designed to accommodate an additional 5% volume ullage margin, which results in approximately 80 in³ of additional tank volume. This ullage space protects against any safety issues because of potentially large pressure drops after engine start, which could cause damage to the Oxidizer Tank's structural integrity. With this additional ullage volume, the total Oxidizer Tank volume desired was determined to be 1663 in³. This number was used in the design of the multiple Oxidizer Tank components.

Aluminum 6061-T6 was chosen as the ideal material for the Oxidizer Tank. This is because it is fairly lightweight, yet it has a high enough yield strength to withstand the maximum-expected 915 psi of nitrous oxide with a reasonably small wall thickness, and is financially viable. This combination of features, combined with Rice Eclipse's familiarity with this material, makes aluminum 6061-T6 an ideal metal for the design of this Oxidizer Tank.

It was decided that the tank should be split into three components for ease of manufacturing and structural integrity: the Body Cylinder, the Forward Bulkhead, and the Injection Bulkhead. The Body Cylinder was chosen to be a simple cylinder, while the Forward Bulkhead was designed as a modified dome with ports for plumbing and additional material for fastener holes to allow the Oxidizer Tank to be secured to the airframe. The Injection Bulkhead was designed as an integration of the aft oxidizer bulkhead and the thrust chamber bulkhead. This decision was made to reduce the material needed to manufacture these components by combining their respective functions into one machined piece, as well as to eliminate the possible failure mode of plumbing yielding under stress. All three components will be welded together at the location of the shoulder extensions. The following sections contain more information about the specific components.

2. Body Cylinder

The Body Cylinder is a tube that contains the majority of the engine's necessary oxidizer. Its outer diameter is the same as the airframe at 6.25 in, and its thickness is determined from wall stress calculations. Knowing these dimensions and the volume of oxidizer the cylinder must be able to carry, its length can be determined.

Table 5. Body Cylinder Design Specifications	
Available Oxidizer Volume	1495.64 in ³
Total Mass	19.17 lb
Total Length	55.10 in
Minimum Wall Thickness	3/16 in

The design of the Body Cylinder began with the calculation of the necessary wall thickness throughout the tank to house the nitrous oxide. Although the performance of the engine has been designed around the expected nitrous oxide pressure of 750 psi, the Oxidizer Tank's wall thickness was designed to withstand a maximum expected pressure of 915 psi. Similar to how the team defined the estimated nitrous oxide liquid density, this value was calculated by

studying the average temperature of past Spaceport America Cup competitions at 11 AM, which was determined to be approximately 30°C. Using this temperature, the team calculated the expected rise in pressure of nitrous oxide, which resulted in a total pressure of 915 psi. Nitrous oxide's density decreases rapidly as the temperature continues to rise beyond 30°C, which would require a much larger tank volume to house the same amount of mass, so the team decided that 915 psi will be the highest pressure that the nitrous oxide will be allowed to reach. Any pressure beyond this point will trigger the Oxidizer Tank's relief valve to vent nitrous oxide until the pressure settles below 915 psi.

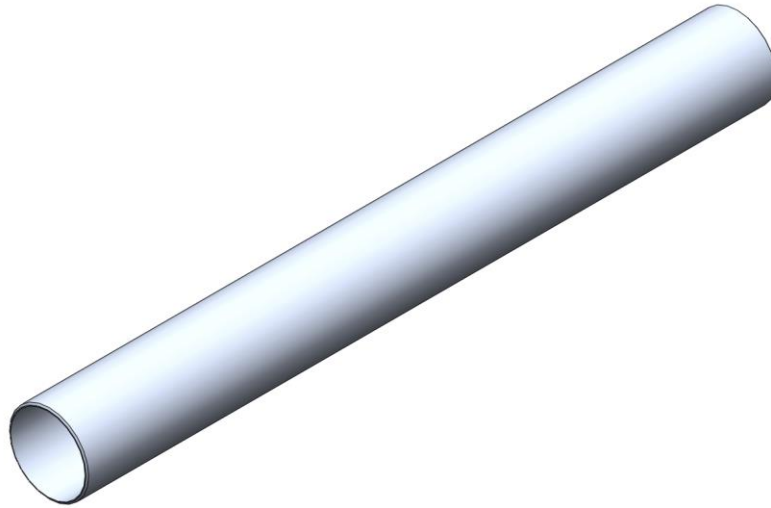


Figure 7. Body Cylinder

The wall thickness of the Oxidizer Tank was calculated using hoop stress and axial stress equations. The maximum nominal pressure used for the calculation is 915 psi, and the Oxidizer Tank outer diameter is known to be 6.25 in, since it will match the outer diameter of the overall rocket airframe. Since 3/16 in was the smallest standardized value that meets the safety requirements, it was chosen to be the wall thickness of the entire Oxidizer Tank. The calculations can be found in *Appendix VIII, Calculation B.1*. In addition to the stress calculations, an FEA static study of the tank was performed in SolidWorks Simulation to verify that the tank will not yield when pressurized with nitrous oxide. This simulation includes the Forward Bulkhead, Body Cylinder, and Injection Bulkhead, and is discussed in detail in *Appendix IX, Simulation B.1*.

With the inner diameter of the Body Cylinder now known due to its fixed outer diameter and wall thickness, the length can be determined. The Body Cylinder holds the majority of the oxidizer, a volume which amounts to 1663 in³ minus the combined internal volumes of the Forward Bulkhead dome and the Injection Bulkhead dome. As will be discussed in *Section IV.A.3* and *Section IV.B.1* respectively, the volume of the Forward Bulkhead is 111.58 in³ and the volume of the Injection Bulkhead is 57.57 in³. Using a simple equation for the volume of a cylinder, the length of the Body Cylinder was found to be 55.1 in. Finally, the Body Cylinder has a chamfer on either end which allows the part to be welded to both bulkheads. More details on this feature and the welding requirements for the Oxidizer Tank components are given in *Section IV.D.1*.

3. Forward Bulkhead

The Forward Bulkhead serves as the forward dome of the Oxidizer Tank, and is welded to the forward end of the Body Cylinder in order to create a sealed and rigid connection. It is also used for integration with the airframe that is forward from the Oxidizer Tank, and contains a shoulder extension to have a secure connection to the airframe. The Forward Bulkhead also contains connection points for the vent valve, relief valve, and a pressure transducer and temperature probe that collects data from the Oxidizer Tank during static testing. Its design was chosen to allow for easy integration and assembly with its surrounding components, meet all safety criteria, and eliminate unnecessary mass. The cylindrical geometry of the Forward Bulkhead will be machined using a manual lathe, the forward face (including the ports) will be machined using a CNC mill, and the complicated geometry of the forward dome will be manufactured via a CNC lathe.



Figure 8. Forward Bulkhead (isometric view)

Table 6. Forward Bulkhead Design Specifications	
Available Oxidizer Volume	111.58 in ³
Total Mass	3.48 lb
Total Length	5.57 in
Minimum Wall Thickness	3/16 in

As the Forward Bulkhead is welded to the Body Cylinder, it meets the same welding requirements as the Body Cylinder (see *Section IV.D.I*). A 3 in cylindrical extension was added to the end of the bulkhead as this is the minimum length orbital welding requires to safely secure the component. This extension has the same thickness as the Body Cylinder (3/16 in) in order to meet the same safety factor.

The dome on the Forward Bulkhead was optimized to minimize mass while still upholding a factor of safety above 2.0 when loaded with oxidizer at its maximum pressure before being vented, which is 915 psi. An ordinary, spherical design was initially considered for the dome because of its safety and verifiability due to the fact that there are known equations to calculate the stress inside a perfect dome. However, this simple design was found to add a significant amount of unnecessary mass to the bulkhead. Through iterative simulations, a new dome geometry was chosen. This design ensures that the minimum wall thickness above the orbital welding extrusion is 0.2 in, which is larger than the minimum Body Cylinder wall thickness of 3/16 in. Additionally, fillets of a radius greater than or equal to 0.5 in were added to any location with a sharp angle in order to reduce stress concentrations. However, this alone is not enough to ensure that this complicated geometry will have a safety factor above 2.0 because there are no standard equations to calculate the stress on the dome walls like there are for spherical geometries. In order to ensure the bulkhead can safely handle the worst case scenario of the loads it could see, the Forward Bulkhead was included in the Oxidizer Tank FEA study. The details of that study (which is the same as the study for the Body Cylinder) are given in *Appendix IX, Simulation B.1*. As seen below, Figure 9 gives the results of the study -- all of the stresses on the Forward Bulkhead are significantly lower than the yield stress of 6061 T-6 (35,000 psi when in tension), and the component has a factor of safety well above 2.

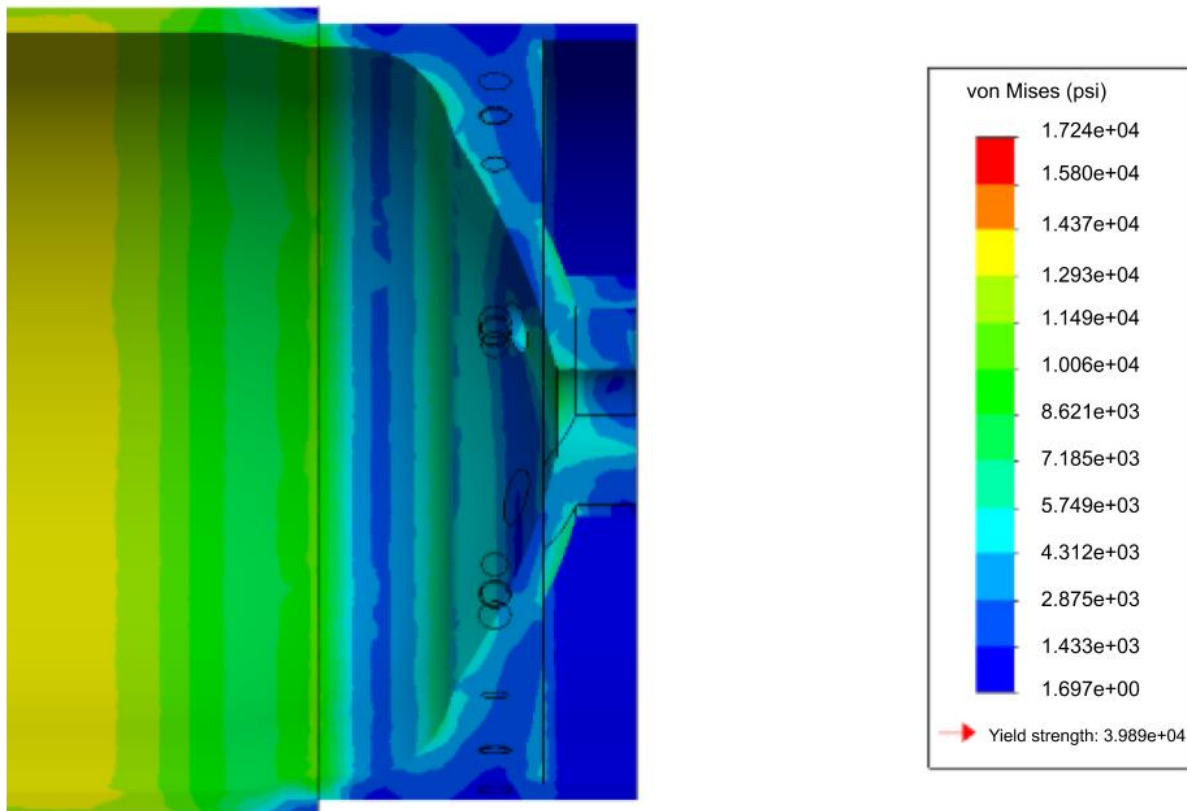


Figure 9. Forward Bulkhead Stress Results from Oxidizer Tank FEA Simulation

An additional concern regarding the dome design of the Forward Bulkhead was machinability. The machines at the team’s workspace, Rice University’s Oshman Engineering Design Kitchen (OEDK), are not equipped to manufacture either the traditional spherical dome geometry or the complicated geometry of the Forward Bulkhead. Curved geometry (such as the arcs in the dome) cannot be easily made on a standard manual lathe, and the part is too large to be machined on the CNC lathe at the OEDK. Therefore, the team has no choice but to find a separate makerspace where the bulkhead can be manufactured. In order to make sure the chosen design is manufacturable on a CNC lathe using a boring bar, the dome geometry design does not contain any sections that curve back around towards the aft end of the engine.

The Forward Bulkhead was designed to include a ring of fasteners, as well as custom threaded ports for the attachment of the Vent/Relief System. To attach the Forward Bulkhead to the rocket airframe, there will be eight ¼ in fasteners, which are further discussed in *Section IV.D.2.1*. Additionally, the Forward Bulkhead has three ports: one ¼” FNPT port for the installation of the Vent Valve Assembly, one ½” FNPT port for the installation of the Relief Valve Assembly, and one 7/16-20 SAE Straight Thread port for the pressure transducer and thermal probe used during ground tests, all of which is discussed in detail in *Section IV.C*.

The geometry of the Forward Bulkhead was also optimized to integrate with the airframe and minimize difficulty when assembling the rocket that contains the Titan II engine. The distance between the bottom of the fastener holes and the ledge the airframe sits on is 1.25 in, which is the minimum length to have a secure connection with the airframe. In order to have as much overlap as possible between the Forward Bulkhead and the airframe, a 0.72 in long shoulder extension was added to the bulkhead.

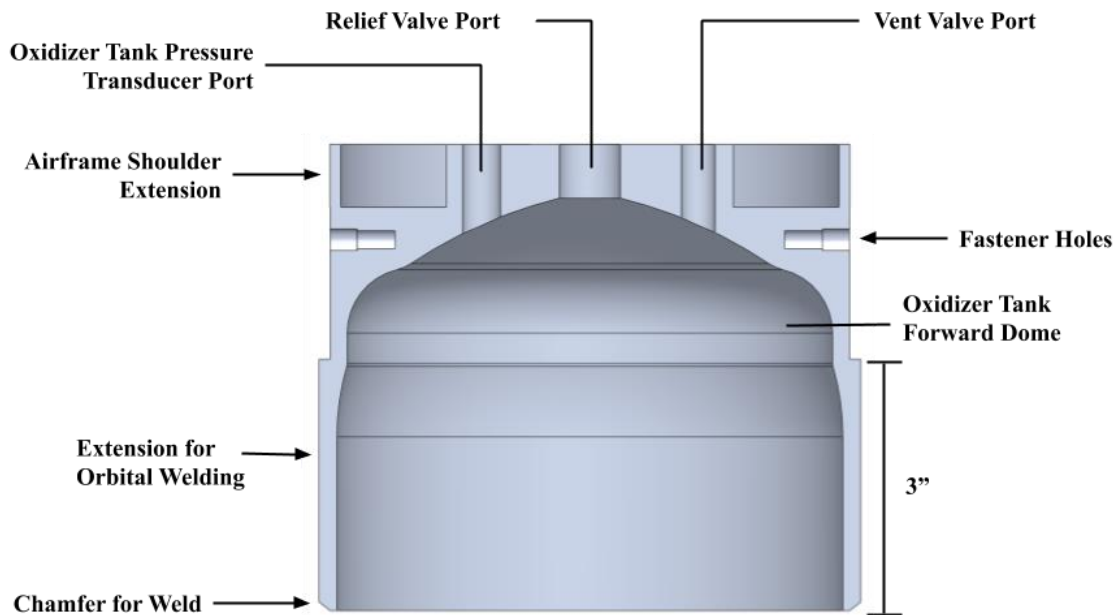


Figure 10. Forward Bulkhead (cross-section view)

B. Injection Assembly

The Injection Assembly consists of three distinct components: the Injection Bulkhead, the Oxidizer Feed Conduit, and the Injector Plate. The bulkhead itself is machined from a single piece of aluminum stock; it includes the aft end of the Oxidizer Tank pressure vessel, a pre-injection chamber, and two ports for pressure transducers. The Injection Bulkhead is welded to the Body Cylinder in order to create a seal for the main pressure vessel. The Oxidizer Feed Conduit is a bore through the Injection Bulkhead that allows oxidizer to flow into the pre-injection chamber. To secure the Injection Assembly to Thrust Chamber and the rocket airframe, there will be 24 ¼” radial fasteners on the aft side of the Injection Bulkhead, which are further discussed in *Section IV.D.2.2*. The functions and rationales behind each component in the assembly are discussed in further detail below.

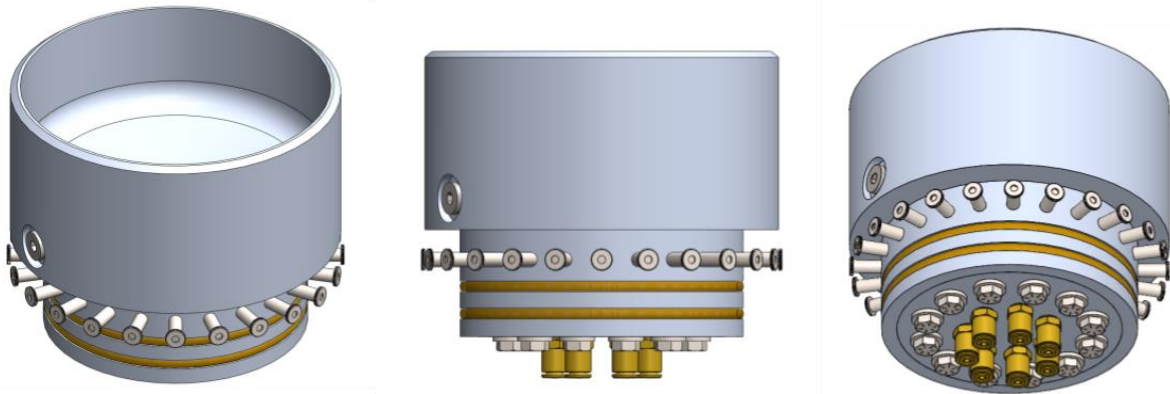


Figure 11: Injection Assembly (three views)

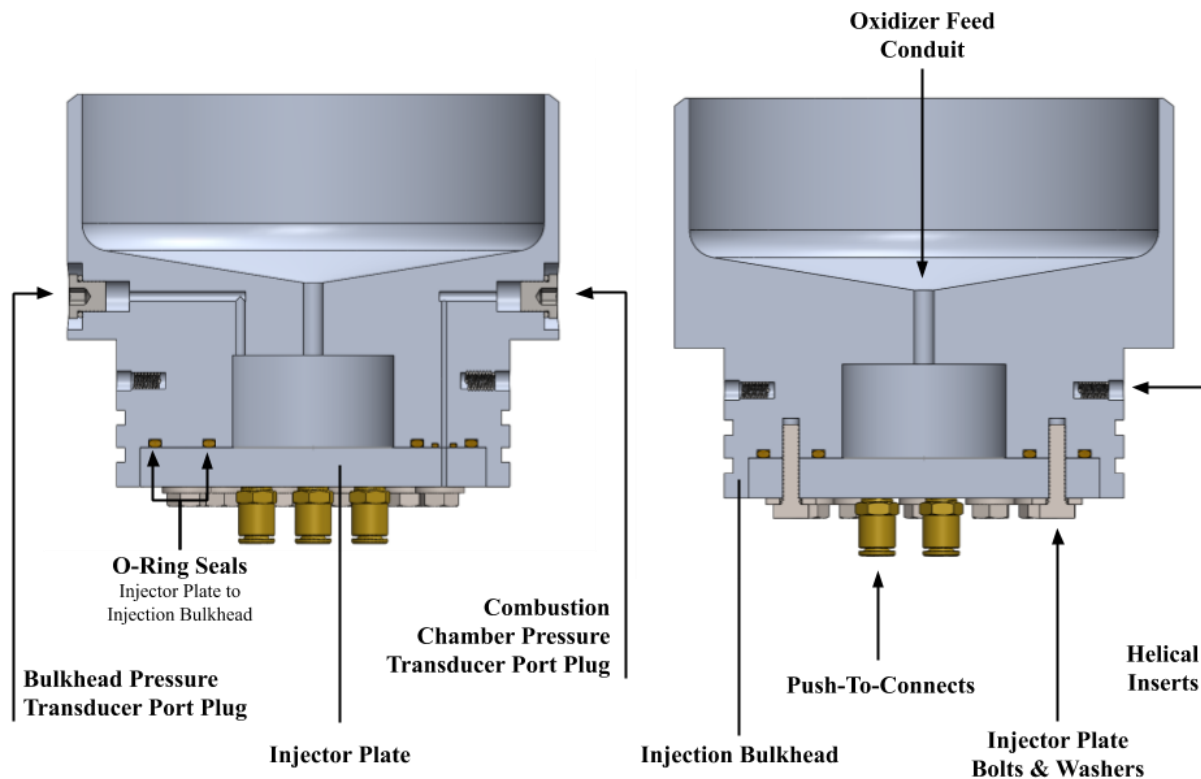


Figure 12. Injection Assembly (cross-section views)

1. Injection Bulkhead

The Injection Bulkhead serves as both the dome on the aft side of the Oxidizer Tank and the bulkhead that connects to the forward side of the Thrust Chamber that houses the Injector Plate. The team originally considered having two separate bulkheads, one being the aft end of the tank and the other housing the Injector Plate with a thin line of plumbing connecting the two, instead of this component. However, the team decided that a single component is a better design than the two bulkheads connected by a feed line since high loads could damage the thin line of plumbing. Additionally, combining the two bulkheads into a single component reduces the total mass and length of the engine. The design of the Injection Bulkhead includes the Aft Dome for the Oxidizer Tank, a Pre-Injection Chamber, 24 radial holes for fasteners which attach to the Combustion Chamber and the airframe, and two pressure transducer (PT) ports. The thin line of plumbing was replaced by the Oxidizer Feed Conduit, which goes through the center of the Injection Bulkhead and is discussed further in *Section IV.B.2*.

The Injection Bulkhead is welded to the Body Cylinder, and its forward end meets the requirements for orbital welding specified in *Section IV.D.1*. The Injection Bulkhead sits on the forward side of the Combustion Chamber and houses the Injector Plate. Aluminum 6061-T6 was chosen as the material for the bulkhead -- it is chemically compatible with nitrous oxide, and although it may not be as strong as stainless steel or 7075 aluminum, it is cheaper, lighter and easier to machine. With the exception of the Aft Dome, the Injection Bulkhead will be manufactured using manual lathes and CNC mills at Rice's OEDK. Due to its complicated geometry, the Aft Dome will be machined on a CNC lathe.



Figure 13: Injection Bulkhead (three views)

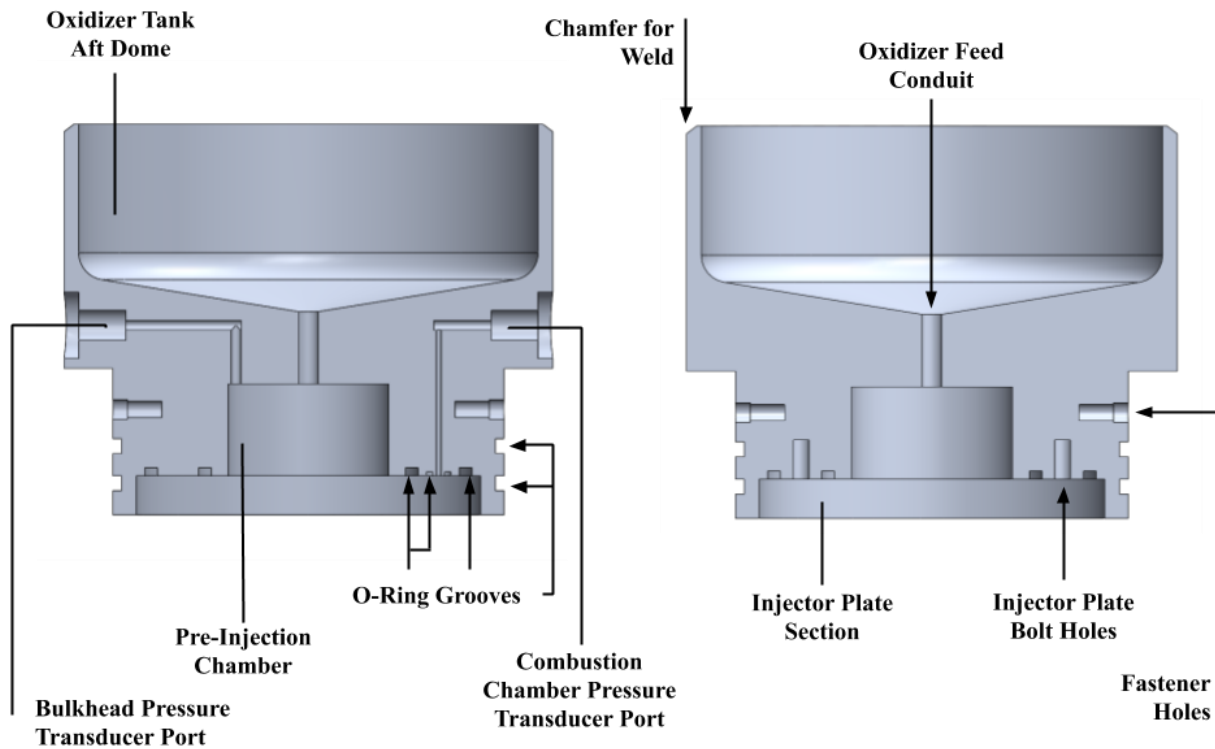


Figure 14: Injection Bulkhead (two cross-section views, labeled)

The following objectives drove the design of the bulkhead:

- Must contain the nitrous oxide held in the Oxidizer Tank
- Must be compatible for welding to Oxidizer Tank
- Must contain the combustion chamber gases produced in the Combustion Chamber
- Must be compatible with Combustion Chamber dimensions
- Must keep the Injector Plate in place
- Must include two pressure transducers: one for gathering data from the bulkhead and one for gathering data from the Combustion Chamber

The outer diameter of the forward side of the Injection Bulkhead is 6.25 in to integrate with the Body Cylinder. The outer diameter of the aft side of the Injection Bulkhead is 5.0 in, as this is the inner diameter of the Combustion Chamber it integrates with. The Injection Bulkhead contains 24 ¼ in radial holes for the fasteners that

secure it to the Combustion Chamber and the airframe. More details on the Combustion Chamber are given in *Section V.A.2*. The Injection Bulkhead fasteners are discussed in *Section IV.D.2.2*.

Table 7: Injection Bulkhead Design Specifications	
Material	Aluminum 6061-T6
Aft Dome Outer Diameter	6.25 in
Pre-Injection Chamber Diameter	2.050 in
Injector Plate Section Outer Diameter	5.00 in
Available Oxidizer Volume	57.57 in ³
Total Mass	5.95 lbm
Pressure Transducer Ports	7/16-20 SAE Straight Thread Port
Minimum Wall Thickness	0.1875 in
Total Length	5.0 in

1.1 Aft Dome

Similar to the dome on the Forward Bulkhead, the Aft Dome on the Injection Bulkhead is designed to uphold a safety factor greater than 2.0 while minimizing mass. A spherical geometry was initially considered, but was found to have a safety factor well beyond what was needed and take up a significant amount of volume. Instead, a thinner design consisting of a conical face meeting a cylindrical face with a fillet of radius 0.5 in was chosen. This design decreased the mass of the bulkhead by nearly 2 lbm when compared to the spherical dome. For safety, the minimum thickness anywhere on the dome (except for the extension which mimics the geometry of the Body Cylinder) is 0.21 in, which is more than the Body Cylinder's 3/16 in. Like the Forward bulkhead, the geometry is not standard, so there are no equations the team can use to ensure the safety factor is above 2.0. Instead, the team included the Injection Bulkhead in the Oxidizer Tank FEA simulation with the Aft Dome experiencing its maximum pressure of 915 psi. The details of this study are given in *Appendix IX, Simulation B.1* and the stress results on the Aft Dome are shown in Figure 15 below. The highest stress is 17.2 ksi, which gives the Aft Dome a factor of safety just above 2 when compared the yield strength of 6061 T-6 aluminum in tension (35 ksi).

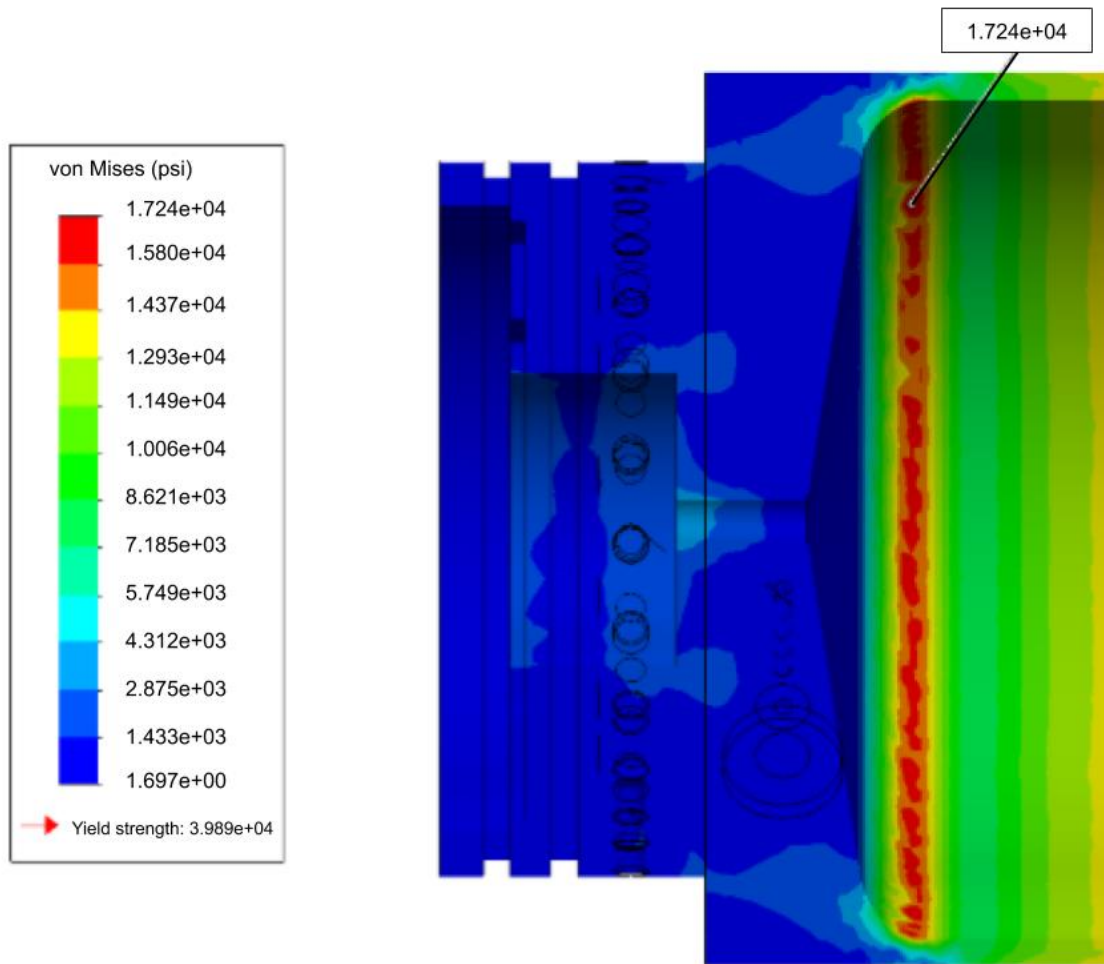


Figure 15. Forward Bulkhead Stress Results from Oxidizer Tank FEA Simulation

1.2 Pre-Injection Chamber and Injector Plate Section

The bottom half of the Injection Bulkhead (i.e. everything below the Aft Dome) will be inserted into the Combustion Chamber. This is why there is a shoulder in between the fastener holes and the pressure transducer ports. Inserting the Injection Bulkhead into the Combustion Chamber ensures that the top of the component is sealed. This lower section of the Injection Bulkhead contains both the Pre-Injection Chamber and the Injector Plate Section. The Pre-Injection Chamber is located between the Oxidizer Feed Conduit and the Injector Plate. It allows nitrous oxide to accumulate and expand so that it is able to pass through all of the Injector Plate holes. The height of the Pre-Injection Chamber is 1.175 in while the radius was set to 1.025 in. This radius was chosen in order to ensure that all of the injection holes lie within the Pre-Injection Chamber. This value also allows the team to minimize the area that the Pre-Injection Chamber occupies, and thus allows ample room for other components, mainly O-ring grooves and bolt holes, on the bottom face of the Injection Bulkhead.

1.3 Wall Stress Considerations

Hoop and axial stress calculations were performed in order to determine the safety factor of the Injection Bulkhead walls, which are inserted into the Combustion Chamber. These calculations can be found in *Appendix VIII, Calculation B.2.1*. It was determined that the safety factor at room temperature is 6.38.

There will be cold nitrous oxide flowing through the Injection Bulkhead, and the walls under consideration will be exposed to the hot combustion chamber gases. The team does not know what the temperature of the nitrous might be nor is the temperature of the combustion chamber gases known. As a result, the team has not performed a rigorous heat transfer analysis and the team has not determined what the Injection Bulkhead's temperature might be. However, by looking up the yield strength of 6061-T6 at different temperatures, the team was able to determine that the Injection Bulkhead will maintain a factor of safety greater than 2 for any temperature lower than 399°F. The team

also used linear interpolation to determine the temperature at which it is expected that the factor of safety to fall below 2, which was found to be 468°F. For more details on these calculations, please refer to *Appendix VIII, Calculation B.2.1*.

As will be discussed in *Section IV.B.3.4*, the Injector Plate is mounted to the Injection Bulkhead via 12 vertical 1/4 in - 20 bolts that thread into the aft face of the bulkhead. These bolts thread into helical inserts which are permanently situated inside the Injection Bulkhead. Although these helical inserts are 0.49 in long and have a 0.06 in gap from the end of the bolt holes, the bolt holes inside the Injection Bulkhead are designed to be 0.62 in deep. This is in order to give a 0.07 in gap from the start of the bolt hole to the start of the helical insert. The majority of the force on the Bulkhead due to these fasteners is on the first few threads, and the team decided to move this location deeper inside the bolt hole in order to reduce the stress on the bulkhead. This is due to the fact that the material surrounding the front of the bolt holes is thinner than the rest of the bulkhead as the Injector Plate O-ring grooves are only 0.135 in away from the bolt hole in the radial direction.

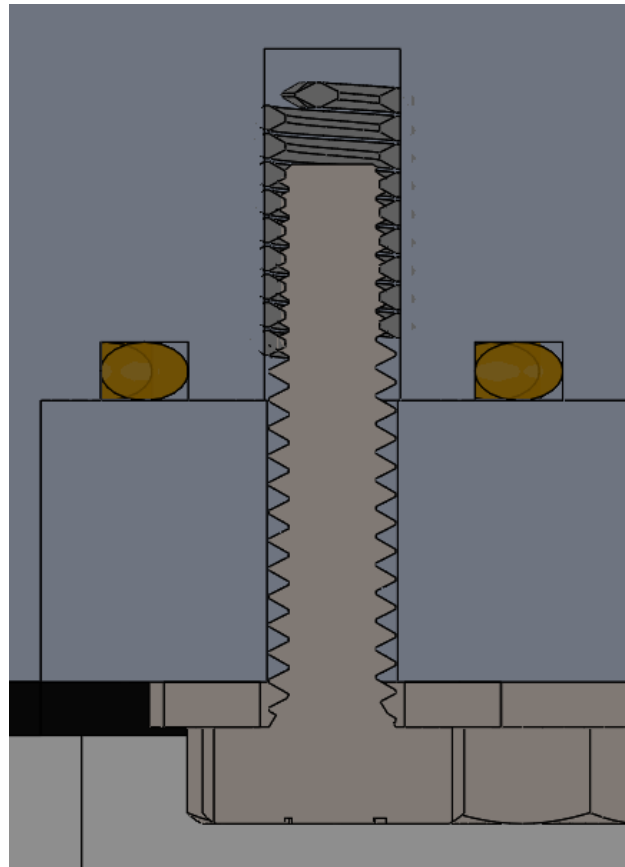


Figure 16. Injector Plate Bolts and Helical Inserts Cross Section

While the Injection Bulkhead is included in the Oxidizer Tank pressure simulation, this only includes the loads on the Aft Dome section of the bulkhead. Due to the fact that the Injection Bulkhead contains the Injector Plate and is exposed to gases stemming from the Combustion Chamber, many of its other walls will be subject to a 500 psi pressure load. In order to ensure the Injection Bulkhead has a factor of safety greater than or equal to 2 for yield when subjected to all of its expected loads, a separate FEA simulation focused entirely on the Injection Bulkhead was conducted. The setup and results of that study are presented in *Appendix IX, Simulation B.2*.

1.4 Pressure Ports

One of the key features on the Injection Bulkhead is the inclusion of two ports for measuring the pressure in relevant locations during test fires and cold flows. The ports are machined directly into the side of the Injection Bulkhead -- allowing for a 7/16-20 SAE straight thread adapter to thread directly into the part. The ports themselves are directly connected to channels carefully machined inside of the bulkhead that direct to the desired location inside of the engine. One port's internal channel leads to the Pre-Injection Chamber, while the other leads to the Pre-

Combustion Chamber. Note that the port leading to the Pre-Combustion Chamber uses a channel that goes through an associated hole in the Injector Plate. This hole allows for pressure readings to be taken on the aft side of the plate. The channels, which both consist of 1/8 in horizontal channels that meet a 1/8 in diameter hole (Pre-Injection Chamber port) or 1/16 in diameter hole (Pre-Combustion Chamber port) at a 90 degree angle, will be carefully machined with a CNC mill.

The ports are located on the forward half of the Injection Bulkhead (i.e. the side that does not insert into the Combustion Chamber), as they need to be accessible to insert the pressure transducers. The ports themselves are machined with straight threads that allow for a simple boss-style fitting with built-in O-ring seal. The nominal diameter of these fittings is 0.385 in. As seen in Figure 14, the ports are given an additional groove around the perimeter to allow for a socket head torque wrench to fit around the hex portion of the fitting to securely tighten it.

Pressure data from the Pre-Injection Chamber and the Pre-Combustion Chamber will only be necessary when collecting data during static testing. During flight, no pressure transducers will be used on this section of the engine, so standard COTS plugs will be used in the ports. Details about the pressure transducers, as well as other instrumentation, are given in *Section VI.E*.

1.5 O-Ring Grooves and Seals

In order to contain the combustion gases, two radial O-rings were placed around the outer diameter of the main bulkhead body; these O-rings will create a seal when pressed against the Combustion Chamber walls and thus prevent any gases from escaping. In order to be compatible with the dimensions of the Combustion Chamber, the outer diameter of the main body of the bulkhead will be 5.00 in. This bore diameter led the team to select No. 2-248 O-rings for this particular application. Even though only one O-ring is necessary, a second O-ring was added for redundancy. Thermal expansion and contraction calculations show that the injection bulkhead walls can have a temperature differential as high as 380°F with the combustion chamber wall, and still maintain the required 0.002” diameter difference needed to maintain the required O-ring squeeze to hold the seal.

There are three O-ring grooves along the bottom face of the Injection Bulkhead. Two of these O-ring grooves surround the ring of axial bolt holes. These grooves are sized for a No. 2-230 O-ring and a No. 2-241 O-ring. The purpose of this pair of O-rings is to prevent nitrous oxide in the Pre-Injection Chamber from leaking around the sides of the Injector Plate, prevent combustion gasses that leak through the bolt holes from entering the Pre-Injection Chamber, and prevent combustion gases from traveling up the sides of the Injector Plate and into the Pre-Injection Chamber. An additional O-ring groove was placed around the hole leading up to the Combustion Chamber PT port. This O-ring groove is designed for a No. 2-008 O-ring and it is meant to prevent combustion gases from leaking out from the PT hole. The Injector Plate Bolts outer O-ring, Combustion Chamber PT O-ring, and Injection Bulkhead outer diameter O-rings will all be subject to hot combustion gases and will use Moly-Graph, a high temperature Molybdenum grease, as lubricant. The Injector Plate Bolt Inner O-ring is directly exposed to the cold temperatures of nitrous oxide and will use Krytox, a cold temperature synthetic grease, as lubricant.

Table 8: Injection Bulkhead O-rings			
O-ring Set	Size Specifications	Material	Lubrication
Injector Plate Bolt Inner O-ring (Face Seal)	1 x No. 2-230	Silicone	Krytox
Injector Plate Bolt Outer O-ring (Face Seal)	1 x No. 2-241	Silicone	Moly-Graph
Combustion Chamber PT O-ring (Face Seal)	1 x No. 2-008	Silicone	Moly-Graph
Injection Bulkhead OD O-rings (Radial Seal)	2 x No. 2-248	Silicone	Moly-Graph

2. Oxidizer Feed Conduit

The Oxidizer Feed Conduit includes the internal geometry of the Injection Bulkhead that connects the Aft Dome of the Oxidizer Tank to the Pre-Injection Chamber. The purpose of this system is to route the oxidizer in the tank to the Combustion Chamber efficiently and effectively. The Feed Conduit effectively replaces the concept of an “oxidizer feed line” that connects the tank to the Thrust Chamber -- this conduit connects the two regions together without using an additional external component.

Table 9: Oxidizer Feed Conduit Specifications	
Conduit Length	0.925 in
Conduit Radius	0.22655

When designing the Oxidizer Feed Conduit, the main concern was the potential hazard of exothermic decomposition; nitrous oxide will exothermically decompose into molecular nitrogen and oxygen if heated to a high enough temperature. Nitrous oxide decomposition can become a positive feedback mechanism, rapidly cascading through all available oxidizer and accelerated by higher temperatures and pressures. These processes can be mitigated by quenching, during which the heat needed to ignite other decomposition or combustion reactions anew is absorbed by other materials acting like a heat sink -- in this case, the aluminum wall of the Oxidizer Feed Conduit. The Injection Bulkhead’s Feed Conduit is sized to decrease the chances of spontaneous decomposition or combustion from propagating into the Oxidizer Tank and causing catastrophic failure. This fluid choke point will draw a significant amount of thermal energy from the small volume of free-stream oxidizer flow to the comparatively larger inner surface area of the Feed Conduit.

The higher liquid oxidizer velocity in the conduit also helps prevent combustion or decomposition for propagating against the flow. Thus, for any section of the choke, it is important to ensure that the volume of oxidizer enclosed is small compared to the surface area of the aluminum bulkhead surrounding the oxidizer. Studies concerning the propagation of the nitrous oxide decomposition reaction in various pipes do exist, but are not rigorously conclusive as to what conduit geometry will effectively quench a reaction in the oxidizer flow. However, it was found that when using a circular conduit, a length:diameter ratio of at least 2 would ensure that combustion/ decomposition propagation would be very unlikely.

The competing consideration driving the conduit design is the need for the conduit to be short and simple to reduce the pressure drop and flow cavitation through the bulkhead, so the oxidizer flow rate isn’t significantly reduced by the geometry preceding the Injector Plate. The conduit was chosen to have a 0.22655 in radius, which is machineable by a 29/64 in ANSI standard drill bit and is slightly larger than the size that would have the same area as the injector holes (a 0.212 in radius). Additionally, its length:diameter ratio is slightly over two. A slightly larger size than the combined area of the injection holes was chosen because it would cause the cavitation-induced choke point in the saturated nitrous flow to be the Injector Plate rather than the conduit. Additionally, the team can adjust the Injector Plate after testing but not the conduit due to the fact that it is part of the Injection Bulkhead which is welded to the Oxidizer Tank. Making the conduit slightly larger than the absolute minimum size gives the team a small margin to make the injector holes larger if it is deemed necessary while still preventing the conduit from being the choke point for the nitrous flow. Making the difference between the minimum radius and the actual radius less than 0.02 in balances the competing drivers of minimizing reaction propagation risk and maximizing flow rate. The calculations that were performed to determine the radius of the Oxidizer Feed Conduit are detailed in *Appendix VIII, Calculation B.2.2.1*.

The pressure drop along the conduit was calculated in order to find the best pressure to design the Injector Plate holes around. The analysis assumes incompressible, single-phase liquid flow with no cavitation in the oxidizer stream. These assumptions are probably not representative of what will actually happen in the engine. The nitrous oxide in the tank will be at (or close to) its vapor pressure and so any loss in pressure --which the feed line will likely create because it contracts the oxidizer flow area-- will lead to some cavitation. Despite this, the team decided to use a single phase model because developing an accurate two phase model requires the team to have accurate experimental data about the temperature and pressure at different points, including the Oxidizer Tank, the Pre-Injection Chamber, and the Combustion Chamber. Rather than developing a complicated model based on inaccurate estimates and approximations, the team has decided to design this component using a simpler model, and revisit the

design once the engine has been tested. Static tests will provide the team with data that can be used to learn about the flaws of the current models, and develop a more accurate two phase model.

The current pressure drop calculations, which are detailed in *Appendix VIII, Calculation B.2.2.2*, resulted in a total pressure drop of 59.75 psi. This pressure drop is assumed to be significant relative to the pressure variation in the Oxidizer Tank as the oxidizer cools due to vaporization during a burn, so the Injector Plate is designed around a 690.25 psi Pre-Injection Chamber pressure.

3. Injector Plate

The Injector Plate is responsible for producing the desired flow rate of oxidizer and atomizing the nitrous oxide before it enters the Combustion Chamber. Atomization increases the surface area of the nitrous flow entering the combustion chamber, in turn improving the rate of reaction of the oxidizer with the fuel grain.⁶ This also allows for a more even distribution of oxidizer throughout the cross section of the Combustion Chamber.

Some additional features of the Injector Plate include its role in allowing the team to gather Combustion Chamber pressure data and its compatibility with the engine's fill system. The Injector Plate will be connected to a set of nylon tubes via push-to-connect fittings that will transport nitrous oxide into the Oxidizer tank. More details about the engine's fill system can be found in *Sections VI.A* and *VI.B*.

The following design objectives drove the design of the injector plate:

- Must produce an oxidizer mass flow rate of 5.132 lb s^{-1} (2.328 kg s^{-1})
- Must atomize the flow of nitrous oxide
- Must be compatible with the engine's fill system
- Must allow for combustion chamber pressure readings

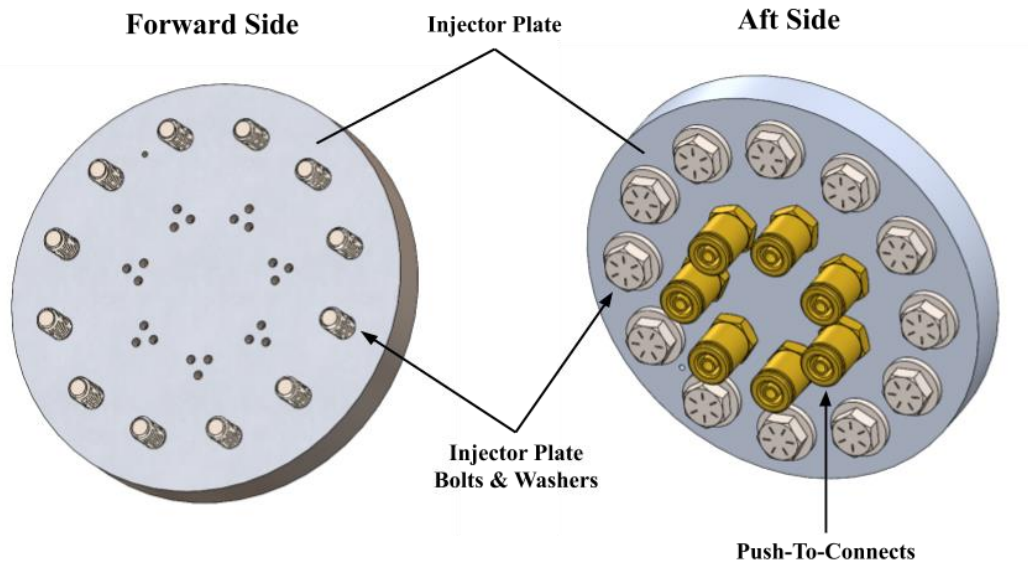


Figure 17: Injector Plate Assembly (forward & aft views, labeled)

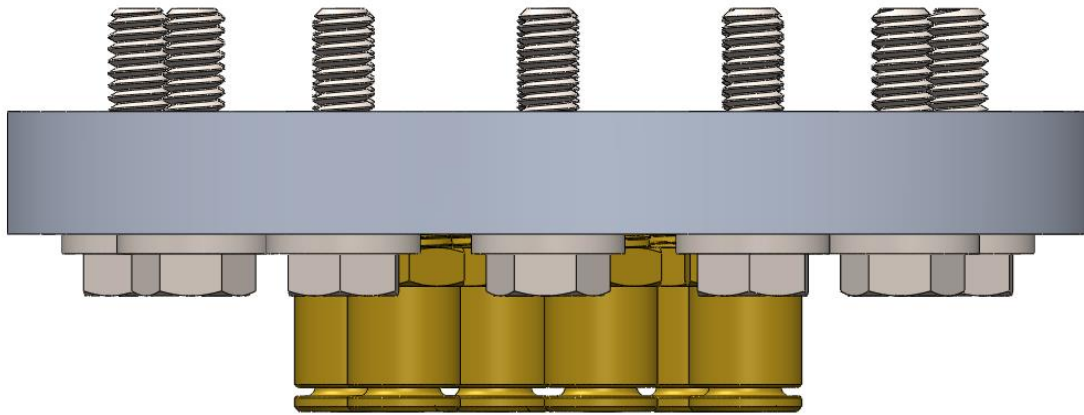


Figure 18: Injector Plate Assembly (front view)

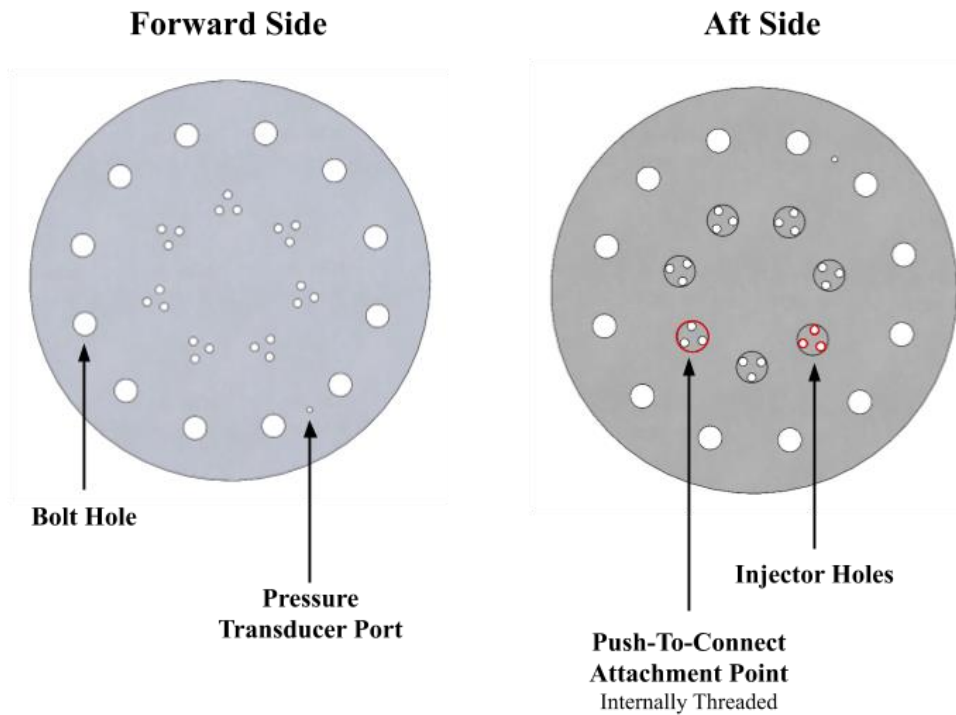


Figure 19: Injector Plate (forward & aft side views, labeled)

3.1 Injector Holes

In order to be compatible with the fill system (*Sections VI.A and VI.B*), it was decided that the Injector Plate would need a “showerhead” hole geometry. This geometry allows for the placement of the injector holes inside a larger hole that in turn attaches to a push to connect (PTC). The seven PTCs allow the team to connect the injector to nylon tubes and thus fill the oxidizer tank with ease. The team decided to use seven PTCs to maximize the number of PTCs on the surface of the plate while also maintaining sufficient spacing between the bolts and PTCs to allow for easy installation. Using seven PTCs gives the team the ability to use 21 injector holes, which ensures that the combined area of the injector holes is smaller than the combined area of the PTCs. This means that the injector holes will be the limiting factor in the flow of oxidizer rather than the PTCs. Since the flow rate through the injector plate is dependent on both the number of holes and the area of each hole, using 21 holes allows the team to shrink the area of these holes and thus better atomize the flow of nitrous.

The Injector Plate's holes can be modeled as small orifices. Under a single phase flow model, the expected oxidizer mass flow rate through the Injector Plate is given by the following expression.⁴

$$\dot{m} = C_d \cdot A \cdot n \cdot \sqrt{2 \cdot \Delta p \cdot \rho}$$

Where \dot{m} represents the mass flow rate through the orifice, A is the cross section of the orifice, n is the number of holes on the plate, Δp is the change in pressure across the plate (the pressure in the bulkhead minus the pressure in the Combustion Chamber), ρ is the density of nitrous oxide, and C_d is the discharge coefficient.

However, because nitrous oxide is a self-pressurizing gas, it will be near its vapor pressure when it is in the Oxidizer Tank. As a result, any change in pressure -- which the Injector Plate is designed to induce -- will lead to the formation of vapor. This leads to cavitation and two phase-flow. With this in mind, the equation above does not account for two phase flow and so it cannot accurately predict the oxidizer mass flow-rate.

It has been noted that for cavitating systems, the value of the discharge coefficient can be adjusted to simulate the effects of cavitation. In cavitating systems the discharge coefficient is solely dependent on the ratio of the orifice diameter to the diameter of pipe that surrounds the orifice (in this case the Pre-Combustion Chamber).^{7,8} The following equations give the mass flow rate with this corrected discharge coefficient.

$$\beta = \frac{d_{hole}}{d_{pipe}}$$

$$A = \frac{1}{4} \pi (d_{hole})^2$$

$$C_d = 0.5542 + 0.5626\beta - 1.652\beta^2 + 1.68\beta^3$$

$$\dot{m} - (0.5542 + 0.5626\beta - 1.652\beta^2 + 1.68\beta^3) \cdot A \cdot n \cdot \sqrt{2 \cdot \Delta p \cdot \rho} = 0$$

The pressure drop across the Injector Plate will vary over time, because although the Combustion Chamber pressure should be fairly constant, the pressure in the Oxidizer Tank is expected to decrease over the course of the burn. Static testing data from the team's 50 lb thrust hybrid engine, Luna, shows that there is a slight decrease in the average feed pressure over the course of a burn. Although Luna's feed pressure transducer is not reading data from the Oxidizer Tank, it is reading data from the feed line attached to the tank which is at an equivalent pressure.

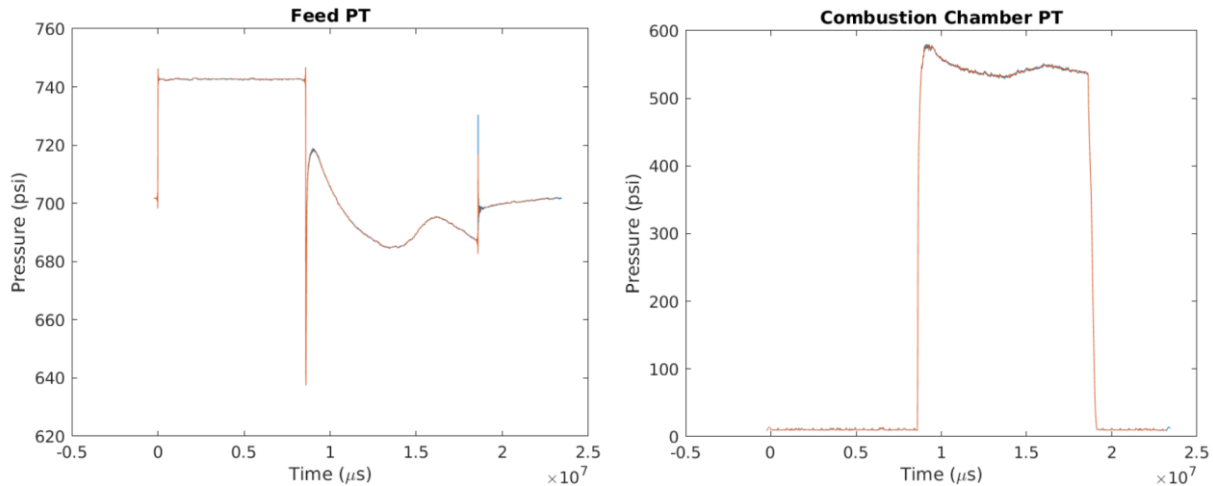


Figure 20. Luna Feed PT and Combustion Chamber PT data from Test #1, 3/3/19

Until the team tests the engine or develops a high-fidelity tanking and de-tanking thermodynamic model, it isn't possible to know the average oxidizer feed pressure. For now, the team assumes this pressure is 750 psi, corresponding to nitrous oxide at 70°F. As a result $\Delta p = 750 - 500 - \Delta P_{FC} - \Delta P_{ML} = 190.25 \text{ psi}$, and $\rho =$

778.7 kg/m^3 (density of nitrous at 70°F). This is a different density than the value used for the Oxidizer Tank since the Injector Plate will be designed to be optimized for static testing, in which an average temperature of 70°F is far more likely than the chosen New Mexico temperature of 86°F . This is because the team will get more useful data from the test if the Injector Plate is optimal for that day, and unlike the Oxidizer Tank it is feasible for the team to remachine the Injector Plate in between a static test and flight. Once a hot-fire test is performed (or a full thermodynamic model is developed), the team will be able to develop a better estimate for the average Pre-Injection Chamber pressure and the density of nitrous oxide.

The team will use $d_{pipe} = 4.25 \text{ in}$ (inner diameter of the Pre-Combustion Chamber) and $\dot{m} = 2.328 \text{ kg/s}$. In order to solve the polynomial equation above in terms of d_{hole} , a MATLAB script was written to iterate from $n = 4$ to $n = 25$. These values were chosen based on the fact that any combination with less than four holes would probably not provide sufficient atomization whereas more than 25 holes would make machining impractical. When these values of n were plugged into the equation, the result was a single variable polynomial equation in terms of d_{hole} . The roots of this equation (and thereby the injector hole diameter) were found by using the bisection method. More information can be found in *Appendix X*. The results are illustrated below in Figure 21.

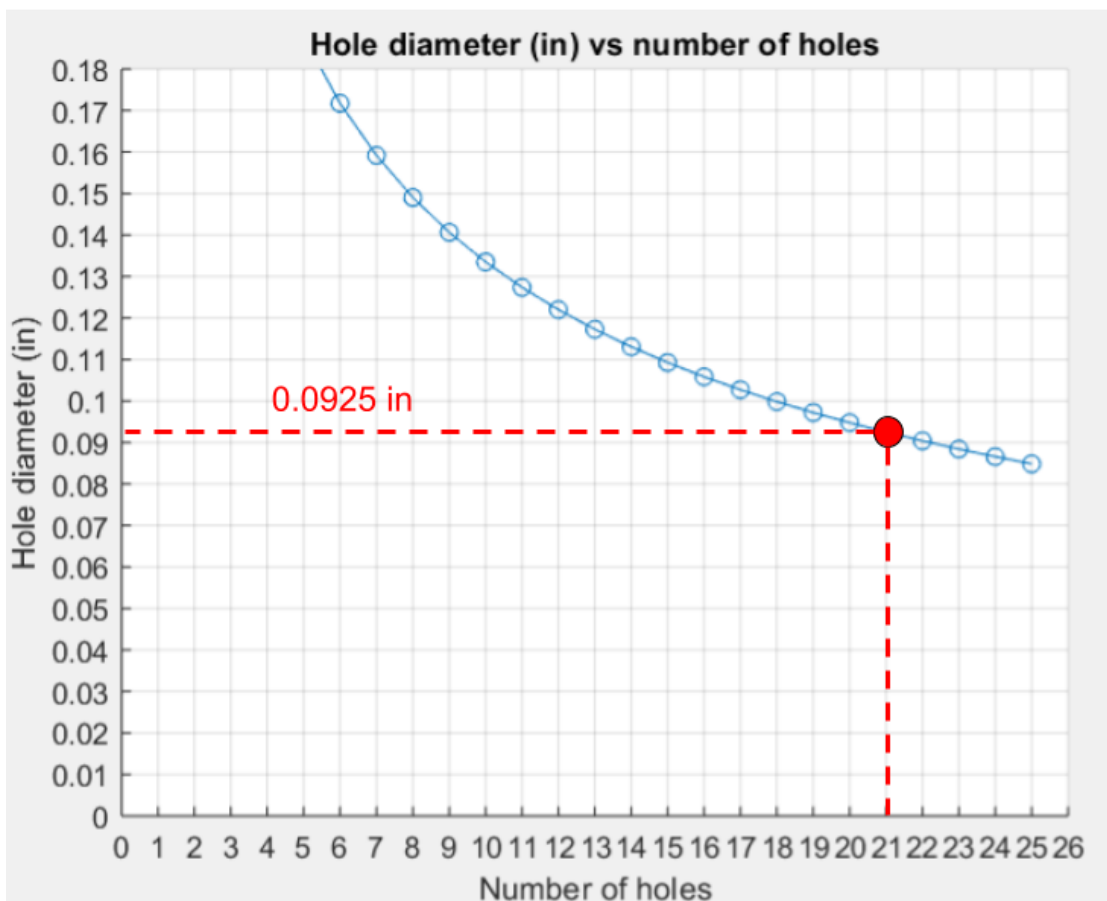


Figure 21. Acceptable Hole Diameter and Number of Holes Combinations

Using these results, it was determined that the best combination to produce atomization and work with the design would use 21 injector holes, each with a 0.09251 in diameter. However, the injector holes must be machined with a standard drill bit⁹, so the diameter was rounded down to 0.0925 in, or 2.35 mm. Three of these holes can comfortably fit inside each of the 1/8 in NPT tapped holes used for the PTCs.

In order to achieve an even distribution of oxidizer in the Combustion Chamber, the holes on the plate will be evenly and symmetrically spaced within a 2 in diameter circle. It is important that the entirety of the holes lie within the inner diameter of the fuel grain (2.26 in). If the injector holes are not within this diameter, it is possible for the

oxidizer flow to collide directly with the fuel grain. This may lead to uneven fuel regression or potentially chip away at large sections of the fuel grain and clog the Nozzle.¹⁰

3.2 Data Collection

In addition to atomizing the nitrous oxide, the Injector Plate will also allow the team to collect pressure data from the Combustion Chamber. As discussed in the Injection Bulkhead section, there will be a 1/16 in hole on the Injector Plate that aligns with a hole that runs through the bulkhead; this will allow for the attachment of a pressure transducer on the side of the Injection Bulkhead to record necessary pressure data of the Combustion Chamber as discussed in *Section IV.B.1.4*.

3.3 Plate Material Selection

The Injector Plate will be constructed out of aluminum 6061-T6 because it is a lightweight alloy that is chemically compatible with nitrous oxide, and relatively easy to machine. A plate thickness of 0.5 in was chosen in order to allow the PTCs to fully thread into the plate and to prevent the plate from yielding when subjected to pressure.

To ensure that this material could withstand the stress that the injector would be subjected to and the deformation of the plate would be negligible, a static SolidWorks simulation was performed. Details on this simulation can be found in *Appendix IX, Simulation B.3*. Through this simulation, the team determined that the Injector Plate achieves a factor of safety that is above 2. The simulation showed that the Injector Holes would experience the greatest stress -- at these points, there was a maximum Von Mises stress of 14.57 ksi, which is less than half the yield strength of 6061-T6 in tension (35 ksi). It was also determined that the stresses acting on the Injector Plate would lead to negligible displacement (3.5×10^{-3} in).

3.4 Injector Plate Retention

In order to fasten the Injector Plate to the Injection Bulkhead, there will be twelve 1/4 in - 20 bolts that thread into helical inserts in the Injection Bulkhead. This would result in a safety factor of 2 as computed in *Appendix VIII, Calculation B.2.3*.

The team originally intended to use a retaining ring to keep the Injector Plate in place with the intention of saving mass. However, retaining rings have multiple disadvantages that make them less favorable to a bolted, although more massive, alternative. First, they only come in specific sizes -- having to select one would place additional design constraints on the geometry of the Injection Bulkhead. Second, the team has found that inserting and removing a retaining ring can be difficult, time consuming, and pose a safety hazard. Finally, bolts are easier to use and are able to apply a clamping force, compressing the O-rings into the bottom face of the Injection Bulkhead.

Once the decision was made to use bolts, the team realized that steel bolts would be threading directly into the 6061-T6 aluminum Injection Bulkhead. The shear yield strength of aluminum is lower than that of steel, meaning that the most probable failure mode would be internal thread tearout. This consideration motivated the team to use helical inserts and a relatively large number of bolts. Steel helical inserts strengthen the threads and improve the material compatibility of the assembly. The team decided to use 1/4 in - 20 bolts because twelve of these bolts could easily fit on the Injector Plate and because they were the largest diameter bolts that can be used with helical inserts given the existing geometries in the bulkhead.

Thread tearout also influenced the bolt preload calculations. Due to the low yield strength of 6061-T6 aluminum, it was not possible to achieve a factor of safety of 2 using the recommended preload force of 2862 lbf ($0.75 \cdot \text{proof load} \cdot \text{tensile stress area} = 0.75 \cdot 120 \text{ ksi} \cdot 0.0318 \text{ in}^2$). As a result, the team calculated the maximum preload force that would ensure the design remains within a factor of safety of 2. The maximum preload force was calculated to be 1,529.723 lbf. Using this preload value, the factor of safety was determined against the static stress experienced by the bolts: 2.014 (see *Appendix VIII, Calculation B.2.3*).

Table 10. Injector Plate Specifications	
Material	Aluminum 6061-T6
Injector Holes	21 equally spaced 0.0925 in diameter holes 3 per PTC Attachment point
PTC Attachment Point	7 equally spaced 1/8 in NPT taps
PT hole	One 1/16 in diameter hole in between two bolt holes
Diameter and Thickness	4.4 in and 0.5 in
Total Mass	0.69 lb

C. Oxidizer Tank Vent and Relief System

The design of the tank's vent and relief system is highly dependent on the highest pressure the team is comfortable with letting the nitrous oxide inside the Oxidizer Tank reach. Since the engine is designed for the Spaceport America Cup, which is held in the New Mexico desert, it is possible that a higher than expected temperature causes the nitrous oxide pressure to rise. If the pressure inside the tank is slightly above the targeted pressure of 750 psi or the volume of oxidizer begins to tap into the excess volume the Oxidizer Tank has capacity for, the team aims to controllably vent the nitrous oxide until the pressure is lowered back down to 750 psi so that the engine can still fire. However, if the pressure increases beyond 915 psi, it poses a serious safety concern due to high stresses on the Oxidizer Tank, and the tank will automatically be rapidly vented until the pressure is below 915 psi in order to prevent a dangerous failure mode. These functions are achieved with a vent valve and a relief valve, respectively. Note that a main oxidizer valve will not be included in the engine during flight because the nylon tube fill system (see *Sections VI.A* and *VI.B*) used on this engine seals the oxidizer in the Oxidizer Tank before ignition, and this engine will not need to be shut down or restarted during flight before draining its Oxidizer Tank.

The Oxidizer Tank's Forward Bulkhead holds two valves that perform vent and relief functions. In flight configuration, the valves direct the gas outwards into the atmosphere, through holes in the flight vehicle airframe. Table 11 summarizes the valve specifications and performance. Supporting calculations for the valve vent rates can be found in *Appendix VIII, Calculations B.3*. Figure 22 shows the overall piping and instrumentation diagram of the Oxidizer Tank's vent/relief system. Both valves are discussed in more detail in the proceeding sections.

Table 11. Oxidizer Tank Valve Specifications		
Specification	Vent Valve	Relief Valve
Manufacturer	Clark Cooper	Generant
Model Number	EH30-042-D012-OXCY	HPRV-500 SS-T-915
Valve Type	2-way solenoid valve	Inline, mechanical, spring-actuated relief valve
Default (No-Power) Position	Normally Closed	Normally Closed
Maximum Allowable Working Pressure (psi)	6300	3700 (set to open at 915)
Rated Temperature Range (°F)	-238 to 400	-428 to 399
Seal Material	Teflon	Teflon
Orifice Diameter (in)	0.032	0.515
Flow Coefficient (C_v) or Discharge Coefficient (C_d)	$C_v = 0.02$	$C_d = 0.2$
Flow Capacity** (lb/sec)	0.016	7.879
Power Requirements	22 W, 12 volt DC	N/A
Notes and Purchase Options	Cleaned for oxygen service with cryogenic service options	Cleaned for oxygen service

**Assumes worst-case venting of gaseous nitrous oxide out of the tank ullage at 915 psi to atmospheric pressure

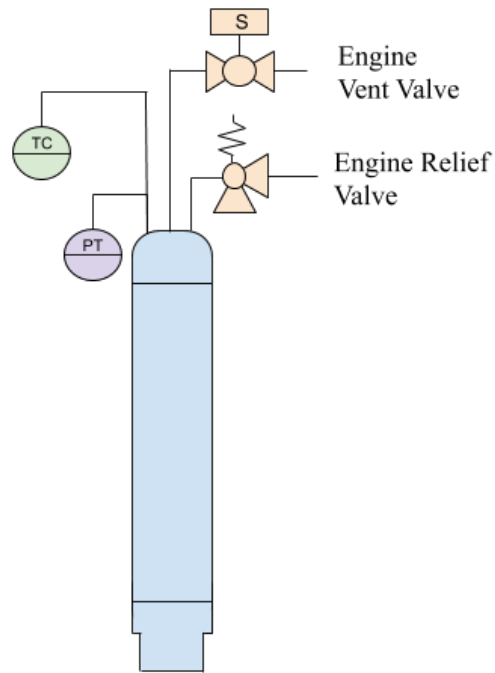


Figure 22. Oxidizer tank piping and instrumentation diagram (PT and TC only present on ground testing setup)

1. Vent Valve

The engine's vent valve is a Clark Cooper EH30 series normally-closed, electronically-actuated solenoid valve with the larger 0.032 in orifice option. The valve is configured with cryogenic and oxygen-cleaning options to make it compatible with nitrous oxide service. It operates up to 6300 psig and has 1/4 in NPT inlet and outlet ports. It was chosen because it is small enough to fit within the inner diameter of the engine's airframe, but is still rated to the pressures and cold-temperature oxidizer conditions needed. This vent valve will be actuated open during the oxidizer fill sequence to allow the air inside the tank at atmospheric pressure to escape as nitrous oxide fills the tank. The vent valve will be assembled with a dip tube that reaches into the Oxidizer Tank, which is designed to ensure a 5% ullage volume in the headspace of the tank. The valve's flow channel is small, so it doesn't allow a significant flow rate of nitrous oxide when the tank reaches its 915 psi peak pressure (see above table). It will be used to vent during oxidizer loading only -- its primary function is not an emergency vent valve. Emergency venting will be performed by the high flow rate relief valve on the tank and the high flow rate ground vent valve on the ground support equipment. Images of the vent valve assembly and vent valve are seen below.

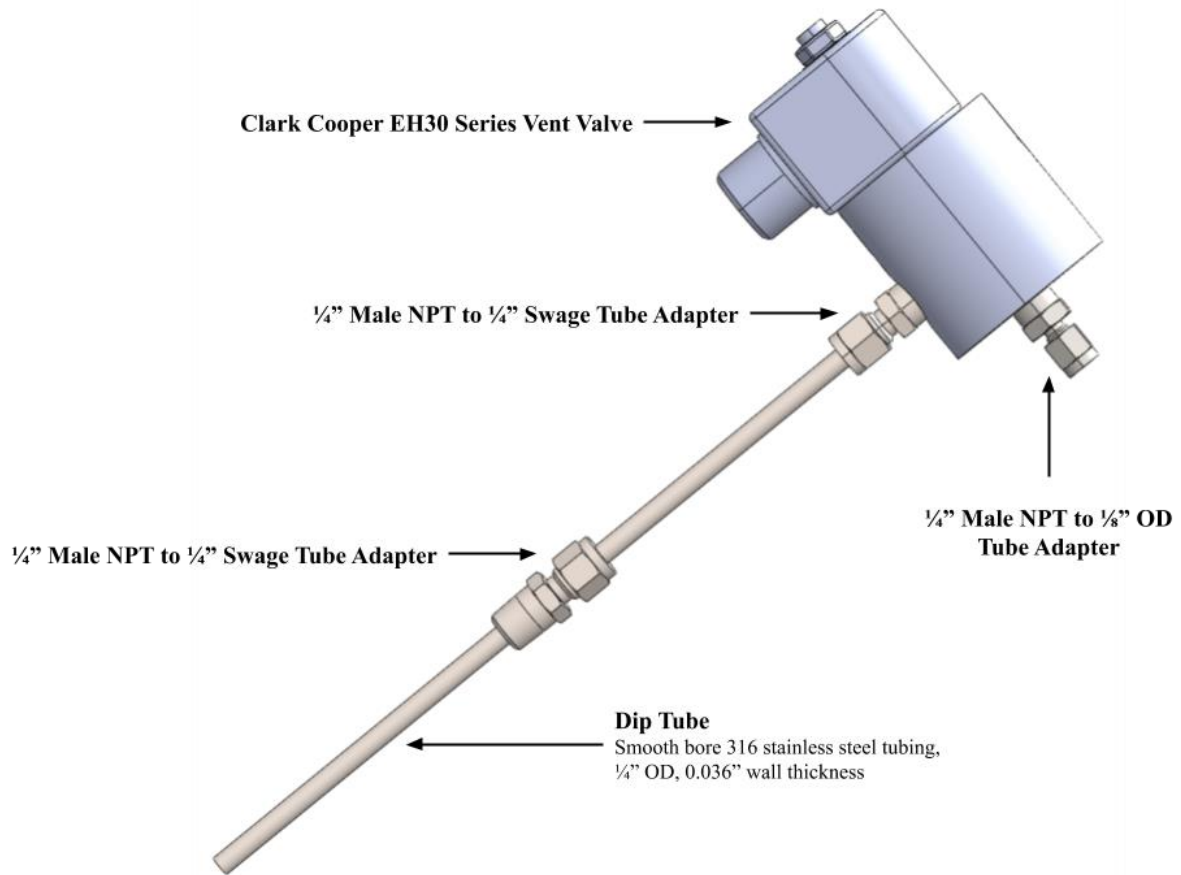


Figure 23. Engine vent valve assembly



Figure 24. Clark Cooper EH30 Series Vent Valve

The dip tube on the vent valve drives the maximum fill point of the Oxidizer Tank, as it will cause oxidizer to be vented from the tank as it reaches its entry point. Once the oxidizer does reach this point, it will begin to flow

through the dip tube and out of the system through the vent valve, causing a white plume of nitrous oxide to visibly exit the plumbing system. This white plume serves as a signal to the team, indicating that the Oxidizer Tank is fully filled. The dip tube dimensions are extremely important to the functionality of the fill system as the dip tube length directly determines the amount of oxidizer in the tank.

For sizing the length of the dip tube for a full burn, a calculation was conducted using the known volume of desired nitrous oxide, as well as the known dimensions of the Oxidizer Tank. The calculations, which can be found in detail in *Appendix VIII, Calculation B.3.2*, determined a necessary dip tube length of 3.78 in from the top of the Forward Bulkhead to the end of the dip tube. The tube will be made out of 316 stainless steel, with a 0.036 in wall thickness, and will be connected to the vent valve and the bulkhead via MNPT to Swage Tube adapters, as shown in Figure 23. Because of varying oxidizer amounts for shorter burn ground tests, the length of the dip tube differs based on the length of the burn. The dip tube sizing for shorter burns, as will be used in the team's initial static hot fires, is detailed in *Section VII.D*.

After the fill procedure, the vent valve can be closed to prevent any escaping nitrous oxide gas, but, in the case of overpressurization due to temperature (as measured in the pressure transducer in the Forward Bulkhead), the valve can be reopened to provide limited pressure relief. This overpressurization pressure is set at 915 psi, which has been used as the maximum allowable pressure value that the Oxidizer Tank will experience before venting, as explained in *Section IV.A*.

2. Relief Valve

The relief valve is a high-pressure relief valve (HPRV) manufactured by Generant. This mechanical relief valve is the primary pressure relief device on the Oxidizer Tank in case the tank exceeds 915 psi, with additional pressure relief provided by the emergency vent valve on the ground support equipment in case the relief valve fails closed. The valve is rated to 3700 psi and is set to open at 915 psi, which is the maximum allowable working pressure of the Oxidizer Tank. The valve body is 316 stainless steel for corrosion resistance against the oxidizer flow, and the seals are Teflon, which function at temperatures as low as -320°F, which is necessary for cold, expanding nitrous flow. As the temperature of the nitrous oxide held in the Oxidizer Tank is far higher than the -320°F operating temperature specified by Generant, the potential freezing of the valve will not be a concern. Before being implemented on the engine, the relief valve will undergo rigorous low temperature testing in order to confirm its reliability.

Normally, the flow capacity of a relief valve is sized by determining the maximum flow rate that could occur in a pressure system due to the failure of an upstream flow-limiting component, like a pressure regulator or a metering valve. However, the oxidizer loading system of Titan II does not contain a regulator or any flow control valve. The mechanism driving pressure buildup in the engine's Oxidizer Tank after loading is the rising temperature of the nitrous oxide in the tank and the ground systems due to ambient solar flux. With the team's current lack of experimental data and the uncertainty of the thermal environment at the Spaceport America Cup launch site, it would be too risky to solely entrust a heat transfer model that determines this pressure rise. As an alternative, the team opted for the more conservative relief valve sizing criterion that it must permit a mass flow rate of gaseous nitrous oxide out of the tank ullage of at least 5.132 lb/sec at the tank's peak 915 psi of pressure. This is the flow rate of oxidizer through the Injector Plate during engine operation, which was assumed to be a large enough flow rate to counteract any heating-induced pressure rise in the tank based on experience in the original Titan engine hot fire. The smallest HPRV size that meets this criterion is the 1/2 in NPT port size, which has an orifice diameter of 0.515 in and a discharge coefficient of 0.2, which allows 915 psi gaseous nitrous oxide vent at 7.879 lbs/sec. This exceeds the minimum required flow rate by a factor of 2.3. Calculations can be found in *Appendix VIII, Calculation B.3.3*. The valve outlet is connected to a 1/2 in NPT tee connector routed to two 3/8 in stainless steel tubes, which provide enough flow capacity downstream of the valve to minimize further flow rate restriction. The piping and fittings in the Relief Valve Assembly are shown in Figure 25. The overall Oxidizer Tank piping and instrumentation diagram is shown in Figure 22.

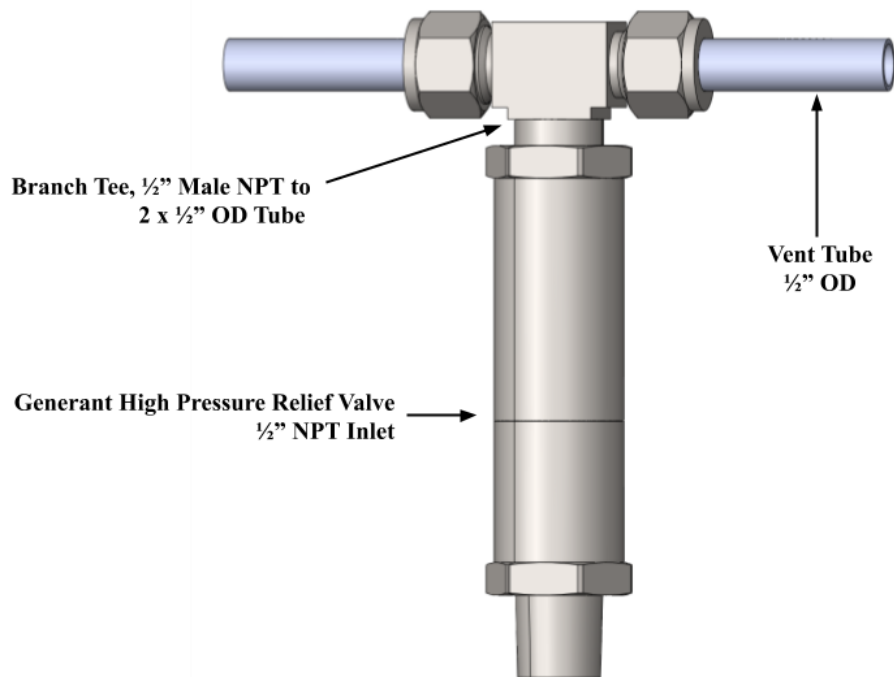


Figure 25. Engine relief valve assembly

D. Oxidizer Tank and Bulkhead Retention

1. Orbital Welding

The Forward Bulkhead and Injection Bulkhead will be welded onto either end of the main body cylinder of the Oxidizer Tank by a professional welder external to Rice Eclipse. Welding was chosen as the form of connecting the bulkheads to the cylinders because it is permanent, and because it eliminates the need for sealing elements or connectors that would add weight to the overall engine.¹¹

The components will be bonded together using an orbital weld, the preferred method for tube-to-tube joining, such as the Oxidizer Tank components. During orbital welding, the two tubes are clamped in place while an orbital weld head rotates an electrode and electric arc around the weld joint to make the required weld.¹² Specifically, the team will use a V-Butt, full penetration orbital weld for the components. To enable this type of weld, the cylindrical ends of the Forward Bulkhead and Injection Bulkhead were extended to provide enough cylindrical surface for the orbital welding equipment. Additionally, the ends of the two bulkheads and body cylinder were adjusted with the necessary geometry (root and “V”) to form the joint.

To determine the necessary geometry for the weld, calculations were conducted based on orbital welding standards.¹³ These calculations can be found in the *Appendix VIII, Calculation B.4.1*. The final welding parameters were set to 37.5° angled cut starting at an axial offset of 0.1 in. and a root of 0.0575 in. as seen in Figure 26.

In order to ensure the area around the two welds retains its strength, the Oxidizer Tank will undergo heat treatment after welding. This process and the fact that the safety factor for the Oxidizer Tank is over 2.7 when compared to the yield strength of 6061 give the team confidence that the welds will not cause the tank to fail. However, since this is not guaranteed, the Oxidizer Tank will be hydrostatically tested to 1.5x its maximum nominal operating pressure before being used in a hot fire⁷, as will be discussed in *Section VII.A*.

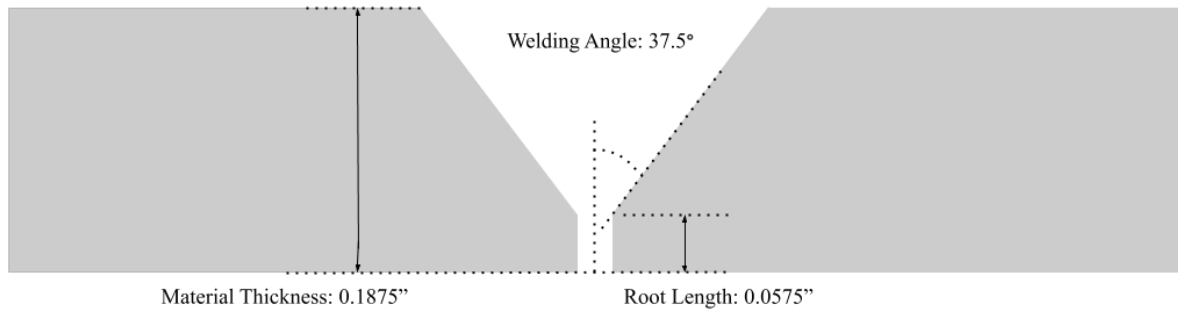


Figure 26. Welding Preparation Diagram

2. Fasteners

Fasteners are needed to hold the Oxidizer Tank in place with respect to the airframe of the rocket. One set of fasteners is needed to connect the Forward Bulkhead to the airframe above it, while another set of fasteners is required to connect the Injection Bulkhead to the airframe below it. For these rings of fasteners, the team chose to use a pin that goes through the components with a threaded end to clamp the components to the airframe. Using a pin surface ensures an even distribution of the load that is being supported by the fastener, when compared to a threaded bolt which has force acting on the peaks of each thread, crushing the thread and deforming the bolt. Therefore, using a pin section on the fastener allows the team to use a smaller number and smaller size of fastener while still achieving the same factor of safety. With this in mind, the team decided to use McMaster-Carr’s shoulder screw as it has both the pin, or shoulder, and threaded section that the team had desired. The team performed the calculations shown in *Appendix VIII, Calculations B.4.2 and B.4.3* with many different shoulder screws, with varying shear stress, shoulder diameter, and head types to determine the best fastener for the Forward Bulkhead to airframe connection. Ultimately, the team decided to use Ultra-Low-Profile Shoulder Screws from McMaster-Carr for both rings of fasteners as they have a very thin head, allowing for a minimal increase on aerodynamic drag. Additionally, there are many options for shoulder diameter and length as well as thread length and size.

Both sets of fasteners will thread into stainless steel helical inserts. The use of stainless steel helical inserts will ensure that the threads in the aluminum bulkheads will not wear out over time with use. Both rings of fasteners will also use threadlocker, such as Loctite 243, to ensure that the fasteners do not loosen during flight due to vibrations of the engine. The details of both the Forward Bulkhead fasteners and Injection Bulkhead fasteners are discussed in more detail below.

2.1 Forward Bulkhead Fasteners

The fasteners on the forward end of the Oxidizer Tank will connect the airframe directly to the Forward Bulkhead. For this ring of fasteners, the team chose to use eight Ultra-Low-Profile Shoulder Screws, with 1/4 in shoulder diameter, 3/8 in shoulder length, and 10-24 thread, as seen in Figure 27 below, that are evenly spaced around the circumference of the Forward Bulkhead. The shoulder length of 3/8 in was chosen so that the pin would fit through the airframe, which has a thickness of 1/8 in, with 1/4 in of the pin inside of the Forward Bulkhead. The thread size of 10-24 was chosen based on availability of shoulder screws from McMaster Carr with the given shoulder diameter.



Figure 27. Forward Bulkhead to Airframe Shoulder Screw

In addition, stainless steel 10-24 helical thread inserts that are 0.380 inches in length will be placed inside of the holes in the bulkhead. The holes for the shoulder screw in the Forward Bulkhead are designed to ensure that the shoulder screw is actually clamping the airframe and Forward Bulkhead together, rather than bottoming out.

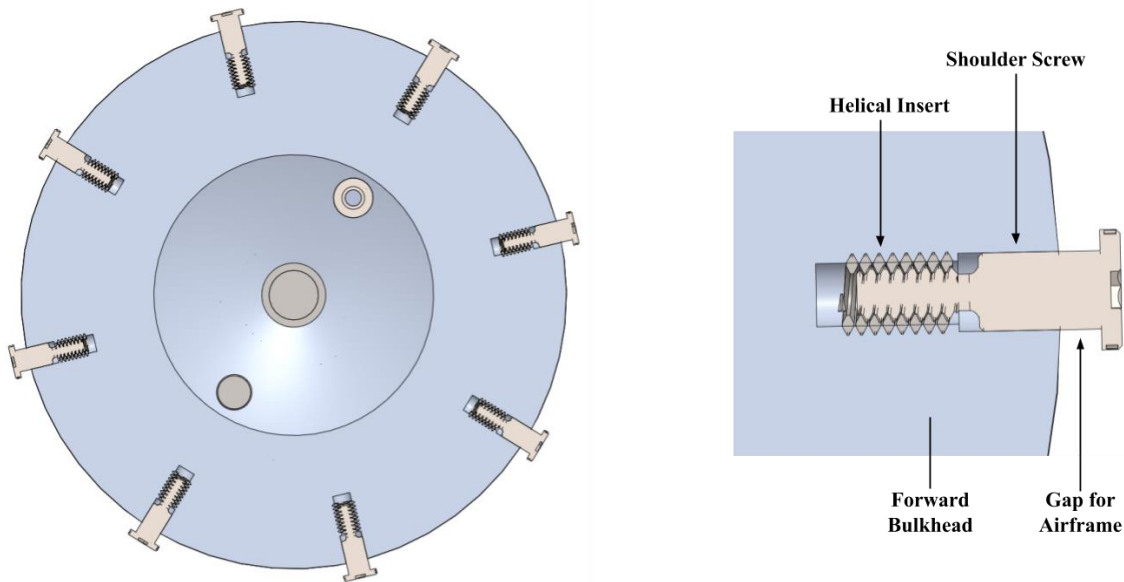


Figure 28. Forward Bulkhead Fasteners with Cross Section View

To ensure that these shoulder screws are sufficient for attaching the Forward Bulkhead to the airframe, three calculations were performed: bearing stress and tearout stress on the shoulder screw holes within the Forward Bulkhead as well as shear stress on the shoulder screw. These calculations can be found in *Appendix VIII, Calculation B.4.2*. Additionally, preload calculations were performed to determine the maximum preload that can be applied to the Forward Bulkhead fasteners. These calculations are found in *Appendix VIII, Calculation B.4.2.4*.

2.2 Injection Bulkhead Fasteners

The fasteners on the aft side of the Oxidizer Tank are designed to connect the Injection Bulkhead to the Airframe below it, as well as connecting the Injection Bulkhead to the Combustion Chamber. Because of this, the team chose to use a pin that goes through the airframe, Forward Combustion Chamber Spacer (a spacer between the airframe and Combustion Chamber - see *Section V.A.5* for detail), Combustion Chamber, and Injection Bulkhead, with a threaded end to clamp the four components together. These fasteners were primarily designed based on requirements of the Combustion Chamber stresses. Based on the bearing stress calculations performed on the Combustion Chamber, discussed in detail in *Appendix VIII, Section C.2.2*, it was determined that there must be 24 fasteners on either end, each 1/4 inches in diameter evenly spaced around the circumference of the Combustion Chamber and the respective components. This unusual number of fasteners is due to a high bearing stress load on the fastener holes in the Combustion Chamber, discussed in detail in *Section V.A.2*. The team decided to use twenty-four Ultra-Low-Profile Shoulder Screw, with a 1/4 in shoulder diameter, 3/4 in shoulder length, and 10-24 thread as seen in Figure 29 below.



Figure 29. Injection Bulkhead to Airframe Fastener

This exact shoulder screw was primarily chosen based on availability of 1/4 in shoulder diameter shoulder screws from McMaster-Carr. This total shoulder length was chosen so that the pin will fit through the airframe,

Combustion Chamber Forward Spacer, and Combustion Chamber, with a total thickness of 5/8 in, with 1/8 in of the pin left to sit inside of the Injection Bulkhead. The engagement between the shoulder of the shoulder screw and the Injection Bulkhead casing is the minimum thickness of the Combustion Chamber, 1/8 in. This ensures that the safety factor with regards to the bearing stress on the Injection Bulkhead is equivalent to that of the Combustion Chamber.

In addition, there will be 10-24 thread and 0.380 in long helical inserts inside of the fastener holes within the Injection Bulkhead. Just like the Forward Bulkhead, the holes for the shoulder screw in the Injection Bulkhead are designed to ensure that the shoulder screw is actually clamping the components together, rather than bottoming out.

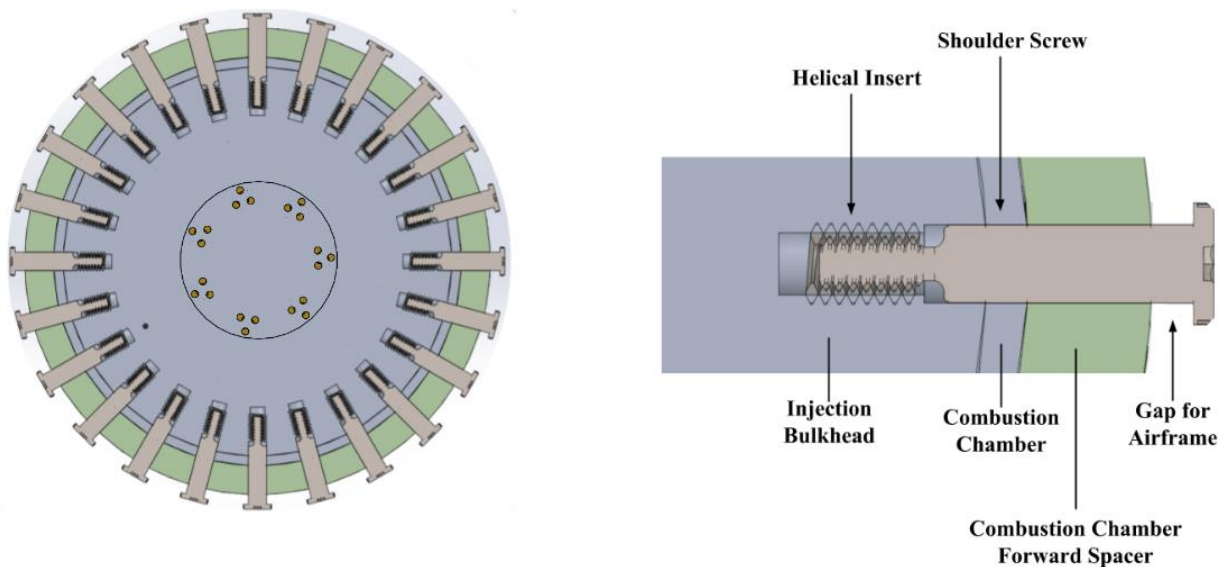


Figure 30. Injection Bulkhead Fasteners

To ensure that these shoulder screws are sufficient for attaching the Injection Bulkhead to the Combustion Chamber, Forward Combustion Chamber Spacer, and airframe, three calculations were performed -- bearing stress and tearout stress on the shoulder screw holes within the Injection Bulkhead as well as shear stress on the shoulder screw. These calculations can be found in *Appendix VIII, Calculation B.4.3*. Just as with the Forward Bulkhead, preload calculations were performed to determine the maximum preload that can be applied during assembly to the Injection Bulkhead fasteners. These calculations are found in *Appendix VIII, Calculation B.4.3.4*.

V. Thrust Chamber Assembly

The Thrust Chamber Assembly allows for propellant to be burned and accelerated to produce thrust. It contains the Combustion Chamber Assembly, which houses the Fuel Grain as well as thermally protective phenolic liners. Additionally, it contains the Nozzle Assembly, which consists of the Nozzle Insert and the Nozzle Casing that protects it. Nitrous oxide enters the Thrust Chamber through holes in the Injector Plate at the aft end of the Oxidizer Storage and Feed Assembly, where it reacts with the fuel grain inside the Combustion Chamber. Combustion gases are accelerated out of the Nozzle Insert to produce 1,200 lbs of thrust. The Thrust Chamber Assembly is fastened to the Oxidizer Storage and Feed Assembly through the Injection Bulkhead Fasteners. This integration is highlighted below in Figures 32 and 33.

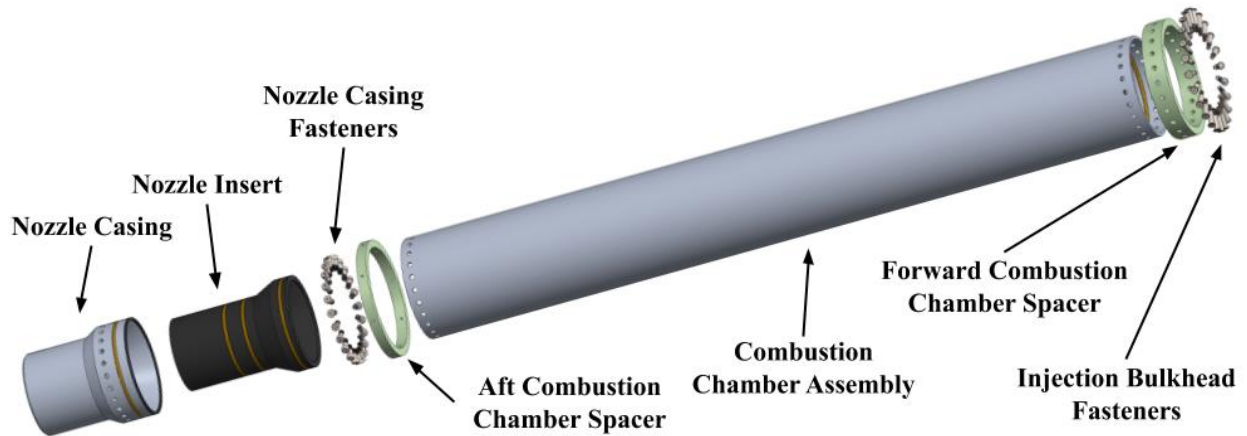


Figure 31. Thrust Chamber Assembly (exploded view)

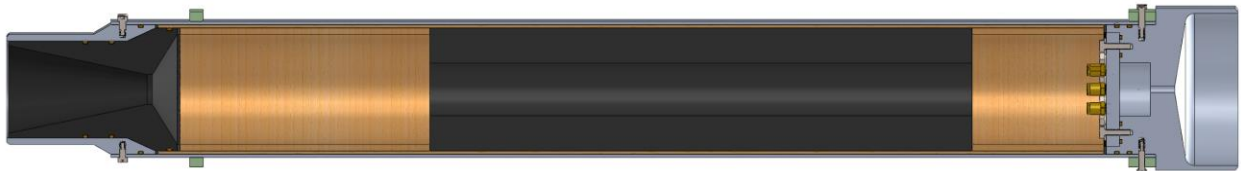


Figure 32. Thrust Chamber Assembly and Injection Assembly (cross-section view)

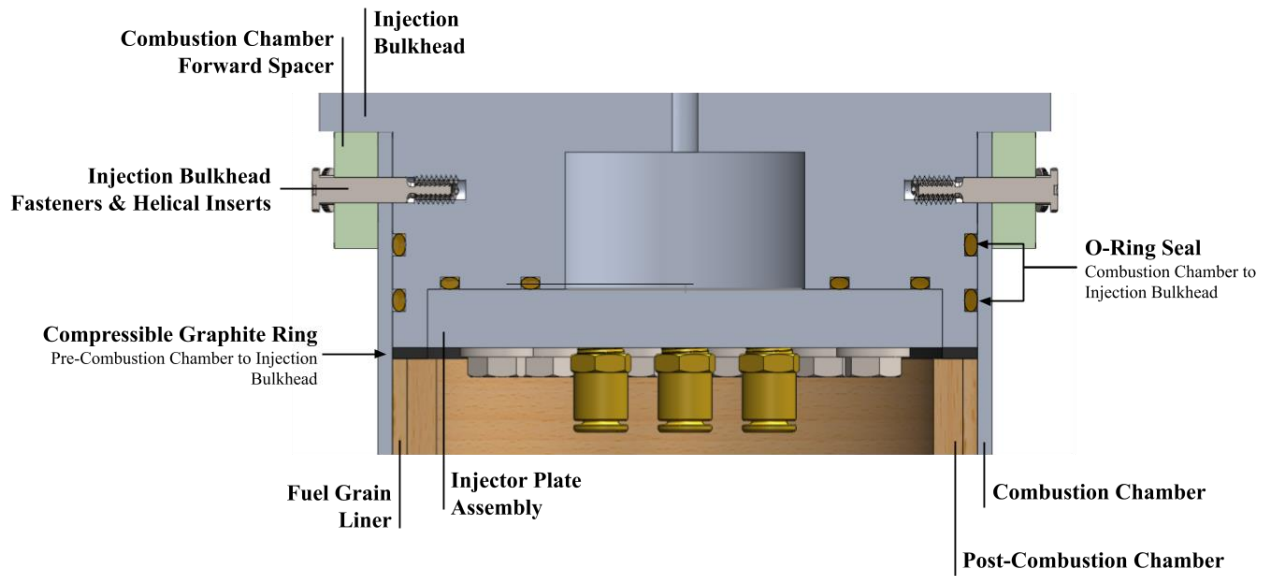


Figure 33. Integration of Injection Assembly and Thrust Chamber Assembly

A. Combustion Chamber Assembly

The Combustion Chamber Assembly consists of the Combustion Chamber, which is supported within the airframe by two spacers and surrounds a phenolic Fuel Grain Liner. The Fuel Grain Liner encloses the HTPB Fuel Grain and the Pre- and Post-Combustion Chambers. All images in the Combustion Chamber assembly sections (Section V.A.1 through V.A.5) show the components as they will be tested in the first hot fire.



Figure 34. Combustion Chamber Assembly, aftside facing to the left (cross-section view)

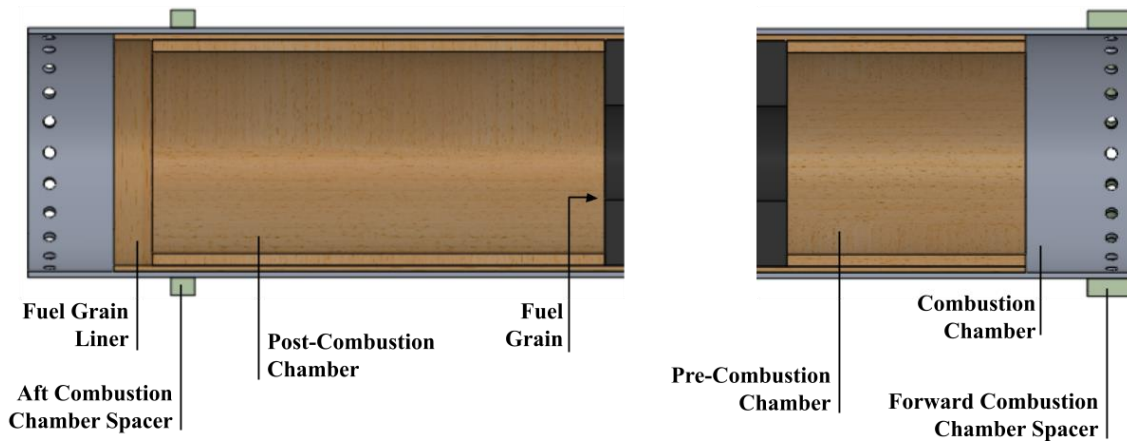


Figure 35. Combustion chamber assembly, aftside on the left (cross-section view, labeled)

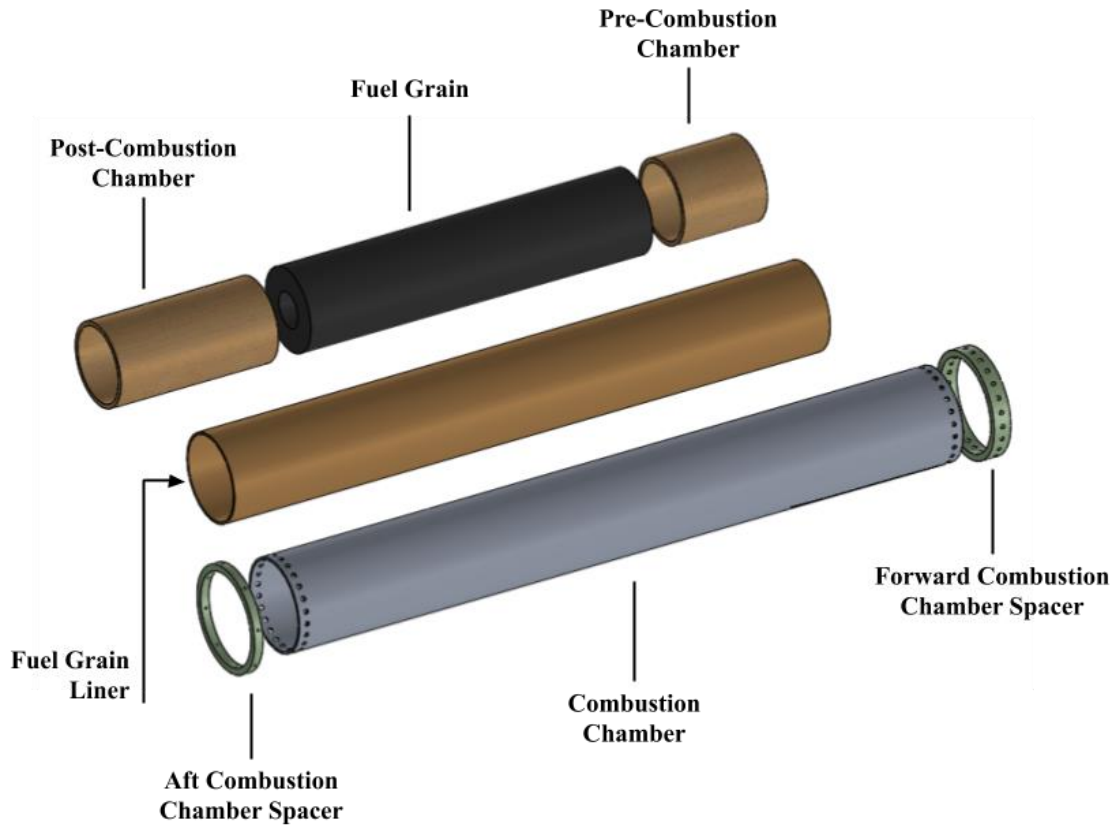


Figure 36. Combustion Chamber Assembly (exploded view)

1. Fuel Grain

The Fuel Grain contains the entirety of the engine’s solid propellant. As discussed in *Section II.A*, its composition is 83% HTPB, 17% curative, and 3% of its combined mass of carbon black. It is housed inside the phenolic liner for thermal protection and between the Pre- and Post-Combustion Chamber for optimal combustion.

Table 12. Fuel Grain Parameters	
Geometry	Circular with Uniform Cross-Section
Outer Diameter	4.75 in
Initial Port Radius	1.1352 in
Final Port Radius	2 in
Mass at Start of Burn	11.24 lb
Mass of Fuel Burned	7.00 lb
Average Fuel Mass Flow Rate ($\dot{m}_{f,avg}$)	0.9140 lb/s
Fuel Grain Length	22.5391 in

Average Fuel Grain Regression Rate	0.1129 in/s
---	-------------

The Fuel Grain parameters are almost entirely dependent on its regression over the 7.67 second burn. The outer diameter of the Fuel Grain has to be the same as the inner diameter of the phenolic liner at 4.75 in, as it is cast inside of the liner (for more information about this component see *Section V.A.4*), but the length and initial port radius of the Fuel Grain are determined from the regression rate. The relatively lengthy process of characterizing the theoretical burn of the engine is detailed below.

1.1 Grain Geometry

Before in-depth regression and thermal penetration analysis could be started, the geometry of the Fuel Grain needed to be selected as a reference when running calculations. There are two relevant geometries that impact the performance of the grains burn: cross section geometry and side section geometry.

The cross section geometry -- the geometry seen when looking at the Fuel Grain port from fore to aft -- was chosen to be a simple circle. The cylindrical port shape was chosen because it enables relatively efficient combustion¹⁴ without introducing the safety concerns associated with more complex geometries such as star shaped or wagon wheel (see Figure 37 below.) These alternative Fuel Grain geometries have been shown to slightly improve performance, but due to their spokes can more easily have chunks of unburned fuel break off, which can become lodged in the nozzle.

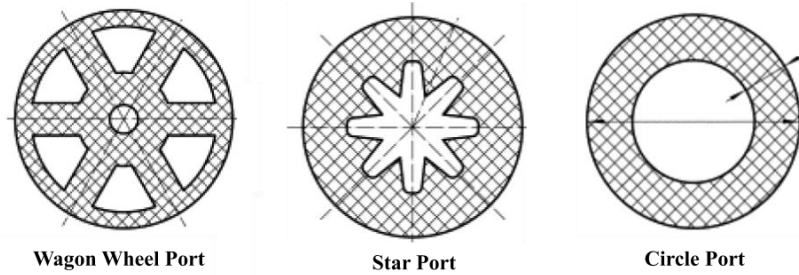


Figure 37. “Wagon Wheel”, “Star”, and “Circle” Fuel Grain Cross Sectional Geometry¹⁵

The side section geometry was also chosen to a simple, uniform cylinder. This is seen in the port diameter being constant all the way through the grain. The cylindrical shape was chosen because it is easy to pour and cast, and therefore eliminates safety or performance issues that can arise from a Fuel Grain that is not cured in its proper shape, such as cracking, bulging, or deformation. Eclipse’s 50 lb thrust test engine, Luna, implements a “dog bone” geometry along its length, which utilizes a circular cross section whose radius changes over the Fuel Grain length. Specifically, the “dog bone” geometry had a smaller port radius in the center of the Fuel Grain compared to either end, as this is where the regression rate was found to be the highest. However, pouring a dog bone Fuel Grain at the scale of Titan II is far more difficult than for Luna, and a cylindrical geometry is far easier to manufacture. Additionally, a simple cylinder minimizes additional safety concerns a more complicated dog bone geometry introduces, such as exposing the phenolic at areas where the thickness of the Fuel Grain is lower. More complex cross and side section geometries will be explored by the team in the future.

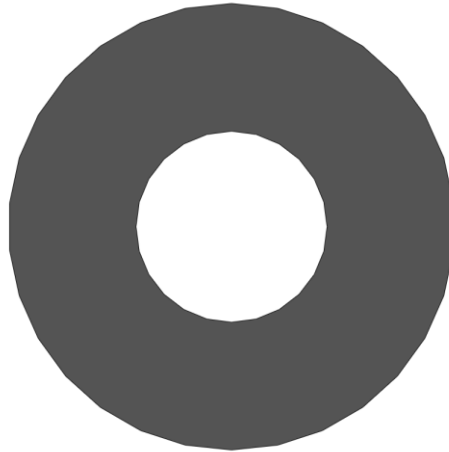


Figure 38. Fuel grain (Head-on view)

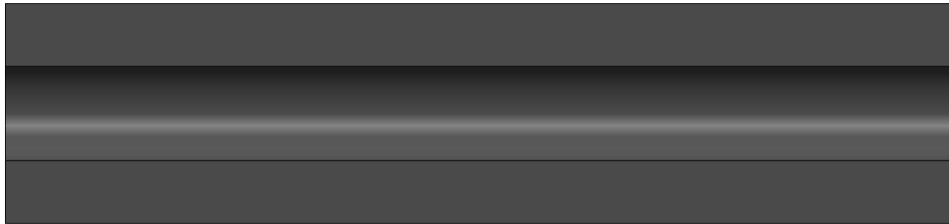


Figure 39. Fuel grain (side section view)

1.2 Fuel Regression Characterization

The team explored several ways to attempt to characterize the Fuel Grain regression rate as accurately as possible based on the composition of the fuel mixture, but were not able to find comparable data that could be affirmed as a valid representation of the team's Fuel Grain performance. Much of the literature on HTPB-fuel engines discuss engines that utilize a fuel with different chemical compositions than that of Eclipse's (and therefore burn and perform differently) or utilize a different oxidizer. Until the engine is built and regression rate data is taken from a hot fire, there is no way for the team to have confidence in a model for the regression rate. Instead, the team decided to characterize the regression of the team's 50 lb thrust hybrid rocket engine, Luna, and use the results to design Titan II's Fuel Grain. The regression equation of a hybrid rocket scales relatively well as long as the fuel and oxidizer combination is the same and changes in engine parameters are limited. Luna uses the same HTPB for fuel and nitrous oxide for oxidizer as Titan II and operates at the same chamber pressure of 500 psi, ensuring that data found from Luna can be applied to Titan II more accurately than data obtained from external sources.

A general equation for the regression rate of a hybrid rocket engine is given by,

Where: $\frac{dr}{dt}$ = the regression rate as a function of time (in/s)
 m'_{ox} = the mass flow rate of oxidizer (lb/s)
 A = the area of the port (in²)
 a = an experimentally determined constant
 n = an experimentally determined constant

$$\frac{dr}{dt} = a \left(\frac{m'_{ox}}{A} \right)^n$$

In order to determine Luna's regression characteristics, the team collected experimental data on the initial and final Fuel Grain radius, mass flow rate of oxidizer, and burn time from multiple Luna tests. This data was inputted into a MATLAB script which used exponential regression to find an accurate equation for the Fuel Grain regression

rate as a function of time. These computations can be found in the MATLAB script titled “Titan_II_Regression” in *Appendix X*. They resulted in $a = 0.1605$ and $n = 0.8288$.

Since the regression of a hybrid rocket scales well, the same a and n values from Luna’s regression rate formula can be used to characterize the regression of Titan II’s Fuel Grain, and appropriate values for the average internal port area and mass flow rate of oxidizer can be substituted. Knowing the average mass flow rate of oxidizer, 5.132 lb/s, the differential equation can be solved to give the Titan II Fuel Grain radius as a function of time,

Where: m'_{ox} = the mass flow rate of oxidizer (lb/s)

$r(t)$ = the radius of the Fuel Grain port (in) as a function of time (s)

r_0 = the initial port radius (in)

a = an experimentally determined constant (taken from Luna analysis)

n = an experimentally determined constant (taken from Luna analysis)

t = time (seconds)

$$r(t) = \left[(2n + 1) \cdot t \cdot a \cdot \left(\frac{m'_{ox}}{\pi} \right)^n + r_0^{2n+1} \right]^{\frac{1}{2n+1}}$$

HTPB is an excellent insulator, and leaving a small amount of fuel at the end of the burn ensures that there is an additional additional layer to prevent the Combustion Chamber from heating up a significant amount and weakening. The team decided to make the Fuel Grain thickness 0.375 in at the end of the burn, which equates to a final port radius of exactly 2 in. This final radius and the regression model can be used to work backwards and calculate the initial Fuel Grain radius, which is computed in *Appendix VIII, Calculation C.1.1*.

As the result of these calculations, the initial radius was established to be 1.1352 in, which corresponds to an average regression rate of 0.1129 in/s. This initial radius is perfect because it is safely larger than the nozzle throat radius, minimizing the chance of a piece of HTPB breaking off and clogging the nozzle throat. Since the Fuel Grain regression rate decreases as port area increases, the fact that the initial radius is not overly large leads to the desirable result of having a high regression rate which allows the Fuel Grain to be shortened. Plotting the port radius as a function of time results in the following graph:

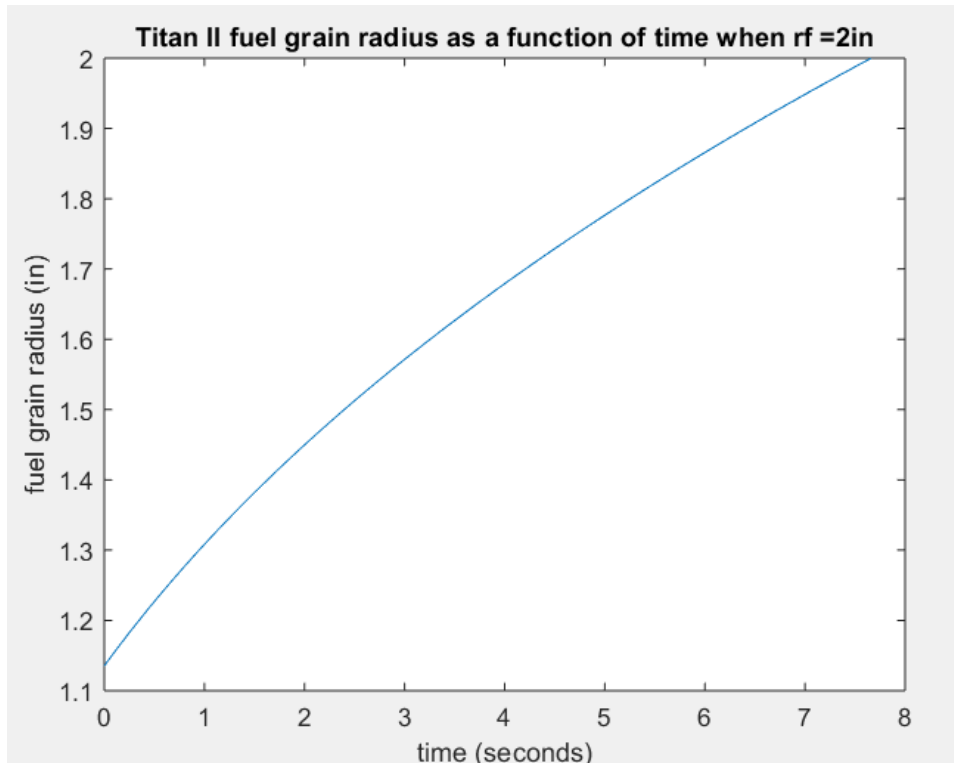


Figure 40. Titan II Fuel Grain Regression Plot

As stated in the Engine Performance Requirements section, the optimal average fuel mass flow rate is 0.9140 lbm/s. The Fuel Grain length that gives the optimal mass flow rate of fuel was determined via calculations in *Appendix VIII, Calculation C.1.2*. The optimal length was found to be 22.5391 in. The Fuel Grain is cast in a mold that has to be machined, so for the sake of machinability the length was rounded to 22.54 in.

The differences between the Luna and Titan II engines must be noted, however, such as the fact that Luna was designed to produce only 50 lbf of thrust. These differences are likely to produce different regression rates. Because of this, the team will conduct a number of rigorous test fires throughout the 2020-2021 school year to characterize the regression rate of the Titan II Fuel Grain with as many data points as possible. The engine will be tested through a series of 4-second and 6-second test fires and is currently designed with a final port radius of 2.0 in, which corresponds to a 0.375 in thick wall at the end of a full 7.67 second burn. This is to mitigate the risk of the fuel's regression rate being larger than anticipated, which could lead to damage to the Combustion Chamber Assembly if all of the fuel is consumed and the Fuel Grain Liner is exposed to direct combustion for an extended period of time. The team plans to use the characterization of the regression rate to perform design changes to the Fuel Grain's dimensions, in order to best optimize the performance of the engine.

1.3 Thermal Protection and Properties

The Fuel Grain also provides substantial thermal protection for the Combustion Chamber walls during combustion. Using a calculation given in *Appendix VIII, Calculation C.1.3*, the characteristic penetration distance was found to be 0.002 in, an extremely small penetration distance. The chosen final Fuel Grain thickness is 0.375 in, which is more than enough to protect the chamber from conduction of combustion heat over the full burn. This final thickness will be reduced when the grain is resized to decrease the fuel margin, but the 0.375 in margin will ensure that the final thickness will be on the order of tenths of an inch, rather than thousandths. Through testing and optimizing the fuel, the team will ensure that the chamber is fully thermally protected while maximizing the utility of the Fuel Grain.

1.4 Grain Manufacture and Pre-Test Manual Inspection

To pour a Fuel Grain, the HTPB and carbon black are initially mixed together to an even consistency, then left under vacuum for at least 24 hours to remove air bubbles. The curative is then added and mixed in quickly to minimize the amount of air reintroduced, and the fuel is then poured into the mold. The mold is created from a combination of 3D printed and machined parts, and is designed to let the HTPB cure inside of its phenolic liner. The pot life (amount of time that the fuel remains liquid enough to pour after the addition of the curative) is approximately 35 minutes, though the fuel requires at least five days to cure completely. Before the engine's first hot fire, test pours will be made to help the team decide how long the grain needs to cure. Once the fuel has been poured, the mold is left undisturbed for a week to cure, after which the Fuel Grain is removed from the mold and is ready to use.

Pouring of the Fuel Grain for the hot fire is preceded by a "schedule" test -- pouring samples of the fuel grain into small containers for quick curing. Once poured in a small cylindrical mold, the quality of the Fuel Grain will be inspected via a manual stiffness test to quantify if it is hard enough and will be carefully assessed for the amount of bubbles. Bubbles pose a significant safety hazard since the pieces of fuel around them are likely to break off and clog the nozzle, resulting in catastrophic failure. After it has been certified that the characteristics of the Fuel Grain appear as nominal, the grain will be ready to be used in an engine hot fire.

2. Combustion Chamber

The engine's Combustion Chamber contains the combustion reaction that generates the exhaust gas used to produce thrust. The chamber is fastened to the Injection Bulkhead on the forward end. The shoulder screws that fasten the Combustion Chamber and Injection Bulkhead together will also go through the airframe. This single attachment point to the airframe will allow the Combustion Chamber to safely thermally expand without causing damage to the airframe in the process. The Combustion Chamber houses the Fuel Grain Liner and Fuel Grain Assembly, as well as Pre- and Post-Combustion Chamber phenolic tubes. On the aft end, the Nozzle Assembly attaches to the engine via the Nozzle Casing fastened through the Combustion Chamber. In addition, two fiberglass spacers hold the Combustion Chamber to the airframe with the forward spacer fastened to the Injection Bulkhead as well. These spacers are discussed in more depth in *Section V.A.5*. The images below show the Combustion Chamber as it will be fired in the first hot fire.

Table 13. Combustion Chamber Parameters

Material	Aluminum 6061-T6
Combustion Chamber OD	5.25 in
Combustion Chamber Thickness	0.125 in
Combustion Chamber Initial Mass	8.05 lb
Initial Combustion Chamber Length	41.2 in
Optimal Combustion Chamber Length	34.2 in

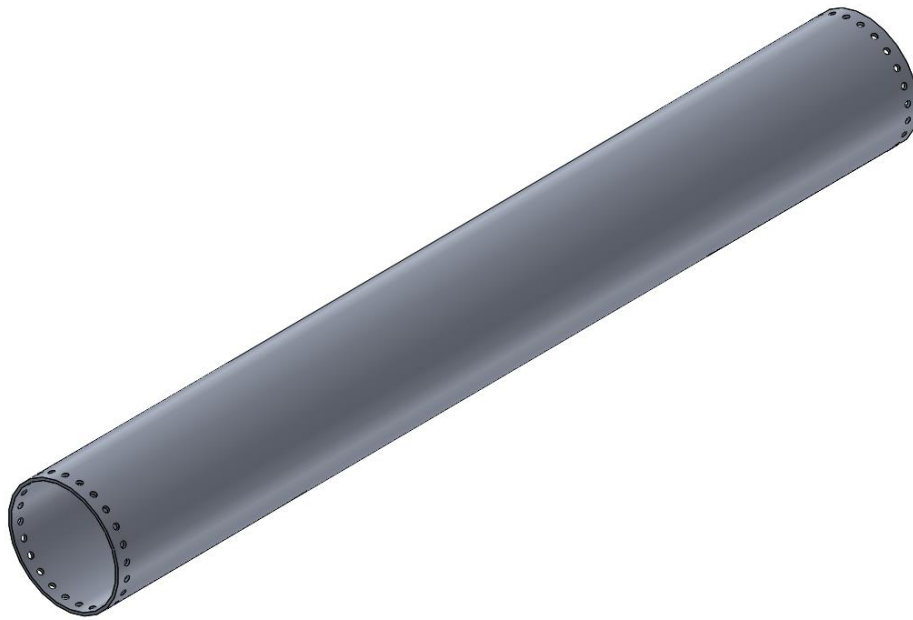


Figure 41. Combustion chamber isometric view

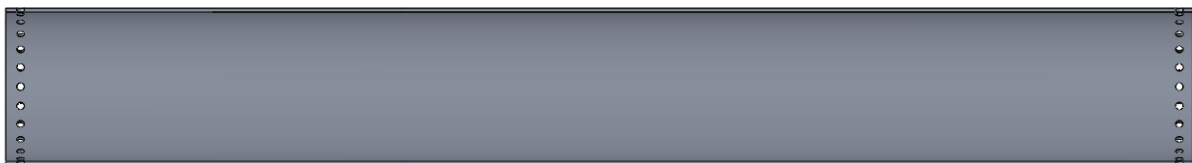


Figure 42. Combustion chamber (side section view)

The Combustion Chamber for the Titan II engine is constructed out of a machined drawn-over-mandrel 6061-T6 aluminum tube. 6061-T6 aluminum was selected for the chamber because of its relatively high strength-to-weight ratio, low cost, and its favorable fracture mechanics versus materials like steel. Steels are in general more brittle than aluminum alloys, and have a less favorable impact toughness. If the combustion chamber was subject to a short, high intensity load due to its internal pressure distribution, a steel chamber would be more likely to fracture or shatter while an aluminum chamber would be more likely to simply unzip.¹⁶ Unzipping is a far safer failure mode compared to fracturing, so the team decided aluminum would be the safer material. 7075 aluminum was considered for the chamber because of its higher strength, but 6061 aluminum's strength was found to be sufficient for the expected loads while

being significantly less expensive and easier to procure. The tube, purchased at a size of 5.25 in outer diameter by 5 in inner diameter and 4 ft long, is cut and faced down to the final 39.67 in length. The Chamber has 24 radial 0.25 in holes whose centers are located 0.5 in from the forward face which hold the fasteners that thread into the Injection Bulkhead, as well as 24 radial 0.25 in holes whose centers are located 0.45 in from the aft face which hold the fasteners that thread into the Nozzle Casing. Tearout stress calculations for the fastener holes can be found in *Appendix VIII, Calculation C.2.3*.

The Combustion Chamber must be able to contain the expected 500 psi chamber pressure generated during a burn while simultaneously fastening to the Injection Bulkhead and restraining the Nozzle Casing. The Combustion Chamber must also be insulated from the expected 5627°F combustion temperature. The chamber wall thickness and outer diameter were selected by examining the pressure-induced hoop stress on the chamber as well as the pressure-induced bearing stress experienced in the fastener holes. The number and diameter of the fastener holes on either end of the Combustion Chamber were also selected by examining the pressure-induced bearing stress. The hoop stress analysis calculation and the bearing stress calculation are computed in *Appendix VIII, Calculation C.2.1* and *C.2.2* respectively. The factor of safety due to hoop stress is 3.33 and the factor of safety due to bearing stress is 2.60.

The Combustion Chamber wall could be made thinner and still withstand the pressure-induced hoop stress, however 0.125 in was chosen as the desired wall thickness as it is readily available for purchase and would not require extra machining. Additionally, decreasing the Combustion Chamber wall thickness would increase the bearing stress on the wall through the fastener holes on either end. The high factor of safety for hoop stress also leaves room to increase the inner diameter of the Combustion Chamber to 5.75 in such that the outer diameter of the Combustion Chamber is flush with the inner diameter of the airframe at 6 in. However, this was avoided because increasing the diameter also increases the bearing stress, which had a far lower factor of safety than for hoop stress. Since the fastener hole configuration is the same on either side of the Combustion Chamber (24 equally spaced 0.25 in holes), the bearing stress will be the same on either end.

The bearing stress factor of safety does not leave as much room for change as the hoop stress factor of safety. If the outer diameter of the Combustion Chamber were kept at 6 in (the inner diameter of the airframe), the factor of safety would be lower than the team's objective of 2.0. The team recognizes that having 24 fasteners in a single ring is not common, but this was found to be the best option that resulted in a safety factor larger than 2.0. A chamber with a 0.25 in wall thickness was considered, but the extra mass added would ensure that the rocket that contained the Titan II engine would not reach 30,000 ft, which was the original goal of the engine. A wall thickness between 1/8 in and 0.25 in was considered, but would not be able to be purchased directly and the added machining costs make this solution less than optimal. Switching from 24 x 0.25 in fasteners to 12 x 0.5 in fasteners would result in the same factor of safety in regards to the bearing stress calculations, but the larger fasteners would not integrate well with the thin walls of the Injection Bulkhead and Nozzle Casing.

The team also performed a static study in SolidWorks Simulation to check for any significant areas of increased stress in the chamber wall due to the bolt hole stress concentration or any interaction between the bearing and hoop stresses. These simulations are detailed in *Appendix IX, Simulation C.1* and the results are given in the figures below. The maximum stress on the inner wall of the Combustion Chamber is below 17,500 psi (half of the yield strength), which results in a factor of safety that is above 2. A stress concentration up to 27,000 psi exists on a small area above and below both the forward fastener holes and aft fastener holes. Figures 44 and 45 show the stresses that exceed 17,500 psi from the study on these holes. However, because this is a bearing load case, these stress concentrations will be relieved by localized micro-yielding in the material. Since these FEA simulations do not take this plastic model into account, hand calculations are the most reliable method so the team is acceptable with this safety factor that is lower than 2 from FEA results.^{16, 28} It is noteworthy that although these results depict a factor of safety lower than 2 around the fastener holes, the stress still does not reach the yield strength of 6061-T6 aluminum.



Figure 43. Combustion Chamber FEA Study Results

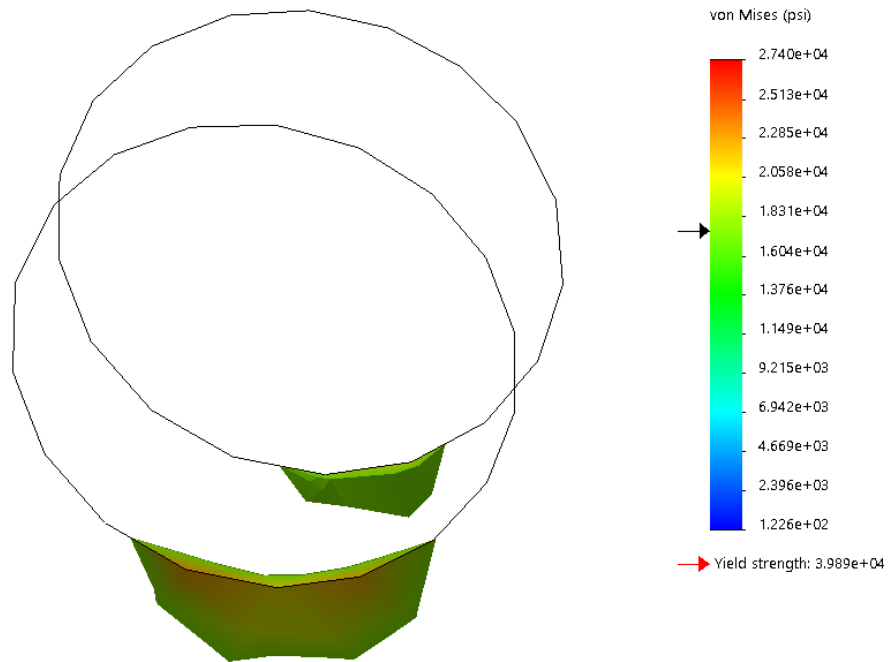


Figure 44. Forward Combustion Chamber Holes Stress Concentrations

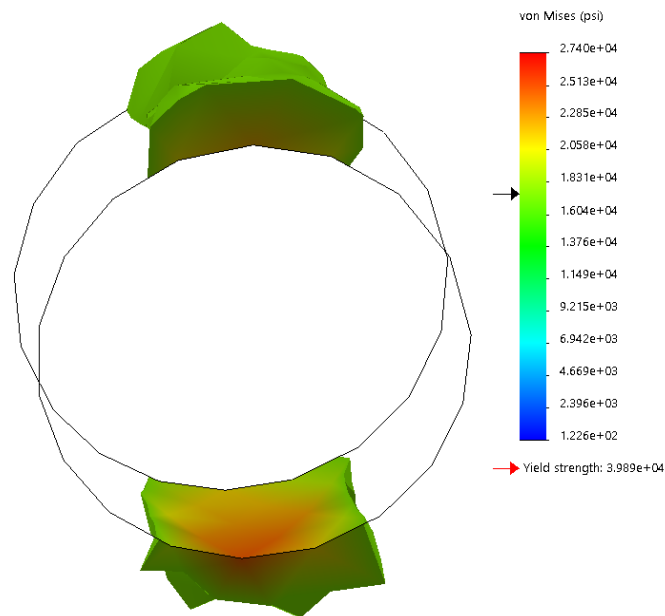


Figure 45. Aft Combustion Chamber Holes Stress Concentrations

Although the Fuel Grain is dimensioned to be 22.54 in, the Combustion Chamber is designed to be 7 in longer than needed in order to be able to contain a 29.54 in long Fuel Grain if necessary. This is because the team recognizes that using Luna data as a model for the Titan II Fuel Grain is not entirely accurate, and the length of the Fuel Grain may change as empirical data on the regression rate is gained after ground testing. The team does not have the resources to rebuild the Combustion Chamber if it is empirically determined that the fuel is too short and there is no extra room in the Combustion Chamber to lengthen the fuel. On the other hand, it is much more reasonable for the team to design the Combustion Chamber longer than necessary given the current data, cut the Combustion Chamber length after static testing, and remachine the fastener holes. The optimal Fuel Grain length will be determined after Titan II undergoes two static tests, and the difference between 29.54 in and the length of the experimentally determined optimal Fuel Grain will be the amount the team cuts down the Combustion Chamber length by. If the difference is determined to be less than 0.625 in, the team will not cut the Combustion Chamber as the fastener holes will not be able to be remachined. If the regression matches the team's current model, the optimal Combustion Chamber length is 34.2 in. Until the Combustion Chamber is shortened to its optimal length, the extra length within the Combustion Chamber will be compensated for by extending the lengths of the Pre- and Post-Combustion Chambers, as will be further discussed in *Section V.A.3*.

The Combustion Chamber must also have adequate thermal protection from the expected 5627°F combustion temperature, which is provided by the Fuel Grain, its phenolic liner, and the phenolic Pre- and Post-Combustion Chambers. The melting point of 6061-T6 aluminum is 1205°F, so any direct exposure of the Chamber wall to the combustion products will compromise the integrity of the Chamber. In addition, the yield strength of 6061-T6 aluminum drops dramatically with increasing temperature. The Combustion Chamber thermal expansion analysis in the Injection Bulkhead section of this document (*Section IV.B.1*) identifies the critical chamber wall temperature as 460.2°F (237.9°C) based on the hoop stress and decreased yield strength. If the chamber wall becomes any hotter, it will yield. Therefore, beyond direct exposure to exhaust gas, the chamber's thermal protection must insulate the aluminum wall from any conductive heat transfer to keep the wall temperature below 460.2°F. This insulation is provided by the phenolic Pre- and Post-Combustion Chambers and Fuel Grain Liner, as well as the Fuel Grain itself. *Sections V.A.3, V.A.4, and V.A.1*, respectively, discuss these components and their thermal protection capabilities.

3. Pre- and Post-Combustion Chambers

3.1 Pre-Combustion Chamber

The Pre-Combustion Chamber is a phenolic component on the forward end of the Combustion Chamber whose aft face is flush with the forward face of the Fuel Grain. It provides the injected oxidizer enough residence time in the chamber to fully vaporize before combusting with the Fuel Grain, improving the efficiency of the combustion reaction.

Table 14. Pre/Post-Combustion Chambers Parameters	
Material	Linen Cloth and Phenolic Resin Composite
Pre- / Post-Combustion Chamber OD	4.75 in
Pre- / Post-Combustion Chamber Thickness	0.25 in
Initial Pre-Combustion Chamber Length	5.0 in
Optimal Pre-Combustion Chamber Length	2.5 in
Initial Post-Combustion Chamber Length	9.5 in
Optimal Post-Combustion Chamber Length	5.0 in

Most hybrid engines use a Pre-Combustion Chamber with a length-to-diameter ratio of 0.5 to achieve the required oxidizer residence time, where the length is the Pre-Combustion Chamber length and the diameter is the inner diameter of the Combustion Chamber.¹⁷ For the 5.0 in inner diameter Combustion Chamber used on this engine, this results in a Pre-Combustion Chamber length of 2.5 in. However, until the Combustion Chamber is shortened when the team is confident about a Fuel Grain length, the additional length is accounted for by extending the Pre- and Post-Combustion Chambers. As standards typically set the Post-Combustion Chamber to be twice as long as the Pre-Combustion Chamber¹⁷, roughly 1/3 of the extra 7 in will be contained by the Pre-Combustion Chamber. The team wanted to make the Pre-Combustion Chamber with an easily manufacturable length that is near this value, which was decided to be 5.0 in.

With the length selected, the Pre-Combustion Chamber section of the Combustion Chamber must also be protected from the hot combustion gases. To add thermal protection beyond the Fuel Grain Liner, a 5.00 in long, 0.25 in thick tube of the same linen phenolic material as the Fuel Grain Liner is attached inside the liner using a foaming polyurethane glue like Gorilla Polyurethane Glue or Elmer’s Glue All-Max. This same type of adhesive is used in assembly of COTS solid propellant motors to adhere grains to an outer liner.¹⁸ The adhesive will hold the Pre- and Post-Combustion Chamber liners in place to prevent them from moving axially along the chamber in case the Fuel Grain burns away fully. This linen phenolic is a composite material made of layers of woven linen cloth impregnated with phenolic resin, which is then heated and cured to make a solid material. A survey of different hybrid rocket engine designs from other research groups showed that this material is a common choice for an ablative Combustion Chamber thermal protection system.¹⁹ Experiments performed by other hybrid rocketry groups shows that a minimum phenolic wall thickness of 0.215 in is required to ensure that burning and ablation of the phenolic interior wall doesn’t compromise the liner outer wall.¹⁹ Rounding up to the nearest standard purchasable size, the Pre-Combustion Chamber liner wall thickness was set to 0.25 in. The Fuel Grain Liner surrounding the Pre-Combustion Chamber liner also provides a 0.125 in thick layer of thermal protection, but this liner is considered a last-resort protection system, and due to potential uncertainty and variation in the burning and ablation behavior of the phenolic, the critical 0.215 in wall thickness was applied to just the Pre-Combustion Chamber liner itself to add extra protection with minimal mass increase.

In addition, a compressible graphite ring will be situated between the Pre-Combustion Chamber and the Injection Bulkhead. At an original thickness of 1/8 in, the compressible graphite will be compressed by 0.025 in, to a final thickness of 0.1 in. Although the graphite has a maximum compression of 35%, this graphite is only compressed by 25% in order to avoid error in this domain. The compressible graphite will aid with tolerancing any unevenness in the cross-sectional surface of the Pre-Combustion Chamber.

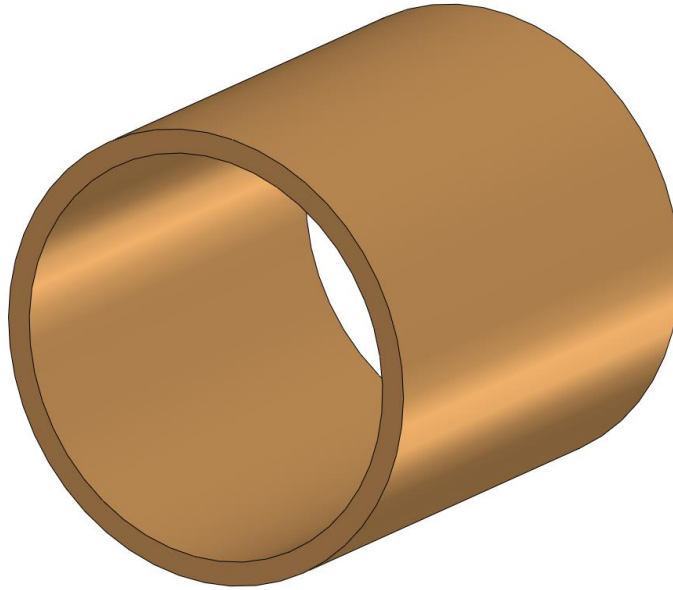


Figure 46. Pre-Combustion Chamber liner

3.2 Post-Combustion Chamber

The Post-Combustion Chamber is the section of the Combustion Chamber between the end of the Fuel Grain and the start of the converging section of the nozzle. It allows the propellants to sufficiently mix and fully combust before exiting the engine through the nozzle. Allowing the fuel and oxidizer to complete their combustion before leaving the Combustion Chamber increases the engine's efficiency. Eclipse currently does not have a high-fidelity combustion model for its hybrid engines, so the exact propellant residence time required after the Fuel Grain to complete all combustion is not known, but a common hybrid engine design criterion is to have a Post-Combustion Chamber with a length-to-diameter ratio of 1.0 with respect to the chamber inner diameter.¹⁷ This results in a 5.0 in long Post-Combustion Chamber for this engine. However, until the Combustion Chamber is shortened, the Post-Combustion Chamber must account for the rest of the 7 in extension. Since 2.5 in were added to the Pre-Combustion Chamber, 4.5 in must be added to the Post-Combustion Chamber. This brings the length of the Post-Combustion Chamber to be 9.5 in for the initial hot fire. While shortening the Pre- and Post-Combustion Chambers would significantly hinder engine performance, there is little evidence to show that extending them will make a large negative impact. Experimental data taken from a University of Washington hybrid engine shows that the thrust with an optimal Post-Combustion Chamber is similar to the thrust when the Post-Combustion Chamber's length was extended by more than 100%.¹⁹ When the optimal length of the Fuel Grain is found and the Combustion Chamber is shortened accordingly, the lengths of the Pre- and Post-Combustion Chambers will also be shortened to their optimal lengths of 2.5 in and 5.0 in, respectively. Like the Pre-Combustion Chamber, the Post-Combustion Chamber requires an additional phenolic liner to protect the chamber wall from the heat of the combustion gases in the absence of an insulating Fuel Grain. By the same design rationale given for the Pre-Combustion Chamber using experiments conducted by other hybrid rocketry groups, the phenolic liner wall thickness was set to be 0.25 in to provide sufficient thermal protection against the exhaust gases.

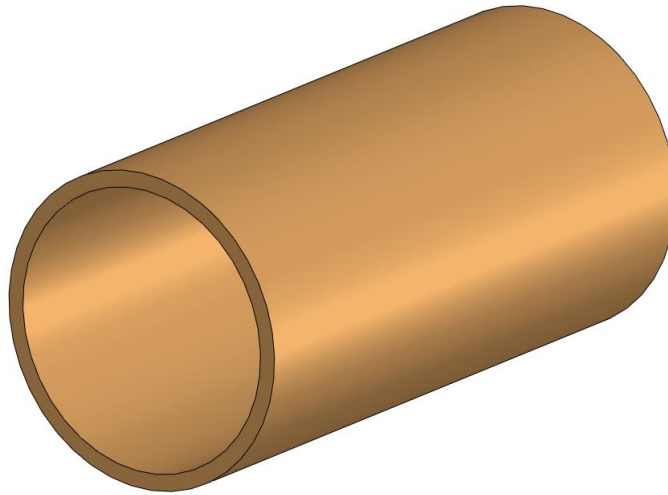


Figure 47. Post-Combustion Chamber liner

4. Fuel Grain Liner

The Fuel Grain Liner, as mentioned in previous sections, is a cylindrical layer of thermal protection for the Combustion Chamber, laying between the aluminum body of the Combustion Chamber and the inner components (Fuel Grain, Pre-Combustion Chamber, and Post-Combustion Chamber). As such, its outer diameter is the same as the inner diameter of the Combustion Chamber at 5.0 in. The liner is designed to provide a 0.125 in thick layer of linen phenolic material, and is meant to act as a risk-mitigation mechanism in the case that the regression rate of the Fuel Grain is much larger than anticipated, and the combustion burns through all of the Fuel Grain or through the linen phenolic Pre- and Post-Combustion Chambers. Additionally, the Fuel Grain Liner provides a convenient way for the Fuel Grain to be poured, cast, and assembled with the engine.

Table 15. Fuel Grain Liner Parameters	
Material	Linen Cloth and Phenolic Resin Composite
Fuel Grain Liner OD	5.0 in
Fuel Grain Liner Thickness	0.125 in
Initial Fuel Grain Liner Length	37.8 in
Optimal Fuel Grain Liner Length	30.8 in

As explained in the Pre- and Post-Combustion Chamber section (*Section V.A.3*), the linen phenolic composite is a combination of multiple layers of woven linen cloth and phenolic resin, which is heated and cured to solidify. The team had also considered using fiberglass instead of this phenolic as the Fuel Grain liner material, since the team has successfully used it as thermal protection in the Titan I engine, but high cost led the team to consider replacements. The team began to conduct research on linen phenolic after reading about the successful use of it as a Fuel Grain liner by the University of Washington in the 2018 Spaceport America Cup¹⁹ and noting that the thermal testing conducted by this team produced favorable results that translated directly to Rice Eclipse’s thermal performance needs. The company Accurate Plastics was found to be a large supplier of composite materials, including both linen phenolic and fiberglass, so price figures could easily be compared. From the site’s prices, it was determined that the linen phenolic is significantly cheaper. Because of its low cost and acceptable thermal properties, Accurate Plastics’ linen phenolic was chosen as the material for the Fuel Grain Liner, as well as for the Pre- and Post-Combustion Chambers.

This liner will extend to encompass the lengths of the Pre-Combustion Chamber, Fuel Grain, and Post-Combustion Chamber. It is flush with the Pre-Combustion Chamber, but must extend 0.81 in past the Post-Combustion Chamber in order to integrate with the nozzle assembly (see Figure 53 in *Section V.B* for more detail on this integration) . As previously discussed, the Pre- and Post-Combustion Chambers will be lengthened for the first hot fire to account for the fact that the Fuel Grain regression may be different from the Luna models. As the liner encompasses these components, it too will have an initial length ready for the first hot fire that is longer than the optimal length given the current regression data. This results in an initial length of 37.8 in and an optimal length of 30.8 in. The chosen wall thickness for this liner is 0.125 in., which will fully fill the gap between the outer diameter of the interior components and the inner diameter of the Combustion Chamber.

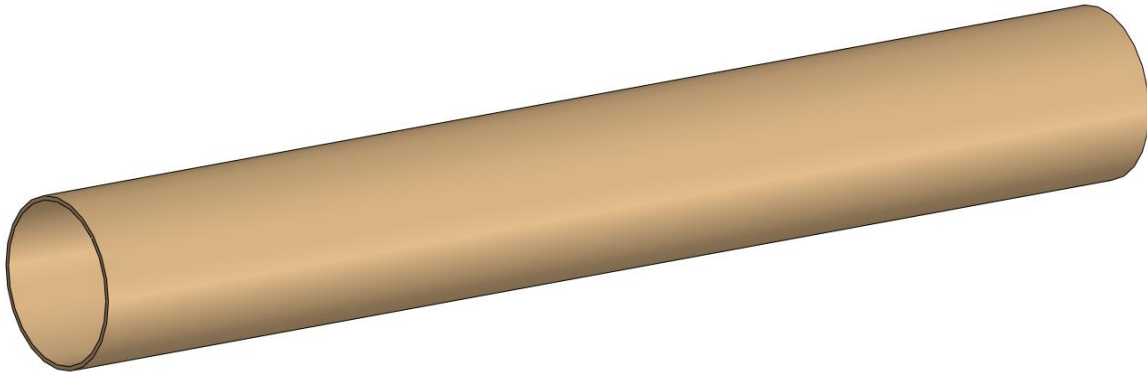


Figure 48. Fuel Grain Liner



Figure 49. Fuel Grain Liner (side section view)

5. Combustion Chamber Spacers

The Combustion Chamber spacers are two fiberglass rings that attach to the airframe and provide support for the Combustion Chamber. The spacers are required since the Combustion Chamber outer diameter of 5.25 in is less than the 6 in inner diameter of the airframe, and they help secure the Combustion Chamber to the airframe as well as prevent it from vibrating within the airframe. Additionally, these spacers are far easier to machine than the Combustion Chamber and will allow the team to avoid problems with the tolerances of the Combustion Chamber as it is purchased. Fiberglass was chosen because although its structural properties are poor compared to other typically used materials such as aluminum or steel, the spacers themselves will not be taking any substantial loads, and fiberglass is far lighter than these alternative options. The Forward Combustion Chamber Spacer is secured to both the airframe and the Combustion Chamber with the same fasteners that secure the Combustion Chamber to the Injection Bulkhead. More information about these fasteners is given in *Section IV.D.2.1*. As such, it contains the same 24 radial 0.25 in fastener holes on its midline as the Combustion Chamber. In order to leave sufficient room on either side of each bolt hole while minimizing weight, its height was determined to be 1 in. Since the forward spacer connects the Combustion Chamber to the airframe, its thickness is 0.375 in.

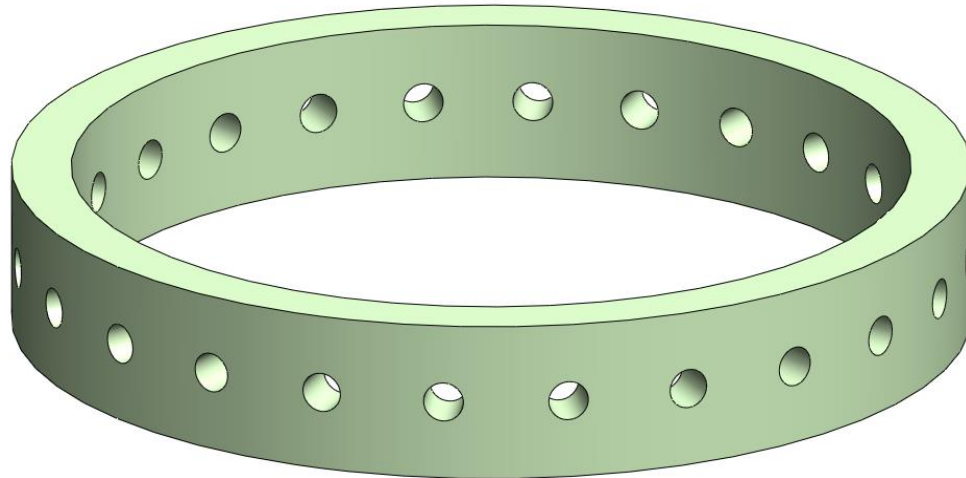


Figure 50. Forward Combustion Chamber Spacer

In order to allow the Combustion Chamber to thermally expand and contract in the vertical direction, the Aft Combustion Chamber Spacer will be fastened to the airframe but not the Combustion Chamber. By having an inner diameter of 5.25 in, the aft spacer will still prevent the Combustion Chamber from vibrating within the airframe but will not constrain its vertical position. The bottom spacer has 8 radial bolt holes on the midline which provide threads for 8-32 bolts that secure the spacer to the airframe. Stress will not pose problems for these bolts nor these bolt holes since the bottom spacer will not be experiencing high loads and does not have to fasten to the Combustion Chamber. In order to leave sufficient room on both sides of each bolt hole, the height of the bottom spacer was determined to be 0.5 in. Since the aft spacer spans the distance between the Combustion Chamber outer diameter and the airframe inner diameter, its thickness is 0.375 in.

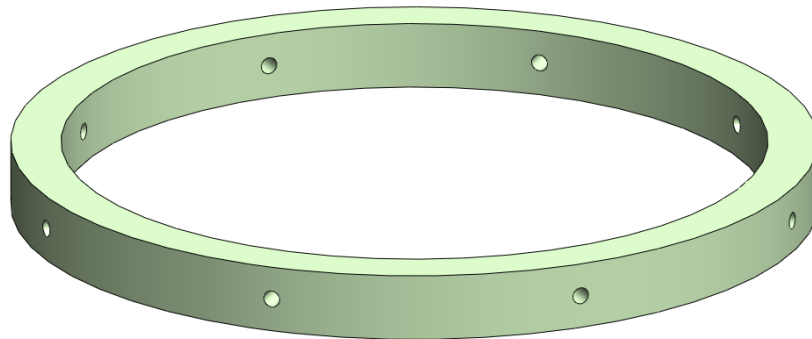


Figure 51. Aft Combustion Chamber Spacer

The Combustion Chamber spacers will not be built until after the engine is statically tested and is ready to be launched in a flight vehicle as they are not integral to the operation of the engine itself. In addition to providing support for the Combustion Chamber, the spacers are helpful for securing external airframe components such as fins and rail buttons. Because of this, the Rice Eclipse Aerodynamics team will optimize the design of the spacers to suit the layout of the rocket airframe that houses Titan II. The position of the forward spacer is fixed, but the exact position of the aft spacer does not need to be finalized by the Propulsion team before Titan II's flight vehicle is designed. Regardless of its final position, the Aft Combustion Chamber Spacer will not be attached to the Combustion Chamber in order to allow for thermal expansion.

B. Nozzle Assembly

The purpose of the Nozzle Assembly is to constrict the flow of the exhaust gases, accelerating them to supersonic velocities and improving the performance of the rocket. To accomplish this objective, a graphite Nozzle Insert has been designed to properly compress and expand the exhaust gases and take the majority of the thermal

loads. While it has incredible thermal properties, graphite has poor strength, so an exterior structure was designed to support the Nozzle Insert and connect the Nozzle Insert to the Combustion Chamber. Together, these two components create the Nozzle Assembly.

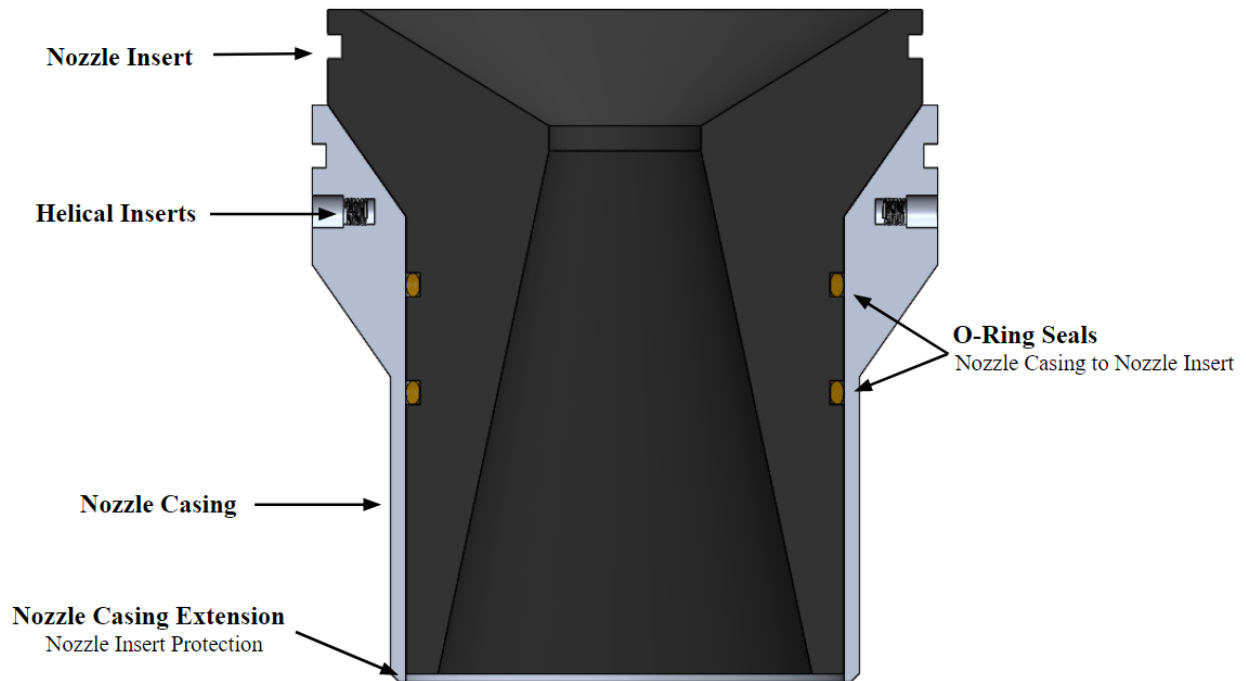


Figure 52. Nozzle Assembly (cross-section view)

Table 16. Design Specification of Nozzle Assembly	
Nozzle Insert Mass	3.10 lb
Nozzle Casing Mass	1.71 lb
Throat Radius	0.6075 in
Exhaust Gas Velocity at Throat	Mach 1
Diverging Angle	12 degrees
Exit Radius	1.494 in
Exhaust Gas Pressure at Exit	10.9 psi
Specific Heat Ratio	1.2524

The nozzle of a rocket is exposed to incredible thermal and structural loads as it bears the full force of the combustion gases while accelerating them to produce thrust. In industry, these problems are solved with a combination of exotic metal alloys, namely Inconel, and highly complex cooling channels which flow fuel as a coolant around the nozzle. While efficient, these solutions are both expensive and complex, which makes them unfeasible with the resources available during the design process of the Nozzle Assembly at the scale of an undergraduate team such as Rice Eclipse. Instead, the team chose to split the nozzle into two separate pieces to each handle different types of loads: a Nozzle Insert which will take the thermal loads and a Nozzle Casing which will take structural loads. With

this approach, the interior geometry of the Nozzle Insert must be designed to properly compress and expand the exhaust gasses while the exterior geometry of the Nozzle Casing must be designed to secure the assembly to the Combustion Chamber. Additionally, the design of the Nozzle Assembly must be such that the Nozzle Casing and Insert can interface with one another to create seals which prevent flow of exhaust gasses between the two components and between the wall of the Combustion Chamber and the Nozzle Assembly.

One of the primary design considerations was preventing gas flow between the Nozzle Casing, the Insert, and the wall of the Combustion Chamber. To address this problem, four O-rings grooves were designed and added, three of which are on the Nozzle Insert. As shown in Table 17 and Figure 53 below, the topmost O-Ring groove holds a size 2-246 seal between the phenolic of the Combustion Chamber liner and the Graphite Insert. The other two O-ring grooves of size 2-236 are redundant and interface with the Nozzle Casing. Finally, the Nozzle Casing has an O-ring groove of size 2-248 between the wall of the Combustion Chamber, which is intended to prevent hot combustion gases from reaching and causing the shoulder screws which secure the Nozzle Casing to fail. All of the Nozzle Assembly O-rings will be subject to hot combustion gases and will use Moly-Graph, a high temperature Molybdenum grease, as lubricant.

Table 17. Nozzle Assembly O-rings				
O-ring Set	Size Specifications		Material	Lubrication
Nozzle Casing to Combustion Chamber (Gland Seal)	OD 5.00 in	1 x No. 2-248	Silicone	Moly-Graph
Nozzle Insert to Fuel Grain Liner (Gland Seal)	OD 4.75 in	1 x No. 2-246	Silicone	Moly-Graph
Nozzle Casing to Nozzle Insert (Gland Seal)	OD 3.50	2 x No. 2-236	Silicone	Moly-Graph

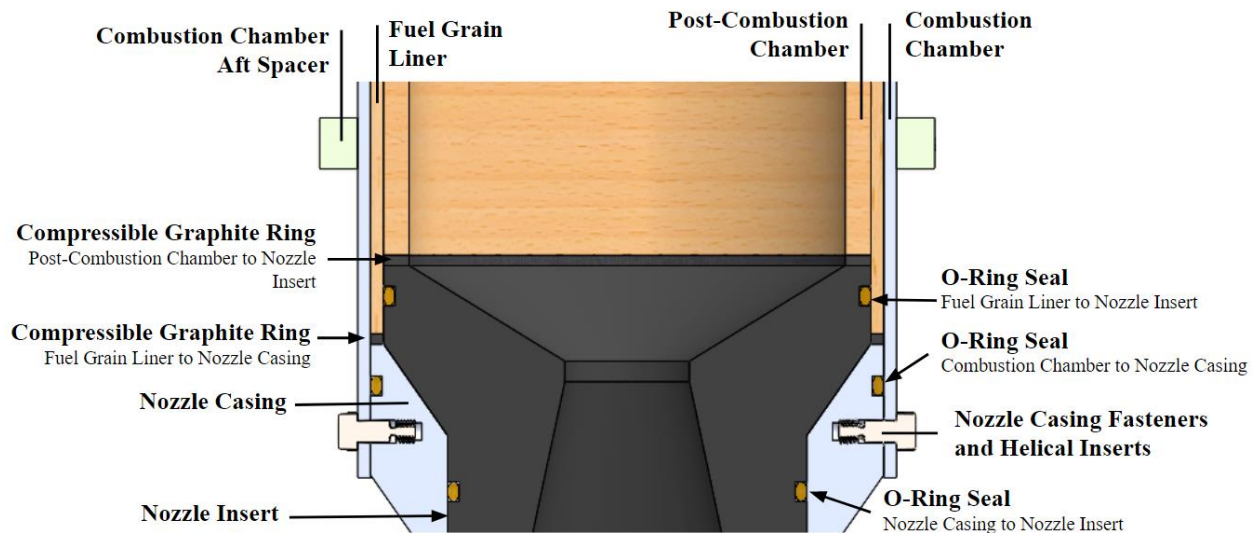


Figure 53. Nozzle Assembly and Combustion Chamber Assembly Integration (cross-section view)

1. Nozzle Insert

The Nozzle Insert is designed to properly compress and expand the exhaust gasses to maximize the thrust and efficiency of the motor. The exhaust gases will accelerate as they are compressed until they reach Mach 1. At this point, the gases will only accelerate further if they are allowed to expand. As such, the interior geometry of the Nozzle

Insert must have a Converging-Diverging structure with a constant diameter throat connecting the two regions. Using the calculations outlined below in *Appendix VIII, Calculation C.3.1*, the radius of the throat was determined to be 0.6075 in and the radius of the exit was determined to be 1.4943 in.

These dimensions ensure that the fluid will be traveling at Mach 1 at the throat and the pressure of the exhaust gas will be 10.9 psi. Spaceport America is located 4,595 ft above sea level, and depending on the final efficiency of the engine (somewhere between 70% at the lowest and 100% at the greatest), engine burnout will occur between 4,750 and 7,000 ft above the launchpad, before coasting the rest of the flight. These burnout boundaries have halfway points of 2375 and 3500 ft above the launchpad, translating to 6,970 and 8,095 ft above sea level. The altitude chosen to optimize to was 8,000 feet, which has a corresponding ambient pressure of 10.9 psi. Optimizing the nozzle for this altitude means that the flow will be underexpanded during ground testing, but flight efficiency will be greater.

As these dimensions are critical to the performance of the engine, the throat and exit radius are intended to be no larger than the stated values and less than three thousandths of an inch smaller. Additionally, the radius of the Nozzle Insert's forward end was chosen to be 2.375 in to allow adequate graphite buffer between the Combustion Chamber and the exhaust gases. The diverging angle was set to 12 degrees, which may be further optimized. Finally, the thickness of the Nozzle Insert decreases linearly as the flow travels down the diverging end of the nozzle. This decision was made to minimize the total mass of the Nozzle Assembly. Additionally, the exhaust gases become significantly cooler as they expand and accelerate past Mach 1, so the need for a thermal buffer decreases drastically throughout the diverging end of the nozzle.

A compressible graphite ring is placed between the top of the Nozzle Insert and the Post-Combustion Chamber (as seen above in Figure 53). At an original thickness of 1/8 in, the compressible graphite will be compressed by 0.025 in, to a final thickness of 0.1 in. Although the graphite can sustain a maximum compression of 35%, this graphite is only compressed by 20% in order to provide leniency in dimensions of the associated parts. This compression will eliminate any unevenness in the bottom faces of the Post-Combustion Chamber and the Fuel Grain Liner, as well as provide a force which presses the Insert into the Casing. In addition to the chamber pressure, the compressible graphite will prevent the Nozzle Insert from shifting before, during, and after the burn.

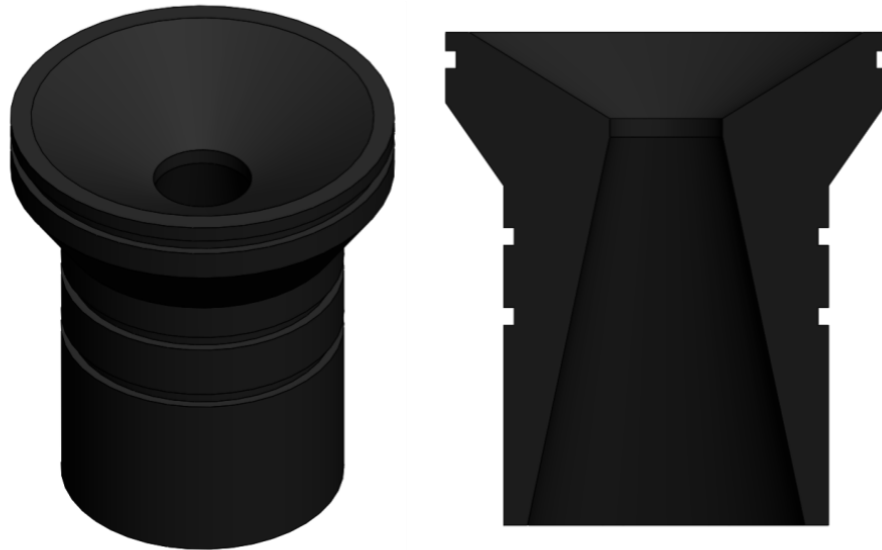


Figure 54. Nozzle Insert

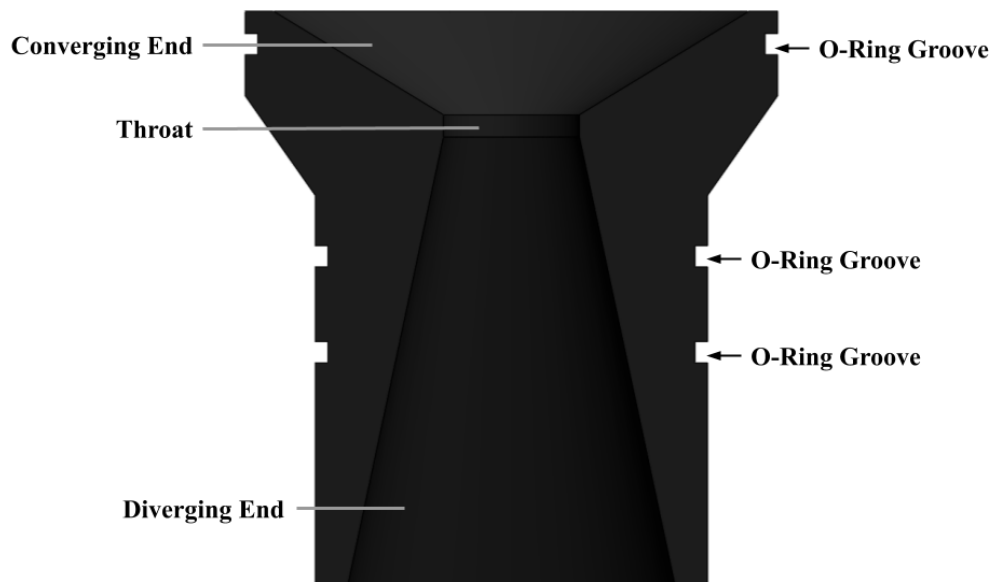


Figure 55. Nozzle Insert (cross section, labeled)

2. Nozzle Casing

The Nozzle Casing structurally supports the graphite insert by fastening into the Combustion Chamber. These fasteners do not interface with the airframe to allow for thermal expansion of the Combustion Chamber. This series of 24 fasteners is discussed at length in *Section V.B.3*. The flat top of the Casing was designed to allow the Fuel Grain Liner to drop below and interface with the topmost O-ring seal on the Nozzle Insert. Another ring of compressible graphite of the same thickness and compression as described in *Section V.B.1* will be situated between the Fuel Grain Liner and the Nozzle Casing. It will eliminate unevenness in the interface of the Post-Combustion Chamber Liner with the Nozzle Casing.

In order to prevent damage to the Insert graphite during assembly, transportation, and flight, the Nozzle Casing extends 1/16 in below the Nozzle Insert so that the graphite is less likely to directly strike the ground upon landing. The outer diameter of the casing drops from 5 in at the end of the Combustion Chamber to 3.75 in at the bottom in order to save mass. This decrease is made possible by the fact that all the loads on the casing will be located at the shoulder screw holes. Below that point, any remaining aluminum exists to protect the enclosed graphite such that the thickness of the Casing below this drop is 0.25 in.

The team also performed a static study in SolidWorks Simulation to check for any areas of stress in the Nozzle Casing due to loads exerted during an engine fire, which can be found in *Appendix IX, Simulation C.2*.



Figure 56. Nozzle casing

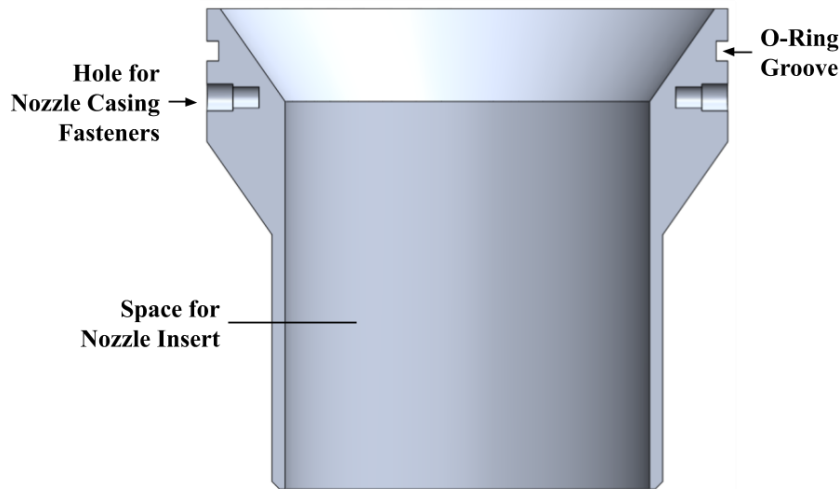


Figure 57. Nozzle Casing (cross-section view, labeled)

3. Nozzle Casing Fasteners

Fasteners are needed to hold the Combustion Chamber in place with respect to the Nozzle Casing on its aft end. These fasteners were designed with the same intuition and reasoning as the Oxidizer Tank fasteners as discussed in *Section IV.D.2*. With this in mind, the team again decided to use McMaster Carr's Shoulder Screws as they have both the pin, or shoulder, and threaded piece that the team is looking for along with a large variety of offered dimensions on the fasteners. Like the Injection Bulkhead fasteners, there must be a ring of twenty-four fasteners, each 1/4 in in diameter, equally spaced around the circumference of the Nozzle Casing. This was based on the bearing stress calculations performed on the Combustion Chamber, discussed in *Section V.A.2* and detailed in *Appendix VIII, Calculation C.2.2*.

Differing from the Injection Bulkhead fasteners, the Nozzle Casing fasteners on the aft side will be used solely to connect the Nozzle Casing to the Combustion Chamber. These fasteners will not continue through the Airframe as to not constrain the Combustion Chamber at two points with respect to the Airframe, allowing for the vertical thermal contraction and expansion of the Combustion Chamber. The team chose to use an Alloy Steel Precision Shoulder Screw, with 1/4 in shoulder diameter, 5/16 in shoulder length, and 10-32 thread, as seen in Figure 58. For this ring of shoulder screws, there was no concern about the aerodynamic drag due to the head of the fastener because it will sit in the gap between the airframe and the Combustion Chamber. This shoulder screw was primarily chosen based on availability of 1/4 in shoulder diameter shoulder screws from McMaster Carr. This total shoulder length is chosen such that the pin will fit through the Combustion Chamber, with a thickness of 1/8 in, with 3/16 in of the pin left to sit inside of the Nozzle Casing. The engagement between the shoulder of the shoulder screw and the Nozzle Casing needs to be, at a minimum, 1/8 in, the thickness of the Combustion Chamber. This ensures that the safety factor with regard to the bearing stress on the Nozzle Casing, is equivalent to, or larger than, that of the Combustion Chamber. This is more than the minimum of 1/8 in of the shoulder inside of the Nozzle Casing, while not protruding too far into the component.



Figure 58. Nozzle Casing to Combustion Chamber Shoulder Screw

In addition, the threads of the rings of shoulder screws will thread into McMaster Carr’s stainless steel helical inserts. Specifically, the nozzle casing will contain 10-32 thread and 0.190 in long helical inserts. The use of stainless steel helical inserts will ensure that the threads in the Nozzle Casing will not wear out with use. Taking into account the length of the helical insert and thread length of the shoulder screw, the depth of the holes in the Nozzle Casing are designed to ensure that there is a gap at the bottom of the hole so the threads are able to fully engage with the helical inserts. Additionally, for the same reasoning as discussed previously with the Forward Bulkhead and Injection Bulkhead fasteners, the ring of fasteners on the Nozzle Casing will use threadlocker to ensure that the fasteners do not loosen during flight due to vibrations of the engine.

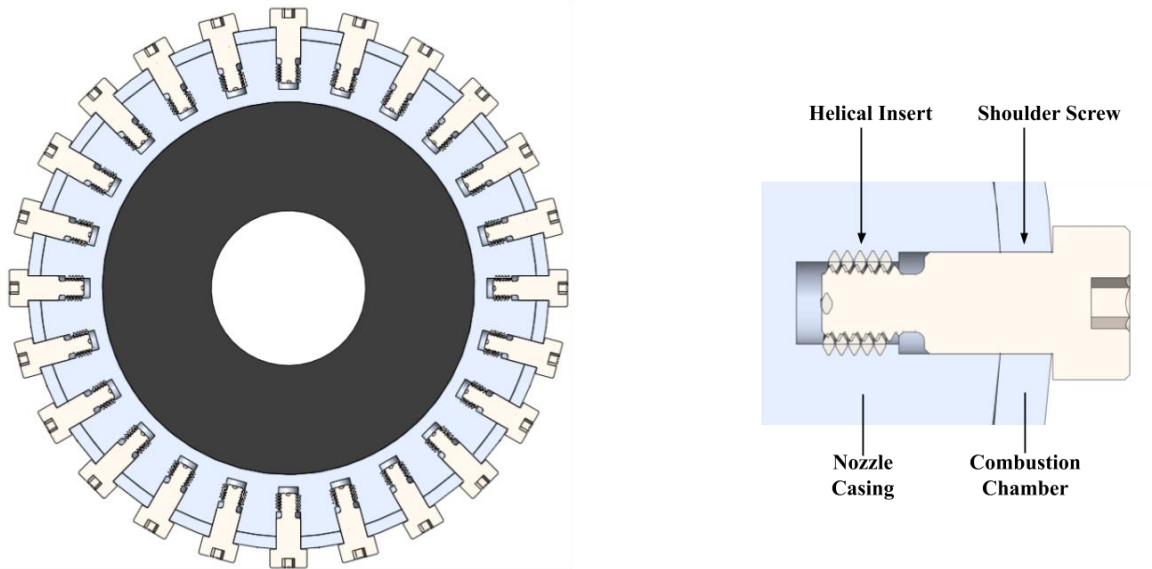


Figure 59. Nozzle Casing Fasteners (top section view)

To ensure that these shoulder screws were sufficient for attaching the Nozzle Casing to the Combustion Chamber, three calculations were performed: bearing stress on the Nozzle Casing fastener holes, shear stress on the shoulder screws, as well as tearout stress on the holes within the Combustion Chamber and Nozzle Casing. These calculations can be found in *Appendix VIII, Calculation C.3.2*. Just as with the Injection Bulkhead and Forward Bulkhead fasteners, preload calculations were performed to determine the maximum preload that can be applied to the Nozzle Casing fasteners during assembly. These calculations are found in *Appendix VIII, Calculation C.3.2.4*.

VI. Ground Support Equipment

The fill system for the Titan II engine begins with two ground nitrous oxide tanks connected via external ground feed plumbing into the flight Oxidizer Tank. The flight Oxidizer Tank will be filled backwards through the engine from flexible nylon tubing which will be severed by the engine’s igniters.

A. Ground Oxidizer Fill System Plumbing Assembly

Two nitrous oxide tanks are each attached to a CGA 660 to 1/4 in NPT fitting, both of which are connected to 1/2 in Swagelok adapters leading into 1/2 in stainless steel tubing that joins the two tanks using a T-fitting. From the now-unified feed line, an additional T-section (1/2 in, 1/2 in, 1/4 in) splits off a 1/4 in tubing section connected with a Swagelok-to-NPT adapter to the main feed line pressure transducer. This pressure transducer allows for the effective reading of the tank pressure without using tank regulators. Further down the feedline, after another section of stainless steel tubing, the oxidizer fill valve is connected. The valve itself is a Triad 60C 1/2 in cryogenic ball valve with a remotely controlled Radius series A AD-008 pneumatic actuator. The valve is actuated using a separate ground nitrogen cylinder, regulated to approximately 100 psi. This valve controls the flow of nitrous oxide into the flight Oxidizer Tank during the pre-flight fill sequence. After the main ball valve is another swagelok T-section (1/2 in, 1/2 in, 1/4 in), which, like the pressure transducer line, splits off into a 1/4 in steel tubing line connected to the ground vent valve. This valve is a 1/4 in ball valve with a remotely controlled Valbia MOD 32 pneumatic actuator designed to vent the entire flight Oxidizer Tank and nylon feed lines in the case of a testing anomaly. From this T junction, a 10 ft section of insulated 1/2 in tubing joins the full ground plumbing assembly to a manifold that splits into six 1/4

in female NPT ports. This manifold is referred to as the start of the oxidizer fill assembly. All stainless steel tubing on the ground support equipment will be insulated to keep the liquid nitrous oxide cold during propellant loading, so the oxidizer is denser and more can be loaded into the engine's Oxidizer Tank. Figure 60 illustrates the Ground Oxidizer Fill System Plumbing Assembly in its flight configuration, and Figure 61 illustrates the Ground Oxidizer Fill System Plumbing Assembly in its static test configuration. Table 18 details the specifications of the fill and vent valves.

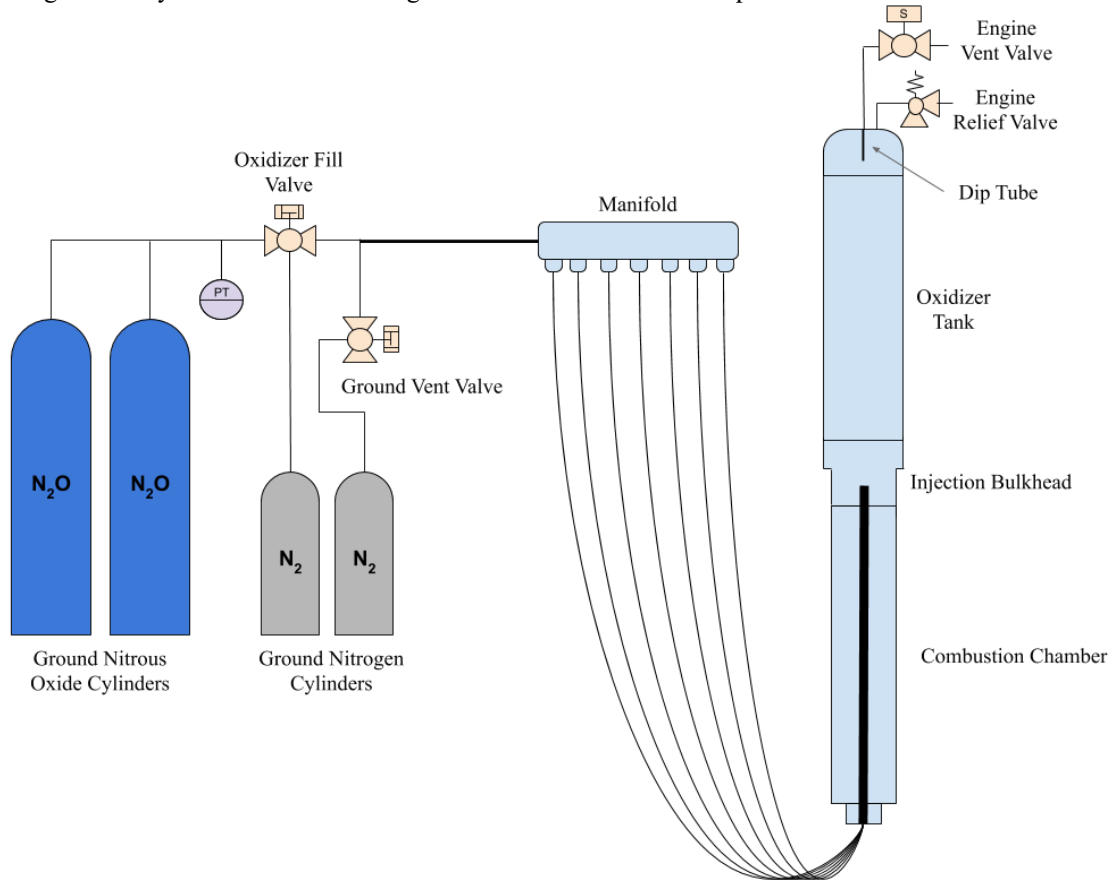


Figure 60. Ground oxidizer fill system piping and instrumentation diagram - flight configuration

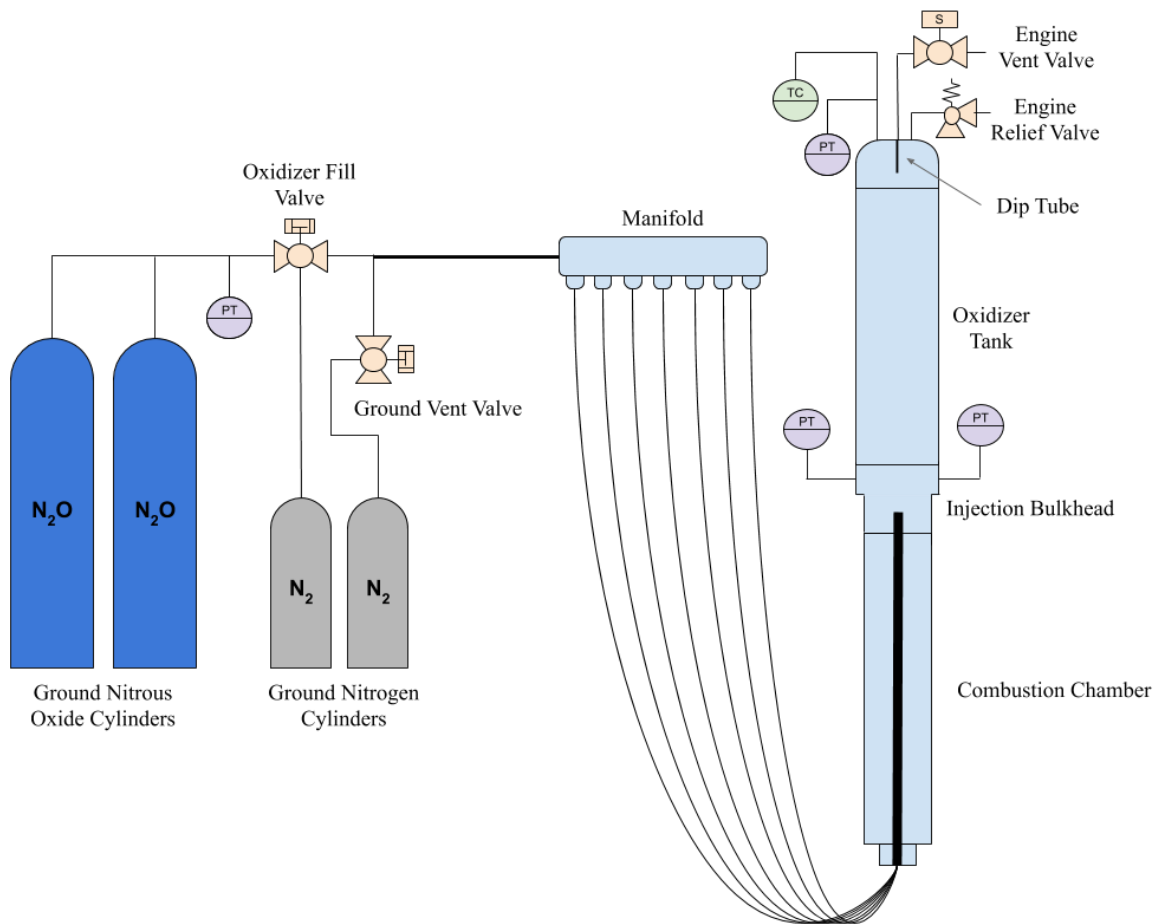


Figure 61. Ground oxidizer fill system piping and instrumentation diagram - static test configuration

Table 18. Ground Support Equipment Valve Specifications		
Specification	Oxidizer Fill Valve	Ground Vent Valve
Manufacturer	Triad Process Equipment - Valve Radius - Actuator	Valbia
Model Number	60C ½” - Valve AD008 - Actuator	8P026300 - Valve MOD 32 - Actuator
Valve Type	Pneumatically-actuated cryogenic ball valve	Pneumatically-actuated ball valve
Default (No-Power) Position	Normally Closed	Normally Open
Maximum Allowable Working Pressure (psi)	2000	1000
Rated Temperature Range (°F)	-196 to 500	0 to 450
Seal Material	Grafoil	PTFE
Orifice Diameter (in)	0.59	0.25
Flow Coefficient (C_v) or Discharge Coefficient (C_d)	C _v = 19	C _v = 6
Power Requirements	12 VDC	12 VDC

B. Oxidizer Fill Assembly

To fill the Oxidizer Tank with nitrous oxide before flight, nitrous flows from the ground tanks through the ground feed plumbing into seven push-to-connect fittings secured in the six 1/4 in NPT port aluminum manifold (A pneumadyne model M30-250-6). The manifold redirects the nitrous oxide flow from the external 1/2 in tubing into six 1/4 in high pressure nylon tubes, rated to 920 psi. The nylon tubing is guided through the Thrust Chamber Assembly into the six corresponding 1/4 in Tube OD x 1/4 in NPTF Male push-to-connect fittings on the aft side of the Injector Plate. The seven 1/4 in nylon tubes are fed through the 1.215 in inner diameter nozzle throat. A circle packing calculator confirms that this throat diameter is large enough to pass all six tubes (see Figure 62). Oxidizer flows into the Oxidizer Tank via the holes in the Injector Plate and through the Oxidizer Feed Conduit during fill.

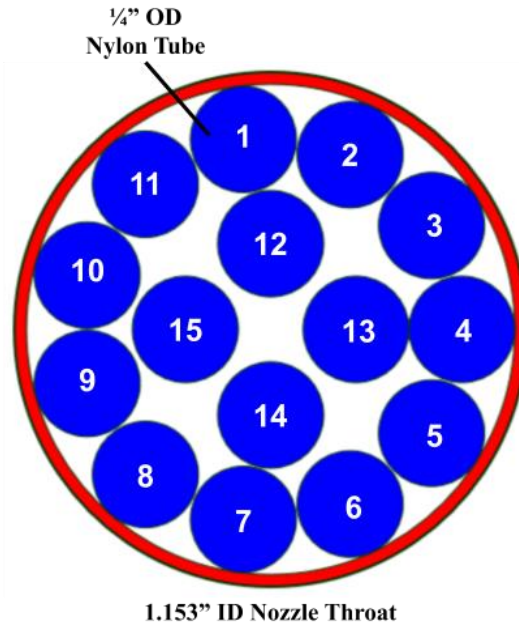


Figure 62. 1.153 in nozzle throat has capacity for 15 1/4 in nylon tubes per circle packing calculation

The team ultimately decided to use this nylon fill system as the Titan II engine oxidizer filling system due to its simplicity, cost, reliable disconnect, lack of added weight, and the team's past experience with this system on the original Titan engine. The other idea seriously considered by the team was a system using a check valve and a pyro valve with quick disconnect. A system was idealized that would involve injecting the nitrous oxide through a port that directly leads to the plumbing between the engine and oxidizer tank. A singular nylon tube would attach to this port, which would have a check valve to prevent any flow outside of the engine even after disconnecting. Another valve would be located right before the bulkhead, to prevent flow from moving to the Injector Plate while filling. This valve would be the main oxidizer valve, which would be actuated to begin the flow of oxidizer. This system would have a clean disconnect system, be reusable, have a simple assembly process, and most importantly give the team freedom with the Injector Plate design. However, it would have a large mass added to the rocket due to the additional valves, add complexity, have a longer development time, and be much more expensive than alternatives.

There was a long discussion for assessing the individual pros and cons of many systems, in which the team determined which points should drive the decision. The main reason that the team chose the nitrous oxide fill system over the check valve and pyro valve with quick disconnect system was that the nitrous fill system had no added weight to the rocket. This is a very important factor since the team's design process has indicated how incredibly valuable it is to save every possible pound in the final rocket. Adding a 4 lb ball valve, as would occur with the previously discussed alternative, could result in the rocket missing out on thousands of feet in altitude. In addition, the nylon fill system is much simpler. Keeping the filling process simple allows the team to focus on perfecting more complex systems, and prevents a rigorous testing procedure to ensure that all components will work. Next, the cost of the nylon fill system is much less than other alternatives. As Eclipse is a student-run team, it is important to reduce cost where possible. Along with the aforementioned benefits, the nylon fill system also has a much faster development time. The project timeline has been constructed with ambitious goals and deadlines, so adding development time for the fill system is not ideal and would take focus away from more important systems. Lastly, the team has used this nylon fill system in the original Titan engine. Team members have experience with designing and implementing this exact system and it has been test proven multiple times on the original engine. Though this fill system limits the Injector Plate design, requires new push-to-connect fittings each test, is difficult to assemble, and requires engine transportation with igniters, the various benefits mentioned above outweigh these cons, leading the team to choose the nylon fill system over alternatives.

C. Fill Process

To begin filling, the Oxidizer Fill Valve is opened, and nitrous oxide flows through the external ground plumbing, through the six nylon tubes, and through the holes in the Injector Plate. The nitrous oxide will then begin

to fill the flight Oxidizer Tank through the Oxidizer Feed Conduit within the Injection Bulkhead. There is a pressure differential between the flight Oxidizer Tank at atmospheric pressure and the ground tanks, making the nitrous oxide flow from the ground tanks into the flight Oxidizer Tank without the need for a pump. The engine's vent valve is open throughout the fill procedure, allowing the atmospheric air originally in the tank to vent as it is replaced with nitrous oxide.

The flight Oxidizer Tank is filled until it contains 39.35 lbm of nitrous oxide based on the oxidizer mass calculations, discussed in *Section III.D* and detailed in *Appendix VIII, Calculation A.2*. To determine when the Oxidizer Tank contains the required mass of nitrous oxide, the ground avionics system will monitor the weight of the ground nitrous tanks throughout the fill process. Once the ground nitrous tanks have lost 39.35 lbm of nitrous oxide, the Oxidizer Fill Valve will be closed. To increase accuracy in this process, the mass of nitrous oxide that remains in the fills lines must be known. To determine this value, an analysis of the system will be performed during early static testing, in which the team will compare the change in weight of the ground tanks to the change in weight data from the axial load cell on the engine test stand. From these data points, the weight of nitrous oxide remaining in the fill lines can be determined. After finding this value, the fill procedure will be adjusted accordingly to ensure the Oxidizer Tank contains 39.35 lbm of nitrous oxide. As a back-up indicator of the oxidizer level in the tank, the outlet port of the engine's vent valve will be monitored for a white plume of liquid nitrous oxide. This will appear when the liquid oxidizer level reaches the bottom of the dip tube (located in the top of the Oxidizer Tank). The dip tube, discussed in detail in *Section IV.C.1*, marks the maximum-allowable liquid level in the tank to maintain its 5% ullage volume when the nitrous reaches its 915 psi vapor pressure state. If the plume is observed before the mass-based fill process is complete, the oxidizer fill valve will be closed to prevent any additional oxidizer from being loaded into the engine.

During the fill process, the tank is heated externally in order to keep a desirable pressure as nitrous oxide is moved from the ground tanks to the on-board Oxidizer Tank. While keeping the tanks at room temperature is easier in the midday sun at Spaceport, the process requires some effort when testing during the colder months. In order to achieve this, the tank is wrapped in electronic heating tape made for heating piping. The tape is connected to the same ground support avionics system used to control valves and ignition. The tape is activated after fill to slowly increase the pressure of the tank after propellant loading. The ground avionics operator monitors the pressure transducer located on the Forward Bulkhead. The tape remains on as long as the pressure of the nitrous oxide remains within 50 psi of the 750 psi expected value. The operator can easily toggle the heating off if the pressure gets too high. The heat is turned off before ignition.

Once the flight Oxidizer Tank is completely filled, the Oxidizer Fill Valve and the engine's vent valve will be closed, leaving the engine ready for ignition.

D. Ignition System

The purpose of the ignition system is to reliably start the engine's combustion from a safe distance. This is achieved using multiple igniters that are secured to the fill line tubing near the Injector Plate. The igniters are made from CAT 5 wire strands, with an approximately 1 cm long stripped area at the end wrapped with 32-gauge nichrome bridge wire. Approximately 1 in of the stripped and wrapped end is then coated with magnesium powder mixed with potassium nitrate in aeropoxy. The igniters are cured in small molds to ensure a cylindrical, easy-to-insert shape, and the length of the wire tails that connect to the terminal block is determined based on safety and convenience.

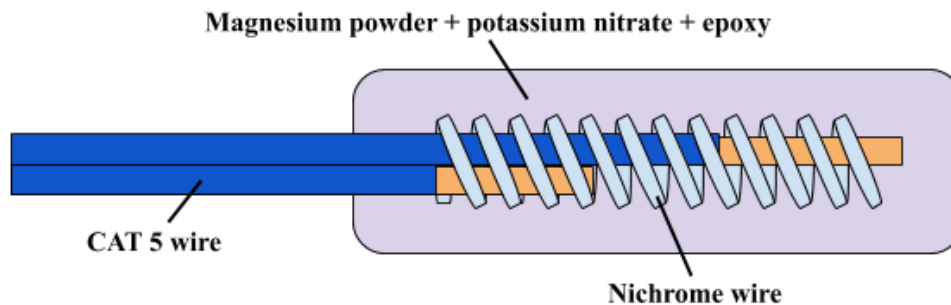


Figure 63. Typical igniter diagram

This ignition system design was chosen because of its inherent reliability. Seven igniters are used for redundancy, greatly reducing the possibility of faulty igniters preventing ignition. By filling and ejecting oxidizer from the same holes, there is no need for an additional valve to start ignition, because severing the nylon tubing by

starting the igniters automatically begins oxidizer flow. With this, the oxidizer flow is entirely dependent on the igniters burning, meaning that there is no concern over oxidizer flow/ignition timing, reducing the possibility of ejecting the igniters before proper ignition can take place. Once the igniters burn through the nylon tubing, full engine ignition begins and the combustion severes each of the fill lines and ejects the loose nylon tubes and igniter wires out through the nozzle.

E. Instrumentation

During ground tests, the team will utilize a variety of instrumentation devices to characterize the performance of Titan II in order to further optimize the engine leading up to flight. A glimpse of this instrumentation is seen in *Section VI.A* above, but more detail in each type of data gathering instrument, where each instrument is located, and reasoning for its placement is discussed below. This instrumentation will be used on all ground tests -- a discussion regarding in-flight instrumentation is also given at the end of this section.

1. Load Cell (LC)

Perhaps the most important sensor in characterizing the performance of Titan II is the load cell to measure the force of thrust produced by the engine exhaust gases. The system utilizes a single, axial load cell mounted at the top of the engine -- serving as the interface between the engine and test stand structure. The engine “pushes” up against the bottom of the load cell during the test, which is in turn fixed to the rigid test stand. The load cell essentially serves as the sole upper mounting point for the engine, ensuring that it experiences the entire thrust of the engine. For the purposes of testing Titan II, only the axial force produced will be measured. In Eclipse’s other engine, Luna, side forces are also measured due to the inclusion of SRAD thrust vector control (TVC); for Titan, however, only the axial thrust is needed for a potential flight vehicle. The team will assume that the side forces are negligible for all flight applications.

The load cell Eclipse uses for this application is a Honeywell pancake-style load cell, capable of measuring up to 3,000 lbs of exerted force. As with all of the team’s instrumentation, the load cell is directly connected to the ground support avionics box, ARCA -- both ground support and flight engine avionics are discussed in an auxiliary document.

The force data can be viewed real time on the team’s data visualization software, RESFET Dashboard, though load cell data is primarily used for post-test analysis off-site. Thrust can be used to determine mass flow rate of oxidizer, fuel regression rate, and more.

2. Pressure Transducers (PTs)

The numerous pressure transducers positioned in the system serve to further characterize the engine. The engine and ground support systems utilize four total PTs in the following locations: feed line, Oxidizer Tank, Pre-Injection Chamber, and Combustion Chamber.

All PTs used are simple low-cost stainless steel compact pressure transducers from Omega sensors. The PTs come with a 1/4 in male NPT pressure port and measure up to 1,000 psi with a 0.5% accuracy. The transducer uses an internal ceramic diaphragm which provides thermal compensation. The same model of pressure transducers have been used by Eclipse for many applications, including on the test engine Luna, as well as the Mk 1, Mk 1.1, and Mk 2 legacy systems.

Note that all pressure transducers are not directly threaded into the engine, and instead are attached via a section of “buffer” tubing, which consists of coiled 1/8 in stainless steel tubing, as seen in Figure 64 below. This small buffer serves to cool down gases slightly to prevent the gases from damaging or destroying the sensitive pressure sensing equipment. This same technique has been used on Luna, and has provided accurate pressure readings throughout the engine’s lifespan. Further trade studies can be conducted to determine exactly how much effect the coils have on temperature and pressure.

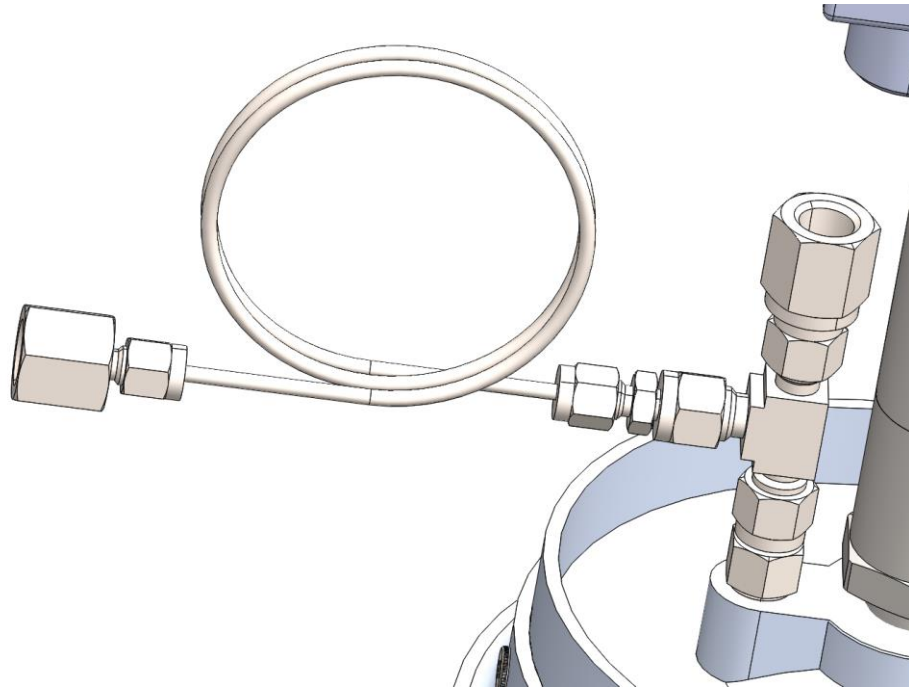


Figure 64. Pressure Transducer Buffer Tubing

The feed line pressure transducer serves to measure the pressure of the nitrous oxide coming from the ground tanks. As detailed above in *Section II.B*, one of the main reasons the team chooses to use nitrous oxide as oxidizer is due to its self-pressurization at 750 psi at room temperature. Because of this, the ground system does not implement pressure regulations on the ground nitrous tanks -- simply opening the tanks allows for the entire system to be pressurized to 750 psi. This eliminates the need for a potentially complex component, but removes the ability to read the pressure of the ground tanks. Though nitrous oxide self-pressurizes at 750 psi, variations in the outside temperature make this pressure variable. In order to read this pressure in real time, and from a safe distance once the tanks are opened, a pressure transducer is placed between the ground tanks and the main feed line valve. Like the load cell, the PT is connected to Eclipse's ground avionics box that transmits data back to the ground station in real time. This allows for a single team member to open the tanks and evacuate the area, while pressure readings can be taken remotely afterwards.

The pre-injector and combustion chamber PTs are sensors that both interface directly into the Injection Bulkhead, as referenced in *Section IV.B.1.4*. The pressure transducers connect to channels that lead directly to the Pre-Injection Chamber and the Combustion Chamber, specifically the Pre-Combustion Chamber fore of the Fuel Grain. Before ignition, only the Pre-Injection Chamber will read above atmospheric pressure, as the pre-fire nitrous fill system does not pressurize the Combustion Chamber. Before a fire, when the system settles into equilibrium, the pre-injection PT should be reading the same or similar as the feed line and tank PTs. During a fire, the pre-injector PT is expected to see a sharp decrease in pressure, slightly less than the tank PT due to pressure losses, starting around 750 psi at $T=0$. The combustion chamber PT is expected to see the calculated chamber pressure of 500 psi during a fire, slightly decreasing closer to the atmosphere as the burn ends. The main purpose of these two sensors is to measure the drop in pressure across the injector plate. The pressure drop is a quantifiable value, that can be calculated, as well as measured empirically. This allows the team to compare the actual performance of the engine to the theoretical. This is also helpful due to the fact that the injector plate is one of the few components in the system that is easy to change and iterate upon from test to test. If post-test analysis finds that the oxidizer mass flow rate is not what is desired, the team can use the available pressure data to evaluate whether the injector hole size is adequate.

Finally, during a static ground test, there is a single pressure transducer at the top of the oxidizer tank, threaded into the forward tank bulkhead. This PT serves to measure the pressure in the headspace of the tank, as the nitrous is being filled, and during a fire. With this pressure data, the team is able to monitor the pressure of the tank during filling in order to watch for over or under pressurization before ignition. This data can be used in conjunction with the temperature data so the appropriate actions can be taken. Post test, this pressure data can be used to further analyze the nitrous oxide flow and engine performance.

3. Thermocouple (TC)

The team will utilize a single thermocouple probe in order to measure the temperature of the oxidizer tank during fill, and during a burn. The thermocouple is a RTD temperature sensor from Omega sensors. The probe is inserted through the forward bulkhead and into the vessel. The probe has a 1/4 in NPT fitting to ensure a seal, and is rated to over 2000 psi. The probe has a 12 in sheath length, allowing the sensor to reach into the oxidizer tank and be totally immersed into the oxidizer.

While thermal data hasn't been emphasized in past Eclipse projects, as the team begins to understand the intricacies of heat propagation and the effects of temperature on the performance of the system, more data is required. This purpose of the oxidizer tank thermal probe is two-fold. For one, in a post-test environment, the logged temperature data can be used to find the exact temperature inside the tank during various points of the testing phases. Generally, the nitrous oxide will cool down when expanding into the empty vessel, and then slowly warm due to ambient heat transfer from the potentially hot testing environments. Knowing the exact temperature before a fire can help to more accurately size the oxidizer dip tube and injector plate by being able to calculate the exact density of the nitrous oxide at any given point. Not only does this allow for the team to further optimize the engine, but to also determine more accurate amounts of propellants to load into the pre-fire system. Secondly, the temperature data can be used in RESFET Dashboard to allow the ground operators to view the nitrous oxide temperature in real time as it fills. Coupled with the ability to toggle heating tape on and off (as discussed in *Section VI.C*), this allows for the operators to precisely control the temperature the nitrous is at before a fire -- even after all of the nitrous is loaded in.

While one thermal probe is all that is needed currently, the ground support avionics can support up to two more sensors to place externally on the engine. With Luna, the team has experience with affixing thermal probes to the exterior of engine casing components in order to measure temperature at the wall during a burn. This process can be done easily with high temperature tape. These same styles of sensors can be easily affixed anywhere on the exterior of the engine if additional thermal analysis is desired.

4. In-Flight Instrumentation

While instrumentation is extremely important to gathering performance data on the engine and making tweaks before flight, the constraints put on the team by the Spaceport America Cup competition restrict the team from implementing engine data collection in flight. Titan II is already at the impulse limit for a vehicle competing at Spaceport. As such, in order to reach the intended target altitude of 30,000 feet, the team cannot afford to have heavy instrumentation inside of the vehicle. Additionally, after three successful fires, the team plans to have quantified all of the values needed to optimize the engine for the team's purpose, so on-board instrumentation will not be needed for the team's first attempt at flying a hybrid.

There will be no engine instrumentation on-board the flight vehicle, but the team will still utilize instrumentation on the ground support hardware. This mainly refers to the PT that monitors feed line pressure immediately out of the nitrous oxide ground tanks. However, the team may also opt to implement a thermocouple on the ground system, or a mass measuring system if mass-based propellant loading is pursued. In short, for ground tests, the team wants as much data as possible to help characterize engine performance so tweaks can be made. For flight, however, only the minimum instrumentation is utilized in order to ensure a safe launch.

F. Static Test Stand

The static test stand serves as the basis for all testing operations conducted on the engine. Its primary tasks are to support the weight of the engine during transport to and from the test site, completely restrain the engine during firing to ensure safety, and provide a platform to accurately assess engine flight performance. As the static test stand is a project necessitating its own documentation entirely, this section will simply provide a brief overview of the general systems of the static test stand; a complete and comprehensive investigation of the entire static test stand installation, including all calculations and justifications, can be found in the separate *Ground Systems Documentation*. Of particular interest in this document are two major aspects of the test stand; how the engine is mounted on the test stand to ensure accurate measurements of its capabilities, and how the engine is supported to ensure structural rigidity and safety during engine firings.

The engine block is the part of the test stand where the engine resides during testing, and accomplishes the task of ensuring proper measurement of the engine's output. The engine block contains four main units: the engine itself, the retaining rings, the load plate, and the load cell. The retaining rings are two components directly connecting the engine to the other structures in the test stand. The retaining rings are machined to fit the geometry of the engine and both rings have the same outer diameter. Each retaining ring contains two series of holes; the first series allows for shoulder screws to attach each ring to the engine, and the second series allows for bolts to attach each ring to several unistrut bars vertically mounted around the engine. These unistrut bars surround the engine and provide the

mounting point to support the engine in a vertical position. The unistrut bars are bolted to the steel load plate, which is solely suspended by the aforementioned Honeywell load cell. Such a design means that all force generated by the engine firing has no alternate path to be dissipated throughout the engine and will be measured by the load cell exclusively, ensuring proper measurement of the engine's thrust output capability.

The engine is supported by a large structure, designated as the strongback. It acts as the spine of the testing stand, providing a sturdy backing for the engine block during firing and transport. The strongback connects to the trailer used for transporting the engine, and is able to rotate between vertical and horizontal positions for firing and transport respectively. The strongback's rotation is actuated by a pair of pneumatic pistons and, when in the vertical firing position, is also anchored to the ground with four braided steel cables connecting to eye bolts at the top of the strongback.

The static test stand itself is simply one component of the larger assembly of the testing trailer; however, discussion of the trailer is beyond the scope of this document and can be found in the separate *Ground Systems Documentation*.

VII. Propulsion System Testing and Results

A. Oxidizer Tank Pressure Testing

The engine's Oxidizer Tank will be hydrostatically tested to a pressure of 1373 psi and will be held at that pressure for at least one hour. This satisfies the IREC Design, Test, and Evaluation guide requirement of testing all SRAD pressure vessels up to 1.5 times the maximum expected operating pressure (915 psi) for at least two times the maximum expected system working time (30 minutes).²⁰ This test will be performed at Rice University's South Annex test site, using a high pressure water pump provided by DaVinci Maker Labs. The Oxidizer Tank's valve and sensor ports will be plugged, and the injector plate will be replaced by a boilerplate version with no injection holes.

B. Thrust Chamber Assembly Pressure Testing

The engine's Thrust Chamber Assembly will be hydrostatically tested to a pressure of 750 psi, and will be held at that pressure for at least 15.34 seconds. This satisfies the IREC Design, Test, and Evaluation guide requirement of testing all SRAD pressure vessels up to 1.5 times the maximum expected operating pressure (500 psi) for at least two times the maximum expected system working time (7.67 seconds).²⁰ This test will be performed at Rice University's South Annex test site, using a high pressure water pump provided by DaVinci Maker Labs. The Thrust Chamber Assembly will be hydrostatically tested while integrated with the Oxidizer Tank. The full Thrust Chamber and Oxidizer Tank volume will be filled with water and pressurized to 750 psi, with all valve and sensor ports plugged, and the nozzle casing replaced by a plugged casing.

C. Engine Tanking and De-Tanking

The engine will complete at least one full nitrous oxide loading and off-loading test in its flight configuration prior to beginning the hot fire test campaign. This test will entail filling the engine's Oxidizer Tank with nitrous oxide using the ground support equipment fill system, and then fully venting the nitrous oxide from the tank using the ground support system's ground vent valve.²⁰ This testing will be performed at Rice University's South Annex test site, with the engine configured in its static test configuration (see Figure 61). This test may be performed with carbon dioxide instead, which is a less expensive fluid that has very similar properties to nitrous oxide at the engine's operating pressures.

D. Static Hot Fire Testing

The engine will complete three static hot fire tests before flight. The first will be a 4 second burn, followed by a 6 second burn, and finally a full 7.67 second burn. The short initial burn is to ensure that safety hazards during the initial burn will be minimized; in particular that the Fuel Grain will not regress to the point of exposing the Combustion Chamber even if the regression rate modeling proves to be incorrect. 4 seconds was chosen for the first burn because this time will ensure that less than half of the fuel grain is burnt by radius. Once this is achieved, longer burns better simulate what the engine will experience in flight and will provide better data. The test data will be used to check the performance of each engine system, and a post-test analysis of the Fuel Grain will reveal whether the team's predicted regression rate model is accurate. The Oxidizer Tank will be weighed before and after each burn using the load cell on Eclipse's mobile test stand in order to give the team an experimental value for the average mass flow rate of oxidizer.²⁰

In order to run a 4 second burn and 6 second burn, the amount of oxidizer in the tank that is required is decreased proportionally to the time of the test. As discussed in *Section IV.C.1*, the dip tube is what drives the maximum fill point of the Oxidizer Tank, as it will cause oxidizer to be vented from the tank as it reaches its entry point. In order to determine the desired dip tube lengths, the calculations outlined in *Appendix VIII, Calculation D.1*, were performed again with the required oxidizer volume. All calculations assume the nitrous oxide enters the tank at 68°F, corresponding to a density of 0.0284 lb/in³. This lower temperature and higher density is assumed because the nitrous oxide expands and cools when entering the tank. From previous Titan I tests, it is known that this temperature is lower than the engine's ideal oxidizer inlet temperature of 70°F. The results are summarized in the table below:

Table 19. Volume of Oxidizer and Dip Tube Length for Static Hot Fire Tests (Assuming 68°F Nitrous Fill Temperature)			
Test Number	Length of Burn (s)	Volume of Oxidizer Required (in³)	Length of Dip Tube (in)
1	4	722.39	36.27
2	6	1083.61	22.95
3	7.67	1384.64	11.10

E. Planned Engine Optimization after Testing

If the first static hot fire proceeds nominally, changes to the majority of the engine will not be drastic. Thrust and pressure data will be analyzed to determine if the Injector Plate and nozzle performed as expected, and appropriate changes to the designs will be made if this is not the case. Before Titan II is launched in a flight vehicle, the Injector Plate will be altered such that the holes are optimized for the expected oxidizer inlet conditions at Spaceport. An experimental specific impulse will also be measured, which will be used as a more accurate measurement for designing the airframe the Titan II engine will power.

As the fuel's regression is modeled off the team's 50 lb hybrid rocket engine, Luna, there is a high likelihood that the experimental regression rate is different from what is to be expected. Since the Combustion Chamber is longer than necessary to accommodate for these potential differences, the optimal dimensions of the Fuel Grain will be determined after the second static hot fire and the Combustion Chamber length will be cut down accordingly. If the regression rate is higher than anticipated, the Fuel Grain can be shortened and more than the extra 7 in currently on the Combustion Chamber will be cut off and the bolt holes re-machined. If the regression rate is lower than expected, less than the extra 7 in of the Combustion Chamber will be cut off the end, if at all, and bolt holes will be re-machined as necessary.

A higher regression rate would be much better for the engine because the shortened Combustion Chamber, Fuel Grain, and phenolic liner would shave a lot of weight off the engine. Because of this, the Rice Eclipse Chemicals team is experimenting with doping the HTPB fuel grain with aluminum powder for the smaller Luna engine, as this has been shown to improve performance in other hybrid rocket engines.²¹ Additionally, the low immediate acceleration of Titan II compared to rockets with solid motors means that the rocket that houses Titan II will need a very long launch rail, but a successful doped Fuel Grain will help mitigate this issue. If a percentage of aluminum powder is proven to be successful at a Luna static fire it will be implemented in Titan II in order to raise the regression rate, as well as overall engine performance. The team aims to implement a doped Fuel Grain on the second hot fire of Titan II, and if successful will also be implemented for the third hot fire and the engine's first flight. The second hot fire was chosen because the doped fuel adds risk and the team aims for the first hot fire to be as safe as possible, as there will be many unknowns during the engine's first trial. Additionally, the doped fuel may have a large effect on the regression rate, and experimenting with it during the second hot fire allows the team to analyze regression data of this fuel before the Combustion Chamber is cut down to the final length before the third and final hot fire.

F. Planned Engine Optimization after Flight

A number of potential projects to optimize the engine have been pitched that would not be implemented until after the Titan II engine flies at the 2022 Spaceport America Cup. This includes a nozzle with a bell shaped diverging end, an active cooling system that would allow the Nozzle Insert and Nozzle Casing to be a single component, and a pressurization system that would inject inert gas into the Oxidizer Tank in order to keep it at a constant pressure.

VIII. Appendix - Detailed Calculations

A. Engine Performance Requirements Definition Calculations

1. Oxidizer to Fuel Ratio as a function of HTPB Mass Calculations

To keep the total propellant mass at a constant 44 lbs, the parameter varied in the analysis was the mass of HTPB, which was coupled to the masses of each other propellant component per the calculations outlined below,

$$O/F = \frac{m_{ox}}{m_f}$$

$$O/F = \frac{m_{nitrous\ oxide}}{m_{HTPB} + m_{curative} + m_{carbon\ black}}$$

Where,

$$m_{HTPB} = m_{HTPB}$$

$$m_{curative} = \frac{0.23}{0.77} m_{HTPB}$$

$$m_{carbon\ black} = 0.03 \cdot m_{HTPB} \left(1 + \frac{0.23}{0.77}\right)$$

$$m_{nitrous\ oxide} = m_{propellant} - (m_{HTPB} + m_{curative} + m_{carbon\ black})$$

Which were then used to express the O/F ratio as a function of HTPB mass with a total $m_{propellant}$ of 44 lbm (20 kg),

$$O/F = \frac{20\ kg - [m_{HTPB} \cdot (1 + \frac{0.23}{0.77} + 0.03 \cdot (1 + \frac{0.23}{0.77}))]}{m_{HTPB} (1 + \frac{0.23}{0.77} + 0.03 \cdot (1 + \frac{0.23}{0.77}))}$$

$$O/F = \frac{20\ kg - (1.3378\ m_{HTPB})}{1.3378\ m_{HTPB}}$$

2. Total Mass and Required Mass Flow Rate of both the Fuel and Oxidizer Calculations

The specific impulse equation below was used to calculate the mass flow rate of propellant required for the 11.5 second burn at 800 lbf average thrust:

$$I_{sp} \cdot g = \frac{F_{t,avg}}{m'_{prop}}$$

The equation was then rearranged to solve for the required propellant mass flow rate. For this calculation, the specific impulse was decreased by 2% in order to account for the expected oxidizer-rich O/F shift during the burn

and other engine inefficiencies, per the hybrid engine design recommendations given on pg. 410 of the *Space Propulsion Analysis and Design* reference book.¹⁷

$$\dot{m}_{prop} = \frac{F_{t,avg}}{(0.98)(I_{sp})(g)}$$

$$\dot{m}_{prop} = \frac{(1200 \text{ lbf})(4.4482 \text{ N/lbf})}{(0.98)(202.47 \text{ sec})(9.81 \text{ m/s}^2)}$$

$$\dot{m}_{prop} = 2.742 \text{ kg/s}$$

This total mass flow rate can be written as the sum of the fuel and oxidizer mass flow rates:

$$\dot{m}_{prop} = \dot{m}_f + \dot{m}_{ox}$$

Which can be written in terms of the fuel mass flow rate using the O/F ratio, where $\dot{m}_{ox} = (O/F)\dot{m}_f$:

$$\dot{m}_{prop} = \dot{m}_f + (O/F)\dot{m}_f$$

Solving for the required fuel mass flow rate:

$$\dot{m}_f = \frac{\dot{m}_{prop}}{(1 + O/F)}$$

$$\dot{m}_f = \frac{2.742 \text{ kg/s}}{(1 + 5.62)}$$

$$\dot{m}_f = 0.414 \text{ kg/s} \cdot \left(\frac{2.2 \text{ lbm}}{1 \text{ kg}}\right)$$

$$\dot{m}_f = 0.9108 \text{ lbm/s}$$

The fuel mass flow rate and the O/F ratio were then used to solve for the required oxidizer mass flow rate:

$$\dot{m}_{ox} = (O/F)\dot{m}_f$$

$$\dot{m}_{ox} = (5.62)(0.9108 \text{ lbm/s})$$

$$\dot{m}_{ox} = 5.119 \text{ lbm/s}$$

Using the 7.667 second burn time, the required total masses of fuel and oxidizer were then calculated:

$$m_f = (\dot{m}_f)(t_{burn})$$

$$m_f = (0.9108 \text{ lbm/s})(7.667 \text{ s})$$

$$m_f = 7.00 \text{ lbm}$$

$$m_{ox} = (\dot{m}_{ox})(t_{burn})$$

$$m_{ox} = (5.119 \text{ lbm/s})(7.667 \text{ s})$$

$$m_{ox} = 39.35 \text{ lbm}$$

B. Oxidizer Storage and Feed Assembly Calculations

1. Hoop stress and axial stress calculations to determine Oxidizer Tank Body Cylinder wall thickness

The wall thickness of the Body Cylinder was calculated using hoop stress and axial stress equations. The maximum nominal pressure used for the calculation is 915 psi, and the Oxidizer Tank outer diameter is known to be 6.25 in, since it will match the outer diameter of the overall rocket airframe. The yield strength of Aluminum 6061-T6 in tension is 35,000 psi. Using the engine's minimum factor of safety to yield of 2.0, the calculation was conducted as shown below:

$$P_{nominal} = 915 \text{ psi}$$

$$SF = 2.0$$

$$d_{outer} = 6.25 \text{ in}$$

$$\sigma_{yield} = 35,000 \text{ psi}$$

$$P_{sf} = SF * P_{nominal} = 1,830 \text{ psi}$$

For ease of manufacturing, standard values for wall thickness were used to calculate how much stress would be experienced by the tank. The first wall thickness value used was 1/8 in.

$$t_{wall} = \frac{1}{8} \text{ in}$$

$$r_{inner} = \frac{d_{outer} - 2t_{wall}}{2} = 3.00 \text{ in}$$

$$\sigma_{hoop} = \frac{P_{sf} * (r_{inner} + \frac{t_{wall}}{2})}{t_{wall}} = 44,835 \text{ psi}$$

$$\sigma_{axial} = \frac{P_{sf} * (d_{outer} - t_{wall})}{4t_{wall}} = 22,417.5 \text{ psi}$$

$$\sigma' = \sqrt{\sigma_{hoop}^2 + \sigma_{axial}^2} = 38,828.25 \text{ psi}$$

$$sf = \gamma_s / \frac{1}{2} \sigma' = 35,000 \text{ psi} / (0.5 * 38,828.25 \text{ psi}) = 1.803$$

This factor of safety is below 2, so a 1/8 in wall thickness would not work. This analysis also makes idealized assumptions, such as that there are no stress concentrations in the tank geometry that need to be accounted for. These assumptions are likely not reflective of the actual Oxidizer Tank, and the team had additional concerns about machining a several foot long aluminum cylinder with a 1/8 in thin wall, so a slightly higher wall thickness was tried next. The second wall thickness value used was 3/16 in.

$$t_{wall} = \frac{3}{16} \text{ in}$$

$$r_{inner} = \frac{d_{outer} - 2t_{wall}}{2} = 2.9375 \text{ in}$$

$$\sigma_{hoop} = \frac{P_{sf} * (r_{inner} + \frac{t_{wall}}{2})}{t_{wall}} = 29,585 \text{ psi}$$

$$\sigma_{axial} = \frac{P_{sf} * (d_{outer} - t_{wall})}{4t_{wall}} = 14,792.5 \text{ psi}$$

$$\sigma' = \sqrt{\sigma_{hoop}^2 + \sigma_{axial}^2} - \sigma_{hoop}\sigma_{axial} = 25,621.36 \text{ psi}$$

$$sf = \gamma_s / \frac{1}{2}\sigma' = 35,000 \text{ psi} / (0.5 * 25,621.36 \text{ psi}) = 2.732$$

This stress is significantly below the yield strength of Aluminum 6061-T6, meaning that this wall thickness value meets the team's needs. Since this was the smallest standardized value that meets the safety requirements, 3/16 in was chosen to be the wall thickness of the entire Oxidizer Tank.

2. Injection Bulkhead Assembly Calculations

2.1 Injection Bulkhead Wall Stress Calculations

The Combustion Chamber pressure is expected to be 500 psi ($P = 500 \text{ psi}$). The outer diameter of the bulkhead is 2.5 in ($r_{out} = 2.5 \text{ in}$). The wall thickness is 0.3 in, except at the O-ring grooves where the wall thickness is 0.19 in. As a result, the Injection Bulkhead is more likely to fail at the O-ring grooves before it fails anywhere else.

In order to account for this worst case scenario, the bulkhead will be treated as a cylinder with wall thickness $t = 0.19 \text{ in}$. This allows the team to use the thin wall cylinder assumption, as the radius to wall thickness ratio is greater than 10 ($r_{out} / t = 13.16$).¹⁶ Using this assumption, the maximum hoop stress is given by:

$$\sigma_h = \frac{P(r_{out} - 0.5t)}{t} = \frac{500 \text{ psi} (2.5 \text{ in} - 0.5 \cdot 0.19 \text{ in})}{0.19 \text{ in}} = 6328.95 \text{ psi}^{16}$$

Meanwhile, the axial stress is given by the following expression:

$$\sigma_{ax} = \frac{P(r_{out} - t)}{2t} = \frac{500 \text{ psi} (2.5 \text{ in} - 0.19 \text{ in})}{2 \cdot 0.19 \text{ in}} = 3039.47 \text{ psi}$$

The Von Mises Stress is thereby:

$$\sigma' = \sqrt{\sigma_h^2 + \sigma_{ax}^2} - \sigma_h \sigma_{ax} = 5482.45 \text{ psi}$$

The yield strength of Aluminum 6061-T6 in tension is 35,000 psi, and so the Injection Bulkhead's wall thickness is sufficient to guarantee a safety factor of above two.

$$SF = \frac{\sigma_{AL}}{\sigma'} = \frac{35,000 \text{ psi}}{5482.454 \text{ psi}} = 6.384$$

Throughout the burn, cold nitrous oxide will be flowing through the bulkhead. However, the aft section of the bulkhead will also be exposed to the hot combustion chamber gases. The team has not developed a heat transfer model for the bulkhead and the temperature of the combustion gases or the temperature of the nitrous oxide in the tank are unknown. However, using the Von Mises stress above and information about the yield strength of aluminum 6061-T6, the temperatures at which the factor of safety will fall below two can be predicted.

The safety factor equals 2 when the yield strength of 6061-T6 equals 10,965 psi. At 399°F (204°C) the yield strength of 6061-T6 is 19,000 psi, while at 500°F (260°C) the yield strength is 7,400 psi²². Using linear interpolation, the temperature at which the yield strength of 6061-T6 reaches 10,965 psi can be approximated.

$$10,965 \text{ psi} = \frac{7,400 \text{ psi} - 19,000 \text{ psi}}{500^\circ\text{F} - 399^\circ\text{F}} (T - 399^\circ\text{F}) + 19,000 \text{ psi}$$

$$T = -8,035 \text{ psi} \left(\frac{500^\circ\text{F} - 399^\circ\text{F}}{7,400 \text{ psi} - 19,000 \text{ psi}} \right) + 399^\circ\text{F} = 469^\circ\text{F}$$

As the temperature of 6061-T6 decreases, its yield strength increases. Thus, the team does not need to worry about the factor of safety being less than two if the nitrous cools the bulkhead more than the combustion chamber gases heat it up.

2.2 Oxidizer Feed Conduit Calculations

2.2.1 Oxidizer Feed Conduit Radius Calculation

To ensure that the Oxidizer Feed Conduit does not limit the flow of oxidizer, its cross-sectional area must be larger than the cross-sectional area of all of the holes in the Injector Plate. The total injection area was calculated below:

$$\text{Total Injection Area} = 21 * \pi r^2 = 21 * \pi \left(\frac{1}{2} * 0.0925 \text{ in} \right)^2 = 0.1411 \text{ in}^2$$

Therefore, the minimum conduit radius could be calculated:

$$\begin{aligned} \text{Total Conduit Area} &= \pi r^2 \\ 0.1411 &= \pi r^2 \\ r_{min} &= 0.212 \text{ in} \end{aligned}$$

The actual conduit radius was chosen to be slightly larger than the minimum radius to reduce the probability of the conduit being a limiting factor in the flow of nitrous. To ensure that the conduit could be machined with a standard drill bit, the radius was chosen to be 0.21875 in (which corresponds to a 7/16 in diameter drill bit), with a total conduit area of:

$$Total\ Conduit\ Area = \pi (0.22655\ in)^2 = 0.161\ in^2$$

2.2.2 Oxidizer Feed Conduit Pressure Drop Calculations

The total pressure drop between the Oxidizer Tank and the Combustion Chamber is given by the following summation:

$$\Delta P_{total} = \Delta P_{FC} + \Delta P_{ML} + \Delta P_{plate}$$

Where:

- ΔP_{total} = total pressure drop between the Oxidizer Tank and the Combustion Chamber (assumed 250 psi)
- ΔP_{FC} = Loss in pressure due to the oxidizer flow area contraction between the Aft Dome and the Oxidizer Feed Conduit, friction throughout the Oxidizer Feed Conduit, and flow area expansion between the Oxidizer Feed Conduit and the Pre-Injection Chamber
- ΔP_{ML} = major-loss pressure drop across the pre-injection chamber (psi)
- ΔP_{plate} = pressure drop across the Injector Plate (psi)

If the major losses in the conduit and Pre-Injection Chamber are small, then the pressure difference can be more accurately computed using a thick orifice model. The result of these computations can be used to solve for the effective pressure drop across the Injector Plate at the target mass flow rate (of 3.4221 lb/sec), so the injector can be sized to compensate for the reduction in flow due to the upstream losses.

The team will use a thick orifice model to calculate the pressure losses in the feed line. The thick orifice model prioritizes the pressure losses due to expansion and contraction over the pressure losses due to friction, but takes into account all of these three losses. Using this model allows the team to perform a single calculation to determine the pressure loss across the oxidizer feed line. Otherwise, the team would have to perform a major pressure loss calculation for the friction losses, and two minor pressure loss calculations for the expansion and contraction. It will first be shown that the pressure losses due to friction are negligible and thus the thick orifice model can be used.

The pressure drop due to major losses in the conduit and the pre-injection chamber was calculated using the Darcy-Weisbach friction loss equation:

$$\Delta P_{major-loss} = f(l/d_h)(\rho u^2/2)$$

Where:

- f = friction factor
- l = length of the flow channel
- d_h = flow channel hydraulic diameter
- ρ = density of the liquid nitrous oxide = 0.0283961 lb/in³ (or 786 kg/m³, assumes 70°F, corresponding to the Injector Plate's 750 psi design pressure. Until the team tests the engine or develops a high-fidelity tanking and de-tanking thermodynamic model, it is not possible to know the average oxidizer feed pressure. For now, the team assumes this pressure is 750 psi, corresponding to nitrous oxide at 70°F)
- u = oxidizer flow velocity

The first major-loss pressure drop calculated was the conduit pressure drop. The conduit has the following geometric parameters:

- $l = 0.925\ in$
- $d_h = 0.4531\ in$

First, the conduit's friction coefficient (a function of Reynold's number) and relative roughness were found.

$$Re = \frac{\rho u D}{\mu}$$

Where:

- u = fluid velocity

D = conduit inner diameter = 0.4375 in
 μ = dynamic viscosity of the liquid nitrous oxide

The dynamic viscosity of the saturated liquid nitrous oxide at 70°F (21.11°C) was calculated using the following curve-fit equation from nitrous oxide steam tables, where θ is a coefficient that compares the critical temperature of Nitrous to the current temperature:⁴

$$\mu = 0.0293423 \cdot \exp[(1.6089)(\theta - 1)^{1/3} + (2.0439)(\theta - 1)^{4/3}],$$

$$\text{where } \theta = (36.42^\circ\text{C} - 5.24)/(T - 5.24)$$

$$\theta = (36.42^\circ\text{C} - 5.24)/(21.11 - 5.24)$$

$$\theta = 1.9647$$

$$\mu = 0.0293423 \cdot \exp[(1.6089)(1.9647 - 1)^{1/3} + (2.0439)(1.9647 - 1)^{4/3}]$$

$$\mu = 1.0093 \times 10^{-3} \text{ Pa} \cdot \text{s}$$

The fluid velocity can be found from a simple mass flow through a circular cross section calculation. With this value, the Reynolds number can be calculated.

$$u = \frac{\dot{m}}{\rho A} = \frac{4\dot{m}}{\rho \pi D^2} = \frac{4(5.132 \text{ lb/s})}{(0.0283961 \text{ lb/in}^3)\pi(0.4531 \text{ in})^2} = 1120.86 \text{ in/s}$$

$$Re = \frac{\rho u D}{\mu}$$

$$= \frac{(0.0283961 \text{ lb/in}^3)(27679 \text{ (kg/m}^3)/(\text{lb/in}^3))(1120.86 \text{ in/s})(0.0254 \text{ m/in})(0.4531 \text{ in})}{(1.0093 \times 10^{-3} \text{ Pa} \cdot \text{s})}$$

$$Re = 255198$$

The relative roughness of the oxidizer feed line was then calculated using the average absolute roughness of finished 6061 aluminum and the hydraulic diameter:

$$\text{Relative Roughness} = \frac{\epsilon}{D_h}$$

$$\text{Relative Roughness} = \frac{0.0015 * 10^{-3} \text{ m}}{0.4531 \text{ in} (0.0254 \text{ m/in})}$$

$$\text{Relative Roughness} = 0.0001303$$

Using both the Reynolds number of the system and the relative roughness, the Colebrook Equation was used to find the appropriate Darcy friction factor. The resulting friction factor is:

$$f = 0.0164$$

Plugging this value into the original pressure loss equation yields:

$$\Delta P_{major-loss} = 0.0164 \left(\frac{0.925}{0.4531} \right) \left(\frac{(0.0283961 \text{ lb/in}^3)(27679 \text{ (kg/m}^3)/(\text{lb/in}^3))(1120.86 \text{ in/s} * 0.0254 \text{ m/in})^2}{2} \right)$$

$$\Delta P_{major-loss} = 1.581 \text{ psi}$$

This pressure drop is pretty negligible, so the team is able to use the thick orifice²³ model to find the pressure drop throughout this system. The mass flow rate through a thick orifice is given by the equation below. Here, \dot{m} represents the mass flow rate, C_d represents the discharge coefficient through the orifice, ΔP is the pressure drop across the orifice, ρ is the density, A_1 is the area of the pipe that the fluid travels through before and after passing through the orifice, and σ is the ratio of the area of the orifice to the area of the pipe.

$$\dot{m} = \frac{C_d A_1}{\sqrt{\frac{1}{\sigma^2} - 1}} \sqrt{2 \cdot \Delta P \cdot \rho} \Leftrightarrow \Delta P = \frac{1}{2\rho} \left(\frac{\dot{m} \sqrt{\frac{1}{\sigma^2} - 1}}{C_d A_1} \right)^2$$

$$\sigma = \frac{A_0}{A_1} = \left(\frac{d_0}{d_1} \right)^2$$

$$\sigma_c = \frac{1}{0.639(1 - \sigma)^{0.5} + 1}$$

$$C_d = \sqrt{\frac{1 - \sigma^2}{\left(\frac{1}{\sigma_c} - 1 \right)^2 + (1 - \sigma)^2}}$$

This calculation is done in the MATLAB script titled “conduit_calculations”. It resulted in a pressure drop of 59.75 psi across the conduit.

Meanwhile, the major losses through the Pre-Injection Chamber can be approximated using an incompressible, turbulent, single phase model for liquid nitrous oxide. In other words, the pressure loss across the Pre-Injection Chamber can be found using the following equation:

$$\Delta P_{ML} = f(l/d_h)(\rho u^2 / 2)$$

Where:

f = friction coefficient

l = length of the flow channel = 1.1750 in (length of Pre-Injection Chamber)

d_h = flow channel hydraulic diameter = 2.05 (diameter of Pre-Injection Chamber)

ρ = density of the liquid nitrous oxide = 0.0283961 lb/in³ (or 786 kg/m³, assumes 70°F, corresponding to the Injector Plate’s 750 psi design pressure)

u = oxidizer flow velocity

Since the desired oxidizer mass flow rate is $\dot{m} = 5.132 \text{ lb/s} = 2.328038 \text{ kg/s}$, the oxidizer flow velocity can be determined as follows:

$$u = \frac{\dot{m}}{\rho A} = \frac{4\dot{m}}{\rho \pi d_h^2} = \frac{4 \cdot 5.132 \text{ lb/s}}{0.0283961 \text{ lb/in}^3 \cdot \pi \cdot 2.05^2 \text{ in}^2} = 54.76 \text{ in/s}$$

The friction coefficient is a function of Reynold's number and the relative roughness of the Pre-Injection Chamber. As a result, the team must calculate these parameters before determining the value of the friction coefficient. These parameters can be found using the equations below:

$$Re = \frac{\rho u d_h}{\mu} \text{ and } Rr = \frac{\epsilon}{d_h}$$

Where:

Re = Reynold's number

u = fluid velocity = 54.76 in/s

d_h = conduit inner diameter = 2.05 in

μ = dynamic viscosity of the liquid nitrous oxide

R_r = Relative roughness

ϵ = average absolute roughness of finished 6061 aluminum = $0.0015 \times 10^{-3} \text{ m}$

The dynamic viscosity of the saturated liquid nitrous oxide at 70°F (21.11°C) will be the same as the value already calculated for the major loss through the conduit and Pre-Injection Chamber, $\mu = 1.0093 \times 10^{-3} \text{ Pa} \cdot \text{s}$. Thus, the Reynolds number and relative roughness are:

$$Re = \frac{(0.0283961 \text{ lb/in}^3)(27679 \text{ (kg/m}^3)/(\text{lb/in}^3))(54.76 \text{ in/s})(0.0254 \text{ m/in})(2.05 \text{ in})(0.0254 \text{ m/in})}{1.0093 \times 10^{-3} \text{ Pa} \cdot \text{s}}$$

$$Re = 56399.28$$

$$Rr = \frac{0.0015 \cdot 10^{-3} \text{ m}}{2.05 \text{ in} \cdot 0.0254 \text{ m/in}} = 2.880737469 \times 10^{-5}$$

Using these two parameters, the Colebrook Equation was used to find the friction coefficient:

$$f = 0.0235$$

Plugging this value into the original pressure loss equation results in:

$$\Delta P_{ML} = 0.022371 \left(\frac{1.1750 \text{ in}}{2.05 \text{ in}} \right) \cdot 0.5 (786 \text{ kg/m}^3 \cdot 36.51 \text{ in/s} \cdot 0.0254 \text{ m/in})$$

$$\Delta P_{ML} = 6.829 Pa = 0.000991 psi$$

Using these values, and the assumption that the total pressure drop would equate to 250 psi, the pressure drop across the Injector Plate can be derived:

$$\Delta P_{plate} = \Delta P_{total} - \Delta P_{FC} - \Delta P_{ML}$$

$$\Delta P_{plate} = 250 psi - 59.75 psi - 0.000991 psi = 190.25 psi$$

2.3 Injector Plate Retention

The team will use 12 ($n = 12$) 1/4 in - 20 grade 8 bolts to retain the injector plate ($d = 0.25 in$ and $N = 20$). The tensile stress area of the bolt is $A_t = 0.0318 in^2$. The washer thickness is $t_0 = 0.065 in$. The injector plate thickness is $t_1 = 0.5 in$. Thus, the minimum bolt length is $L > t_0 + t_1 + 1.5d \Leftrightarrow L > 0.94$ ¹⁶. As a result, a bolt length of $L = 1 in$. Consequently, the length of the bolt that threads into the Injection Bulkhead is $t_2 = 0.435 in$.

The minimum major diameter of the bolt's threads (with helical inserts) is: $D_s = 0.31 in$ ³⁰. Meanwhile, the maximum pitch diameter of the internal threads (using helical inserts) is $E_n = 0.2864 in$ ³⁰. The length of thread engagement is $L_e = \min\{t_2, d\} = 0.25 in$. The shear area of internal threads is given by:

$$A_n = N \cdot \pi \cdot L_e \cdot D_s \left(\frac{1}{2N} + 0.57735(D_s - E_n) \right)$$
³¹

$$\begin{aligned} A_n &= 20\pi \cdot 0.25 in \cdot 0.31 in \cdot \left(\frac{1}{2(20)} + 0.57735(0.31 in - 0.2864 in) \right) \\ &= 0.18809 in^2 \end{aligned}$$

The stress acting on the internal threads is equal to the sum of the forces acting on the bolts, divided by the shear area of the internal threads. The forces acting on the bolts are the preload and the force resulting from the nitrous oxide pushing the injector plate against the bolts. The latter is maximized before ignition. At this point, the nitrous in the Pre-Injection Chamber applies a pressure of up to 915 psi on the injector plate and there is no chamber pressure to act against this. Thus, the stress on the internal threads is:

$$\sigma_{tint} = \frac{CF_{IP}}{nA_n} + \frac{F_{PL}}{A_n} = \frac{CA_P \cdot 915 psi}{nA_n} + \frac{F_{PL}}$$
³²

Where C is the fraction of the load carried by the bolts, F_{IP} is the force resulting from the nitrous pressure, n is the number of bolts, F_{PL} is the preload force and A_P is the area under nitrous pressure. Since the team will not be applying a proper preload to the bolts, in the worst case, the bolts will carry all of the load and so $C = 1$. The area under pressure includes the entirety of the pre-injection chamber and the area between the pre-injection chamber and the first O-ring on the bottom face of the Injection Bulkhead. This combined area has a radius of 1.242 in. Thus:

$$\sigma_{tint} = \frac{1 \cdot \pi \cdot 1.242^2 in^2 \cdot 915 psi}{12 \cdot A_n} + \frac{F_{PL}}{A_n} = \frac{369.5157144 lbf + F_{PL}}{0.18809 in^2}$$

A factor of safety of two must be obtained. Since the shear yield strength of 6061-T6 is equal to $\sigma_{SAL} = 0.577(35,000 psi) = 20,195 psi$ the following expression is used:

$$sf = \frac{\sigma_{SAL}}{\sigma_{tint}} \Leftrightarrow 2 = \frac{20,195 psi}{\sigma_{tint}} \Leftrightarrow 2 \left(\frac{369.5157144 lbf + F_{PL}}{0.18809 in^2} \right) = 20,195 psi$$

$$F_{PL} = \frac{1}{2} \cdot 20,195 \text{ psi} \cdot 0.18809 \text{ in}^2 - 369.515744 = 1,529.7 \text{ lbf}$$

Using this value, the preload torque can be obtained using the following equation:

$$T = \frac{K \cdot F_{PL} \cdot d}{1.35} = \frac{0.2 \cdot 1,529.723 \text{ lbf} \cdot 0.020833 \text{ ft}}{1.35} = 4.721 \text{ lbf} \cdot \text{ft}^{16}$$

Where $K = 0.2$ is the nut factor, and $d = 0.25 \text{ in} = 0.02083333 \text{ ft}$ is the nominal diameter of the bolt. This number is divided by 1.35 because torque wrenches can have an error of up to 35%. This is necessary in order to avoid applying excessive torque and losing the factor of safety of 2.

Now that a preload value is obtained, the factor of safety on the bolts themselves can also be determined. The tensile stress (τ_{bolt}) on the bolts is equal to the sum of the stress resulting from the pressure applied by the nitrous oxide on the Injector Plate, and the stress resulting from the preload.

$$\tau_{bolt} = \frac{CF_{IP}}{nA_t} + \frac{F_{PL}}{A_t} = \frac{369.5157144 \text{ lbf}}{0.0318 \text{ in}^2} + \frac{1,529.723 \text{ lbf}}{0.0318 \text{ in}^2} = 59,573.69 \text{ psi}^{16}$$

The proof strength of a grade 8 bolt is 120,000 psi¹⁶ and so the factor of safety is:

$$sf = \frac{120,000 \text{ psi}}{59,573.69199 \text{ psi}} = 2.014$$

3. Tank Vent/Relief System Calculations

3.1 Clark Cooper EH30-042-D012-OXCY Vent Valve Flow Capacity Calculations

The vent valve's flow capacity was calculated to judge whether it could be used as a redundant emergency vent valve in the event of an Oxidizer Tank overpressurization. The valve is connected to the tank's dip tube, so it may flow liquid nitrous oxide at the start of a vent event, but the majority of the flow will be gaseous once the liquid level dips below the dip tube. Therefore, the inlet fluid conditions at the valve were assumed to be 100% gaseous nitrous oxide at 915 psig and 86°F, which is the maximum allowable working pressure of the tank and the corresponding saturation temperature of the nitrous oxide. This results in the following set of properties for the nitrous oxide flow:

Table 20. Nitrous oxide inlet flow properties for valve flow capacity calculations	
Quality	1.0
Upstream Pressure (P ₁) - psia	929.7
Temperature (T ₁) - °R	546
Gas Specific Heat Ratio (k) ²⁴	1.302256
Molar Mass (M) - g/mol	44.0

The first step in the analysis is to determine if the pressure drop across the valve is large enough to induce sonic or "choked" flow inside the valve. The critical downstream pressure to induce choked flow (P*) was calculated using the equation below²⁵.

$$P^* = P_1 \left(\frac{2}{k+1} \right)^{(k/(k-1))}$$

$$P^* = (915) \left(\frac{2}{1.302256 + 1} \right)^{(1.302256/(1.302256-1))}$$

$$P^* = (915) \left(\frac{2}{1.302256 + 1} \right)^{(1.302256/(1.302256-1))}$$

$$P^* = 499.0 \text{ psig}$$

The downstream pressure of the valve is atmospheric pressure or 0 psig, so gas flow in the valve will be choked. The isentropic flow equations for sonic flow through an orifice were then used to calculate the flow rate through the valve - Q (in SCFH), using its C_v of 0.02²⁵:

$$Q = \frac{A * C_v * P_1}{\sqrt{T_1}}, \text{ where the constant } A = \frac{6413.248}{\sqrt{M}} (\sqrt{k}) \left(\frac{2}{k+1} \right)^{((k/(k-1))-0.5)}$$

$$A = \frac{6413.248}{\sqrt{44}} (\sqrt{1.302256}) \left(\frac{2}{1.302256 + 1} \right)^{((1.302256/(1.302256-1))-0.5)}$$

$$A = 645.526$$

$$Q = \frac{645.526 * 0.02 * 929.7}{\sqrt{546}}$$

$$Q = 513.832 \text{ SCFH at 1 atm and } 70^\circ\text{F}$$

$$Q = 0.016 \text{ lb/sec}$$

This flow rate is well below the 5.121 lb/sec emergency vent requirement, so this valve will only be used to vent the Oxidizer Tank during fill operations. Emergency venting capability will be provided by the tank's relief valve and the high-flow vent valve on the ground support equipment.

3.2 Dip Tube Length Calculations

By knowing the ullage volume needed for the tank, and knowing the calculated volumes of the Forward Bulkhead and the Body Cylinder, the necessary length of the dip tube can be determined. Based on these volumes, it is clear that the entire dome of the Forward Bulkhead will be used as ullage space. Additionally, a portion of the cylindrical part of the Forward Bulkhead will be used as ullage space. The calculation was conducted as follows:

Where, V_{os} = volume of oxidizer required for full burn (1583 in³ assuming nitrous oxide at 86°F)

V_u = ullage volume

V_t = volume of entire oxidizer tank (1663 in³)

L_d = length of dip tube

h_f = height of forward bulkhead dome (2.75 in)

L_u = length of cylinder used as ullage volume

V_f = volume of forward bulkhead dome (51.94 in³)

$r = \text{radius of cylinder, both forward bulkhead \& body cylinder (2.9375 in)}$

$$V_{os} = 1583 \text{ in}^3$$

$$V_u = V_t - V_{os} = 1663 \text{ in}^3 - 1583 \text{ in}^3 = 80 \text{ in}^3$$

$$L_d = h_f + L_u = h_f + \frac{V_u - V_f}{\pi * r^2}$$

$$L_d = 2.75 \text{ in} + \frac{80 \text{ in}^3 - 51.94 \text{ in}^3}{\pi * (2.9375 \text{ in})^2}$$

$$L_{d,7.67 \text{ sec}} = 3.78 \text{ in}$$

3.3 Generant HPRV-500 SS-T-915 Relief Valve Flow Capacity Calculations

The relief valve's flow capacity was calculated to check if it could provide the 5.132 lb/sec flow requirement in case the Oxidizer Tank reaches its emergency vent conditions of 915 psig and 86°F. The relief valve is connected to the Forward Bulkhead of the Oxidizer Tank, so like the vent valve the inlet fluid conditions at the relief valve were assumed to be 100% gaseous nitrous oxide at 915 psig and 86°F. The relevant nitrous oxide properties needed for the flow calculation are given in the table below:

Table 21. Nitrous oxide inlet flow properties for relief valve flow capacity calculations	
Quality	1.0
Upstream Pressure (P ₁) - Pa	6410055.9
Temperature (T) - K	303
Gas Specific Heat Ratio (k) ²⁴	1.302256
Molar Mass (M) - kg/mol	0.044
Compressibility Factor at Given State (Z) ²⁶	0.47

The vent valve flow analysis confirmed that the pressure drop across the relief valve is large enough to induce choked flow. The flow rate Q (kg/sec) through the relief valve was then calculated using the isentropic equations for sonic gas flow through an orifice given the valve's discharge coefficient C_d and orifice area A, which are provided by the relief valve manufacturer.²⁷ The equation uses the terms in the above table and the following additional terms:

- C_d: valve discharge coefficient - 0.2
- A: valve orifice area - 0.000134 m²
- R: ideal gas constant - 8.3145 J/(mol*K)
- g: gravitational acceleration - 9.81 m/s²

- K_b : backpressure correction factor - assumed to be 1.0²⁷

$$Q = C * A * C_d * P_1 * K_b * \sqrt{\frac{M}{T * Z}}, \text{ where } C = \sqrt{\left(\frac{k * g}{R}\right) \left(\frac{2}{k+1}\right)^{(k+1)(k-1)}}$$

$$C = \sqrt{\left(\frac{1.302256 * 9.81}{8.3145}\right) \left(\frac{2}{1.302256 + 1}\right)^{(1.302256+1)(1.302256-1)}}$$

$$C = 1.18031$$

$$Q = (1.18031)(0.000134)(0.2)(6410055.9)(1) \sqrt{\frac{0.044}{(303)(0.47)}}$$

$$Q = 3.575 \text{ kg/sec}$$

$$Q = 7.897 \text{ lb/sec}$$

7.897 lb/sec exceeds the 5.132 lb/sec flow requirement by a factor of 1.5. The same analysis was performed for the next-smallest version of this relief valve with a C_d of 0.27 and an orifice diameter of 0.275 in, but the resulting flow rate was 2.985 lb/sec, which fails to meet the flow requirement. Therefore, the 1/2 in NPT port variant of the valve was selected for the Oxidizer Tank.

4. Oxidizer Tank and Bulkhead Retention

4.1 Orbital Welding Geometry

The most common angles for this kind of weld are 60° - 75°, so 75° was picked for ease of manufacturing. This means that a 37.5° cut will be made on the end of each welded component. Since the Oxidizer Tank is designed to have a 3/16 in wall thickness, the root was determined to be acceptable between the range of 0.03 - 0.09 in. With this range in mind, a calculation can be done to determine the acceptable axial starting point for the angled cut:

$$\text{If root} = 0.03 \text{ in: } x = \tan(37.5) \cdot 0.03 = 0.12085$$

$$\text{If root} = 0.09 \text{ in: } x = \tan(37.5) \cdot 0.09 = 0.074814$$

For further ease of manufacturing, the value of 0.1 in was chosen for the axial starting point. With that dimension, the final root value can be found.

$$y = \frac{0.1}{\tan(37.5)} = 0.130$$

$$\text{root} = (3/16) - 0.130 = 0.0575$$

With this value, the final welding parameters can be set.

4.2 Forward Bulkhead Fasteners

The calculations for the bearing stress and tearout stress on the shoulder screw holes within the Forward Bulkhead as well as shear stress on the shoulder screw can be found below. Additionally, maximum preload torque calculations were performed to determine the maximum torque that can be applied to these bolts during assembly.

An Eclipse mentor suggested designing fasteners that go through the airframe for a 50 G acceleration due to recovery system shock. This shock would occur at apogee, so the weight in consideration is the dry weight of the rocket. Thus, the total force acting on all of the fasteners is equal to the 50 times the dry weight of the rocket:

$$F = 50 * W$$

where W is the dry weight of the total rocket. This bearing stress, and the corresponding safety factor, is calculated below.

4.2.1 Bearing stress calculations on the fastener holes within the Forward Bulkhead

Where: σ_b = bearing stress (*psi*)
 σ_y = 6061-T6 aluminum yield strength in compression (34,000 *psi*)
 SF = factor of safety
 n = number of shoulder screw holes (8)
 t = thickness of oxidizer Forward Bulkhead and pin engagement (0.25 *in*)
 d = hole diameter (0.25 *in*)
 W = dry weight of the total rocket (approximated to be 107 *lb*)

$$\sigma_b = \frac{50 * W}{n * t * d}$$

$$\sigma_b = \frac{50 * 107 \text{ lb}}{8 * 0.25 * 0.25}$$

$$\sigma_b = 10,700 \text{ psi}$$

$$SF = \sigma_y / \sigma_b$$

$$SF = 34,000 \text{ psi} / 10,700 \text{ psi} = 3.18$$

4.2.2 Tearout stress calculations on the fastener holes within the Forward Bulkhead

Where: σ_t = tearout stress (*psi*)
 σ_y = 6061-T6 aluminum yield strength in tension (35,000 *psi*)
 τ = 6061-T6 aluminum shear strength
 SF = factor of safety
 n = number of shoulder screw holes (8)
 t = thickness of Forward Bulkhead and pin engagement (0.25 *in*)
 d = distance of hole from the edge of Forward Bulkhead (0.375 *in*)
 W = dry weight of the total rocket (approximated to be 107 *lb*)

$$\sigma_t = \frac{50 * W}{2 * n * d * t}$$

$$\sigma_t = \frac{50 * 107 \text{ lb}}{2 * 8 * 0.375 \text{ in} * 0.25 \text{ in}}$$

$$\sigma_t = 3566.67 \text{ psi}$$

$$\tau = 0.577 \sigma_y = 0.577(35,000 \text{ psi}) = 20,195 \text{ psi}$$

$$SF = \tau / \sigma_t = 20,195 \text{ psi} / 3566.67 \text{ psi} = 5.66$$

4.2.3 Shear stress calculations on the Forward Bulkhead fasteners

Where: τ_f = shear stress on each fastener (*psi*)
 σ_y = yield strength of alloy steel (140,000 *psi* - as specified by McMaster Carr)
 τ_m = shear strength of alloy steel (*psi*)
SF = factor of safety
n = number of fasteners (8)
 A_f = cross-sectional area of one fastener
 d_f = diameter of one fastener (0.25 *in*)

$$\tau_f = \frac{50 * W}{n * A_f}$$

$$\tau_f = \frac{50 * W}{n * \pi * \left(\frac{1}{2} * d_f\right)^2}$$

$$\tau_f = \frac{50 * 107 \text{ lb}}{8 * \pi * \left(\frac{1}{2} * 0.25 \text{ in}\right)^2}$$

$$\tau_f = 13626.67 \text{ psi}$$

$$\tau_m = 0.577\sigma_y = 0.577(140,000 \text{ psi}) = 80,780 \text{ psi}$$

$$SF = \tau_m / \tau_f = 80,780 \text{ psi} / 13626.67 \text{ psi} = 5.93$$

4.2.4 Maximum preload calculations for Forward Bulkhead fasteners

Normally for bolted connections in shear, a preload of 75% of the bolt proof load would be applied to each bolt to induce a clamping force between the connected components. This clamping force causes substantial friction between the two components, which carries a significant portion of the applied shear load, decreasing the stress in the bolts. The preload also induces a friction force between the bolt head and the component and between the internal and external threads, which stops the bolts from vibrating out of place during high-vibration periods such as engine firing. However, the bolts on this Forward Bulkhead are used in a coaxial cylinder-in-cylinder connection to attach the bulkhead to the airframe. For a radially bolted connection of two cylinders where one cylinder must fit inside the other with some clearance, applying a preload to the bolts does not induce a significant clamping force between the two components, because of the clearance between the rigid cylinders and the equally-preloaded bolt on the opposite side of the cylinder pulling the internal component in the opposite direction. Bolts in this type of connection are effectively pins, and any applied preload only increases the axial stress in the bolt without providing a clamping force that significantly strengthens the joint. The only benefit a preload provides is stopping the bolts from vibrating loose. A required preload also provides a target torque for bolt tightening during engine assembly. Therefore, the Forward Bulkhead bolts (and all other bolts in radially-bolted cylinder-in-cylinder connections on this engine) will only be preloaded to the load such that the stress in the bolt maintains a factor of safety to yield of 2 in the combined shear load with axial preload. The resulting preload will be much less than the standard 75% proof load value, so each bolt will also be secured with a medium-strength thread-locking adhesive to prevent the bolts from vibrating out of place.

The von Mises equivalent stress in the bolts is given by the following equation (where σ_a is the axial stress on the bolt caused by preloading)¹⁰:

$$\sigma' = \sqrt{\sigma_a^2 + 3\tau^2}$$

In order to achieve a factor of safety of 2, the von Mises stress must equal half of the yield strength of the bolts ($\sigma_y = 140,000 \text{ psi}$). Also, note that the axial stress on the bolts is equal to the ratio of the force of the preload $F_{preload}$ to the area of the bolt. In this case, the area is taken to be 0.0137 in^2 , based on the minimum diameter of the shoulder screw (the section between the shoulder and the threaded area). Based on the calculations shown above, the shear stress of the Forward Bulkhead fasteners is $\tau_f = 18164.88 \text{ psi}$. As a result, the preload force is found below:

$$F_{preload} = A_f \sqrt{(0.5 \cdot \sigma_y)^2 - 3\tau_f^2}$$

$$F_{preload} = 0.0137 \text{ in}^2 \sqrt{(0.5 * 140,000 \text{ psi})^2 - 3 * (13626.67 \text{ psi})^2}$$

$$F_{preload} = 902.8 \text{ lbf}$$

The preload torque is related to the preload force by the expression below. Here, $d = 0.132$ is the minimum diameter of the bolt and K is the nut factor which equals 0.2 for black oxide-finish fasteners¹⁰.

$$T = K \cdot F_{preload} \cdot d$$

$$T = 0.2 * 902.8 \text{ lbf} * 0.132 \text{ in}$$

$$T = 23.8 \text{ lbf} \cdot \text{in}$$

However, the torque that can be applied by a torque wrench on an unlubricated bolt can vary by up to 35%²⁹, so a worst case scenario was assumed where the fasteners are over tightened by 35%. With this, the maximum preload torque is calculated as follows:

$$T_{max} = 23.8 \text{ lbf} \cdot \text{in} / 1.35 = 17.65 \text{ lbf} \cdot \text{in} = 1.47 \text{ lbf} \cdot \text{ft}$$

4.3 Injection Bulkhead Fasteners

To ensure that the chosen fasteners were sufficient for attaching the Injection Bulkhead to the Combustion Chamber, three calculations were performed -- shear stress on the shoulder screw as well as tearout stress and bearing stress on the holes within the Injection Bulkhead. Additionally, maximum preload torque calculations were performed to determine the maximum torque that can be applied to these bolts during assembly.

To determine the force applied, it is assumed that the Injection Bulkhead will be pushed upward from the pressure of the Combustion Chamber. Therefore, this load will be distributed evenly into the components and into the fasteners that hold the components in place on the forward end of the Combustion Chamber. The maximum applied force will occur during a hydrostatic test of the Combustion Chamber, so the thrust of the rocket during launch is not accounted for. Additionally, during a hydrostatic test, the injection holes will be solid material, so in these calculations, it is assumed that the total area used is the cross-sectional area of the inside of the Combustion Chamber. Based on these conservative assumptions, the total force on the fasteners is equal to:

$$F = P * A_{cc} = P * \pi * \left(\frac{1}{2} * d_{cc}\right)^2$$

where P is the pressure from the Combustion Chamber, A_{cc} is the cross-sectional area of the Combustion Chamber and d_{cc} is the internal diameter of the Combustion Chamber.

4.3.1 Bearing stress calculations on the fastener holes within the Injection Bulkhead

The number and dimension of pin engagement of the fasteners holes in the Injection Bulkhead are identical to that of the Combustion Chamber. Therefore, the bearing stress on both the Combustion Chamber holes and the Injection Bulkhead holes are identical. For the purpose of brevity, the calculations are only included once, and can be found in *Calculation C.2.2*.

4.3.2 Tearout stress calculations on the fastener holes within the Injection Bulkhead

In these tearout stress calculations on the Injection Bulkhead fastener holes, the distance from the center of the holes to the nearest edge of the O-Ring groove that is directly aft the fastener holes was used.

Where: σ_t = tearout stress (*psi*)

P = chamber pressure (*500 psi*)

d_{cc} = diameter of Combustion Chamber (*5.0 in*)

n = number of shoulder screw holes (*24*)

t = thickness of Injection Bulkhead and pin engagement (*0.125 in*)

d = distance from center of hole to edge of O-Ring groove (*0.37 in*)

SF = factor of safety

σ_y = 6061-T6 aluminum yield strength in tension (*34,000 psi*)

$$\sigma_t = \frac{P * \pi * \left(\frac{1}{2} * d_{cc}\right)^2}{2 * n * d * t}$$

$$\sigma_t = \frac{(500 \text{ psi}) * \pi * \left(\frac{1}{2} * 5.0 \text{ in}\right)^2}{2 * 24 * 0.125 \text{ in} * 0.37 \text{ in}}$$

$$\sigma_t = 4422.3$$

$$\tau = 0.577\sigma_y = 0.577(35,000 \text{ psi}) = 20,195 \text{ psi}$$

$$SF = \tau / \sigma_t = 19,618 \text{ psi} / 4422.3 \text{ psi} = 4.567$$

4.3.3 Shear stress on the Injection Bulkhead fasteners

Where: τ_f = shear stress on each fastener (*psi*)

σ_y = yield strength of alloy steel (*140,000 psi* - as specified by McMaster Carr)

τ_m = shear strength of alloy steel (*psi*)

P = chamber pressure (*500 psi*)

d_{cc} = diameter of Combustion Chamber (*5.0 in*)

SF = factor of safety

n = number of shoulder screw holes (*24*)

A_f = cross-sectional area of one fastener

d_f = diameter of one fastener (*0.25 in*)

$$\tau_f = \frac{F}{n * A_f} = \frac{P * \pi * (\frac{1}{2} * d_{cc})^2}{n * A_f}$$

$$\tau_f = \frac{P * \pi * (\frac{1}{2} * d_{cc})^2}{n * \pi * (\frac{1}{2} * d_f)^2}$$

$$\tau_f = \frac{(500 \text{ psi}) * \pi * (\frac{1}{2} * 5.0 \text{ in})^2}{24 * \pi * (\frac{1}{2} * 0.25 \text{ in})^2}$$

$$\tau_f = 8333.33 \text{ psi}$$

$$\tau_m = 0.577\sigma_y = 0.577(140,000 \text{ psi}) = 80,780 \text{ psi}$$

$$SF = \tau_m / \tau_f = 69,240 \text{ psi} / 8333.33 \text{ psi} = 9.694$$

4.3.4 Maximum preload calculations for Injection Bulkhead fasteners

Based on the same reasoning and process as discussed above in this *Appendix, Calculation B.4.2.4* with the Forward Bulkhead fasteners, the maximum preload force that could be applied to the Injection Bulkhead fasteners was calculated.

Where: σ' = von Mises equivalent stress (psi)

σ_a = axial stress on bolt caused by preloading (psi)

σ_y = yield strength of fastener (140,000 psi)

$F_{preload}$ = force of the preload

A_f = minimum cross-sectional area of fastener (0.0137 in²)

τ_f = shear stress on fastener (8333.3 psi)

T = torque

T_{max} = maximum torque

K = nut factor (0.2 for black oxide finish)

d = diameter of bolt

$$\sigma' = \sqrt{\sigma_a^2 + 3\tau^2}$$

$$F_{preload} = A_f \sqrt{(0.5 \cdot \sigma_y)^2 - 3\tau_f^2}$$

$$F_{preload} = 0.0137 \text{ in}^2 \sqrt{(0.5 * 140,000 \text{ psi})^2 - 3 * (8333.3 \text{ psi})^2}$$

$$F_{preload} = 938.39 \text{ lbf}$$

$$T = K \cdot F_{preload} \cdot d$$

$$T = 0.2 * 938.39 \text{ lbf} * 0.132 \text{ in}$$

$$T = 24.77 \text{ lbf} \cdot \text{in}$$

$$T_{max} = 24.77 \text{ lbf} \cdot \text{in} / 1.35 = 18.35 \text{ lbf} \cdot \text{in} = 1.53 \text{ lbf} \cdot \text{ft}$$

C. Thrust Chamber Assembly Calculations

1. Fuel Grain Calculations

1.1. Fuel Grain Initial Radius

Knowing that the final port radius was fixed to 2 in to leave a safe amount of fuel remaining at the end of the burn, the equation for the port radius as a function of time can be rewritten to solve for the initial port radius as the following function of the final port radius and the length of the burn,

Where:

m'_{ox} = the mass flow rate of oxidizer (lb/s)

r_{fin} = the radius of the fuel grain port at the end of the burn (in)

r_0 = the initial port radius (in)

a = an experimentally determined constant (taken from Luna analysis)

n = an experimentally determined constant (taken from Luna analysis)

t_f = the time at the end of the burn (seconds)

$$r_0 = \left[-(2n + 1) \cdot t_f \cdot a \cdot \left(\frac{m'_{ox}}{\pi} \right)^n + r_{fin}^{2n+1} \right]^{\frac{1}{2n+1}}$$

This computation was done in the MATLAB script titled “Titan_II_Regression” (*Appendix X*). The initial radius was calculated to be 1.1353 in, which corresponds to an average regression rate of 0.1129 in/s.

1.2. Optimal Fuel Grain Length

The initial port radius, final port radius, burn time, and fuel density give the team a model for the mass flow rate of fuel per unit length. Since the optimal mass flow rate is known due to a fixed oxidizer to fuel ratio, the grain length that gives this rate can be calculated with the following equation,

Where:

L^* = optimal Fuel Grain length (in)

m'_{fuel} = optimal average mass flow rate of fuel (lb/s)

t = length of burn (s)

ρ = fuel density (lb/in³)

r_0 = initial port radius (in)

r_{fin} = final port radius (in)

$$L^* = \frac{m'_{fuel} \cdot t}{\pi(r_{fin}^2 - r_0^2) \cdot \rho}$$

This computation was done in the MATLAB script titled “Titan_II_Regression” (*Appendix X*). Using the average fuel mass flow rate is 0.913 lb/s, the optimal length was found to be 22.54 in.

1.3. Fuel Grain Penetration Length

To verify the fuel grain's ability to insulate the Combustion Chamber, its penetration length was calculated. Using a steady-state ablation conduction heat transfer model, the characteristic penetration length of the combustion temperature into the regressing Fuel Grain is given by the following equation,

Where:

L^* = combustion temperature penetration length (m)
 k = fuel thermal conductivity (W/m*K)
 ρ = fuel density (kg/m³)
 c = fuel specific heat capacity (J/kg*K)
 $\frac{dr}{dt}$ = average Fuel Grain regression rate (0.00287 m/s)

$$L^* = \frac{k}{\rho c (dr/dt)}$$

The fuel's thermal conductivity is estimated to be that of pure HTPB, which is 0.22 W/(m*K) or 0.027 lbf/(R*s). The exact heat capacity of the fuel composition is unknown, so the $\rho * c$ term of the equation is approximated by the value $2*10^6$ J/(m³*K) or 158 lbf/(in²*R), which is valid for most fully-dense solids at or above room temperature. The regression rate is assumed to be the average rate found from the model above.

$$L^* = \frac{0.027 \text{ lbf}/(R * s)}{(158 \text{ lbf}/(\text{in}^2 * R))(0.1129 \text{ in}/s)}$$

$$L^* = 0.00152 \text{ in}$$

2. Combustion Chamber Calculations

The chamber wall thickness and outer diameter were selected by examining the pressure-induced hoop stress and the pressure-induced bearing stress experienced in the fastener holes. The amount and diameter of the fastener holes on either end of the Combustion Chamber were also selected by examining the pressure-induced bearing stress.

2.1. Combustion Chamber Hoop Stress Calculations

Where: σ_h = hoop stress (psi)
 σ_y = 6061-T6 aluminum yield strength in tension (35,000 psi)
SF = factor of safety
 P_c = internal Combustion Chamber pressure (500 psi)
 t = Combustion Chamber wall thickness (0.125 in)
 r_i = Combustion Chamber inner radius (2.5 in)

Solving for the factor of safety on hoop stress assuming a wall thickness of 0.125 in,

$$\sigma_h = \frac{(P_c)(r_i + t)}{t}$$
$$\sigma_h = \frac{(500 \text{ psi})(2.5 + 0.125)}{0.125}$$
$$\sigma_h = 10,500 \text{ psi}$$
$$SF = \sigma_y / \sigma_h$$

$$SF = 35,000 \text{ psi} / 10,500 \text{ psi}$$

$$SF = 3.33$$

2.2. Combustion Chamber Holes Bearing Stress Calculations

Where: σ_b = bearing stress (psi)

P = chamber pressure (500 psi)

d_{cc} = diameter of Combustion Chamber (5.0 in)

n = number of shoulder screw holes (24)

t = thickness of Injection Bulkhead and pin engagement (0.125 in)

d = hole diameter (0.25 in)

SF = factor of safety

σ_y = 6061-T6 aluminum yield strength in compression (34,000 psi)

$$\sigma_b = \frac{P * \pi * \left(\frac{1}{2} * d_{cc}\right)^2}{n * t * d}$$

$$\sigma_b = \frac{(500 \text{ psi}) * \pi * \left(\frac{1}{2} * 5.0 \text{ in}\right)^2}{24 * 0.125 * 0.25}$$

$$\sigma_b = 13090.0 \text{ psi}$$

$$SF = \sigma_y / \sigma_b$$

$$SF = 34,000 \text{ psi} / 13090.0 \text{ psi} = 2.60$$

2.3 Combustion Chamber Tearout Stress Calculations

Where: σ_t = tearout stress (psi)

σ_y = 6061-T6 aluminum yield strength in tension (35,000 psi)

τ = 6061-T6 aluminum shear strength

SF = factor of safety

n = number of shoulder screw holes (24)

t = thickness of Combustion Chamber and pin engagement (0.125 in)

d = distance of hole from the edge of Combustion Chamber (0.45 in)

F = total force

P = chamber pressure (500 psi)

d_{cc} = diameter of Combustion Chamber (5.0 in)

$$\sigma_t = \frac{F}{2 * n * d * t} = \frac{P * \pi * \left(\frac{1}{2} * d_{cc}\right)^2}{2 * n * d * t}$$

$$\sigma_t = \frac{500 \text{ psi} * \pi * \left(\frac{1}{2} * 2.5 \text{ in}\right)^2}{2 * 24 * 0.45 \text{ in} * 0.125 \text{ in}}$$

$$\sigma_t = 3636.103 \text{ psi}$$

$$\tau = 0.577\sigma_y = 0.577(35,000 \text{ psi}) = 20,195 \text{ psi}$$

$$SF = \tau / \sigma_t = 20,195 \text{ psi} / 3636.103 \text{ psi} = 5.554$$

This is far greater than the minimum safety factor of 2.0. The above calculation determines the tearout stress on the Combustion Chamber's aft end. The same calculation was performed for the forward end, with a distance, d, from the edge of the Combustion Chamber equivalent to 0.5 in. The tearout stress in that situation results in a safety factor that is greater than 5.395, far greater than the minimum safety factor of 2.0.

3. Nozzle Assembly

3.1 Nozzle Insert Radii Calculations

The radius of the throat was determined to be 0.6075 in using the calculations outlined below. In the following equations:

$$F = C_F \cdot A_T \cdot P_c$$

where F is the Engine Thrust, C_F is the Thrust Coefficient, A_T is the Area of the Throat, and P_c is the Combustion Chamber Pressure.

$$C_F = \sqrt{\frac{2k^2}{k-1} \left(\frac{2}{k+1}\right)^{\frac{k+1}{k-1}} \left(1 - \frac{P_e}{P_c}\right)^{\frac{k-1}{k}} + \frac{P_e - P_{amb}}{P_c} \frac{A_e}{A_t}}$$

where, k is the specific heat ratio, P_{amb} is the Ambient Pressure, and P_e is the Exit Pressure.

As the nozzle is being designed for optimal performance at 10,000 ft, the exit pressure equals the ambient pressure at 10,000 ft.

$$P_e - P_{amb} = 10.9 \text{ psi} - 10.9 \text{ psi} = 0$$

Thus,

$$\frac{P_e - P_{amb}}{P_c} \frac{A_e}{A_t} = 0$$

So,

$$C_F = \sqrt{\frac{2k^2}{k-1} \left(\frac{2}{k+1}\right)^{\frac{k+1}{k-1}} \left(1 - \frac{P_e}{P_c}\right)^{\frac{k-1}{k}}}$$

Using the values found in Table 16 in Section V.B,

$$C_F = \sqrt{\frac{2(1.252427)^2}{1.252427 - 1} \left(\frac{2}{1.252427 + 1}\right)^{\frac{1.252427+1}{1.252427-1}} \left(1 - \frac{10.1}{500}\right)^{\frac{1.252427-1}{1.252427}}}$$

$$C_F = 2.0698$$

Returning to the Thrust Equation,

$$F = C_F \cdot A_T \cdot P_c$$

$$A_T = \frac{F}{C_F \cdot P_c}$$

$$A_T = \frac{1200}{(2.0698)(500)}$$

$$A_T = 1.1595 \text{ in}^2$$

$$R = 0.6075 \text{ in}$$

Now that the area of the throat has been found, it is possible to find the exit area using the following equation:

$$\frac{A_T}{A_E} = \left(\frac{k+1}{2}\right)^{\left(\frac{1}{k-1}\right)} \left(\frac{P_e}{P_c}\right)^{\frac{1}{k}} \sqrt{\frac{k+1}{k-1} \left[1 - \left(\frac{P_e}{P_c}\right)^{\left(\frac{k-1}{k}\right)}\right]}$$

By using the new A_T and values outlined above,

1.1595

$$\frac{A_T}{A_E} = \left(\frac{1.252427 + 1}{2}\right)^{\left(\frac{1}{1.252427-1}\right)} \left(\frac{10.1}{500}\right)^{\frac{1}{1.252427}} \sqrt{\frac{1.252427 + 1}{1.252427 - 1} \left(1 - \left(\frac{10.1}{500}\right)^{\left(\frac{1.252427-1}{1.252427}\right)}\right)}$$

Thus,

$$A_E = 7.0146 \text{ in}^2$$

$$R_{Exit} = 1.4943 \text{ in}$$

3.2 Nozzle Casing Fasteners

To ensure that the chosen shoulder screws were sufficient for the Nozzle Casing to the Combustion Chamber connection, three calculations were performed: bearing stress on the Nozzle Casing fastener holes, shear stress on the shoulder screws that fasten the Nozzle Assembly to the Combustion Chamber, as well as tearout stress on the holes within the Nozzle Casing. Additionally, maximum preload torque calculations were performed to determine the maximum torque that can be applied to these fasteners during assembly.

To determine the force applied, it is assumed that the Nozzle Assembly will be pushed downward from the pressure of the Combustion Chamber. Therefore, this load will be distributed evenly into the components and into the fasteners that hold the components in place on the aft end of the Combustion Chamber. The maximum applied force will occur during a hydrostatic test of the Combustion Chamber, so the thrust of the rocket during launch is not accounted for. Additionally, during a hydrostatic test, the nozzle throat will be solid material, so in these calculations, it is assumed that the total area used is the cross-sectional area of the inside of the Combustion Chamber. Lastly, it is assumed that the force is only applied to the pin surface of the fasteners, not the threads or helical inserts. Based on these conservative assumptions, the total force on the fasteners is equal to:

$$F = P * A_{cc} = P * \pi * \left(\frac{1}{2} * d_{cc}\right)^2$$

where P is the pressure from the Combustion Chamber, A_{cc} is the cross-sectional area of the Combustion Chamber and d_{cc} is the internal diameter of the Combustion Chamber.

3.2.1 Bearing stress calculations on the fastener holes within the Nozzle Casing

Where: σ_b = bearing stress (psi)

P = chamber pressure (500 psi)

d_{cc} = diameter of Combustion Chamber (5.0 in)

n = number of shoulder screw holes (24)

t = thickness of Nozzle Casing and pin engagement (0.1875 in)

d = hole diameter (0.25 in)

SF = factor of safety

σ_y = 6061-T6 aluminum yield strength in compression (34,000 *psi*)

$$\sigma_b = \frac{P * \pi * \left(\frac{1}{2} * d_{cc}\right)^2}{n * t * d}$$
$$\sigma_b = \frac{(500 \text{ psi}) * \pi * \left(\frac{1}{2} * 5.0 \text{ in}\right)^2}{24 * 0.1875 \text{ in} * 0.25 \text{ in}}$$
$$\sigma_b = 8726.6 \text{ psi}$$
$$SF = \sigma_y / \sigma_b$$
$$SF = 34,000 \text{ psi} / 8726.6 \text{ psi} = 3.90$$

3.2.2 Tearout stress calculations on the fastener holes within the Nozzle Casing

The section of the Nozzle Casing that decreases in diameter will be referred to as the boattail.

Where: σ_t = tearout stress (*psi*)

P = chamber pressure (500 *psi*)

d_{cc} = diameter of Combustion Chamber (5.0 *in*)

n = number of shoulder screw holes (24)

t = thickness of Nozzle Casing and pin engagement (0.1875 *in*)

d = distance from center of hole to edge of nozzle boattail (0.45 *in*)

SF = factor of safety

σ_y = 6061-T6 aluminum yield strength in tension (35,000 *psi*)

$$\sigma_t = \frac{P * \pi * \left(\frac{1}{2} * d_{cc}\right)^2}{2 * n * d * t}$$
$$\sigma_t = \frac{(500 \text{ psi}) * \pi * \left(\frac{1}{2} * 5.0 \text{ in}\right)^2}{2 * 24 * 0.1875 \text{ in} * 0.45 \text{ in}}$$
$$\sigma_t = 2424.1$$

$$\tau = 0.577\sigma_y = 0.577(35,000 \text{ psi}) = 20,195 \text{ psi}$$

$$SF = \tau / \sigma_t = 20,195 \text{ psi} / 2424.1 \text{ psi} = 8.33$$

3.2.3. Shear stress on the Nozzle Casing fasteners

The strength, number, and size of the Nozzle Casing fasteners are identical to that of the Injection Bulkhead fasteners. Therefore, the shear stress on both the Nozzle Casing fasteners and the Injection Bulkhead fasteners are identical. For the purpose of brevity, the calculations are only included once, and can be found in this *Appendix, Calculation B.4.3.3.*

3.2.4 Maximum preload calculations for Nozzle Casing fasteners

Based on the same reasoning and process as discussed above in this *Appendix, Calculation B.4.2.4* with the Forward Bulkhead fasteners, the maximum preload force that could be applied to the Nozzle Casing fasteners was calculated. As discussed above, the Nozzle Casing fasteners and the Injection Bulkhead fasteners are identical in terms of strength, number, and size. Additionally, the shear stress on the Nozzle Casing fasteners is identical to that of the Injection Bulkhead fasteners. Therefore, the maximum preload that can be applied to the Nozzle Casing fasteners is also identical to that of the Injection Bulkhead fasteners. Again, in the interest of brevity, the calculations are only included once, and can be found in this *Appendix, Calculation B.4.3.4*.

D. Propulsion System Testing

1. Dip Tube Length Calculations for Static Testing

Exactly as was done for the dip tube length calculations for a full 7.67 second burn, the dip tube length can be determined for the 4 and 6 second burns as well. To determine the Ullage volume required for these burns, additional calculations must be performed as well, assuming that the amount of oxidizer required is proportional to the length of the burn. Additionally, unlike the 7.67 second burn, the 4 and 6 second burns will require that the entire Forward Bulkhead as well as a significant portion of the Body Cylinder be used as ullage space.

Where, $V_{os} =$

volume of oxidizer required for burn (1384.64 in³ for full burn assuming nitrous oxide at 68°F)

$t_f =$ *time of a full burn (7.67 seconds)*

$t_s =$ *time of shortened, test burn (4 seconds or 6 seconds)*

$V_{of} =$ *volume of oxidizer required for full burn*

$V_u =$ *ullage volume*

$V_t =$ *volume of entire oxidizer tank*

$L_d =$ *length of dip tube*

$h_f =$ *height of forward bulkhead dome (2.75 in)*

$L_u =$ *length of cylinder used as ullage volume (1663 in³)*

$V_f =$ *volume of forward bulkhead dome (51.94 in³)*

$r =$ *radius of cylinder, both forward bulkhead & body cylinder (2.9375 in)*

1.1 Four second burn

$$V_{os} = \frac{t_s}{t_f} * V_{of} = \frac{4 \text{ sec}}{7.67 \text{ sec}} * 1384.64 \text{ in}^3 = 722.39 \text{ in}^3$$

$$V_u = V_t - V_{os} = 1683 \text{ in}^3 - 722.39 \text{ in}^3 = 960.61 \text{ in}^3$$

$$L_d = h_f + L_u = h_f + \frac{V_u - V_f}{\pi * r^2}$$

$$L_d = 2.75 \text{ in} + \frac{960.61 \text{ in}^3 - 51.94 \text{ in}^3}{\pi * (2.9375 \text{ in})^2}$$

$$L_{d,4 \text{ sec}} = 36.27 \text{ in}$$

1.2 Six second burn

$$V_{os} = \frac{6 \text{ sec}}{7.67 \text{ sec}} * 1384.64 \text{ in}^3 = 1083.58 \text{ in}^3$$

$$V_u = 1683 \text{ in}^3 - 1083.58 \text{ in}^3 = 599.42 \text{ in}^3$$

$$L_d = 2.75 \text{ in} + \frac{599.42 \text{ in}^3 - 51.94 \text{ in}^3}{\pi * (2.9375 \text{ in})^2}$$

$$L_{d,6 \text{ sec}} = 22.95 \text{ in}$$

1.3 Full burn

$$V_{os} = 1384.64 \text{ in}^3$$

$$V_u = V_t - V_{os} = 1663 \text{ in}^3 - 1384.64 \text{ in}^3 = 278.36 \text{ in}^3$$

$$L_d = 2.75 \text{ in} + \frac{278.36 \text{ in}^3 - 51.94 \text{ in}^3}{\pi * (2.9375 \text{ in})^2}$$

$$L_{d,7.67 \text{ sec}} = 11.10 \text{ in}$$

IX. Appendix - Detailed Simulations

A. Engine Performance with the Chosen Oxidizer to Fuel Ratio Affected by Oxidizer Contamination

Name	Propellant Name	Weight (gr)
NITROUS OXIDE		17491.44
HYDROXYTERMINAT POLYBUTADIEN		2374.33
MDI (143L)		709.24
CARBON BLACK		92.49
SULFUR DIOXIDE		356.97
		0.00
		0.00
		0.00
		0.00
		0.00
		0.00
		0.00
		0.00
		0.00
		0.00
		0.00
		0.00
Total Wt (grams)		21024.47

Operating Conditions

Temp. of Ingredients (K) 303

Chamber Pressure (PSI) 500

Exhaust Pressure (PSI) 10.10

Boost Velocity and Nozzle Design

Calculate Isp* 200.7357

C* 5227.497

Density 0.0622985

Molecular Wt 26.60604

Chamber CP/CV 1.249668

Chamber Temp. 3348.128

Display Results Display Nozzle Graphs

Figure 65. ProPEP 3 Propellant Characterization tool input with final O/F ration and 2% SO₂ contamination

B. Oxidizer Feed and Storage Assembly Simulations

1. Oxidizer Tank FEA Static Simulation

A SolidWorks Simulation was performed on the Oxidizer Tank to verify that a factor of safety greater than or equal to 2 was held to yield. This simulation was particularly important since hand calculations can not be computed on the complex geometries of the Forward Bulkhead's Forward Dome and the Injection Bulkhead's Aft Dome. To accurately model the setup of the Oxidizer Tank, the simulation was conducted on an assembly including the Forward Bulkhead, the Body Cylinder, and the Injection Bulkhead. Each component had their chamfer(s) for orbital welding removed because that would present stress concentrations in the simulation that would not exist, assuming the weld is not a weak point for the tank. The default bonded connection between the components was applied to best resemble the welds. A fixed geometry was applied to the outside surface of the Forward Bulkhead to model the engine's flight configuration, which does not constrain the Oxidizer Tank on both ends.

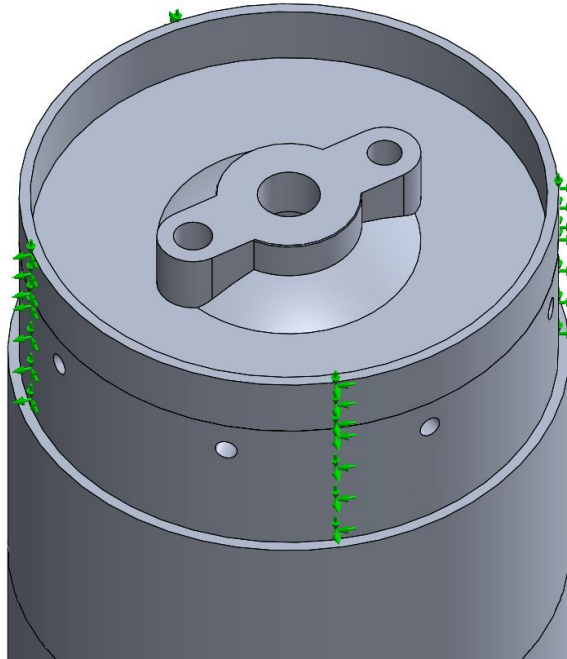


Figure 66. Oxidizer Tank Fixed Geometry

A load of 915 psi, the maximum the Oxidizer Tank will reach before rapid automatic venting, was applied to the Forward Dome, the Body Cylinder, the Aft Dome, and the Oxidizer Feed Conduit. While the Injection Bulkhead experiences different pressures in other areas, these pressures don't pertain to the Oxidizer Tank and are analyzed separately in this *Appendix, Simulation B.2*. Figure 67 shows the pressure applied to the Forward Bulkhead and the Injection Bulkhead and Figure 68 shows the pressure applied to the entire Oxidizer Tank. Note the removal of the chamfers for orbital welding in Figure 67.

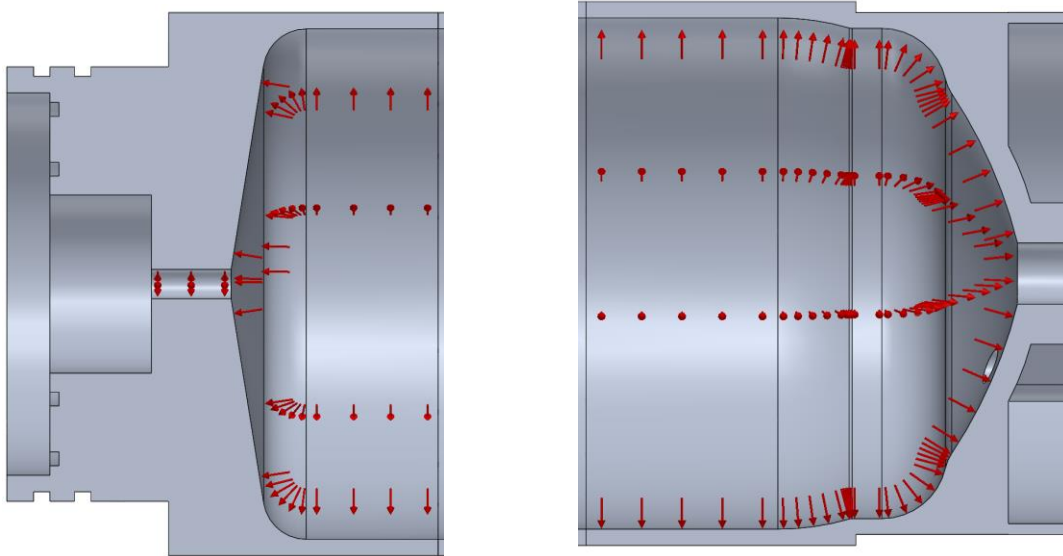


Figure 67. Forward Bulkhead and Injection Bulkhead Pressure Distributions



Figure 68. Oxidizer Tank Pressure Distribution

A global mesh of 0.25 in with a ratio of 1.5 was applied. However, to improve the accuracy of the simulation's results, a mesh control of 0.15 in was applied to all fastener holes and complex geometries on the domes.

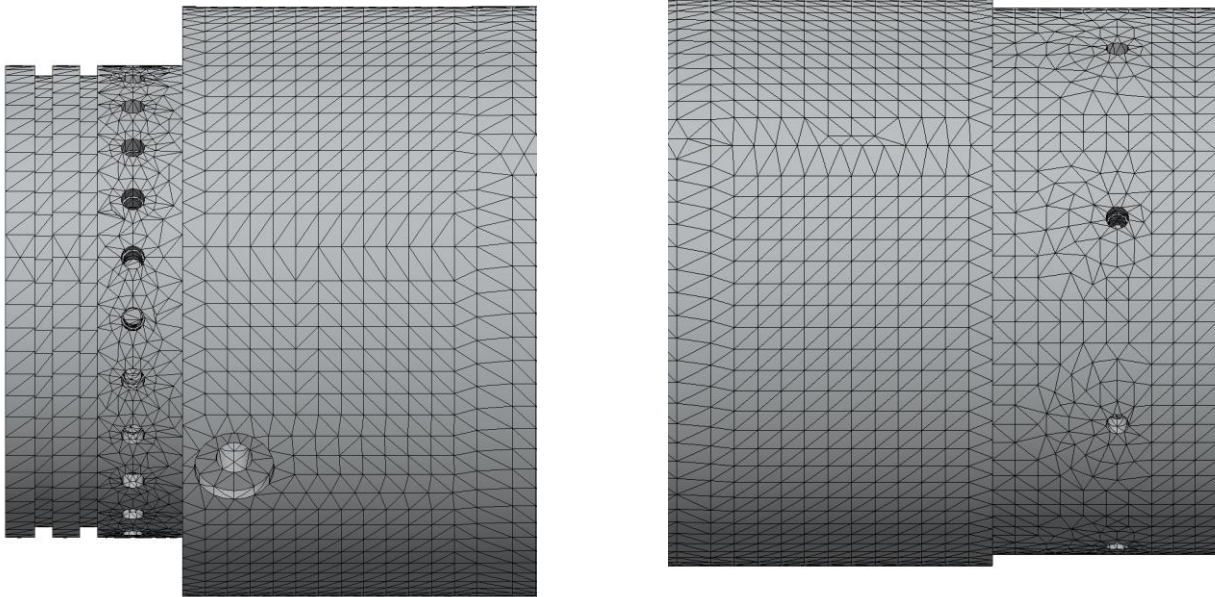


Figure 69. Forward Bulkhead and Injection Bulkhead Mesh



Figure 70. Oxidizer Tank Mesh

The results of the simulation are shown in the figures below. The highest stress is found on the fillet of the Injection Bulkhead, which at 17,240 psi has a factor of safety just above 2 when compared to the yield stress of 6061-T6 Aluminum in tension (35,000 psi). As predicted by the hand calculations, the stress on the Body Cylinder wall has a factor of safety that is far higher than 2.

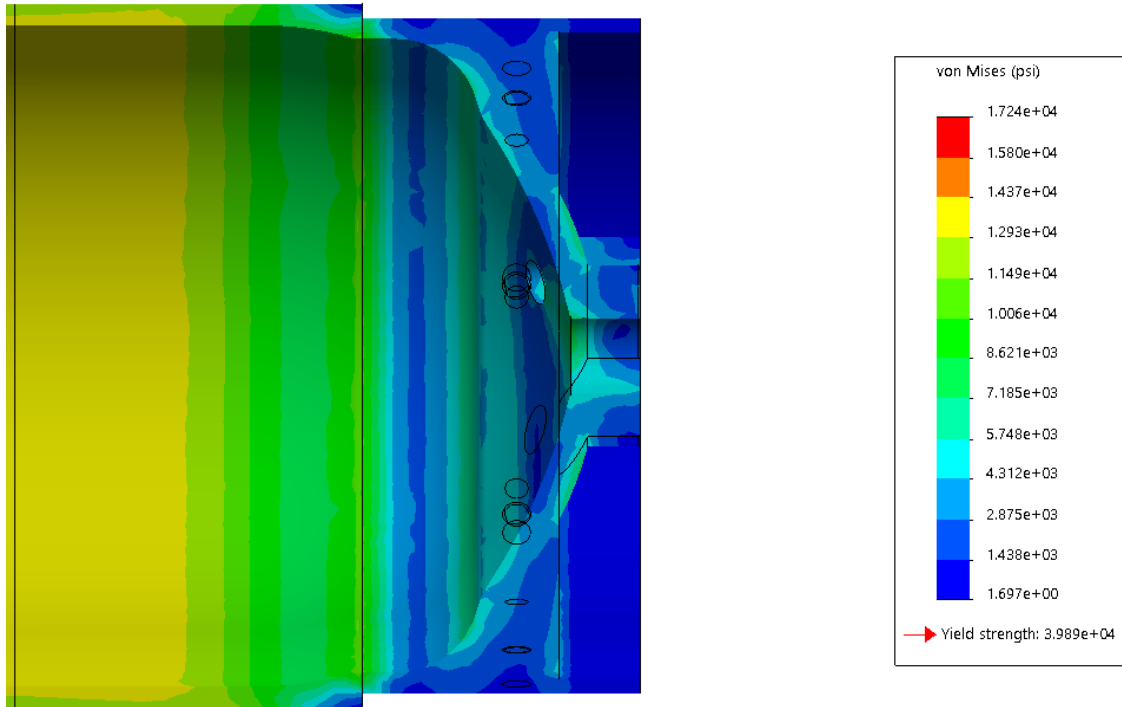


Figure 71. Forward Bulkhead Stress Distribution

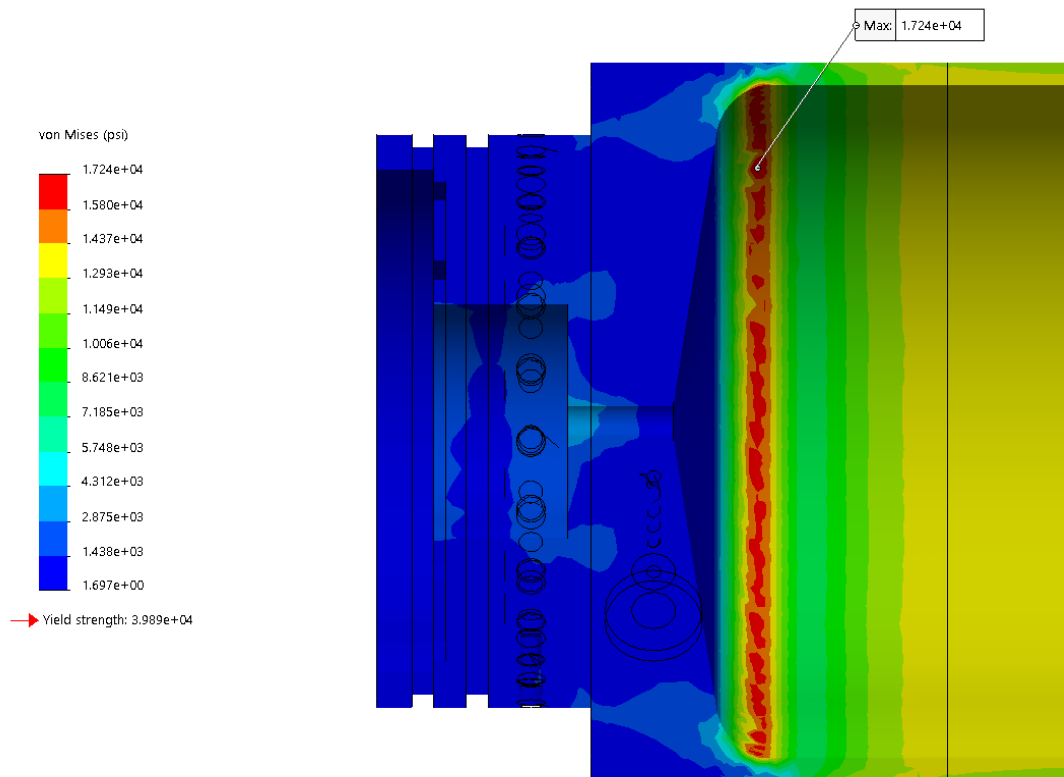


Figure 72. Injection Bulkhead Stress Distribution



Figure 73. Oxidizer Tank Stress Distribution

2. Injection Bulkhead FEA Static Simulation

Although a SolidWorks Simulation was already conducted on the Oxidizer Tank which included the Injection Bulkhead, the focus was on the tank itself and thus the only portion of the Injection Bulkhead that the team looked into was the Aft Dome. Since the Injection Bulkhead experiences other pressures as well due to it containing the Injector Plate, another Solidworks Simulation was conducted that focused entirely on the Injection Bulkhead. Because the Injection Bulkhead is welded to the Oxidizer Tank Body Cylinder, a fixed constraint was applied to the forward face.



Figure 74. Injection Bulkhead Fixed Geometry

A 915 psi pressure was applied to the Aft Dome, Pre-Injection Chamber, and Pre-Injection Chamber PT hole. A 500 psi pressure was applied to the area around the Injector Plate and the Combustion Chamber PT hole. The image below shows the surfaces in which a 500 psi pressure was applied.

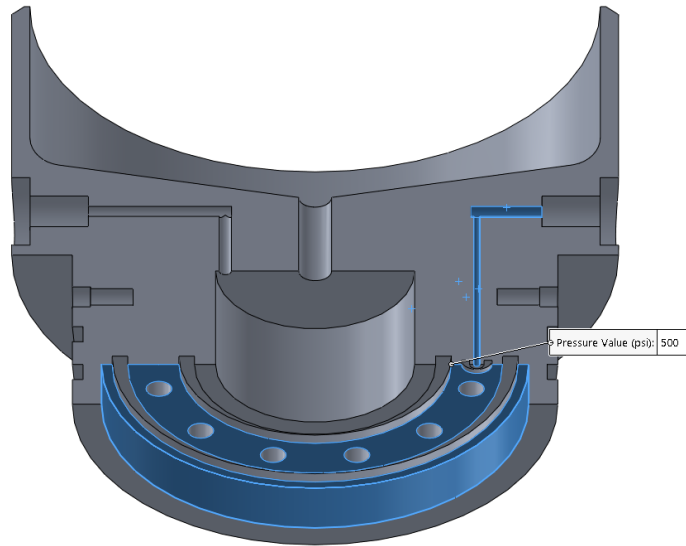


Figure 75. Locations of 500 psi Pressure Load

A global mesh of 0.2 in with a ratio of 1.5 was applied. However, there are many complex geometries on the Injection Bulkhead. The PT ports and O-ring grooves had a mesh control of 0.08 in applied. A mesh control of 0.125 in was applied to the fastener holes. Figure 76 shows the smallest surfaces to which a mesh control of 0.08 in was applied. Figure 77 shows the global mesh on the outside of the bulkhead.

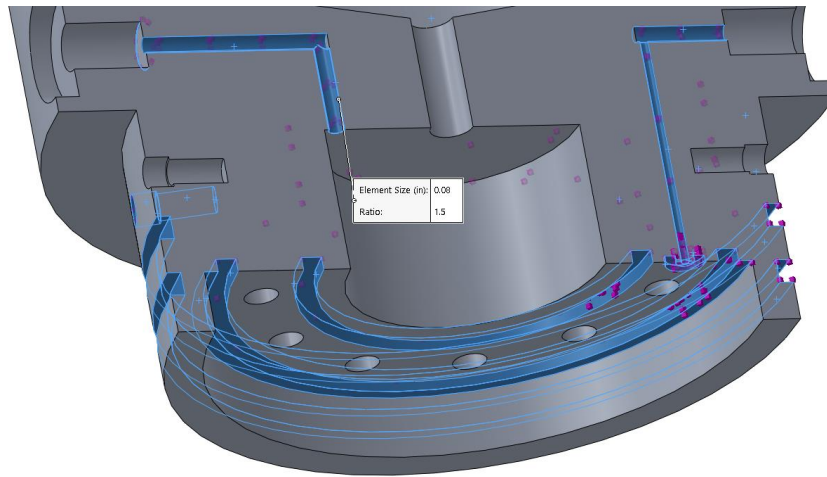


Figure 76. Locations of 0.125 in Mesh Control

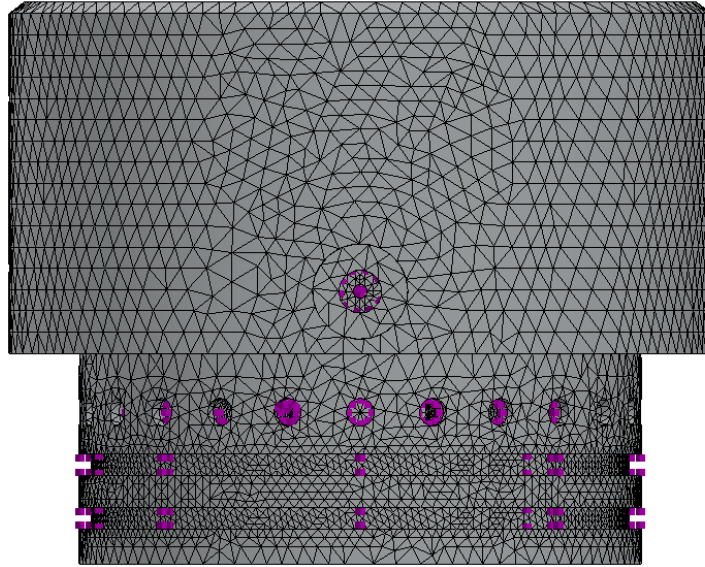


Figure 77. Injection Bulkhead Global Mesh

The results of the study are shown in the image below. All stresses on the Aft Dome, Pre-Injection Chamber, PT ports, fastener holes, and thin walls are far below 17.5 ksi, which is what is required to have a factor of safety above 2.0. The only region that exceeds it is a small section on the most forward part of the Aft Dome. However, this is simply a result of the forward face being a fixed geometry. In reality, the Injection Bulkhead is welded to the Body Cylinder and the stress along this section is the same as the stress along the rest of the Body Cylinder, which has a factor of safety above 2.0. Thus, this simulation proved that the Injection Bulkhead is more than capable of handling the loads the team expects it to receive.

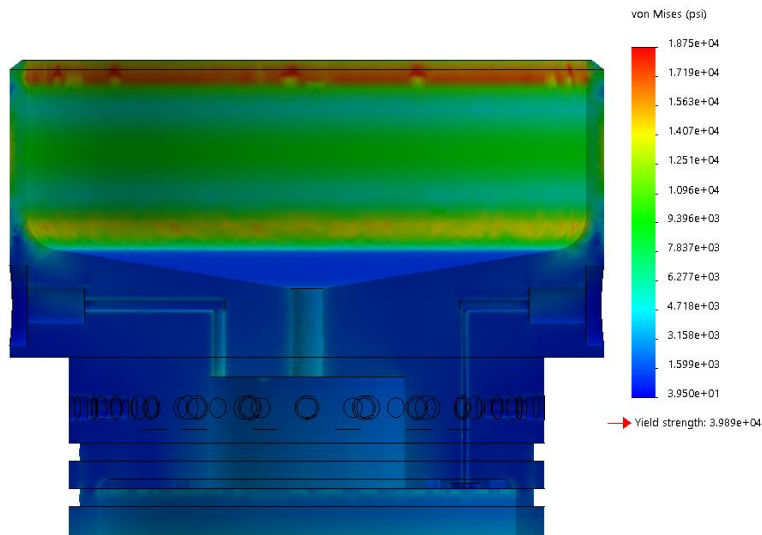


Figure 78. Injection Bulkhead Stress Distribution

3. Injector Plate FEA Static Simulation

A study was run in SolidWorks Simulation in order to verify the stresses in the Injector Plate resulted in a factor of safety above 2. Additionally, the team used the study to check that the deformation in the plate due to the

high pressures acting on it was negligible. Analyzing simply the Injector Plate gives accurate results for the stress distribution but not the deformation, so to find both, the simulation was run with an assembly of the Injector Plate and the Injection Bulkhead. The standard bonded connection between the two components was replaced with a spring connection, which gives accurate deformation as long as the stress is still within the elastic region. The planar face was chosen to be the area of the washers that press against the aft face of the plate, as this is the area of the Injector Plate that is constrained. The parallel face was chosen to be the aft face of the Injection Bulkhead as this surface is flush with the Injector Plate. The normal stiffness of the spring, k , is given by $k = AE/L$. A is the nominal area of bolts retaining the Injector Plate, or 0.0318 in^2 . E is the modulus of elasticity for the steel bolts, or 30 million psi. L is the nominal length, which was chosen to be 0.6 in as this is slightly larger than the thickness of the plate of 0.5 in. This results in a normal stiffness of $1,590,000 \text{ (lbf/in)/in}^2$. Because the forces will be entirely in the vertical direction, tangential stiffness was not necessary.

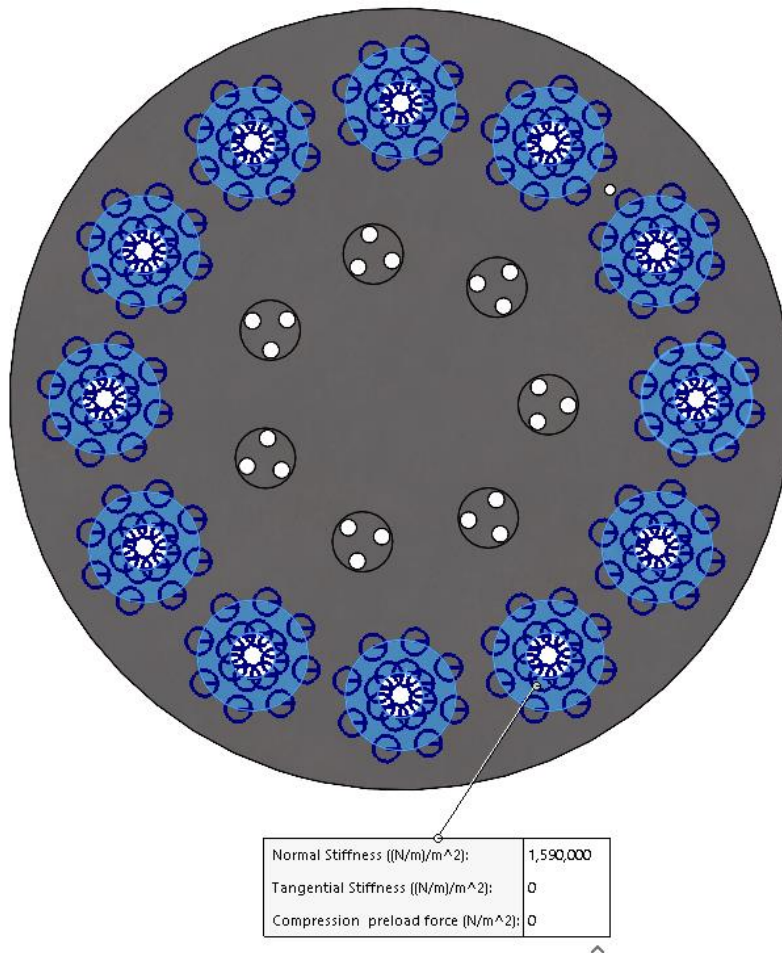


Figure 79. Planar Face Selection (Washers on Aft Side of Injector Plate)

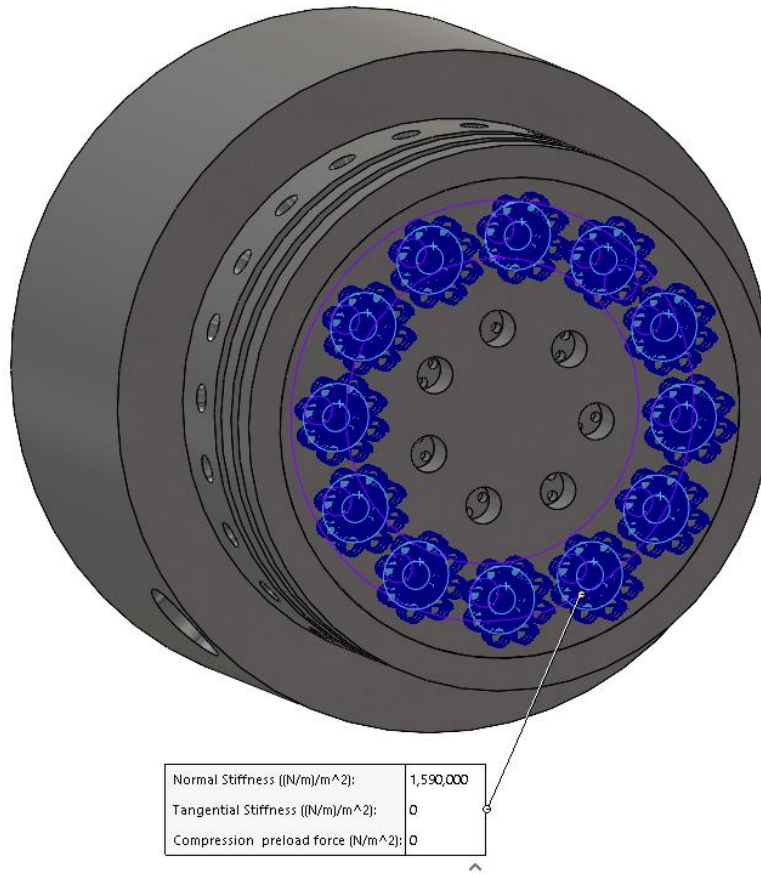


Figure 80. Parallel Face Selection (Aft Face of Injection Bulkhead)

In order to run the simulation, a fixed geometry still had to be applied. The forward face of the Injection Bulkhead was chosen as this surface is welded to the Body Cylinder and will be fixed in flight. However, the selection of this face will have minimal effect on the outcome of the simulation as the spring connection will be constraining the plate.

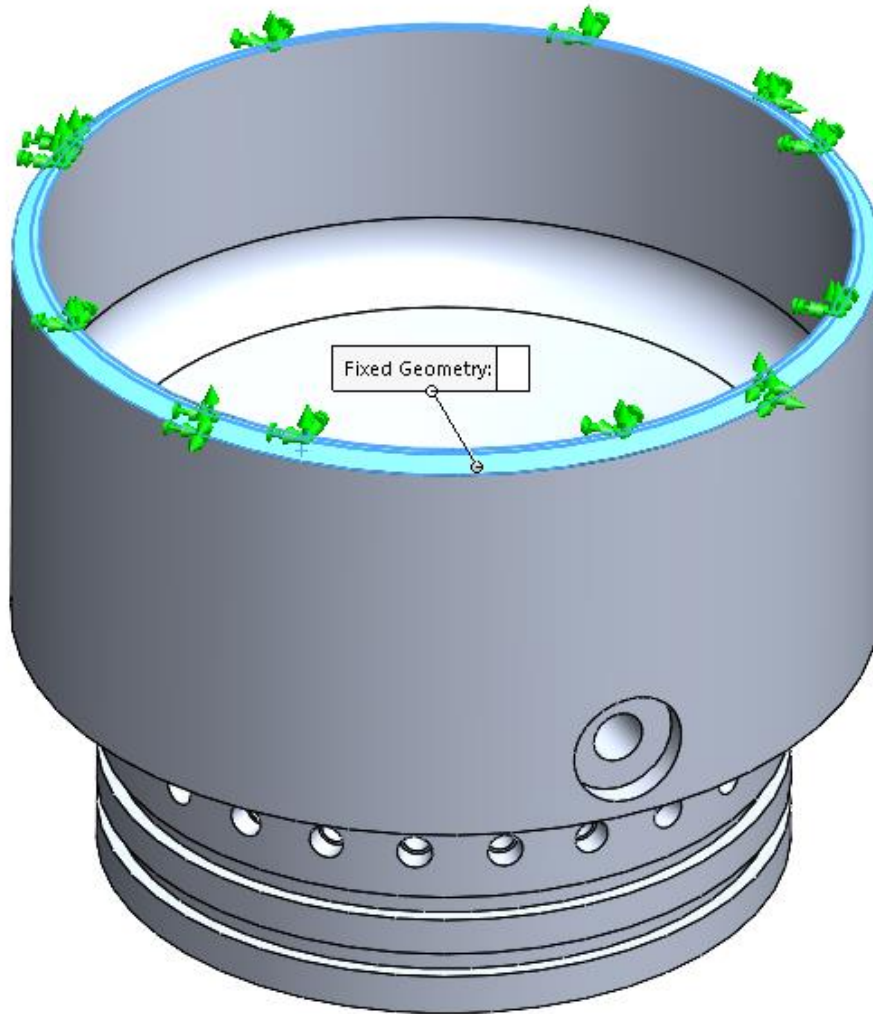


Figure 81. Fixed Geometry Selection

A pressure of 915 psi was applied to the forward face of the Injector Plate on the inside of the Injection Bulkhead's innermost O-ring groove. Although other parts of the Injector Plate will have a pressure exerted on it after ignition, this case, which will be seen during loading, is when the Injector Plate will see the highest stress and deformation.

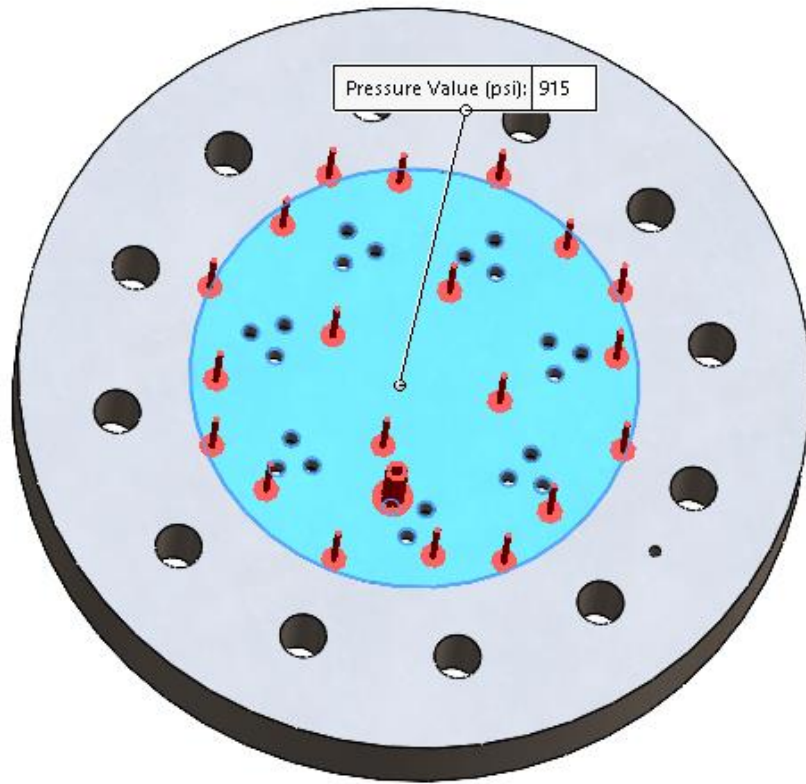


Figure 82. Injector Plate Pressure Distribution

Due to the meshing complexity of the injector plate, a global mesh size of 0.1 was used. While unnecessarily fine in regions away from the injector holes it allowed for simulation without needing mesh controls.

Mesh Details	
Study name	Injector Plate [-Default
Mesh type	Solid Mesh
Mesher Used	Standard mesh
Automatic Transition	Off
Include Mesh Auto Loops	Off
Jacobian points for High quality mesh	16 points
Element size	0.1 in
Tolerance	0.005 in
Mesh quality	High
Total nodes	660234
Total elements	451970
Maximum Aspect Ratio	16.02
Percentage of elements with Aspect Ratio < 3	99.4

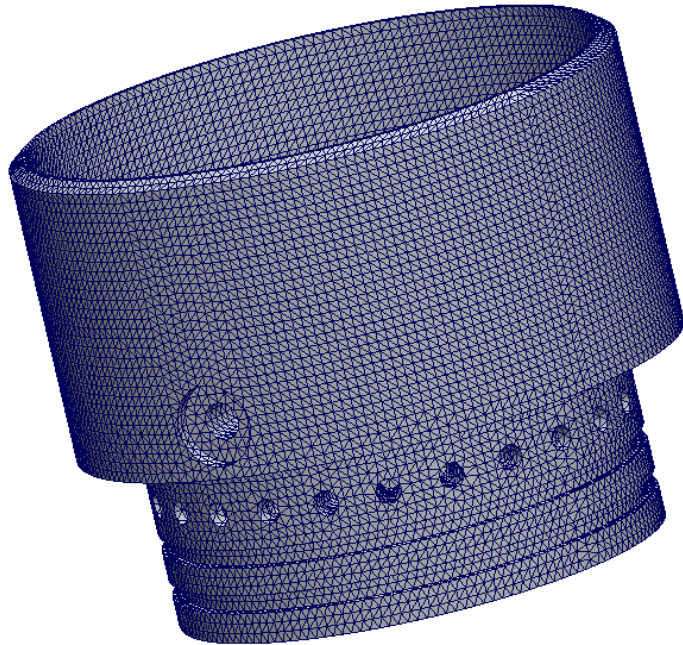


Figure 83. Global Mesh

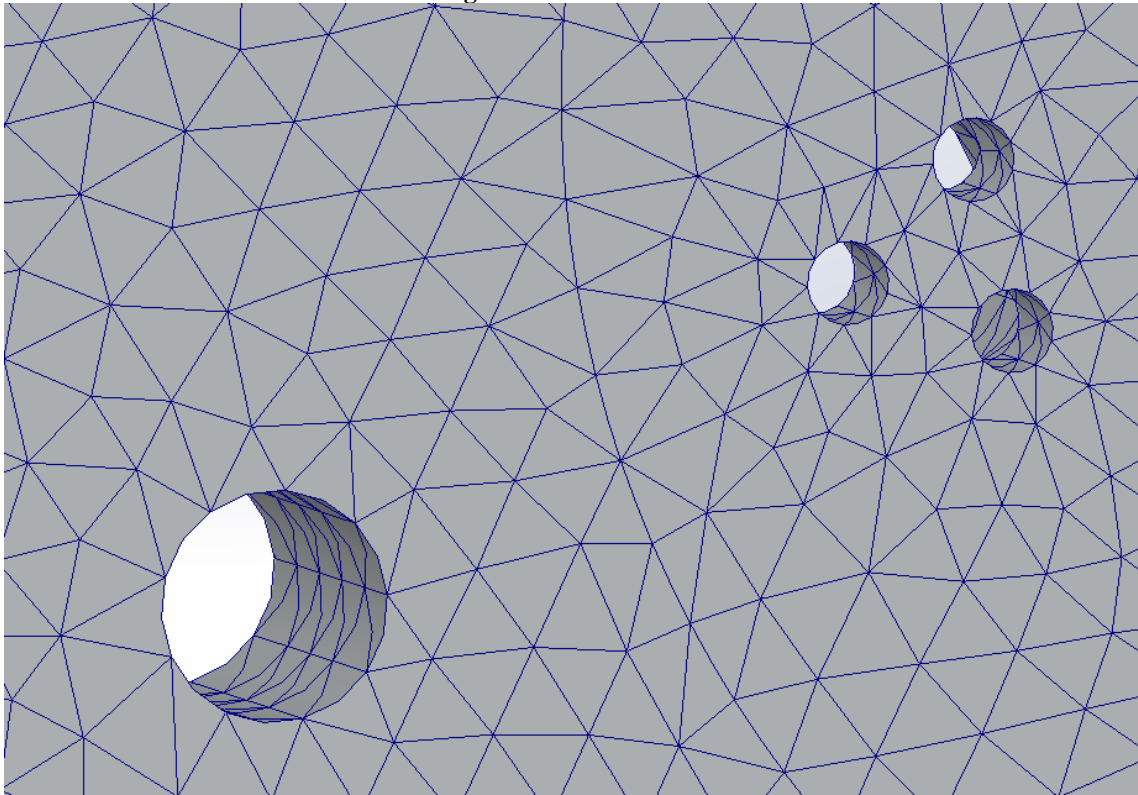


Figure 84. Close Up of Injector Plate Mesh

The results of the study are given in the figures below. The highest stress was found to be 8.077 ksi along the injector plate holes, which results in a factor of safety above 2 when compared to the yield stress of 6061 T-6 aluminum. The maximum displacement is 1.19×10^{-3} in, located at the center of the forward face of the plate. This displacement is small enough to be considered negligible.

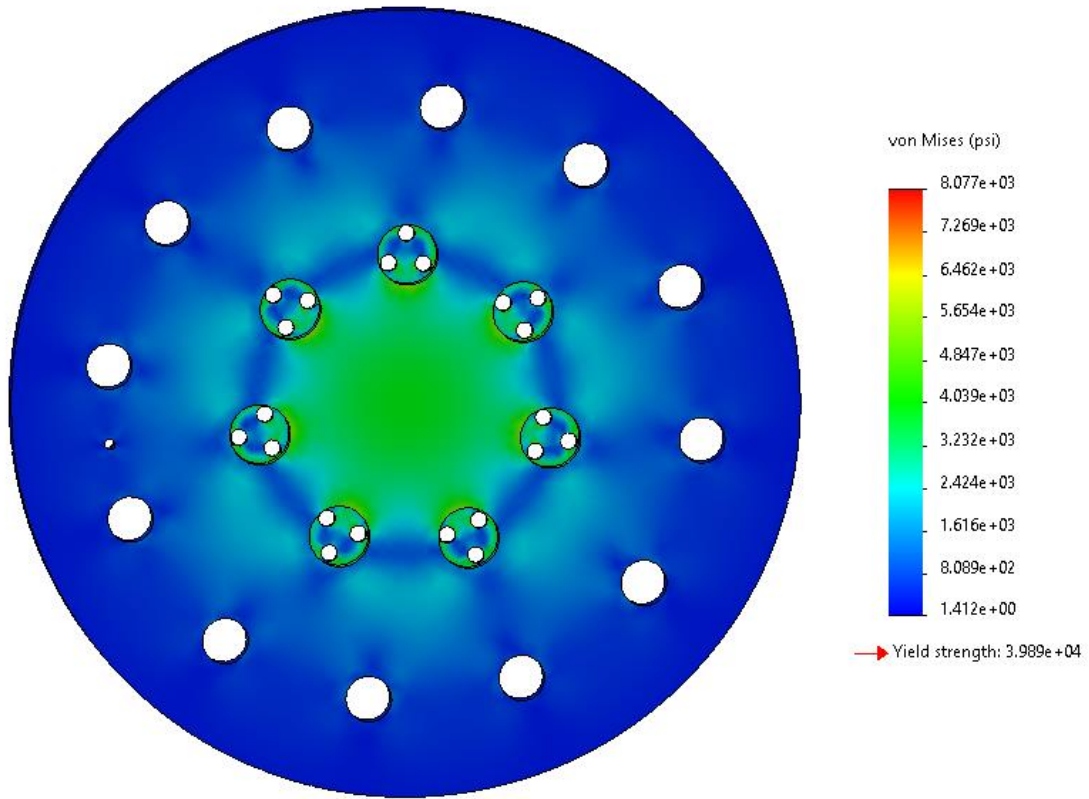


Figure 85. Stress Distribution on the Aft End of the Plate

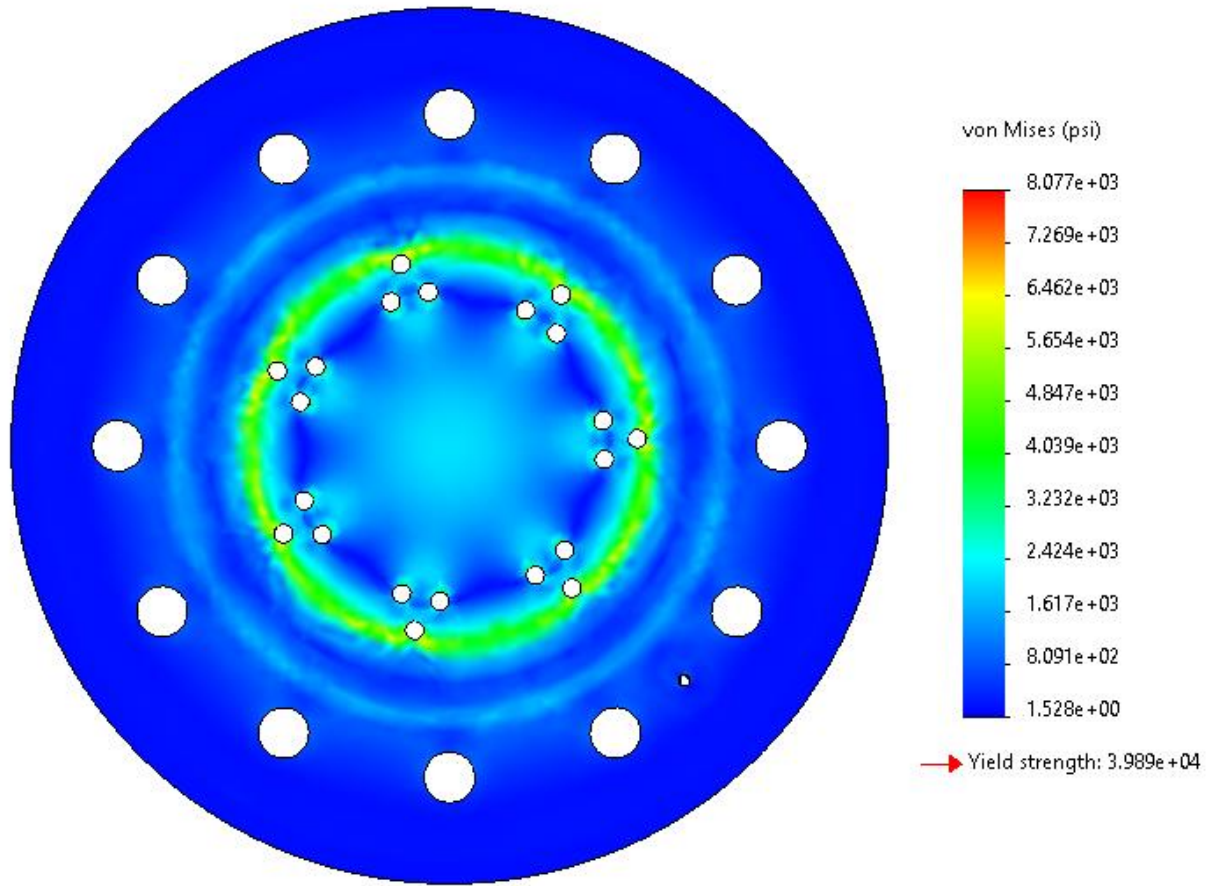


Figure 86. Stress Distribution on the Forward End of the Plate

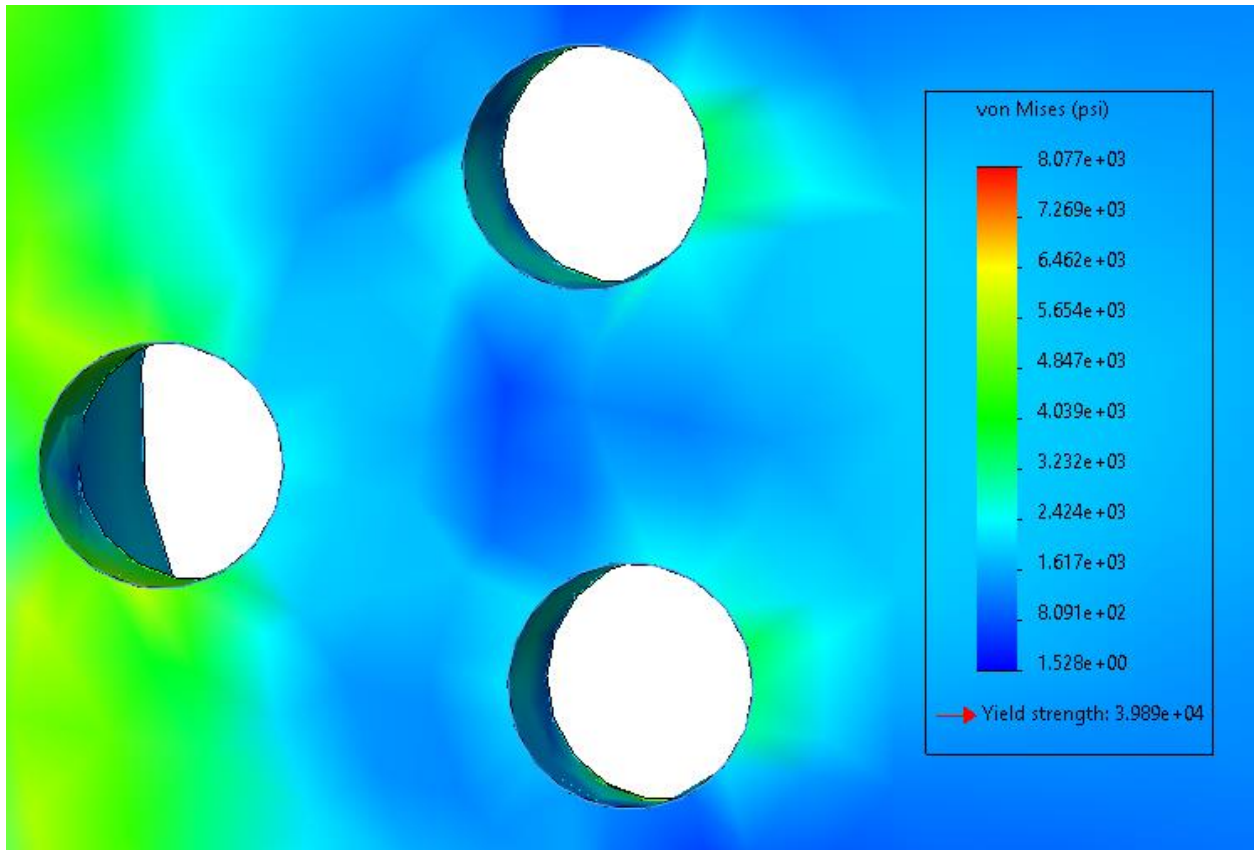


Figure 87. Stress Distribution Along the Injector Holes

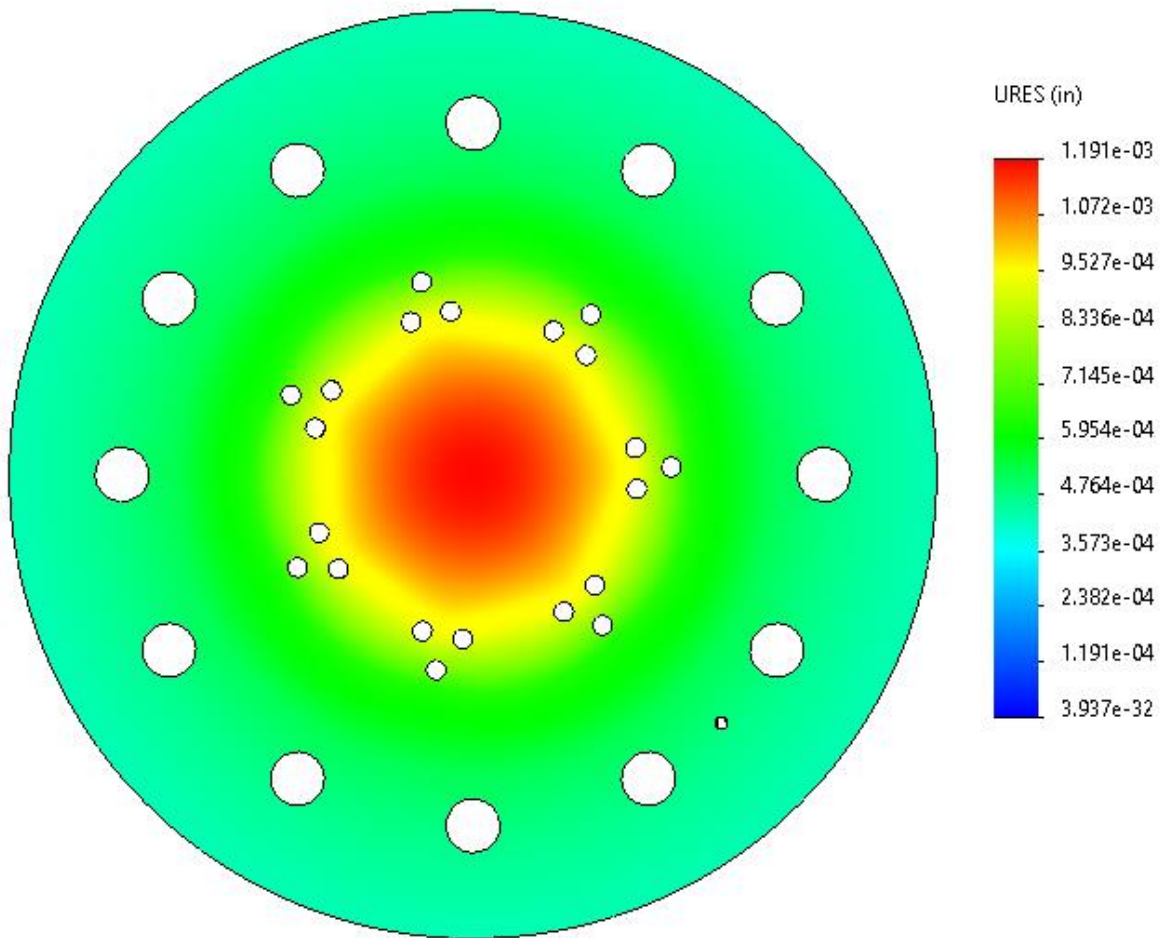


Figure 88. Displacement of Forward End of the Injector Plate

C. Thrust Chamber Assembly Simulations

1. Combustion Chamber Stress Simulations

A static study in SolidWorks Simulation was performed to check for any areas of increased stress in the chamber wall that was not accounted for in the hand calculation. For the simulation, a fixed geometry condition was applied to the fastener holes on the forward end of the chamber. This best emulates the Combustion Chamber's setup since it fastened to the airframe via the holes on the forward end, but is left unconstrained everywhere else to account for thermal expansion.

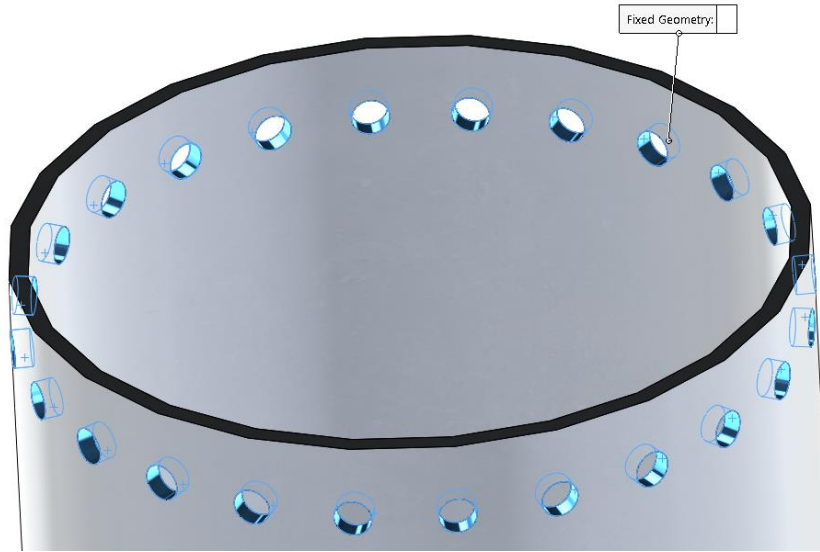


Figure 89. Combustion Chamber Fixed Geometry (Forward Fastener Holes)

A uniform pressure distribution of 500 psi was applied to the inside of the chamber. To be on the side of caution, this pressure was applied to the entirety of the chamber's inner surface.

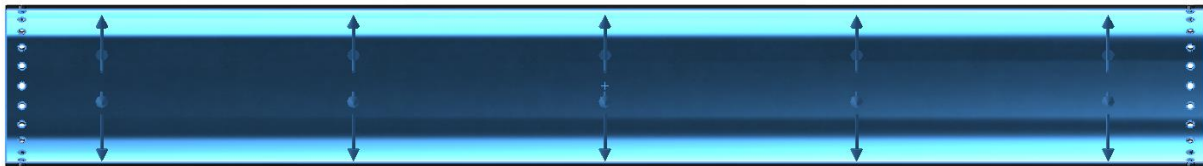


Figure 90. Combustion Chamber Pressure Distribution

Due to the cylinder's simple geometry, a global mesh size of 0.35 in was found to be sufficient. However, a mesh control of 0.15 in was applied to the fastener holes on either side as well as the forward and aft faces in order to produce better results. Again, a standard mesh ratio of 1.5 was applied.

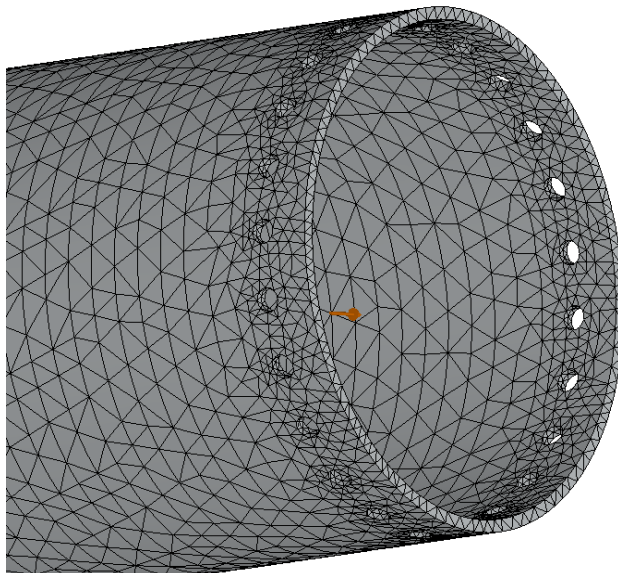


Figure 91. Combustion Chamber Mesh

The results of the simulation are given below. As shown in Figure 92, the stress along the combustion chamber wall is below 16 ksi. The yield stress of Aluminum 6061-T6 in tension is 35 ksi so the factor of safety was found to be above 2.0.



Figure 92. Combustion Chamber Global Stress Distribution

When an isometric view of stresses above 17.5 ksi was applied, the only areas that fell in that region were stress concentrations around the fastener holes. Shown in Figure 93, the highest stress concentration around the forward fastener holes was 21 ksi. Shown in Figure 94, the highest stress concentration around the aft fastener holes was 27.4 ksi. As already discussed in *Section V.A.2*, very localized yielding around the fastener holes is not a large concern for the team since the yielding will relieve the stress concentration. Furthermore, all literature the team has read about this stress points to not designing around the stress concentrations found in FEA results that do not account for plastic deformation. Since the factor of safety along the chamber wall is above two, the team finds these stress concentrations to be acceptable.

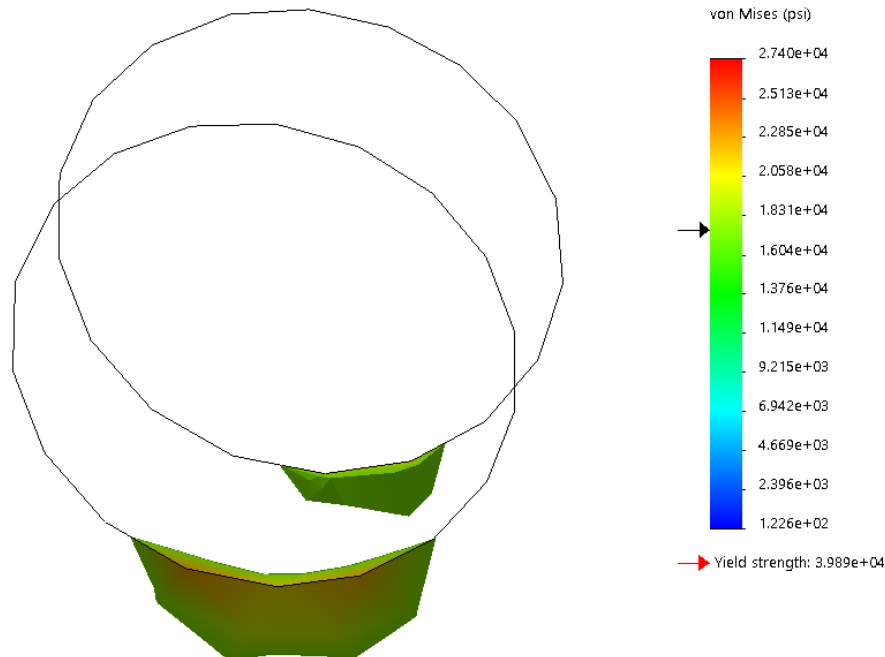


Figure 93. Forward Combustion Chamber Holes Stress Concentration

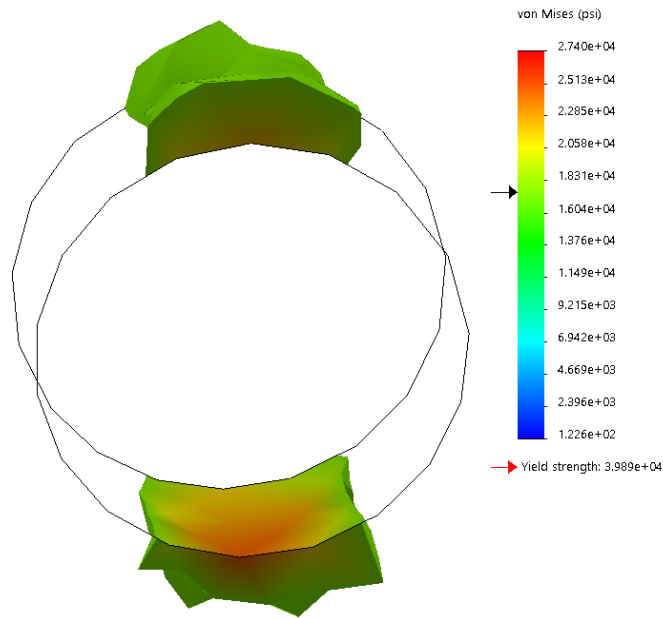


Figure 94. Aft Combustion Chamber Holes Stress Concentration

2. Nozzle Assembly Simulations

To verify the hand calculations for the stress in the Nozzle Assembly and check for stress concentrations that result in a factor of safety less than 2, a SolidWorks simulation was performed. An assembly of the Nozzle Insert and the Nozzle Casing with a bonded connection between the two components was used. A fixed geometry was applied to the 24 radial fastener holes on the Nozzle Casing. The portion of the hole containing the pin was only fixed to examine the worst case scenario in which the threads of the shoulder screws took no load.

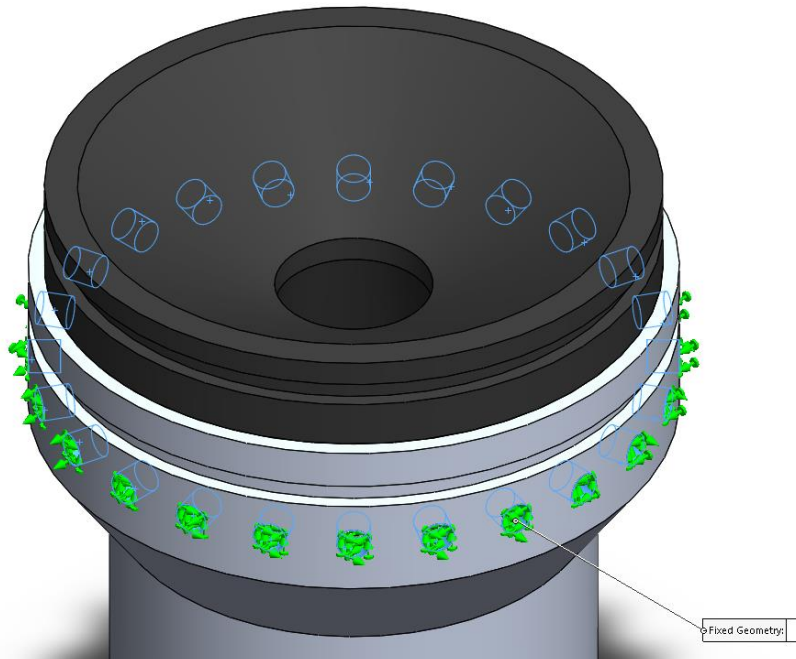


Figure 95. Nozzle Assembly Fixed Geometry

A 500 psi pressure load was applied to the Nozzle Insert's throat and converging end,

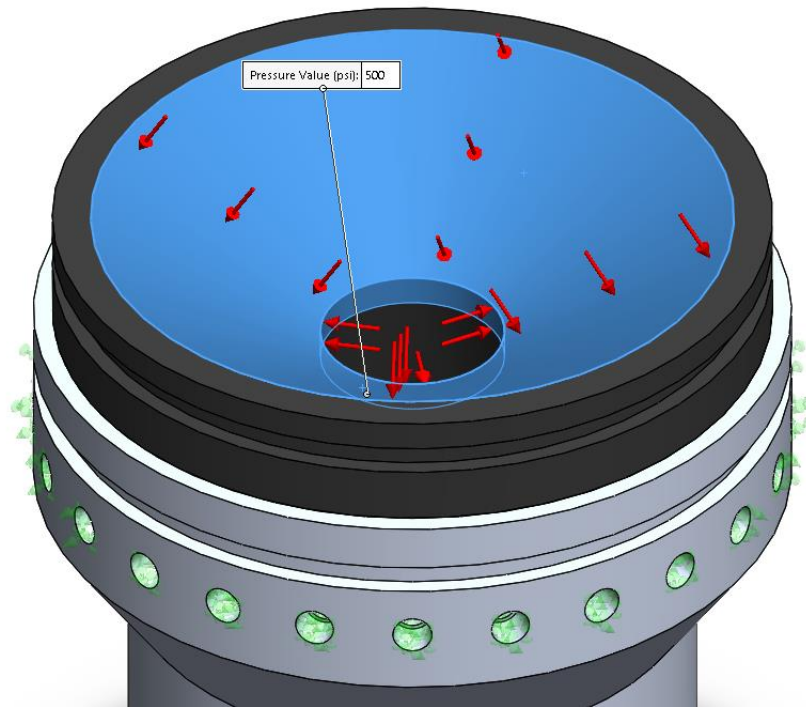


Figure 96. Pressure distribution on nozzle's converging end

A global mesh of 0.2 in with a ratio of 1.5 (default) was applied to the entire assembly. After inspecting the components' most complicated geometry, it was determined that this mesh size was sufficient and a mesh control would not be necessary. A close up view of the fastener holes' mesh is given in Figure 98.

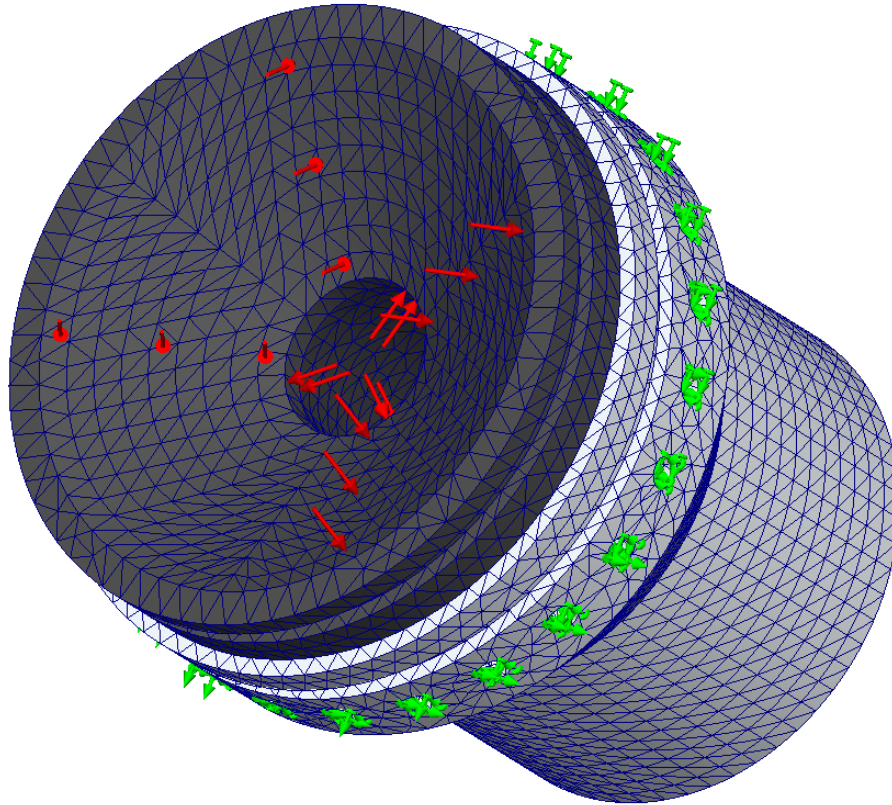


Figure 97. Nozzle Assembly Mesh

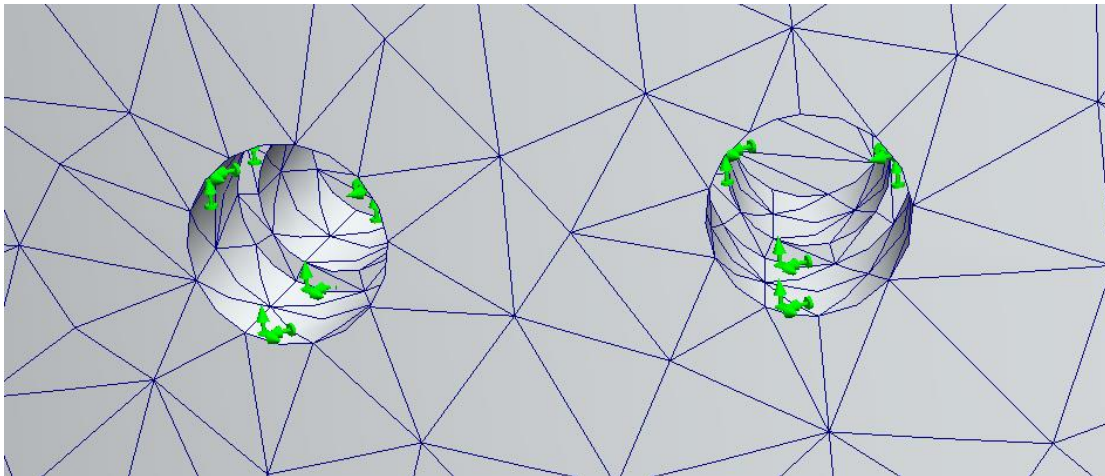


Figure 98. Nozzle Casing Fastener Holes Mesh

The maximum stress was found to be 4.03 ksi at the maximum on the fastener holes. This results in a factor of safety far above 2, meaning that stresses are not a concern for this assembly.

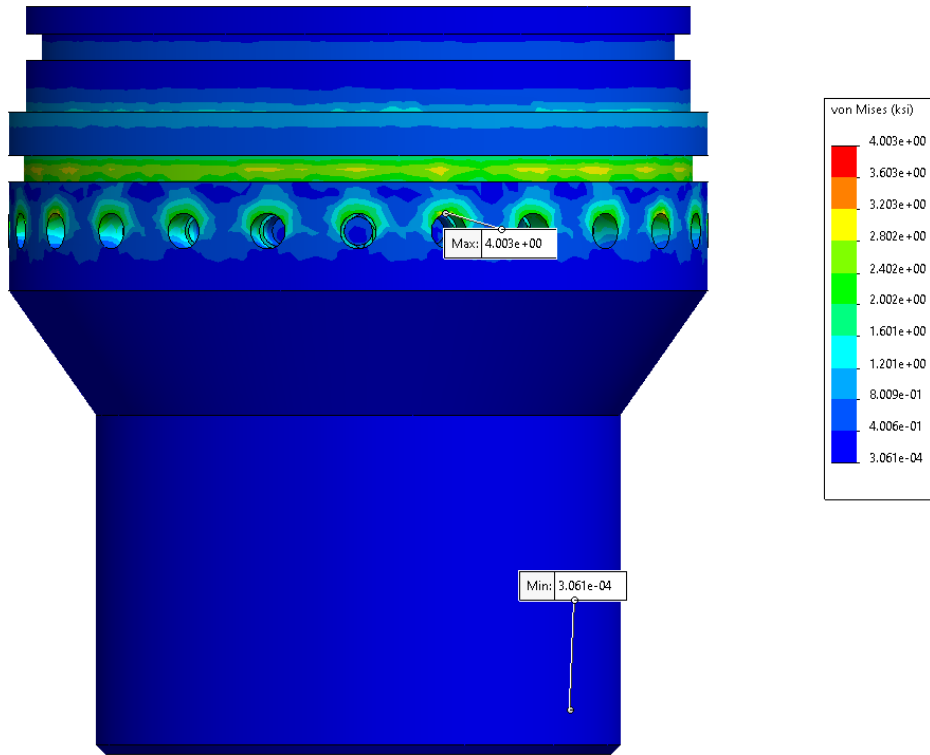


Figure 99. Nozzle Assembly Stress Distribution

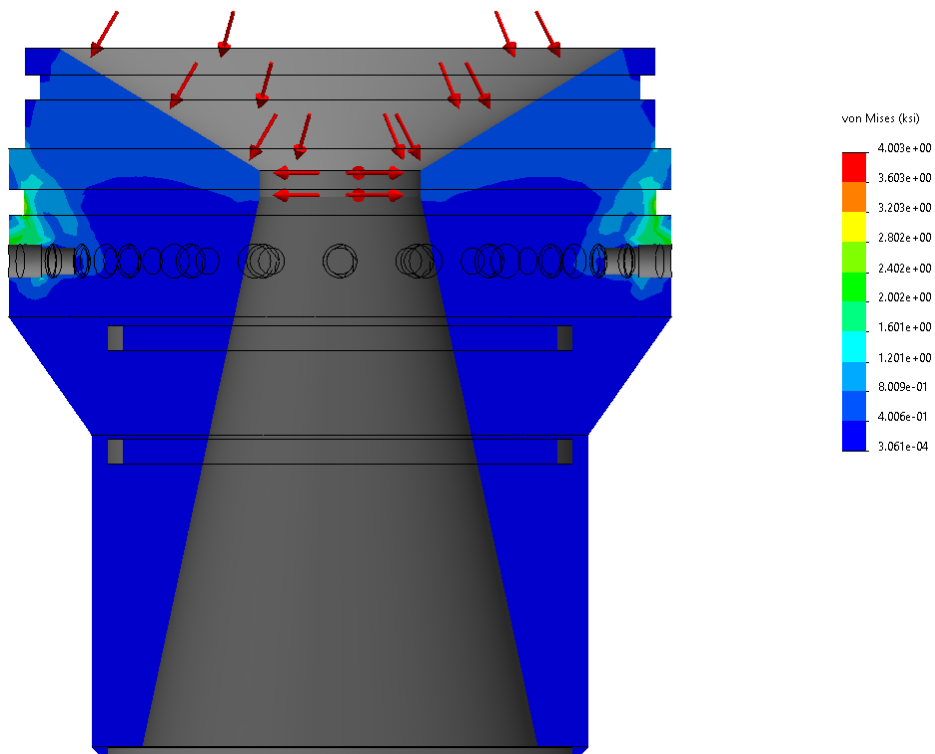


Figure 100. Nozzle Assembly Stress Distribution (Side Section View)

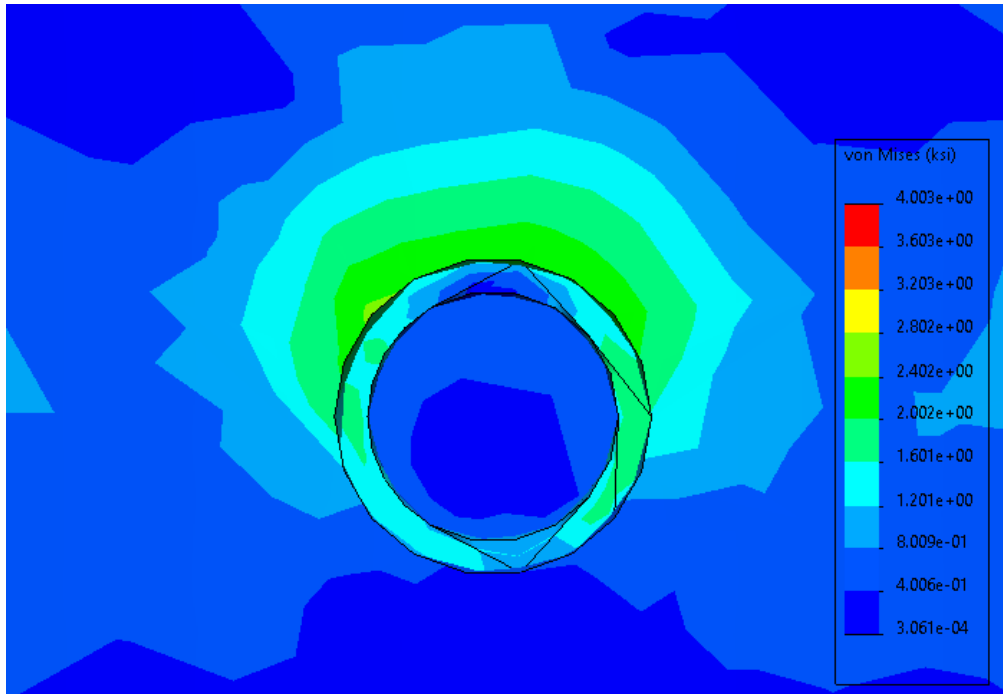


Figure 101. Nozzle Casing Fastener Holes Stress Distribution

X. Appendix - MATLAB Scripts

A. Titan II Engine Parameters

```

% Rice Eclipse Rocketry
% Titan II Team
% 10/11/2019
% This script is intended for the Propulsion-Aerodynamics Integration
%meeting
% on Sunday, Oct. 13th, 2019. The function will take inputs from the
% Aerodynamics team through OpenRocket and will return useful engine
% parameters that will aid in the design of the Titan II engine.
% Fuel: HTPB, Carbon Black, Isocyanate Curative
% Oxidizer: Nitrous Oxide

rho_ox = 688; % oxidizer density, nitrous oxide [kg/m^3]
rho_f = 1009; % fuel density, HTPB + curative + carbon black [kg/m^3]
mix_ratio = 5.62; % oxidizer-fuel mix ratio
isp = 202.47; % specific impulse [sec] - assumes O/F = 5.62 and P_e =
%10.1 psi
g = 9.81; % gravity [m/s^2]
isp = isp * 0.98; % decreases Isp by 2% to account for O/F shift
%during
% burn, per Space Propulsion Design and Analysis pg.
%408

f_tavg = 1200; % average thrust force [lbf]
t_burn = 11.5*800/f_tavg; % burn time [sec]
[vol_f,vol_ox,m_ox,m_f,mdot_ox,mdot_f,m_prop] =
    fuel_mass(f_tavg,isp,g,mix_ratio,t_burn,rho_ox,rho_f);
fprintf('Average Thrust: %f lbf\n', f_tavg);
fprintf('Burn Time: %f sec\n\n', t_burn);
fprintf('Oxidizer Volume: %f in^3\n',vol_ox);
fprintf('Minimum Ox. Tank Volume (5 Percent Margin): %f in^3\n',vol_ox
    * 1.05);
fprintf('Oxidizer Mass: %f lbm\n', m_ox);
fprintf('Oxidizer Mass Flow Rate: %f kg/s\n\n', mdot_ox);
fprintf('Fuel Volume: %f in^3\n',vol_f);
fprintf('Fuel Mass: %f lbm\n', m_f);
fprintf('Fuel Mass Flow Rate: %f kg/s\n\n', mdot_f);
fprintf('Total Propellant Mass: %f lbm\n\n', m_prop);

function [vol_f,vol_ox,m_ox,m_f,mdot_ox,mdot_f,m_prop] =
    fuel_mass(f_tavg,isp,g,mix_ratio,t_burn,rho_ox,rho_f)
% This function calculates the volume, mass, and flow rate of the fuel
% and oxidizer of Titan II.
% Inputs: f_tavg (average thrust force) [lbf]

% isp (specific impulse) [sec]
% g (gravity) [m/s^2]
% mix_ratio (oxidizer-fuel mix ratio)
% t_burn (burn time) [sec]
% Outputs: vol_ox (volume of oxidizer) [in^3]
% vol_f (volume of fuel) [in^3]
% m_ox (mass of oxidizer) [lbm]

```

```

% m_f (mass of fuel) [lbm]
% mdot_ox (mass flow rate of oxidizer) [kg/s]
% mdot_f (mass flow rate of fuel) [kg/s]
% m_prop (mass of propellant) [lbm]
% mdot_prop (mass flow rate of propellant) [kg/s]
f_tavg = f_tavg * 4.44822; % converts f_tavg from lbf to N
m_f = (f_tavg * t_burn) / (isp * g * (1 + mix_ratio));
m_ox = mix_ratio * m_f;
m_prop = m_f + m_ox;
mdot_prop = f_tavg / (isp * g);
mdot_f = mdot_prop / (1 + mix_ratio);
mdot_ox = mix_ratio * mdot_f
vol_f = m_f / rho_f;
vol_f = vol_f * 61023.744; % converts vol_f from m^3 to in^3
vol_ox = m_ox / rho_ox;
vol_ox = vol_ox * 61023.744; % converts vol_ox from m^3 to in^3
m_f = m_f * 2.2046226218488; % converts m_f from kg to lbm
m_ox = m_ox * 2.2046226218488; % converts m_ox from kg to lbm
m_prop = m_prop * 2.2046226218488; % converts m_prop from kg to
%lbm
end

```

```
mdot_ox =
```

```
2.3280
```

```
Average Thrust: 1200.000000 lbf
```

```
Burn Time: 7.666667 sec
```

```
Oxidizer Volume: 1583.095292 in^3
```

```
Minimum Ox. Tank Volume (5 Percent Margin): 1662.250056 in^3
```

```
Oxidizer Mass: 39.348747 lbm
```

```
Oxidizer Mass Flow Rate: 2.328038 kg/s
```

```
Fuel Volume: 192.073749 in^3
```

```
Fuel Mass: 7.001556 lbm
```

```
Fuel Mass Flow Rate: 0.414242 kg/s
```

```
Total Propellant Mass: 46.350303 lbm
```

```
Published with MATLAB® R2018b
```

B. Conduit Calculations

```

%conduit calculations
%Assumes pressure drop due to major loss is negligible, so
%thick orriface model can be used. Also assumes major losses
%in pre-injection chamber are negligible

%constants
rho_ox = 786; %ox density in kg/m^3
d_conduit = .4531/39.37; %converting in to m
d_preinjection = 2.05/39.37;
mdot_ox = 2.328038; %mass flow rate of oxidizer in kg/s

%calculations
sigma = (d_conduit/d_preinjection)^2;
sigma_c = 1/(.639*(1-sigma)^.5+1)';

Cd = sqrt((1-sigma^2)/((1/sigma_c-1)^2+(1-sigma)^2));

delta_P = (1/(2*rho_ox))*((mdot_ox*sqrt(1/(sigma^2)-1)/
(Cd*pi*(d_preinjection/2)^2))^2);

delta_P_psi = delta_P*0.00014503

sigma_c =

    0.6161

delta_P_psi =

    59.7460

```

Published with MATLAB® R2018b

C. Injector Hole Diameter

```

%This script iterates through a range of possible number of holes
%for the Titan II injector plate and identifies the hole diameter
%necessary to achieve the desired oxidizer mass flow rate of
%1.552 kg/s.
%Written by: Eduardo Landin
%Necessary auxiliary files:
    %m_ox.m
    %bisection.m
    %Cd_calc.m
%June 2020

delta_P = (250-59.746)*6894.76;
%converts pressure drop across injector from psi to pascals
%expected average oxidizer tank pressure: 750 psi
%expected combustion chamber pressure: 500 psi.
%Pressure losses in the ox feed line: 62.7924 + 0.000629 psi

num_holes = 4:25;
%will attempt to find the appropriate hole diameter given a number of
%holes. A range of 4 to 25 was chosen as using less holes
%would likely mean too little atomization while more than 25
%may be difficult to machine or fit on the plate with sufficient
%spacing.

hole_diameters = zeros(1, length(num_holes));
iter_vector = zeros(1, length(num_holes));
error_vector = zeros(1, length(num_holes));

for i = 1:length(num_holes)
    f = @(x) m_ox(2.328038, delta_P, 778.7, 0.10795, num_holes(i), x);
    %oxidizer mass flow rate = 2.328 kg/s
    %density of nitrous oxide = 778.7 kg/m^3
    %Pre Combustion Chamber = 4.25 in = 0.10795 m

    [root, iter, error] = bisection(f, 0, 0.0254, 10000, 0.00001);
    %Hole size range: 0 to 1 inch. Given that the last Titan injector
    %hole size did not exceed 0.5 inches it is unlikely that the new
    %Titan II hole size will exceed the 1 inch size. Thus, this
    %will be used as the rightmost end of out root guessing range.

    hole_diameters(i) = root;
    iter_vector(i) = iter;
    error_vector(i) = error;
end

hole_diameters = hole_diameters*39.3701;
%converts meters to inches

%computes the discharge coefficient for each of the hole diameters
Cd_results = zeros(size(hole_diameters));
for i = 1:length(hole_diameters)
    [Cd] = Cd_calc(hole_diameters(i), 5.25);

```

```

        Cd_results(i) = Cd;
    end

varnames = {'holes', 'diameter', 'iterations', 'error', 'Cd'};
table(num_holes', hole_diameters', iter_vector', error_vector',
      Cd_results', 'VariableNames', varnames)

figure
hold on
plot(num_holes, hole_diameters, '-o')
xlim([0 26])
ylim([0 0.18])
xticks([0:26])
yticks([0:0.01:0.18])
title('Hole diameter (in) vs number of holes')
xlabel('Number of holes')
ylabel('Hole diameter (in)')
grid on
hold off

figure
plot(hole_diameters, Cd_results);
title('Discharge coefficient vs. hole diameter')
xlabel('Hole diameter (in)')
ylabel('Cd')
grid on

%test plot to see if graphical results match those of the bisection
%method implemented above (hint: they do).
%f = @(x) m_ox(1.552, delta_P, 778.7, 0.13335, 4, x);
%x = 0:0.001:0.0254;
%y = zeros(size(x));
%for i = 1:length(x)
%    y(i) = f(x(i));
%end
%plot(x, y)

function [root, iter, error] = bisection(f, xleft, xright, maxiter,
    tol)
%bisection
%Uses the bisection method to compute the root of a function over a
%certain interval, given a certain maximum number of iterations and
%an error tolerance.
%Inputs:
%    f - function who's roots we are trying to find
%    xleft - leftmost end of the interval where we're looking for
    roots
%    xright - rightmost end of the interval where we're looking for
    roots
%    maxiter - maximum number of iterations
%    tol - error tolerance
%Outputs:

```

```

    %root - root found
    %iter - number of iterations required
    %error - error
%Written by: Eduardo Landin
%November 2019

error = tol + 1;
iter = 0;
root = (xright + xleft)/2;
if f(xleft)*f(xright) > 0
    disp('no sign change in this range');
else
    while error > tol && iter < maxiter
        if f(root)*f(xright) < 0
            xleft = root;
            %if there is a sign change on the right end of the range
            %proceed to look for roots on the right end of the range.
        else
            xright = root;
            %if there is a sign change on the left end of the range
            %proceed to look for roots on the left end of the range.
        end
        root = (xright + xleft)/2;
        error = abs(f(root));
        iter = iter + 1;
    end
end

end

function [Cd] = Cd_calc(d_hole, d_pipe)
%Cd_calc
%Calculates the discharge coefficient for a small orifice given a
%certain orifice and combustion chamber diameter.
%Inputs:
    %d_pipe - the diameter of the pre-combustion chamber (m)
    %d_hole - the diameter of the holes on the injector (m)
%Outputs:
    %Cd - the estimated discharge coefficient using the polynomial
        %equation for a small orifice with cavitating flow
%Written by: Eduardo Landin
%November 2019

Beta = d_hole/d_pipe;
Cd = 0.5542 + 0.5626*Beta - 1.652*Beta^(2) + 1.68*Beta^(3);

%equation found in "Numerical Study of Cavitation Within Orifice Flow"
%Pengze Yang, December 2015.

%Note: If y'all are still using this equation in 2022 I will be
%incredibly surprised and probably dissapointed
end

```

```

function [val] = m_ox(m_ox, delta_p, rho_ox, d_pipe, num_holes,
    d_hole)
% m_ox_zeros
%A rearranged version of the oxidizer mass flowrate equation for a
% small orifice. Used in the bisection method function to determine
% the diameter of holes needed for a given number of holes (and some
% additional engine parameters)
% Inputs:
    % m_ox - the oxidizer mass flow rate of the engine (kg/s)
    % delta_p - the change in pressure across the injector bulkhead and
    % the combustion chamber. (Pa)
    % rho_ox - the density of the oxidizer used (kg/m^3)
    % d_pipe - the diameter of the pre-combustion chamber (m)
    % num_holes - the number of holes on the injector
    % d_hole - the diameter of the holes on the injector (m)
% Output:
    % val - the value returned by the rearranged equation
% Written by: Eduardo Landin
% November 2019

Beta = d_hole/d_pipe;
C_d = 0.5542 + 0.5626*Beta - 1.652*Beta^(2) + 1.68*Beta^(3);
hole_area = pi*d_hole^(2)/4;
val = (m_ox/num_holes) - C_d*hole_area*sqrt(2*delta_p*rho_ox);

end

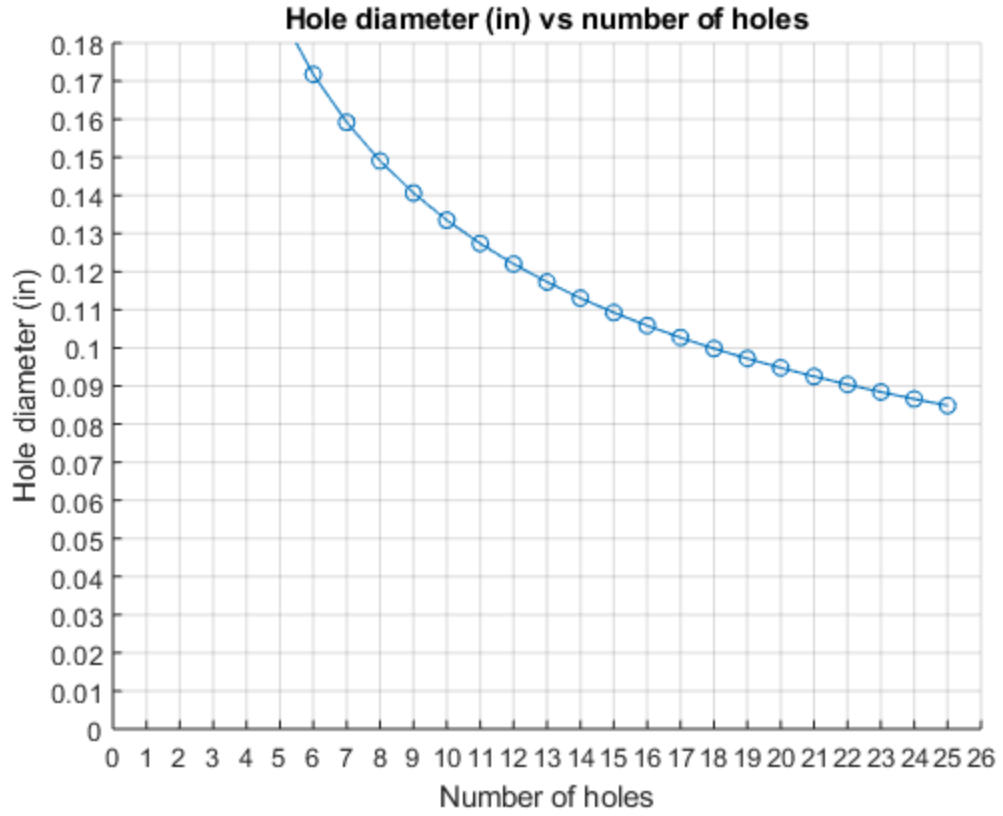
```

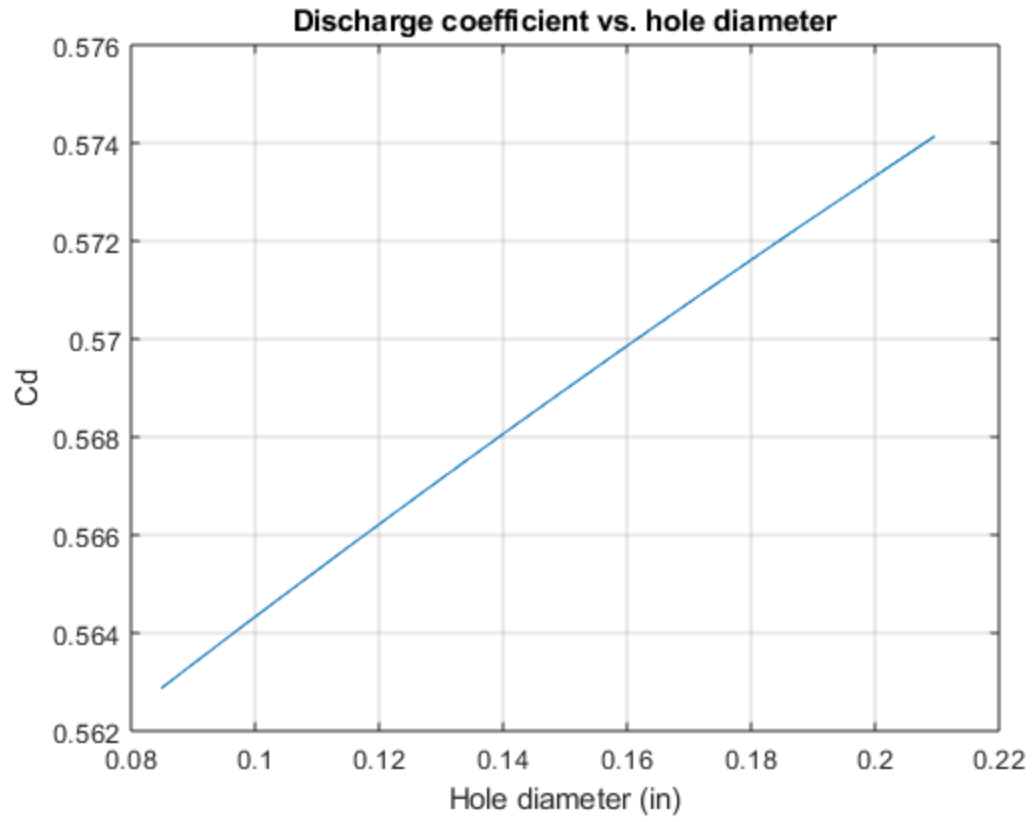
ans =

22x5 table

holes	diameter	iterations	error	Cd
4	0.20966	13	4.479e-06	0.57414
5	0.18787	16	9.7534e-06	0.57229
6	0.17175	16	8.9244e-06	0.5709
7	0.15919	16	2.9108e-06	0.56979
8	0.14905	12	6.2368e-06	0.56888
9	0.14063	16	1.9714e-06	0.56812
10	0.13351	16	7.9884e-09	0.56747
11	0.12737	17	1.5819e-07	0.5669
12	0.12201	13	2.0213e-06	0.5664
13	0.11728	14	4.2455e-06	0.56596
14	0.11306	16	3.9474e-06	0.56557
15	0.10927	15	5.6394e-06	0.56521
16	0.10584	12	5.7519e-06	0.56488
17	0.10271	15	4.4011e-06	0.56459
18	0.099838	15	5.83e-06	0.56431
19	0.097206	16	6.3843e-06	0.56406
20	0.094765	16	2.9689e-06	0.56383
21	0.092506	16	7.1029e-06	0.56361
22	0.090393	13	7.4954e-06	0.56341

23	0.088425	15	5.8416e-06	0.56322
24	0.086578	14	7.9766e-06	0.56304
25	0.084847	16	2.9899e-06	0.56287





Published with MATLAB® R2018b

D. Titan II Regression

```

%Titan_II_Regression
%February 2020
%Written by Daniel Cohen

%This script takes in Luna data for the avg regression rate
%2.5 in down the combustion chamber, an average port area,
%and a constant oxidizer flow rate. It calculates the
%constants for the regression rate equation. Titan II's fuel
%regression is then modeled with these constants and its
%respective average oxidizer flow rate and average port area.
%For a fixed final port radius, the initial port radius and
%optimal fuel grain length (that provide the correct ox fuel
%ratio) are outputted, as well as the port radius over time.

rldot = [.0669; .0442; .0432]; %regression rate data in in/s
y1 = log(rldot);

G1 = [.312;.254;.19]; %G = m'/A, units are lb/(s*in^2)
A1 = [ones(3,1) log(G1)]; %exponential regression matrices

x = (A1'*A1)\(A1'*y1); %finding the projection via normal equations,
    which minimizes error

a1 = exp(x(1))
n1 = x(2)

%a1 and n1 are the a and n values found 2.5 in
%down the combustion chamber

calcrdot = a1*G1.^n1;

figure (1)
plot(G1,calcrdot,'-o');

hold on

Gnew = 0:0.001:1;
calcrdot = a1*Gnew.^n1;
plot(Gnew,calcrdot)

hold off

xlabel('mdot/A (lb/s*in^2)')
ylabel('rdot(in/s)')
title('Luna regression data and calculated regression rate')

t = 0:0.01:11.5*2/3;

mdot_ox = 2.328038/.453592;
tfin = t(end);
rfin = 2; %need to leave .375" thick fuel at the end of the burn for
    safety, fuel grain OD is 4.75"

```

```

r0 = (-(2*n1+1)*tfin*a1*((mdot_ox/pi).^n1)+(rfin.^(2*n1+1))).^(1/
(2*n1+1))

area = pi*(rfin.^2-r0.^2); %cross sectional area of fuel burned
rho_fuel = 2.205*1009*(25.4^3)/(10^9); %density of fuel in lb/ in^3
desired_mass = 2.205* 3.174; %optimal amount of fuel burned
length = desired_mass/(rho_fuel*area) %optimal length of fuel grain

r = ((2*n1+1)*t*a1*((mdot_ox/pi).^n1)+(r0.^(2*n1+1))).^(1/
(2*n1+1)); %solution to the differential equation
rfinal = r(end) %final radius
avgrprime = (r(end)-r(1))/t(end) %avg regression rate in in/s
figure (2)
plot(t,r)
% hold on
% plot(3,r(300), 'o')
% plot(4,r(400),'o')
% hold off
xlabel('time (seconds)')
ylabel('fuel grain radius (in)')
title(strcat('Titan II fuel grain radius as a function of time when rf
=', num2str(rfin), 'in'))

a1 =

    0.1605

n1 =

    0.8288

r0 =

    1.1353

length =

    22.5391

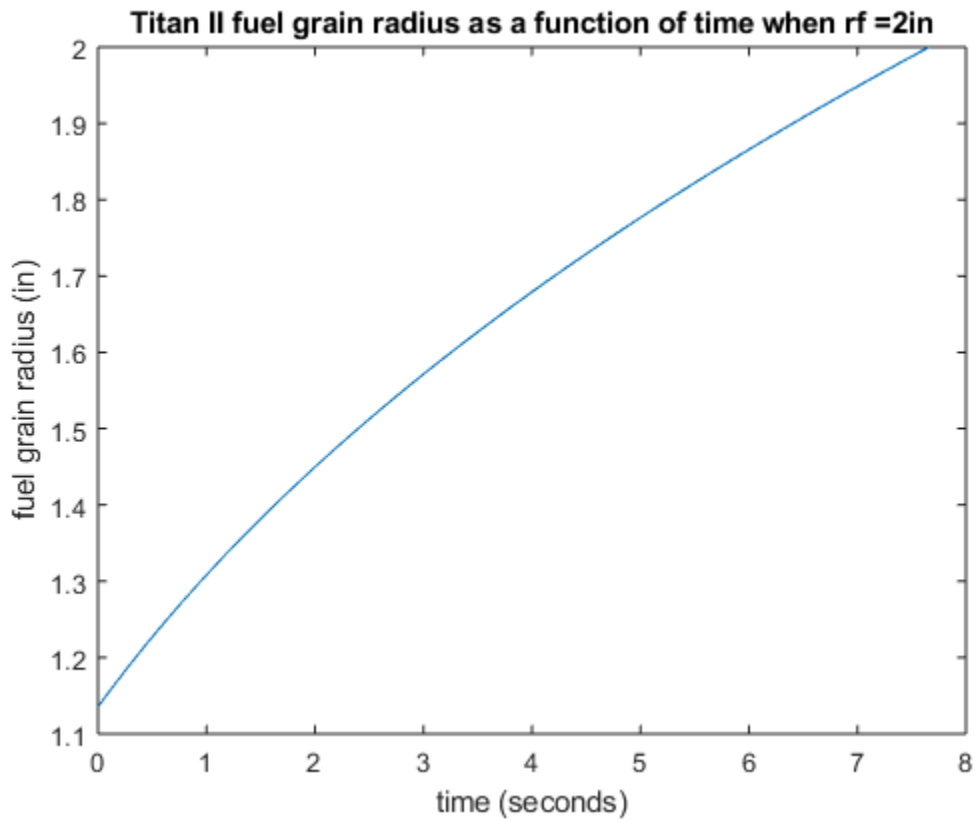
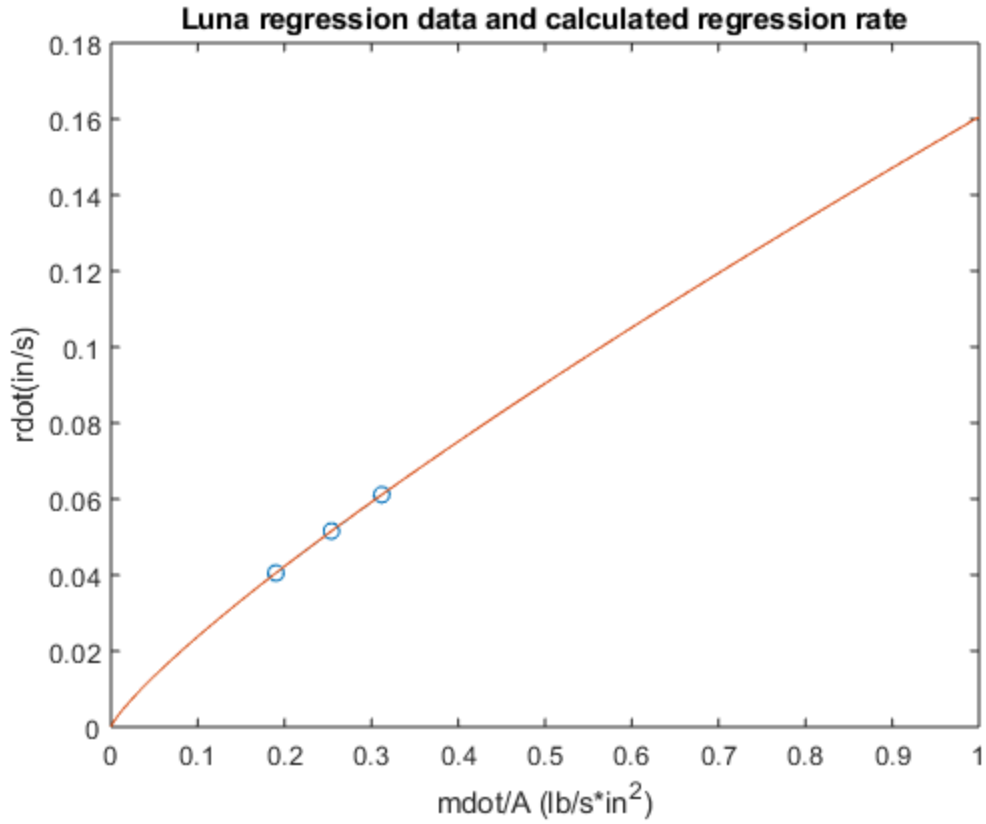
rfinal =

    2

avgrprime =

    0.1129

```



Published with MATLAB® R2018b

XI. Appendix - System Parts and Weights

Table 22. Parts List and Weights					
Part Number	Quantity	Description	Material	Weight (lb)	Weight per Unit (lb)
TII-0000-A	1	Entire Rocket Engine (Wet Weight)	-	105.5	
		Entire Rocket Engine (Dry Weight - assuming 7 lbs of fuel burned)	-	55.91	
TII-1000-A	1	Oxidizer Storage & Feed Assembly	-	35.73	
TII-1100-A	1	Vent Valve Assembly	-	3.21	
EH30-042-D012-OXCY	1	EH30 Series Vent Valve		2.9	2.9
TII-1101-A	1	Dip Tube	316 Stainless Steel	0.07	0.07
SS-400-1-4	2	1/4" MNPT to 1/4" Swage Tube adapter	Stainless Steel	0.16	0.08
SS-200-1-4	1	1/4" MNPT to 1/8" OD Tube adapter	Stainless Steel	0.08	0.08
TII-1200-A	1	Relief Valve Assembly	-	2.09	
HPRV-500 SS-T-915	1	HPRV Relief Valve	AISI 304	1.52	1.52
TII-1201-A	2	Vent Tube	316 Stainless Steel	0.10	0.05
SS-810-3-8TTM	1	Tube Fitting, Male Branch Tee, 1/2 in. Tube OD x 1/2 in. Tube OD x 1/2 in. Male NPT	Stainless Steel	0.47	0.47
TII-1300-A	1	Oxidizer Tank Assembly	-	62.12	
TII-1301-A	1	Forward Bulkhead	6061-T6 Aluminum	3.48	3.48
TII-1302-A	1	Body Cylinder	6061-T6 Aluminum	19.17	19.17
50925K431	1	Compact Extreme-Pressure Steel Pipe Fitting, Plug with Hex Drive, 7/16"-20 UN/UNF Thread Male	Galvanized Steel	0.02	0.02
91732A719	8	Helical Insert, 10-24 Right-Hand Thread, 0.380" Long	18-8 Stainless Steel	0.017	0.002
90969A120	8	Ultra-Low-Profile Shoulder Screw, 1/4" Shoulder Diameter, 3/8" Shoulder Length, 10-24 Thread	Alloy Steel, Black Oxide Finish	0.08	0.01
-	1	Oxidizer	Nitrous Oxide	39.35	39.35
TII-1400-A	1	Injection Bulkhead Assembly	-	7.65	
TII-1401-A	1	Injection Bulkhead, 6061 Aluminum	6061-T6 Aluminum	5.95	5.95

TII-1402-A	1	Injector Plate, 6061 Aluminum	6061-T6 Aluminum	0.69	0.690
50925K431	2	Compact Extreme-Pressure Steel Pipe Fitting, Plug with Hex Drive, 7/16"-20 UN/UNF Thread Male	Galvanized Steel	0.04	0.02
9396T31	7	High-Pressure Push-to-Connect Tube Fitting, for Air and Water, Adapter, 1/4" Tube OD x 1/8 NPTF Male	Nickel-Plated Brass	0.24	0.0341
92620A542	12	Zinc Yellow-Chromate Plated Hex Head Screw, Grade 8 Steel, 1/4"-20 Thread Size, 1" Long	Zinc Yellow-Chromate Plated Steel	0.22	0.018
98023A029	12	Zinc Yellow-Chromate Plated Grade 8 Steel Washer, for 1/4" Screw Size, 0.281" ID, 0.625" OD	Zinc Yellow-Chromate Plated Steel	0.06	0.005
91732A719	24	Helical Insert, 10-24 Right-Hand Thread, 0.380" Long	18-8 Stainless Steel	0.05	0.002
90969A150	24	Ultra-Low-Profile Shoulder Screw, 1/4" Shoulder Diameter, 3/4" Shoulder Length, 10-24 Thread	Alloy Steel, Black Oxide Finish	0.34	0.014
1283N209	2	High-Temperature Silicone O-Ring, 1/8 Fractional Width, Dash Number 248	Silicone	0.015	0.0075
1283N114	1	High-Temperature Silicone O-Ring, 1/8 Fractional Width, Dash Number 241	Silicone	0.0075	0.0075
1283N103	1	High-Temperature Silicone O-Ring, 1/8 Fractional Width, Dash Number 230	Silicone	0.0075	0.0075
1283N18	1	High-Temperature Silicone O-Ring, 1/16 Fractional Width, Dash Number 008	Silicone	0.0075	0.0075
91732A734	12	Helical Insert, 1/4"-20 Right-Hand Thread, 0.5" Long	18-8 Stainless Steel	0.05	0.004
TII-2000-A	1	Thrust Chamber	-	30.38	
TII-2100-A	1	Combustion Chamber	-	25.89	
TII-2101-A	1	Compressible Graphite, Pre-Combustion Chamber to Injection Bulkhead	Compressible Graphite	0.027	0.027
TII-2102-A	1	Pre-Combustion Chamber Phenolic Liner	Phenolic	0.85	0.85
TII-2103-A	1	HTPB Circular Fuel Grain	HTPB	10.87	10.87
TII-2104-A	1	Post-Combustion Chamber Phenolic Liner	Phenolic	1.601	1.61
TII-2105-A	1	Fuel Grain Phenolic Liner	Phenolic	3.30	3.30
TII-2106-A	1	Forward Fiber Glass Combustion Chamber Spacer	G10 Fiberglass	0.42	0.42
TII-2107-A	1	Aft Fiber Glass Combustion Chamber Spacer	G10 Fiberglass	0.22	0.22
TII-2108-A	1	Combustion Chamber	6061-T6 Aluminum	8.05	8.05
TII-2200-A	1	Nozzle Assembly	-	4.49	

TII-2201-A	1	Nozzle Insert, Graphite	Graphite	2.49	2.49
TII-2202-A	1	Nozzle Casing	6061-T6 Aluminum	1.65	1.65
TII-2203-A	1	Compressible Graphite, Post-Combustion Chamber to Nozzle Insert	Compressible Graphite	0.012	0.012
TII-2204-A	1	Compressible Graphite, Fuel Grain Liner to Nozzle Casing	Compressible Graphite	0.023	0.023
91732A511	24	Helical Insert, 10-32 Right-Hand Thread, 0.190" Long	18-8 Stainless Steel	0.024	0.001
92012A532	24	Precision Shoulder Screw, 1/4" Shoulder Diameter, 5/16" Shoulder Length, 10-32 Thread	Alloy Steel, Black Oxide Finish	0.27	0.011
1283N112	2	High-Temperature Silicone O-Ring, 1/8 Fractional Width, Dash Number 236	Silicone	0.015	0.0075
1283N209	1	High-Temperature Silicone O-Ring, 1/8 Fractional Width, Dash Number 248	Silicone	0.0075	0.0075
1283N207	1	High-Temperature Silicone O-Ring, 1/8 Fractional Width, Dash Number 246	Silicone	0.0075	0.0075

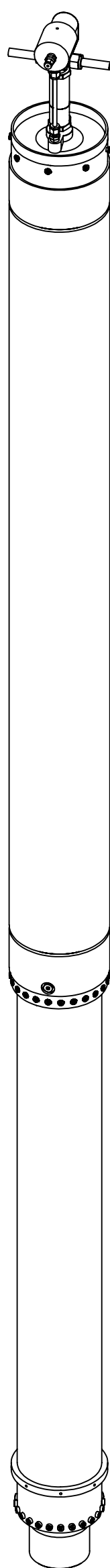
XII. Appendix - Engineering Drawings

NOTES

- 1 DRAWING IS THE SOLE AUTHORITY FOR THE BASIC FORM, LOCATION, ORIENTATION, AND DIMENSIONAL CHARACTERISTICS OF ALL DESIGN FEATURES UNLESS OTHERWISE SPECIFIED.
 - 2 ABBREVIATIONS ARE DEFINED AS FOLLOWS: UOM = UNIT OF MEASUREMENT FS = FAR SIDE
 - 3 SHEET DESIGNATION: \overline{X} X = SHEET
 - 4 ALL HOLES SHALL BE PERPENDICULAR WITHIN .010 DIA TO THE SURFACE INDICATED UNLESS OTHERWISE SPECIFIED
 - 5 BREAK ALL SHARP EDGES AND REMOVE BURRS.
 - 6 ALL THREADS SHALL BE CLASS 2 OR BETTER UNLESS OTHERWISE SPECIFIED.
 - 7 APPLY LOCTITE TO ALL FASTENERS IMMEDIATELY PRIOR TO INSTALLATION UNLESS OTHERWISE SPECIFIED.
 - 8 SAND COMPONENT TO FIT AS NEEDED.
 - 9 CAST FN P09 IN FN P11.
- THE APPLIED PRE-LOAD TORQUE SHOULD NOT EXCEED THE SPECIFIED VALUES FOR THE SPECIFIED FASTENERS:
- 1.4 LB*FT TO FN C08
 - 4.7 LB*FT TO FN C10
 - 1.5 LB*FT TO FN C12 AND C18

SUPPLIERS:

- 1 MCMASTER-CARR SUPPLY COMPANY
WWW.MCMASTER.COM
- 2 SWAGELOK COMPANY
WWW.SWAGELOK.COM
- 3 GENERANT INC
WWW.GENERANT.COM
- 4 CLARK COOPER
WWW.CLARKCOOPER.COM



- A01 ISOMETRIC VIEW FOR REFERENCE ONLY

REVISIONS				
ZONE	REV.	DESCRIPTION	DATE	APPROVED
	A		6/21/2020	

PARTS LIST CONTINUED ON SHEET 2

QTY	PART NUMBER	NOMENCLATURE OR DESCRIPTION	MATERIAL	VENDOR	SHEET	FIND NO.
1	TII-2203-A	MIDDLE COMPRESSIBLE RING	COMPRESSIBLE GRAPHITE		27	P17
1	TII-2202-A	NOZZLE CASING	ALUMINUM 6061-T6		26	P16
1	TII-2201-A	NOZZLE INSERT	GRAPHITE		25	P15
1	TII-2108-A	COMBUSTION CHAMBER	ALUMINUM 6061-T6		24	P14
1	TII-2107-A	AFT SPACER	G10 FIBERGLASS		23	P13
1	TII-2106-A	FORWARD SPACER	G10 FIBERGLASS		22	P12
8	TII-2105-A	FUEL GRAIN LINER	PHENOLIC		21	P11
8	TII-2104-A	POST-COMBUSTION CHAMBER LINER	PHENOLIC		20	P10
1	TII-2103-A	FUEL GRAIN	HTPB		19	P09
8	TII-2102-A	PRE-COMBUSTION CHAMBER LINER	PHENOLIC		18	P08
1	TII-2101-A	FORWARD COMPRESSIBLE RING	COMPRESSIBLE GRAPHITE		17	P07
1	TII-1402-A	INJECTOR PLATE	ALUMINUM 6061-T6		16	P06
1	TII-1401-A	INJECTION BULKHEAD	ALUMINUM 6061-T6		15	P05
1	TII-1302-A	BODY CYLINDER	ALUMINUM 6061-T6		14	P04
1	TII-1301-A	FORWARD BULKHEAD	ALUMINUM 6061-T6		13	P03
2	TII-1201-A	VENT TUBE	STAINLESS STEEL 316		12	P02
1	TII-1101-A	DIP TUBE	STAINLESS STEEL 316		11	P01
1	TII-2200-A	NOZZLE			10	S06
1	TII-2100-A	COMBUSTION CHAMBER			9	S05
1	TII-1400-A	INJECTION BULKHEAD			8	S04
1	TII-1300-A	OXIDIZER TANK			7	S03
1	TII-1200-A	RELIEF VALVE			6	S02
1	TII-1100-A	VENT VALVE			5	S01
1	TII-2000-A	THRUST CHAMBER			4	A02
1	TII-1000-A	OXIDIZER STORAGE AND FEED			3	A01
1	TII-0000-A	TITAN II ENGINE			1	A00

PARTS LIST

UNLESS OTHERWISE SPECIFIED: DIMENSIONS ARE IN INCHES AND APPLY AFTER FINISHES		NAME B. GERWIN	DATE 06/21/20	RICE ECLIPSE TITLE: TITAN II ENGINE
DEFAULT TOLERANCES: FRACTION ± 1/16 ANGLE ± .5° 1 PL ± .1 2 PL ± .03 3 PL ± .010		CHECKED J. KEOGH	06/28/20	
INTERPRET DRAWING PER ASME Y14.100-2004		ENG APPR.		
INTERPRET GEOMETRIC TOLERANCING PER ASME Y14.5M-1994		MFG APPR.		
PROPRIETARY AND CONFIDENTIAL THE INFORMATION CONTAINED IN THIS DRAWING IS THE SOLE PROPERTY OF RICE ECLIPSE. ANY REPRODUCTION IN PART OR AS A WHOLE WITHOUT THE WRITTEN PERMISSION OF RICE ECLIPSE IS PROHIBITED.	NEXT ASSY	USED ON	APPLICATION	COMMENTS: THIS IS RICE ECLIPSE'S FIRST ATTEMPT AT DRAFTING TO ASME Y14.1 AND Y14.5 STANDARDS. AN ATTEMPT WAS MADE TO ESTABLISH TOLERANCES THAT WILL ENSURE ALL PARTS FUNCTION AS INTENDED. FEEDBACK IS APPRECIATED.
SCALE: NONE				SIZE DWG. NO. D TII-0000-A
SHEET 1 OF 29				REV A

8

7

6

5

4

3

2

1

REVISIONS				
ZONE	REV.	DESCRIPTION	DATE	APPROVED
-	-	SEE SHEET 1	-	-

12	91732A734	1/4-20 X 0.5 HELICAL INSERT	STAINLESS STEEL 18-8	△1		C21
1	1283N207	O-RING DASH NUMBER 246	SILICONE	△1		C20
2	1283N109	O-RING DASH NUMBER 236	SILICONE	△1		C19
24	92012A532	10-32 X 5/16" SHOULDER SCREW	ALLOY STEEL	△1		C18
24	91732A511	10-32 X .190 HELICAL INSERT	STAINLESS STEEL 18-8	△1		C17
1	1283N18	O-RING DASH NUMBER 008	SILICONE	△1		C16
1	1283N103	O-RING DASH NUMBER 230	SILICONE	△1		C15
1	1283N114	O-RING DASH NUMBER 241	SILICONE	△1		C14
3	1283N209	O-RING DASH NUMBER 248	SILICONE	△1		C13
24	90969A150	10-24 X 3/4" SHOULDER SCREW	ALLOY STEEL	△1		C12
12	98023A029	1/4 WASHER	GRADE 8 STEEL	△1		C11
12	92620A542	1/4-20 HHS	GRADE 8 STEEL	△1		C10
6	9396T31	PUSH-TO-CONNECT	NICKEL-PLATED BRASS	△1		C09
8	90969A120	10-24 X 3/8" SHOULDER SCREW	ALLOY STEEL	△1		C08
32	91732A719	10-24 X .380 HELICAL INSERT	STAINLESS STEEL 18-8	△1		C07
3	50925K431	PIPE FITTING	GALVANIZED STEEL	△1		C06
1	SS-810-3-8TMM	TUBE FITTING	STAINLESS STEEL 316	△2		C05
1	HPRV-500 SS-T-915	HPRV RELIEF VALVE	AISI 304	△3		C04
1	SS-200-1-4	1/4 MNPT TO 1/8 OD TUBE ADAPTER	STAINLESS STEEL	△2		C03
2	SS-400-1-4	1/4 MNPT TO 1/4 SWAGE ADAPTER	STAINLESS STEEL	△2		C02
1	EH30-042-D012-OXCY	EH30 SERIES VENT VALVE		△4		C01
1	TII-2204-A	AFT COMPRESSIBLE RING	COMPRESSIBLE GRAPHITE		28	P18
QTY	PART NUMBER	NOMENCLATURE OR DESCRIPTION	MATERIAL	VENDOR	SHEET	FIND NO.

PARTS LIST		
SIZE	DWG. NO.	REV
D	TII-0000-A	-
SCALE: NONE		Sheet: 2

5

4

3

2

1

8

7

6

5

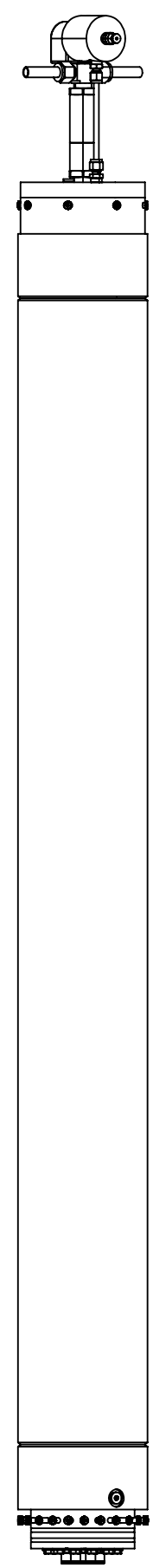
4

3

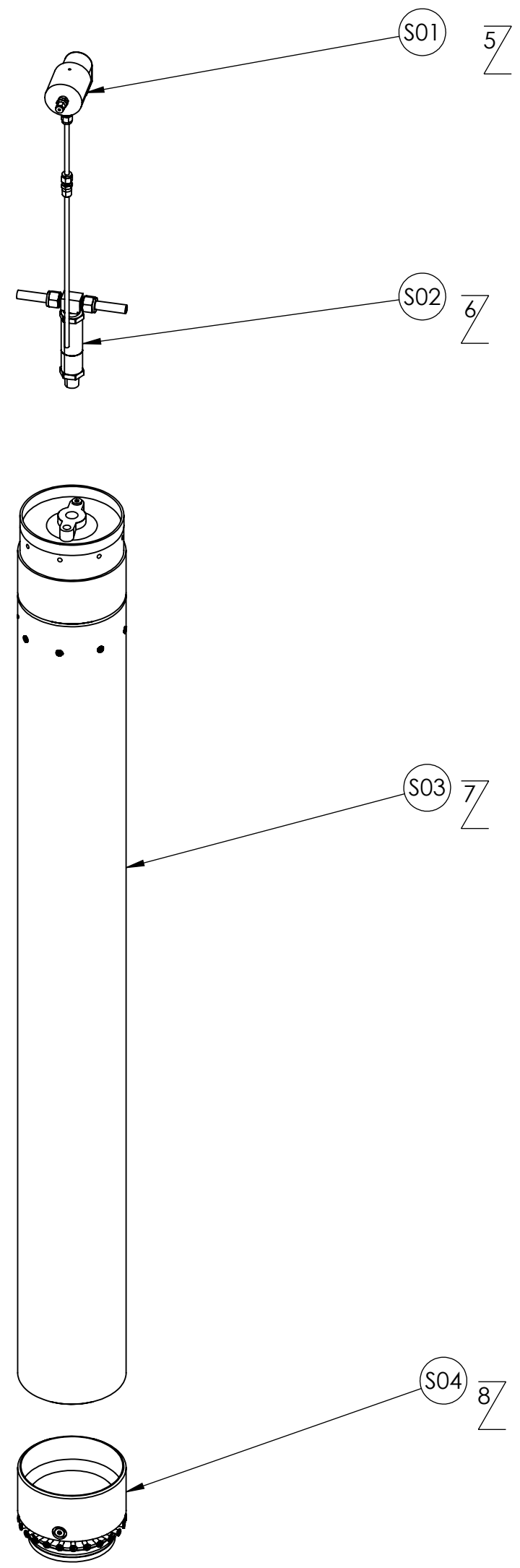
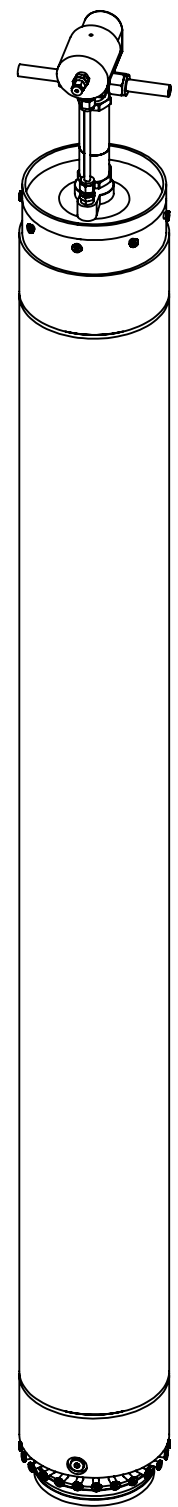
2

1

REVISIONS				
ZONE	REV.	DESCRIPTION	DATE	APPROVED
	-	SEE SHEET 1	-	-



(A01) OXIDIZER STORAGE AND FEED ASSEMBLY

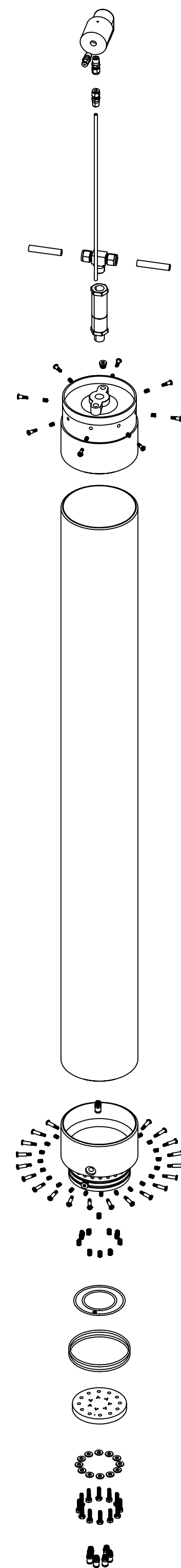


(S01) 5/

(S02) 6/

(S03) 7/

(S04) 8/



5

4

3

2

1

8

7

6

5

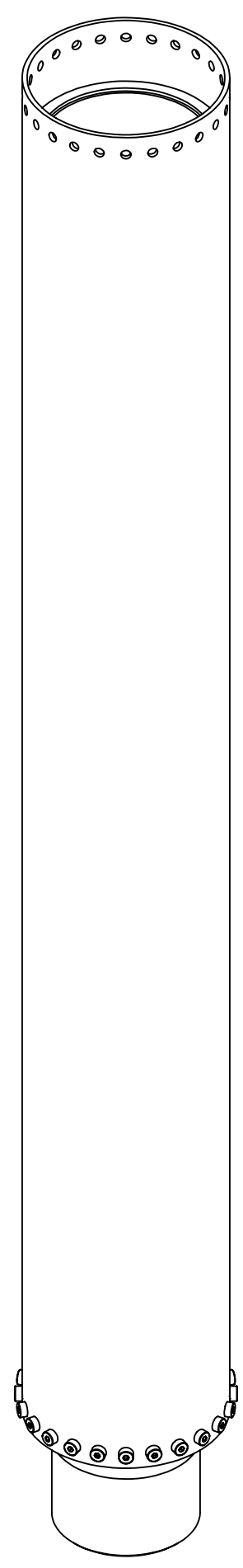
4

3

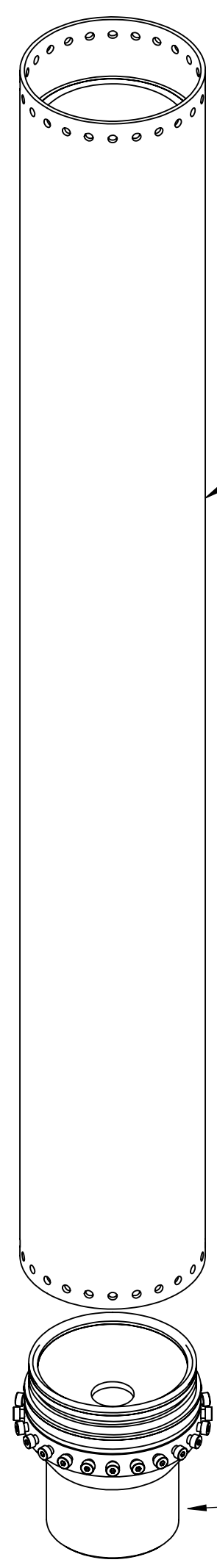
2

1

REVISIONS				
ZONE	REV.	DESCRIPTION	DATE	APPROVED
	-	SEE SHEET 1	-	-

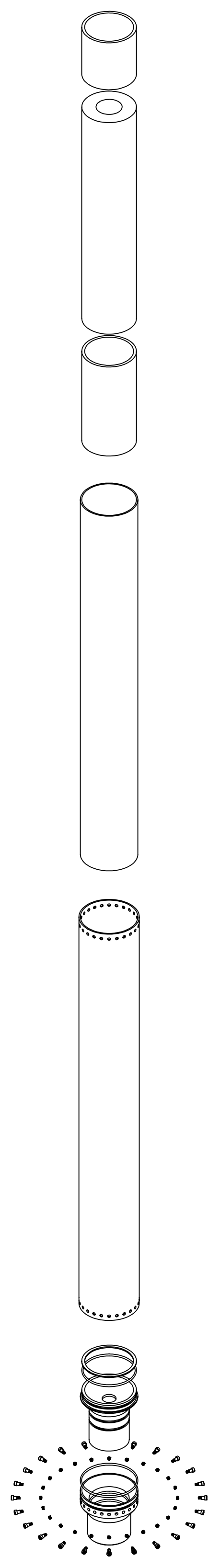


A02 THRUST CHAMBER ASSEMBLY



S05 9

S06 10



8

7

6

5

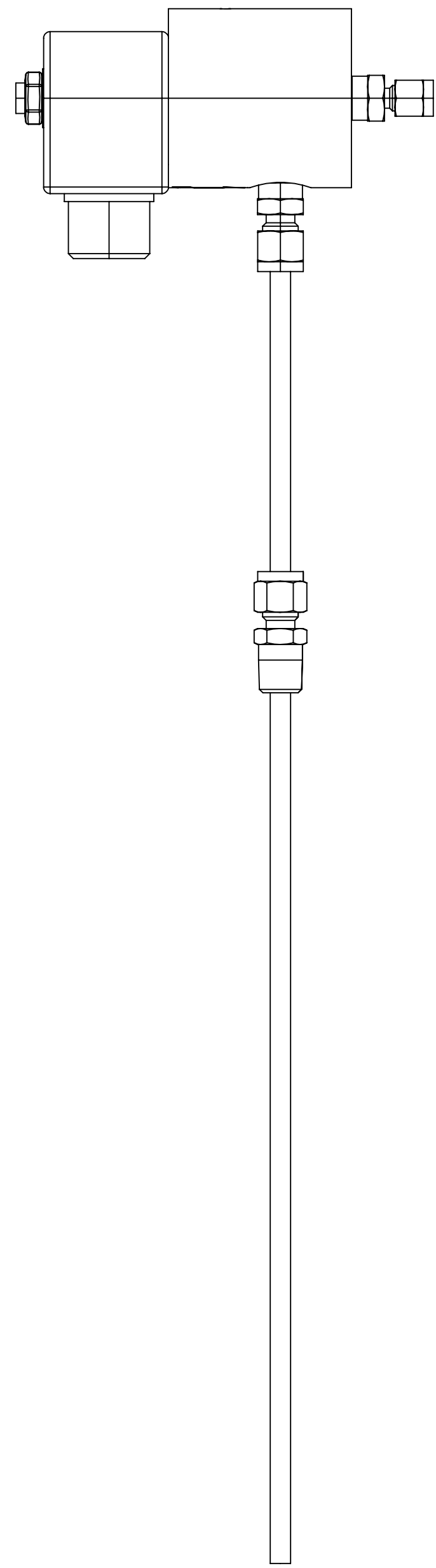
4

3

2

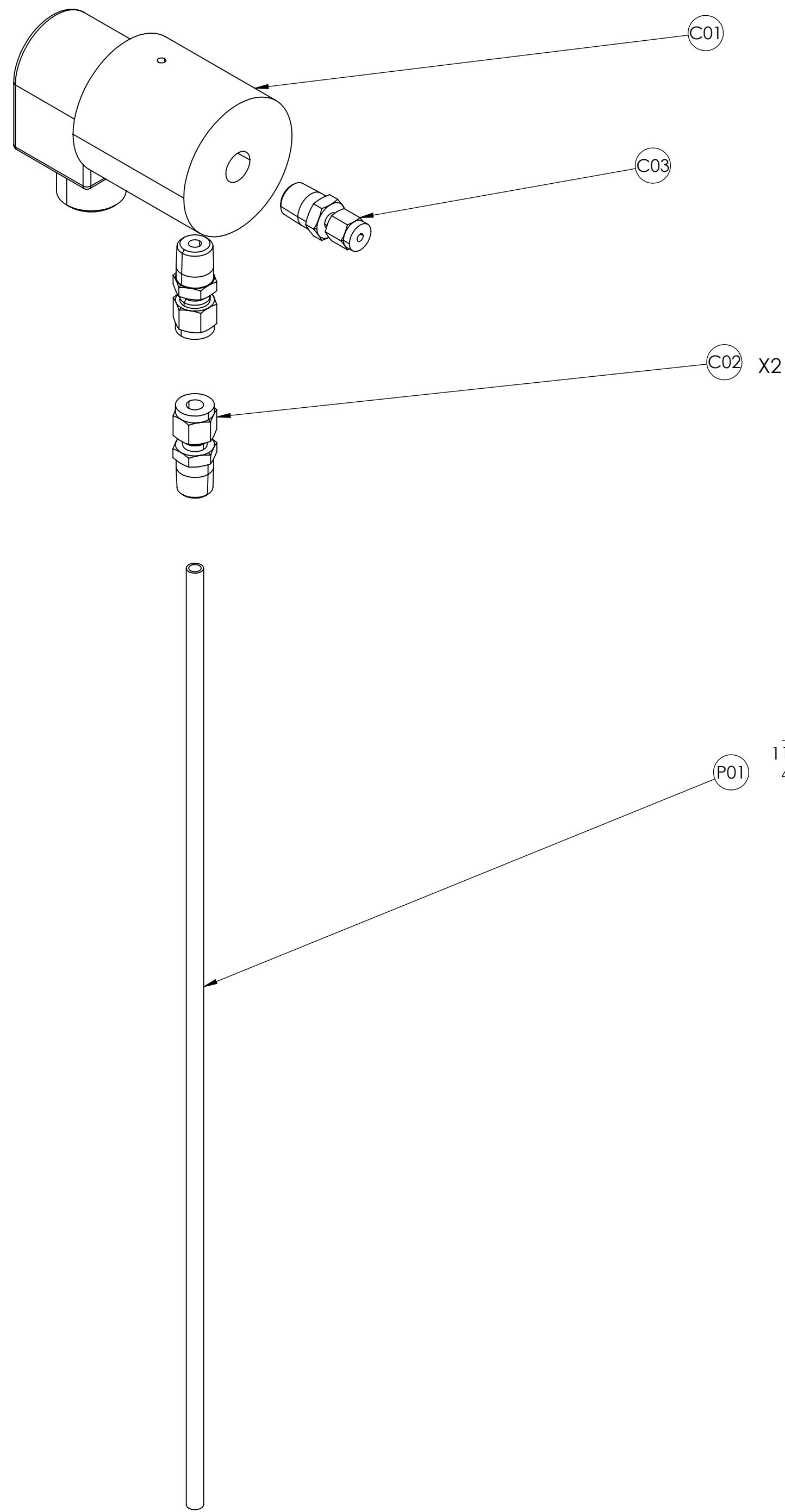
1

REVISIONS				
ZONE	REV.	DESCRIPTION	DATE	APPROVED
	-	SEE SHEET 1	-	-



(S01) VENT VALVE ASSEMBLY

3



(C01)

(C03)

(C02) X2

(P01) 11

8

7

6

5

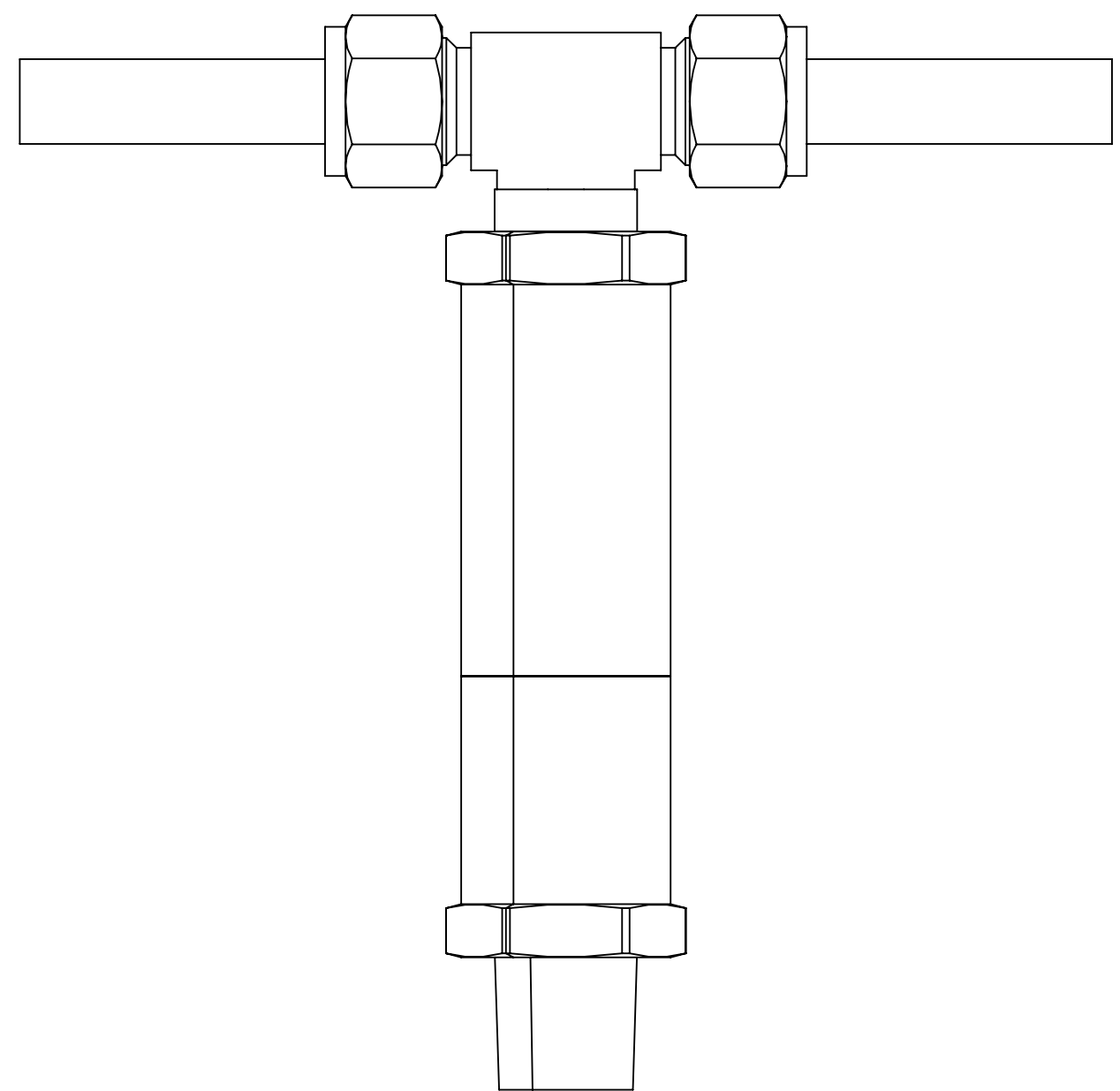
4

3

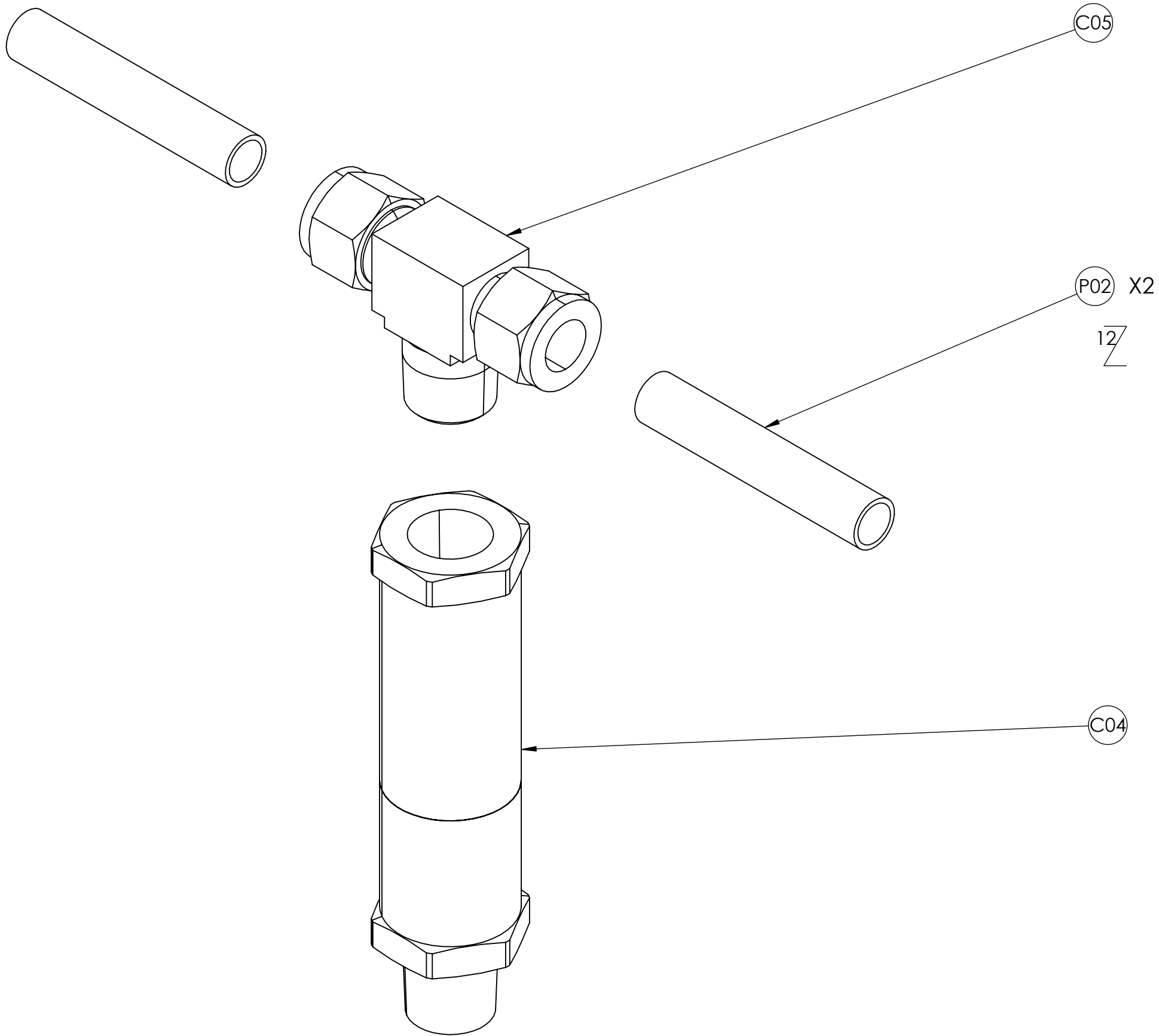
2

1

REVISIONS				
ZONE	REV.	DESCRIPTION	DATE	APPROVED
	-	SEE SHEET 1	-	-



(S02) RELIEF VALVE ASSEMBLY
3/



8

7

6

5

4

3

2

1

REVISIONS				
ZONE	REV.	DESCRIPTION	DATE	APPROVED
	-	SEE SHEET ONE	-	-

D

D

C

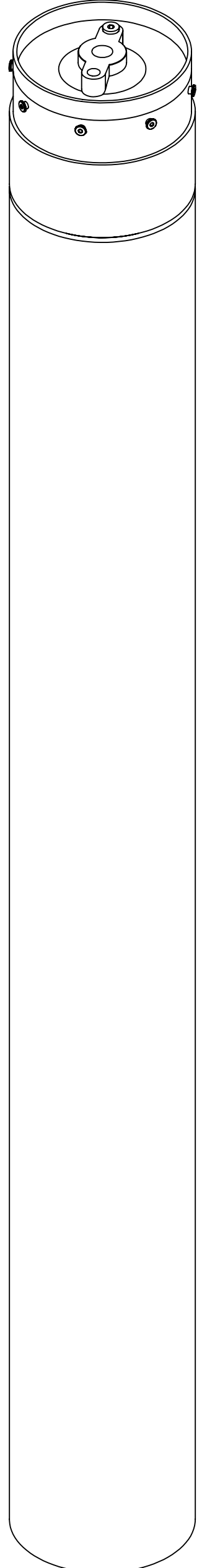
C

B

B

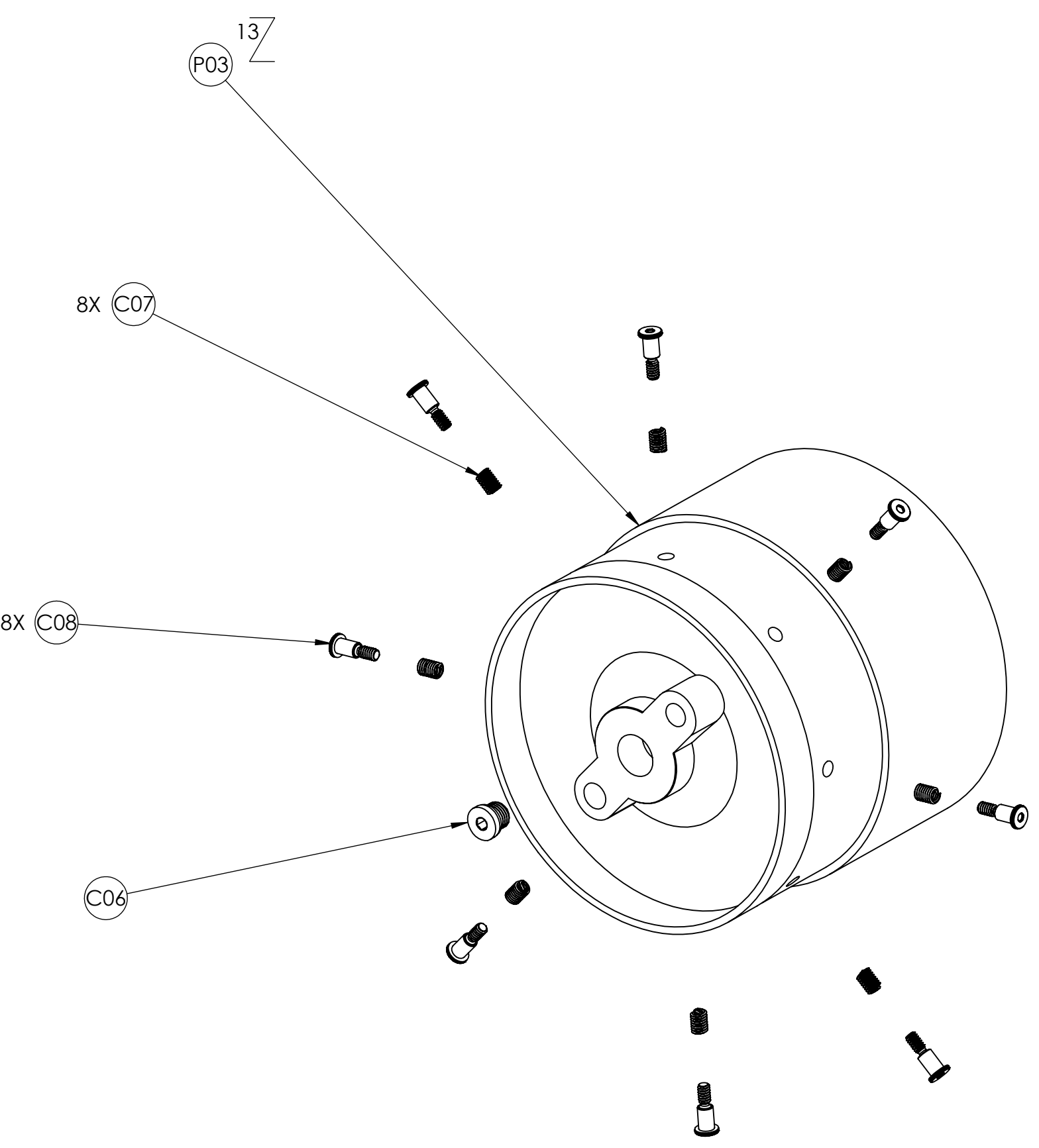
A

A



(S03) OXIDIZER TANK ASSEMBLY

3/



8X (C07)

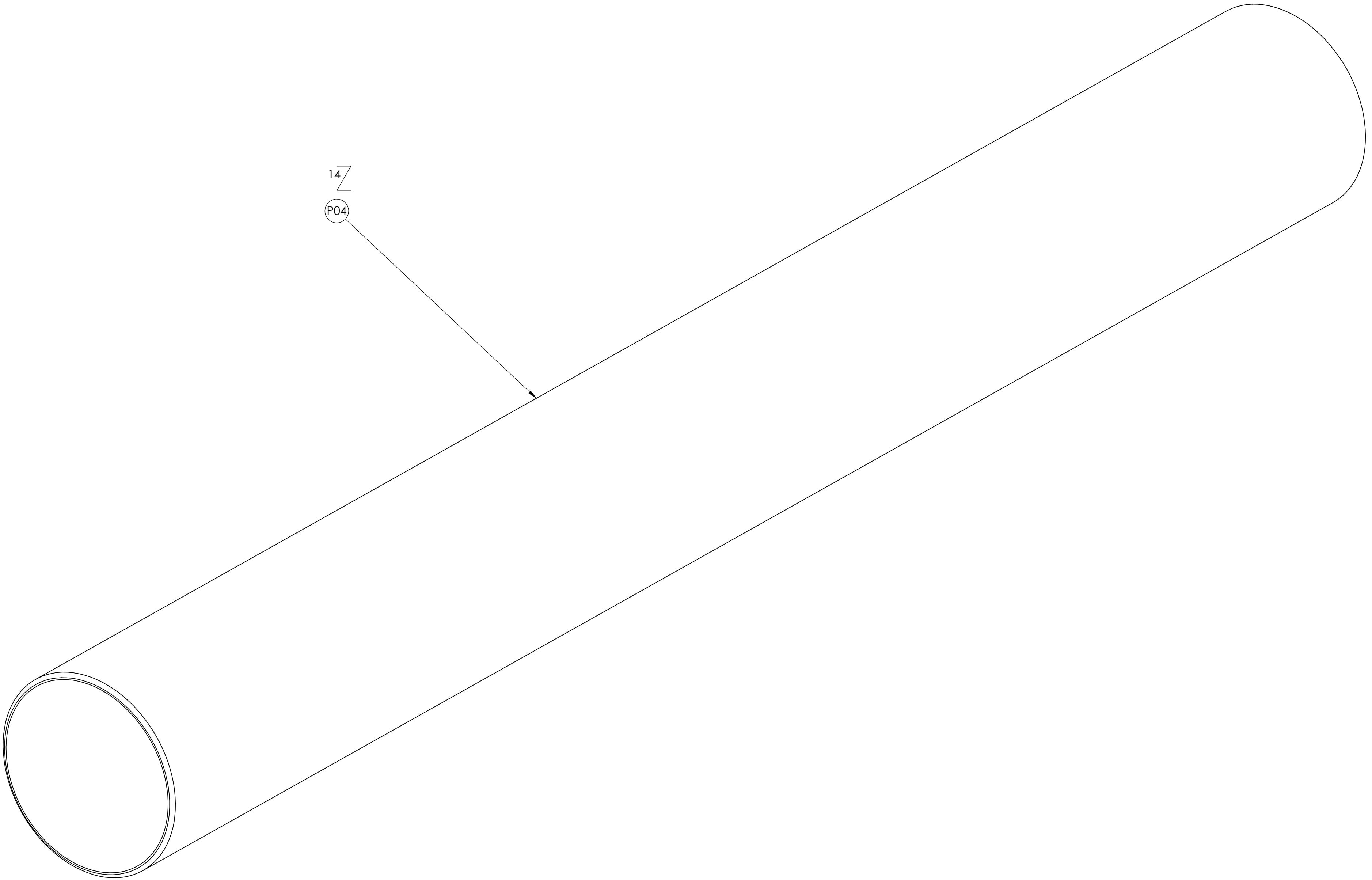
8X (C08)

(C06)

(P03) 13/

14/

(P04)



8

7

6

5

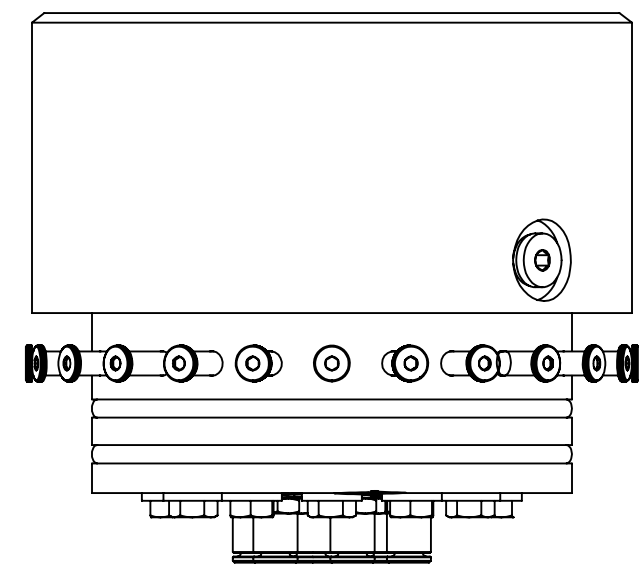
4

3

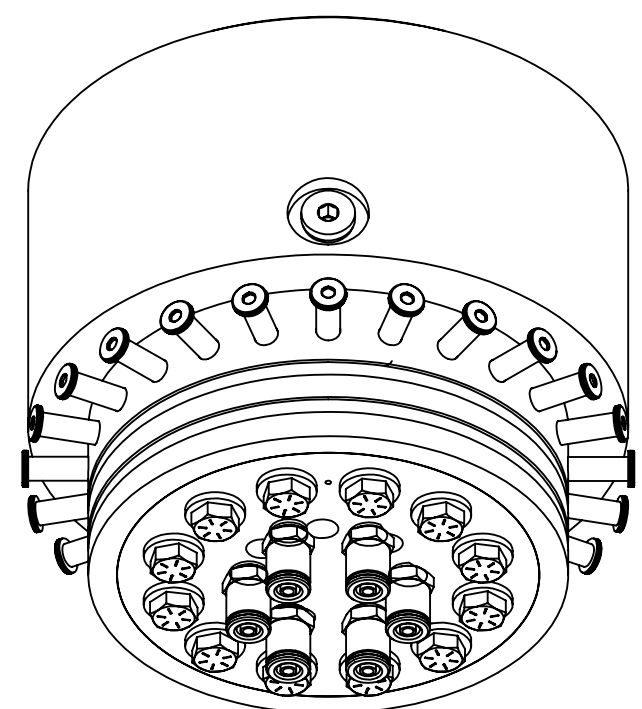
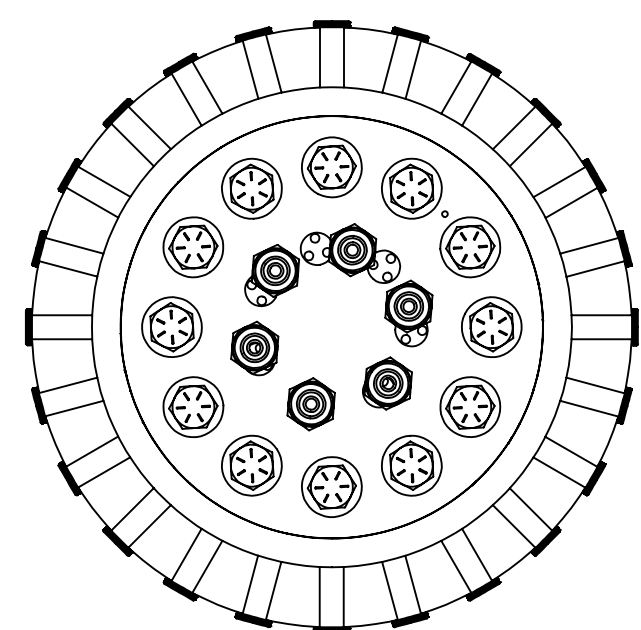
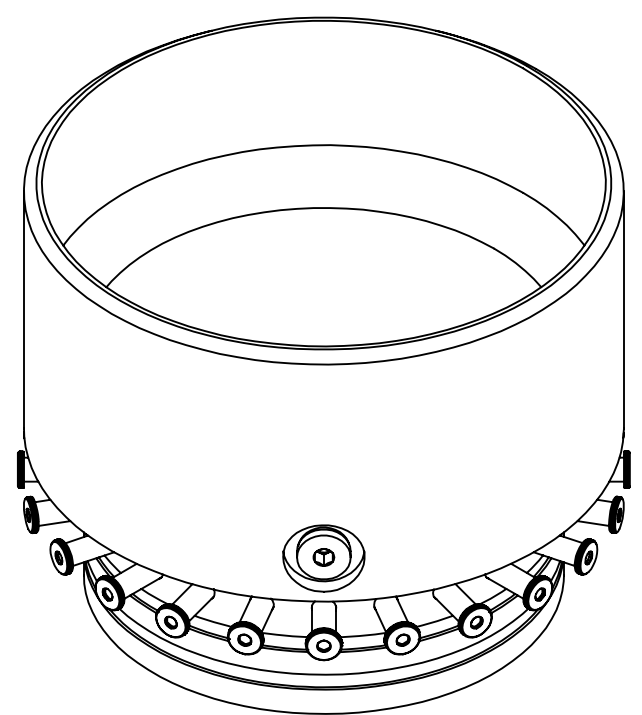
2

1

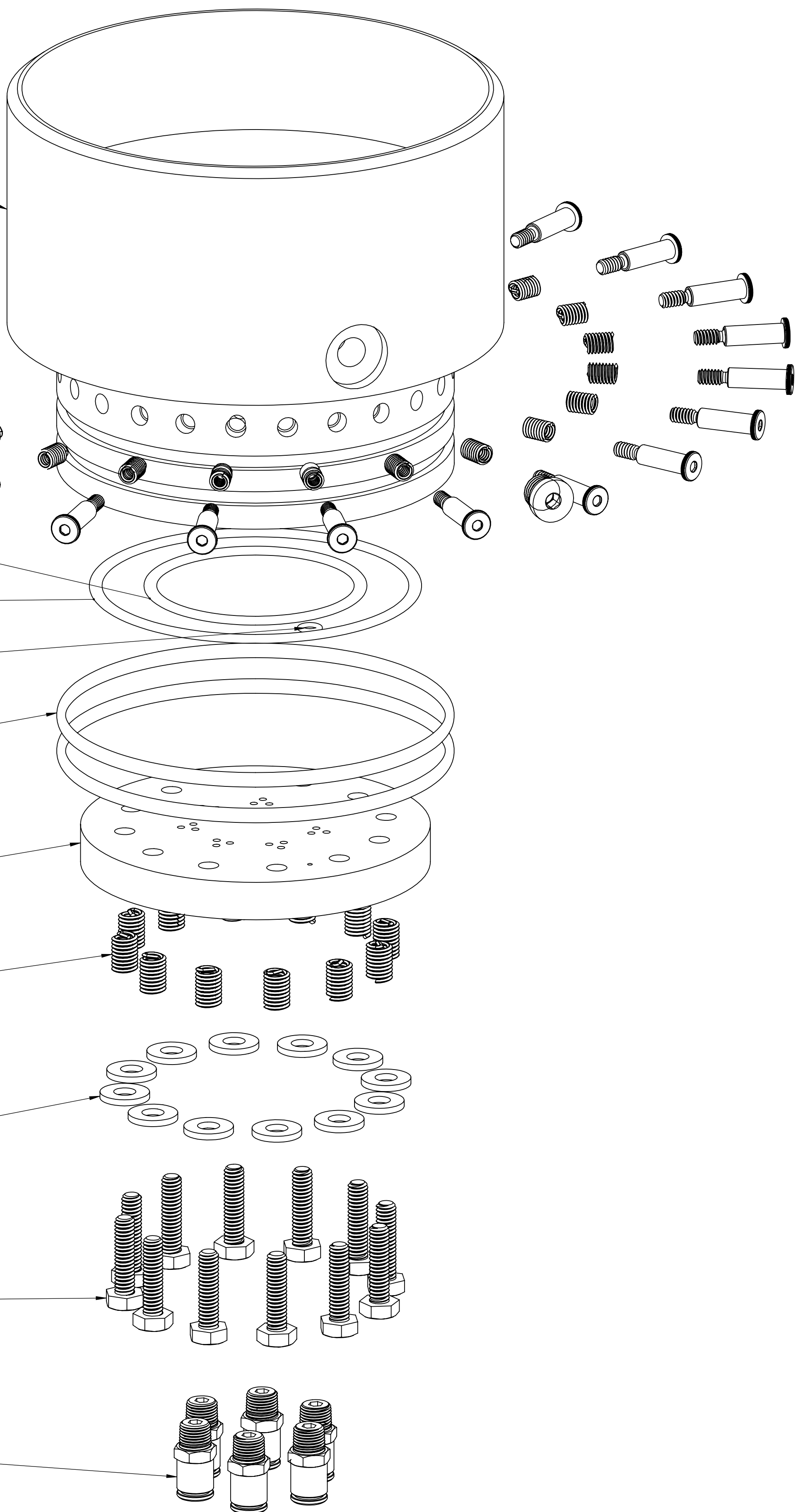
REVISIONS				
ZONE	REV.	DESCRIPTION	DATE	APPROVED
	-	SEE SHEET 1	-	-



(S04) INJECTION BULKHEAD ASSEMBLY
3



- 2X (C06)
- 15 (P05)
- 24X (C07)
- 24X (C12)
- (C15)
- (C14)
- 2X (C16)
- (C13)
- 16 (P06)
- (C21)
- 12X
- 12X (C11)
- 12X (C10)
- 6X (C09)



8

7

6

5

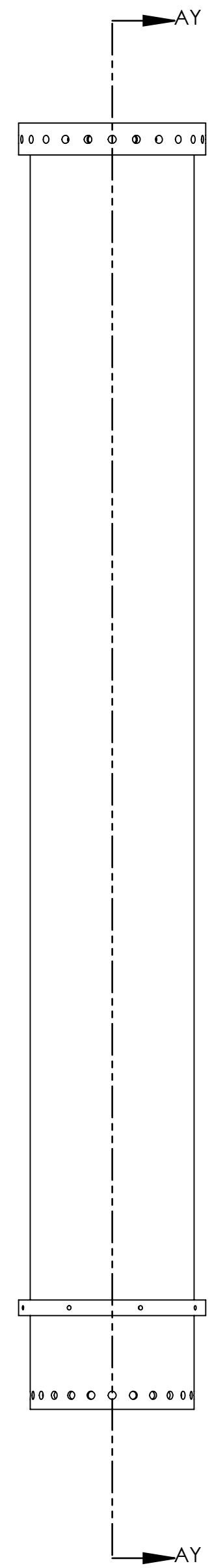
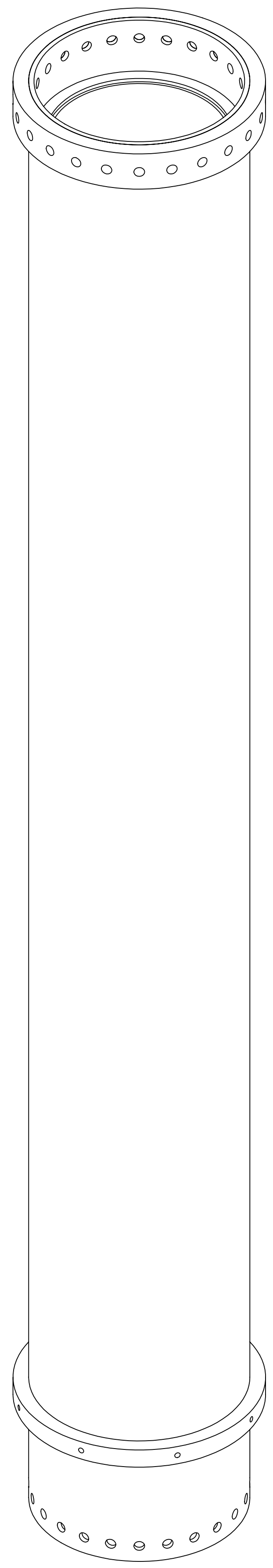
4

3

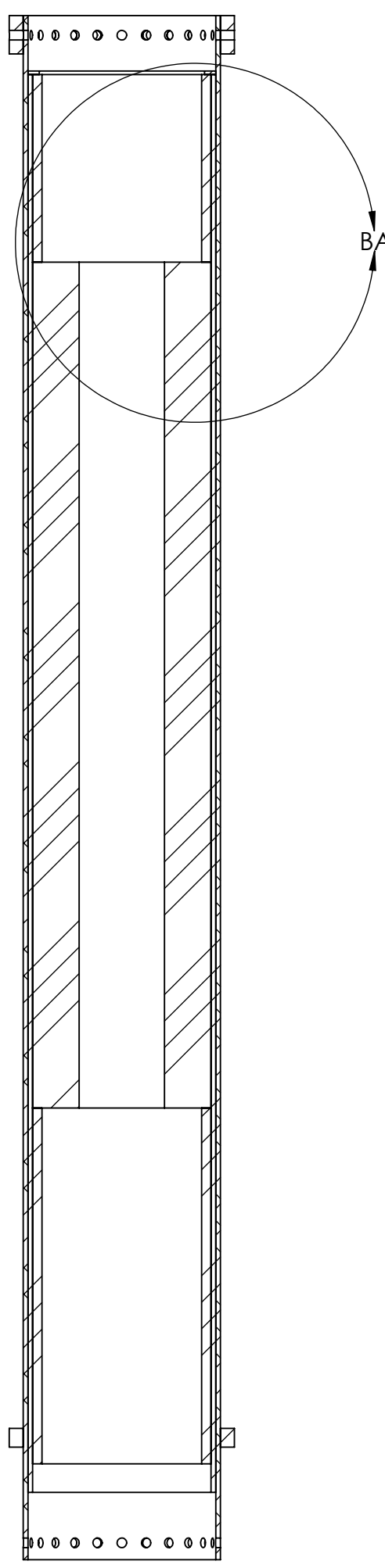
2

1

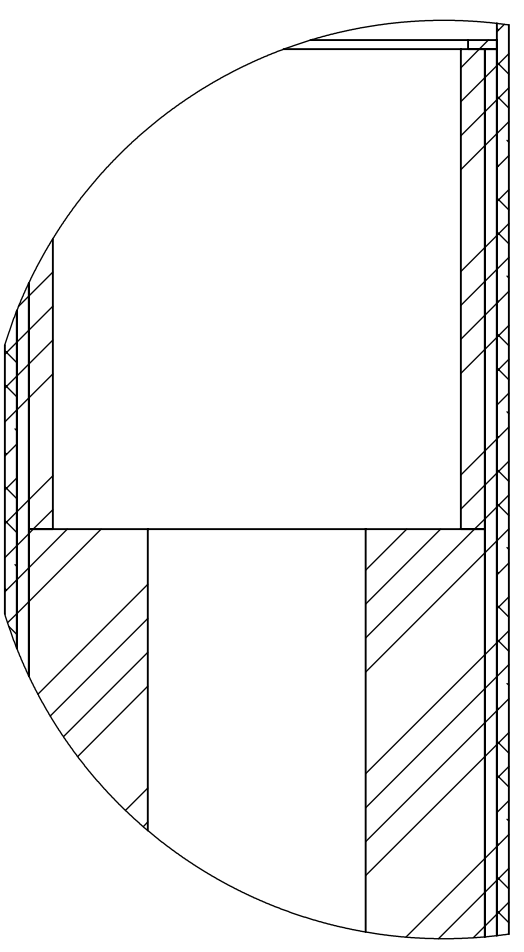
REVISIONS				
ZONE	REV.	DESCRIPTION	DATE	APPROVED
	-	SEE SHEET 1	-	-



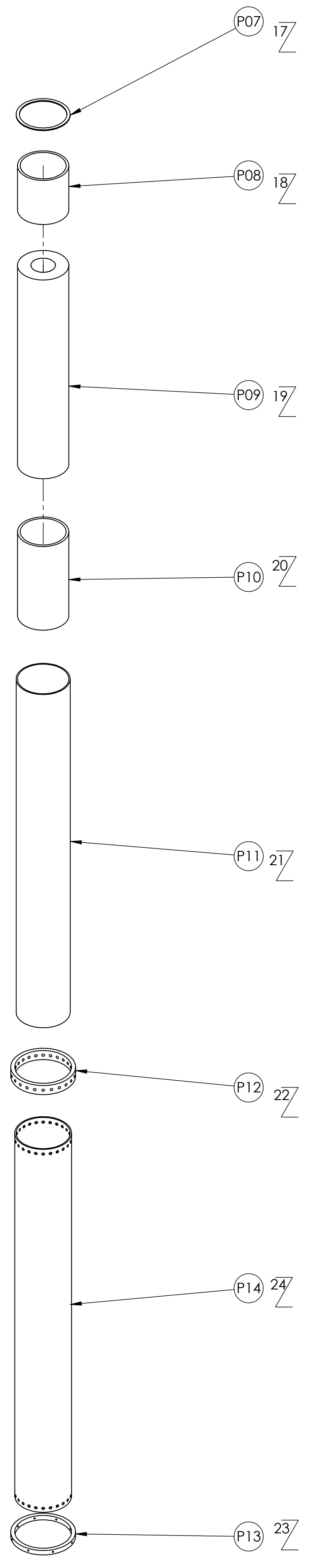
(S05) COMBUSTION CHAMBER ASSEMBLY
SCALE 1 : 4



SECTION AY-AY
SCALE 1 : 4



DETAIL BA
SCALE 1 : 2



SIZE	DWG. NO.	REV
D	TII-2100-A	-
SCALE: N/A	WEIGHT:	SHEET 9 OF 29

8

7

6

5

4

3

2

1

8

7

6

5

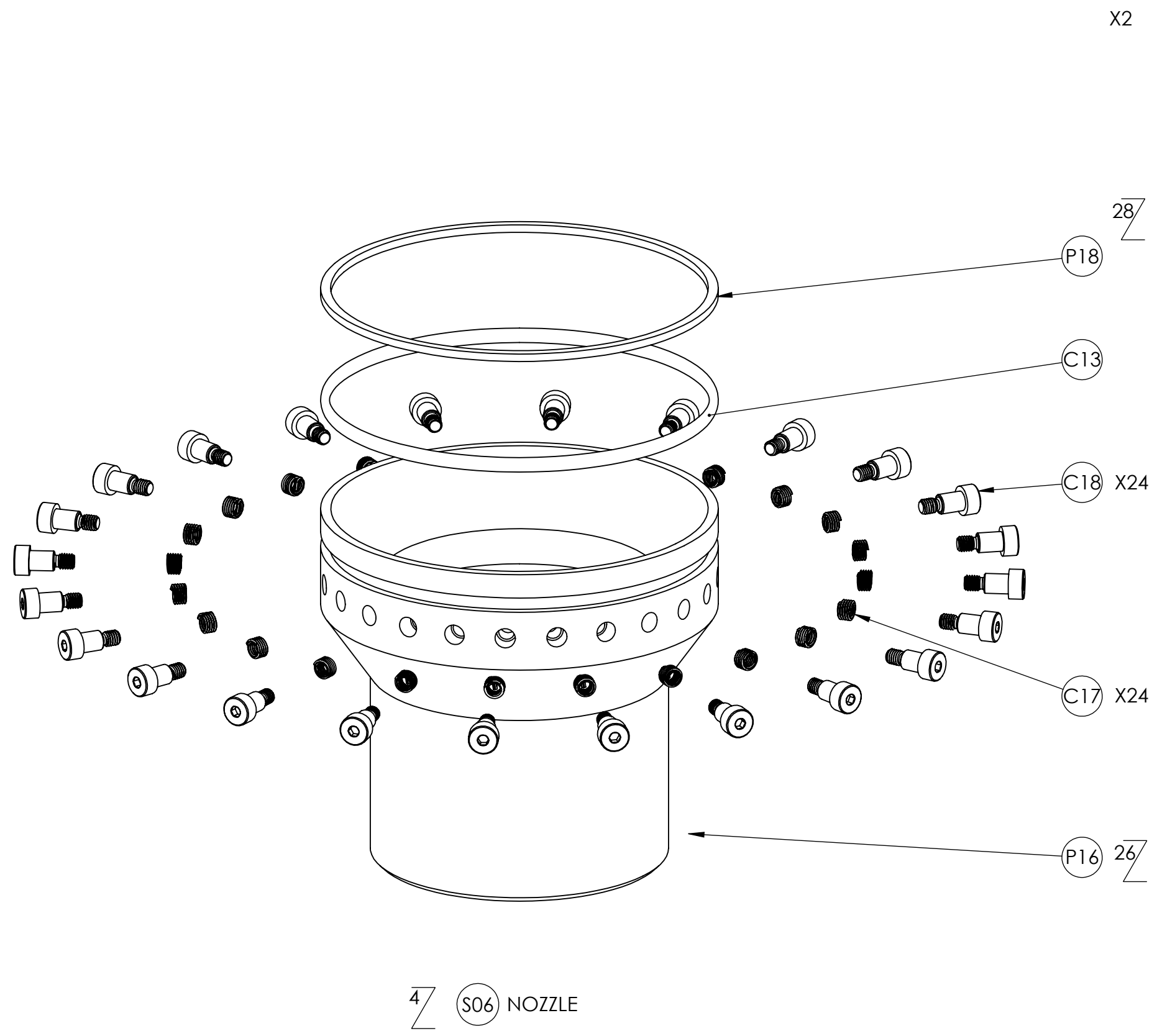
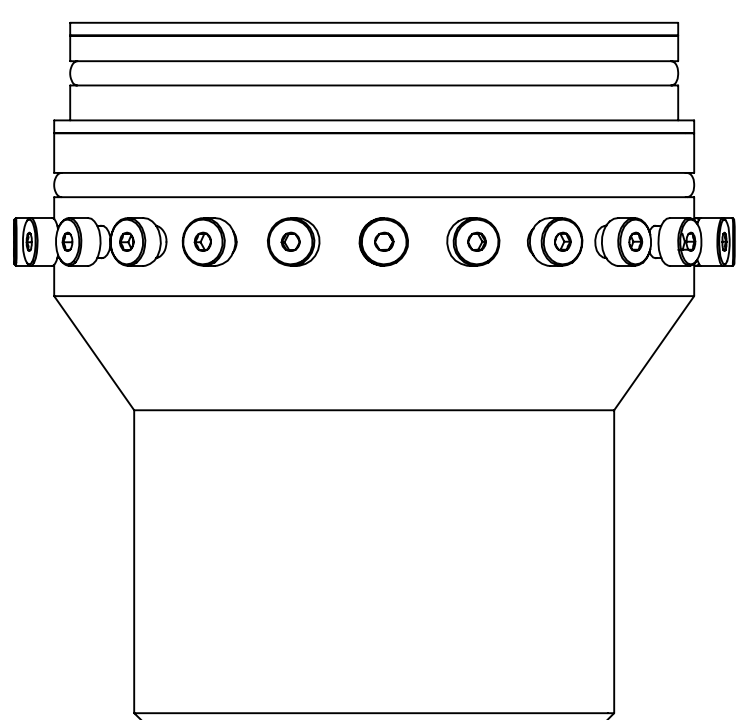
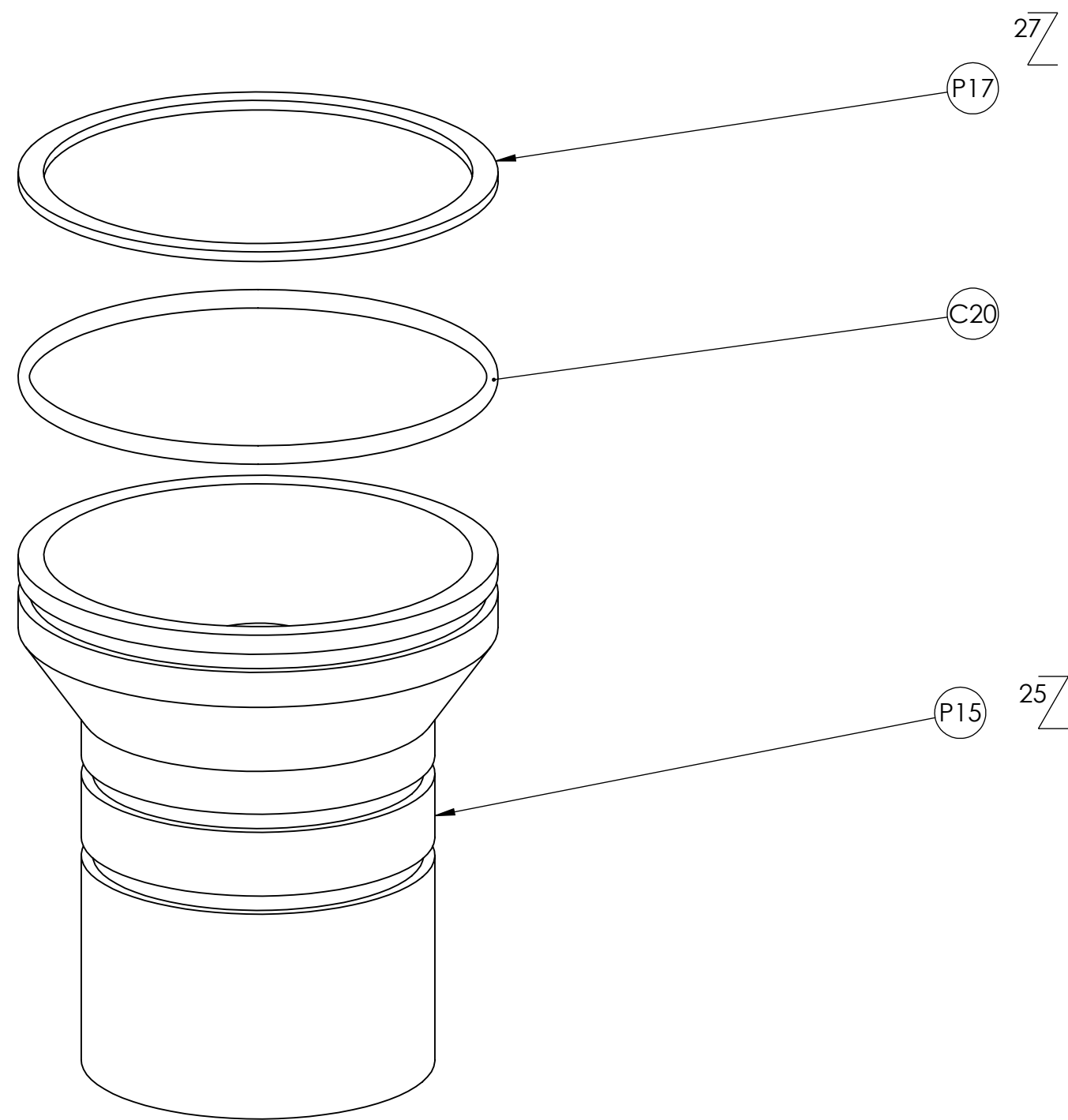
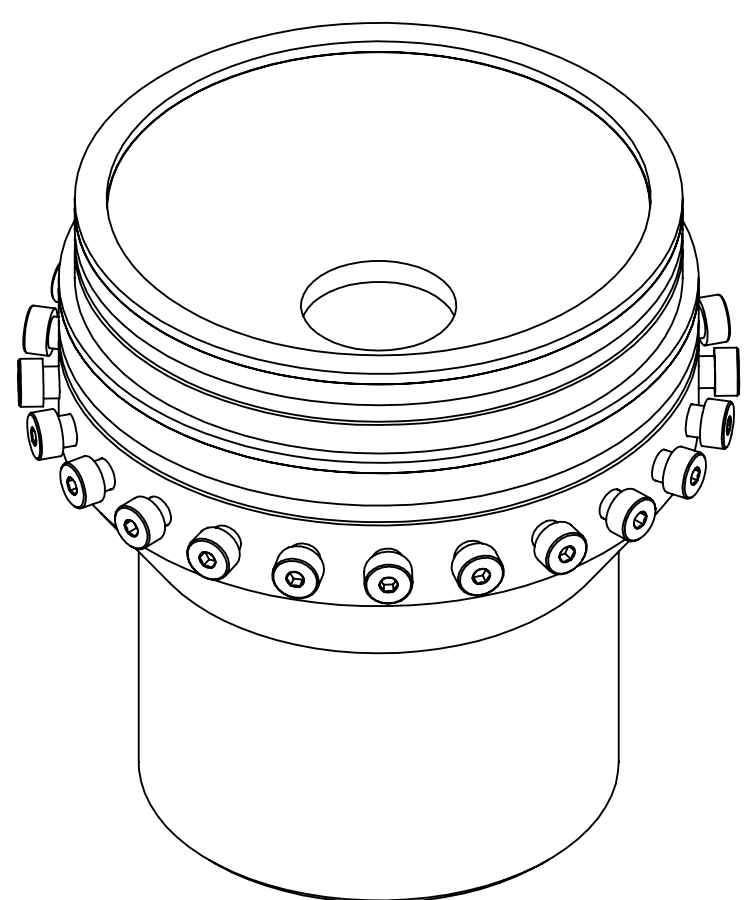
4

3

2

1

REVISIONS				
ZONE	REV.	DESCRIPTION	DATE	APPROVED
	-	SEE SHEET 1	-	-



8

7

6

5

4

3

2

1

REVISIONS				
ZONE	REV.	DESCRIPTION	DATE	APPROVED
	-	SEE SHEET 1	-	-

D

D

C

C

B

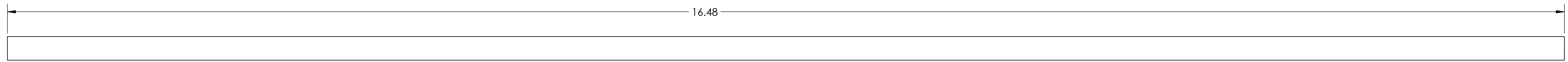
B

A

A



- P01 ISOMETRIC VIEW FOR REFERENCE ONLY

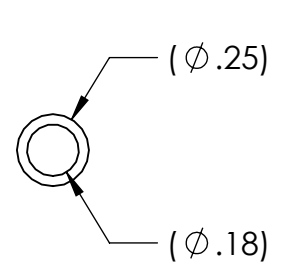


16.48

P01

DIP TUBE

5



(ϕ .25)

(ϕ .18)

8

7

6

5

4

3

2

1

8

7

6

5

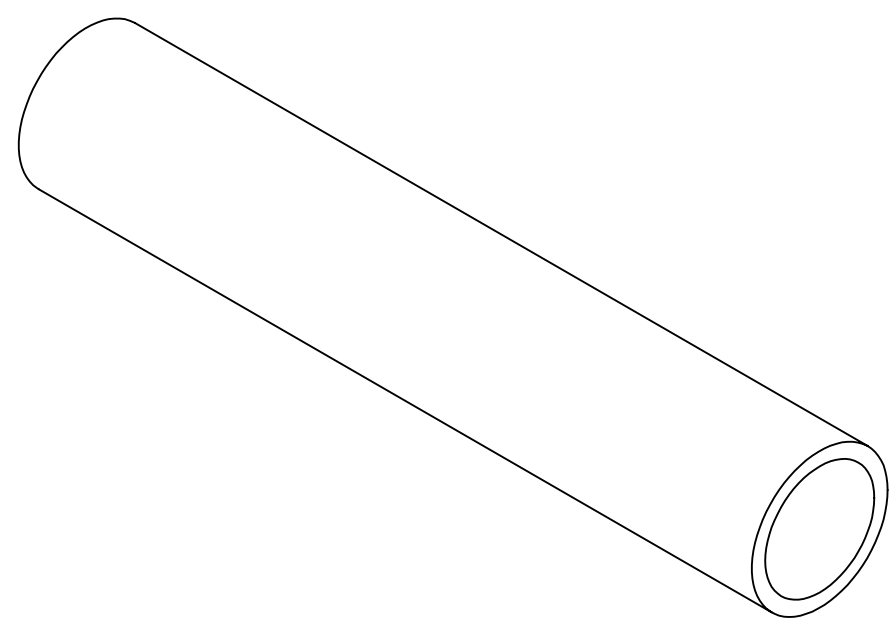
4

3

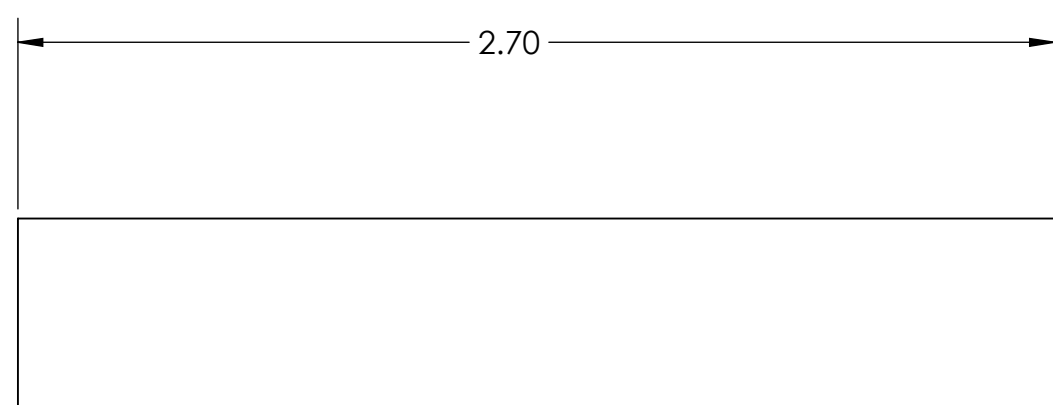
2

1

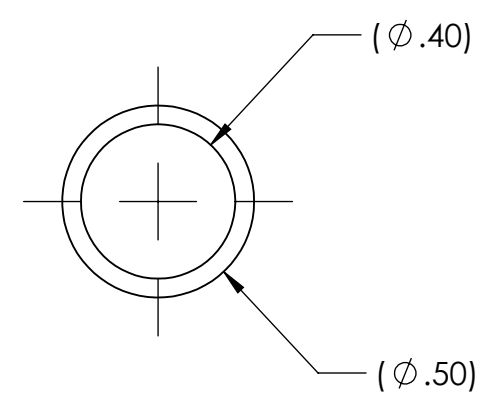
REVISIONS				
ZONE	REV.	DESCRIPTION	DATE	APPROVED
	-	SEE SHEET 1	-	-



- P02 ISOMETRIC VIEW FOR REFERENCE ONLY



P02 VENT TUBE



D

D

C

C

B

B

A

A

8

7

6

5

4

3

2

1

8

7

6

5

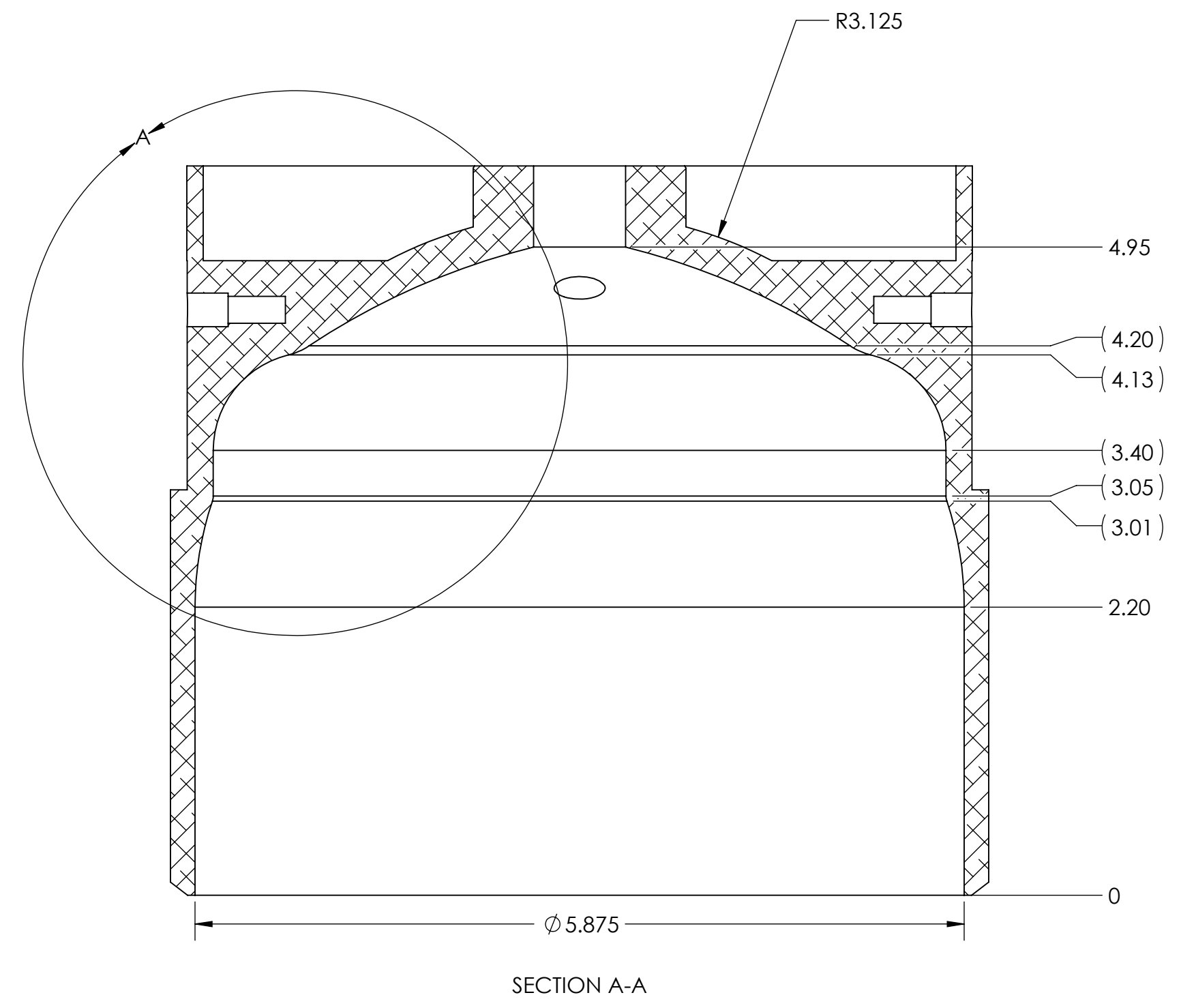
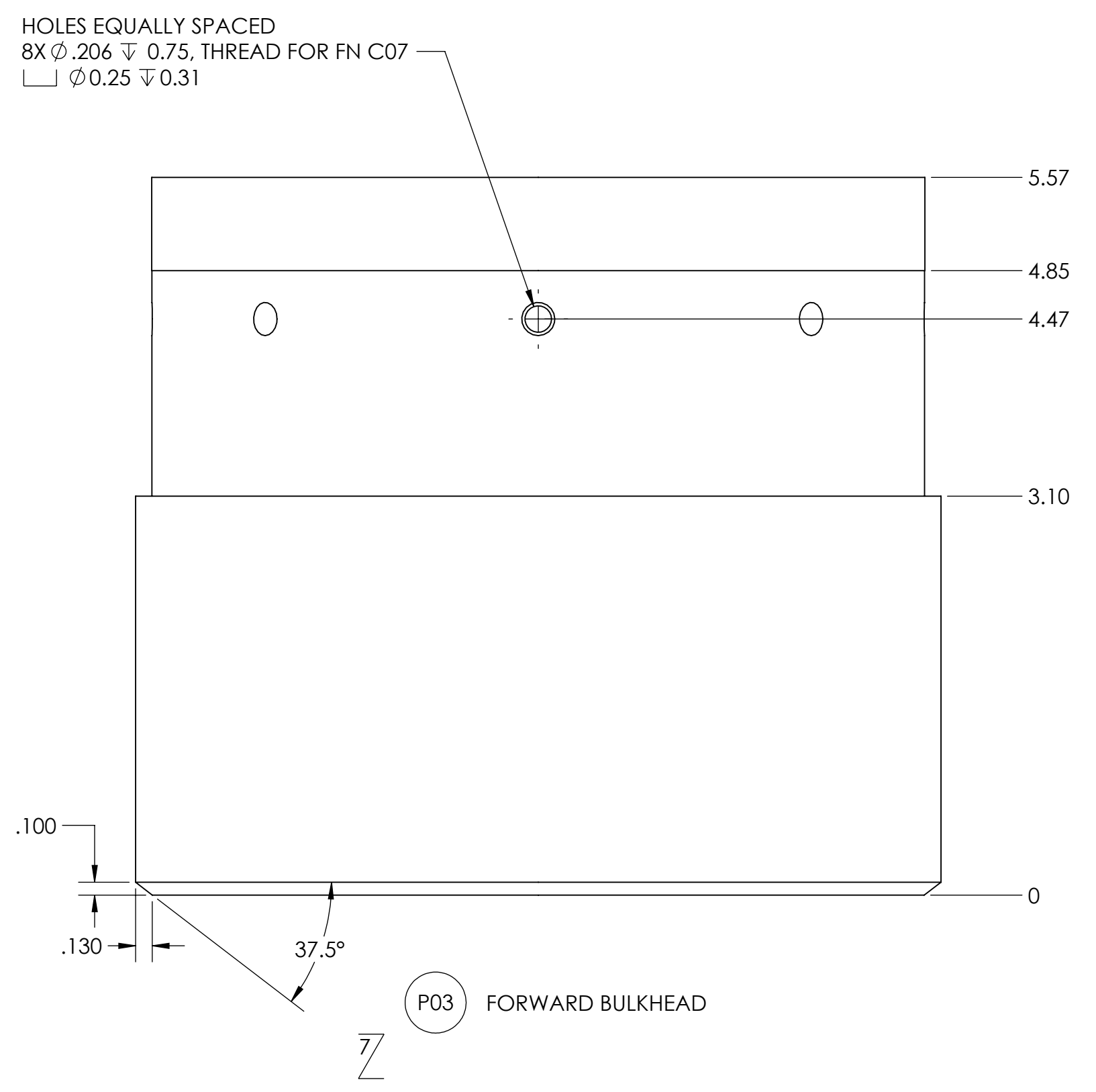
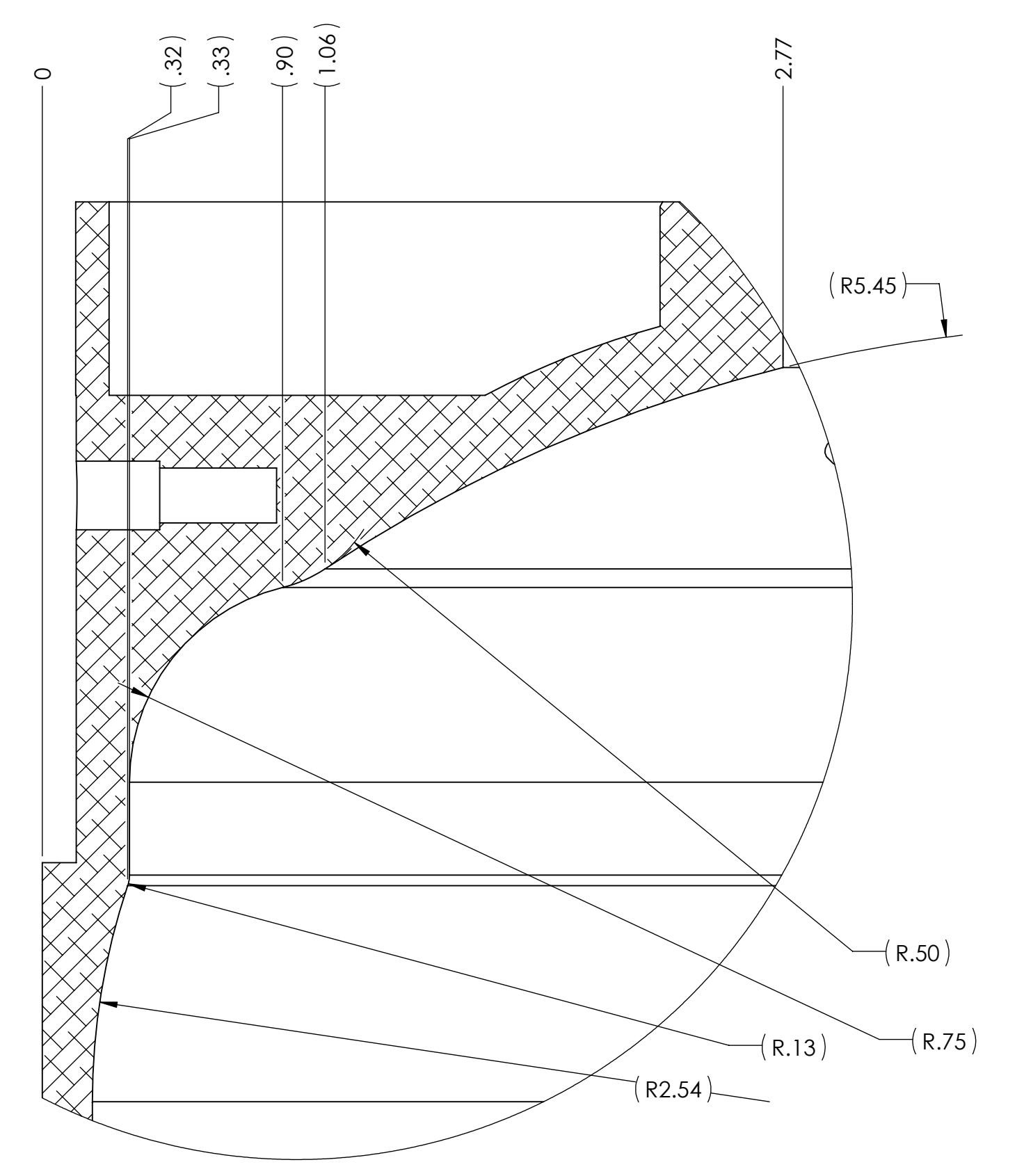
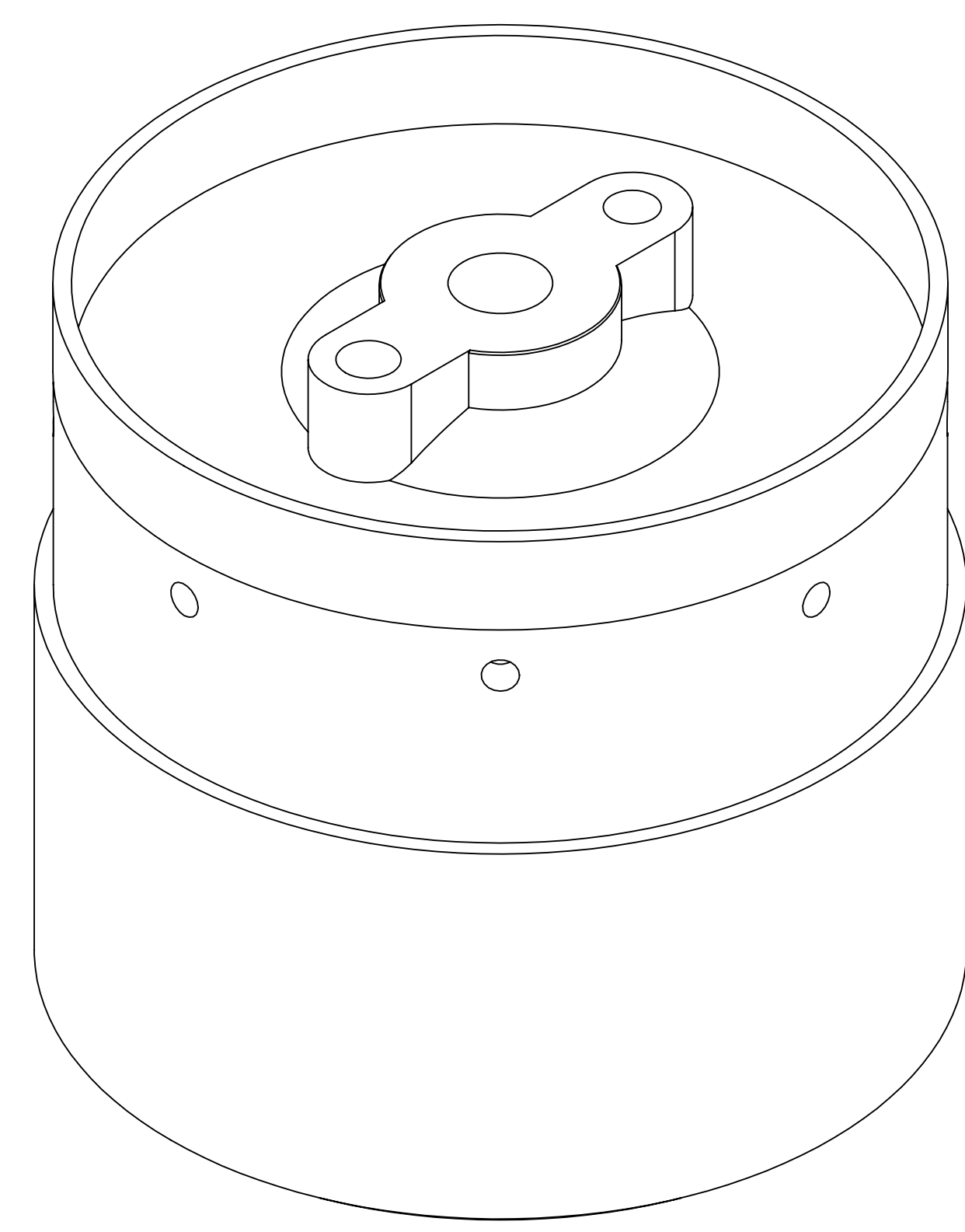
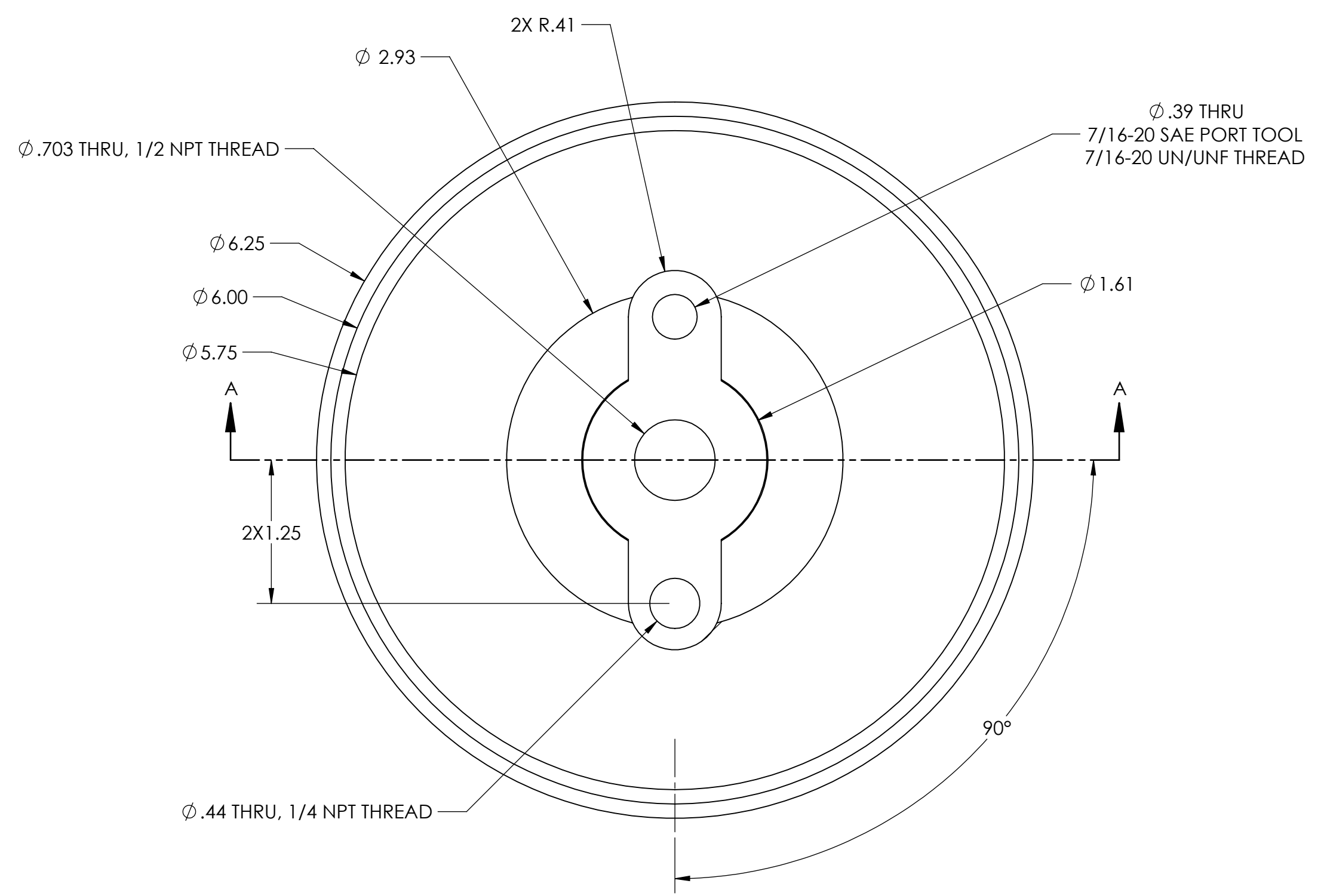
4

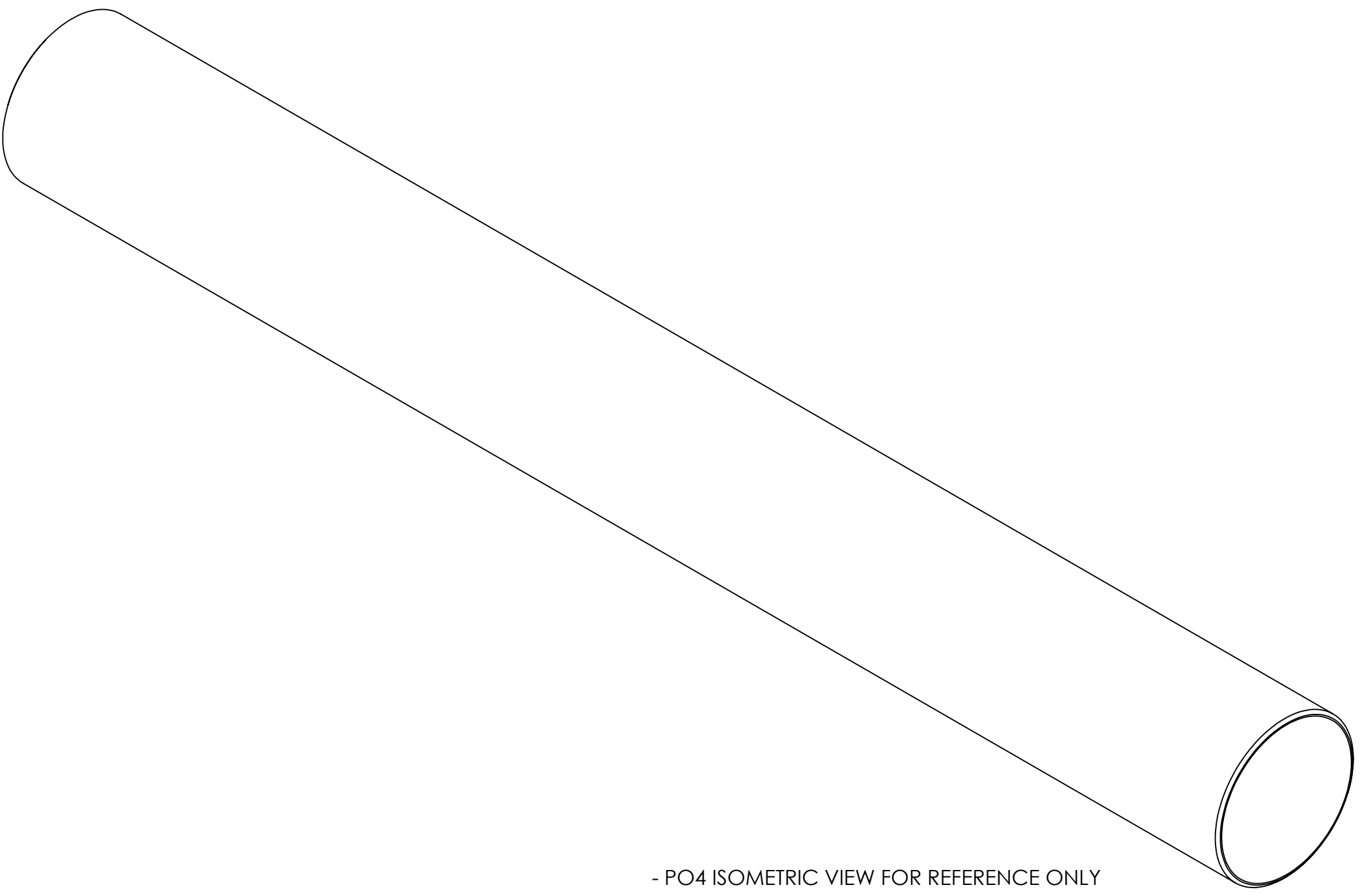
3

2

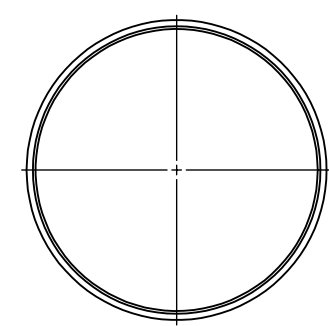
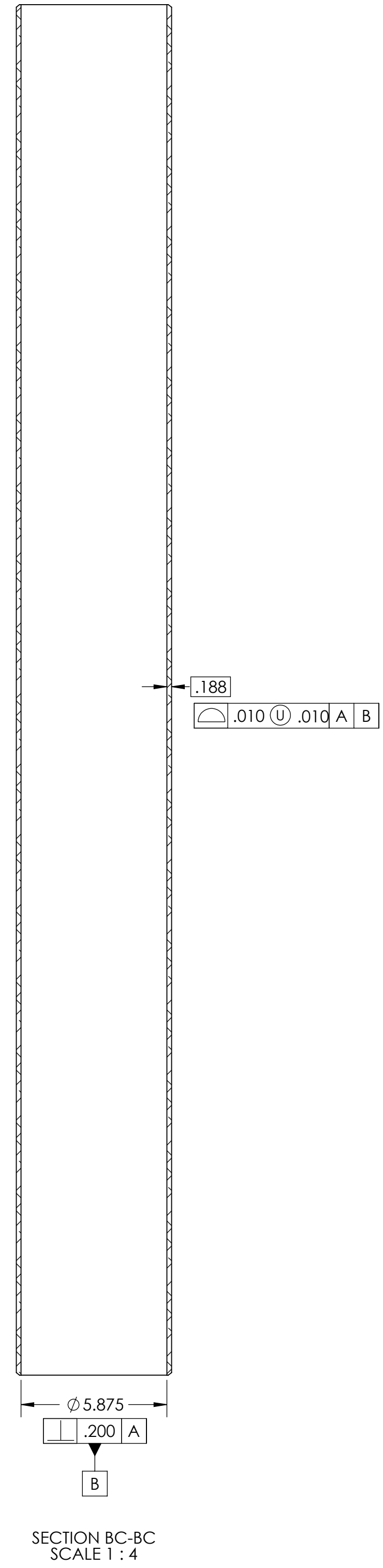
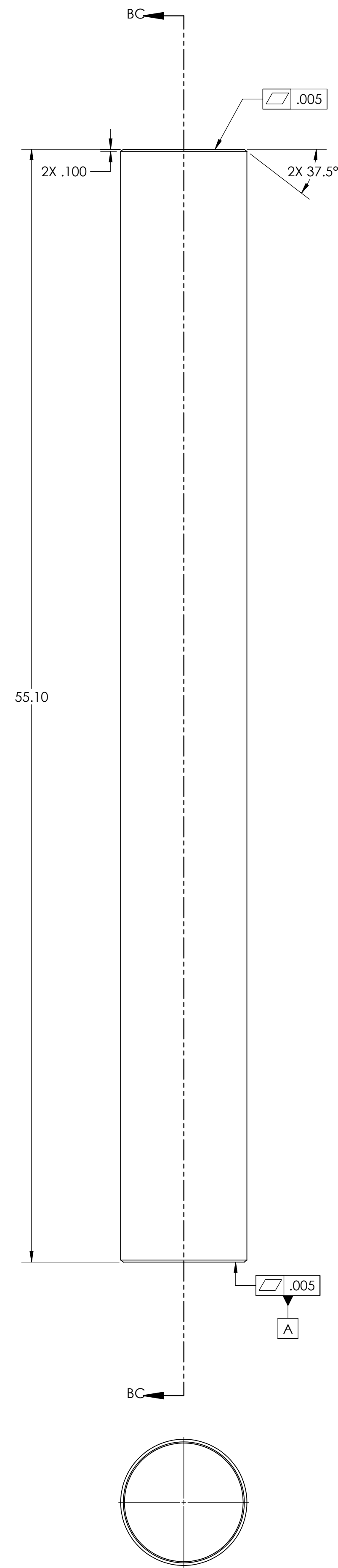
1

REVISIONS				
ZONE	REV.	DESCRIPTION	DATE	APPROVED
	-	SEE SHEET ONE	-	-





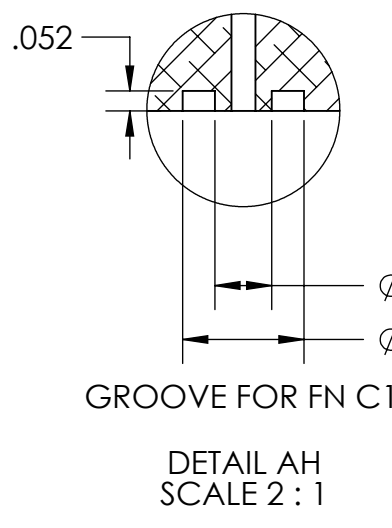
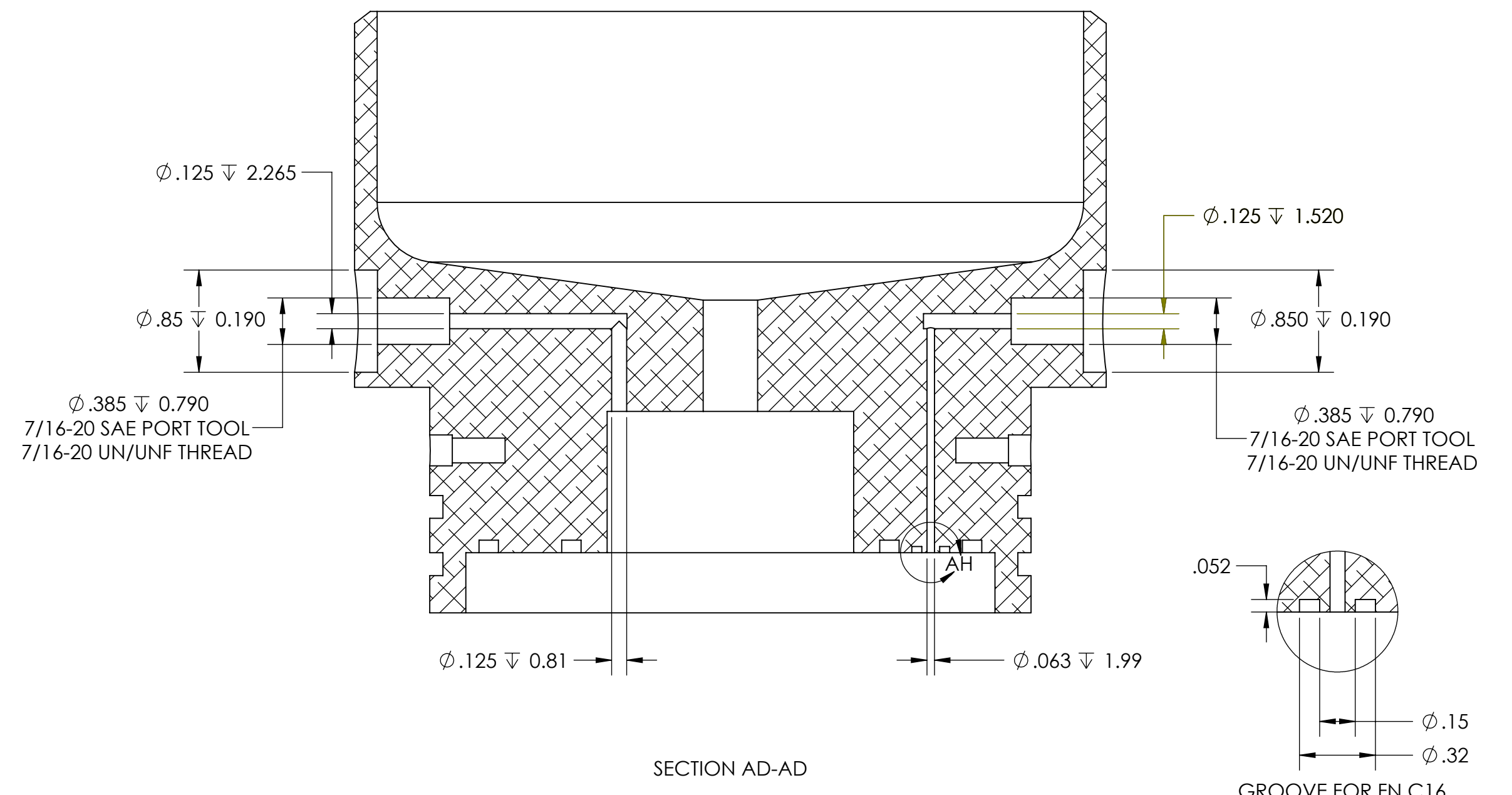
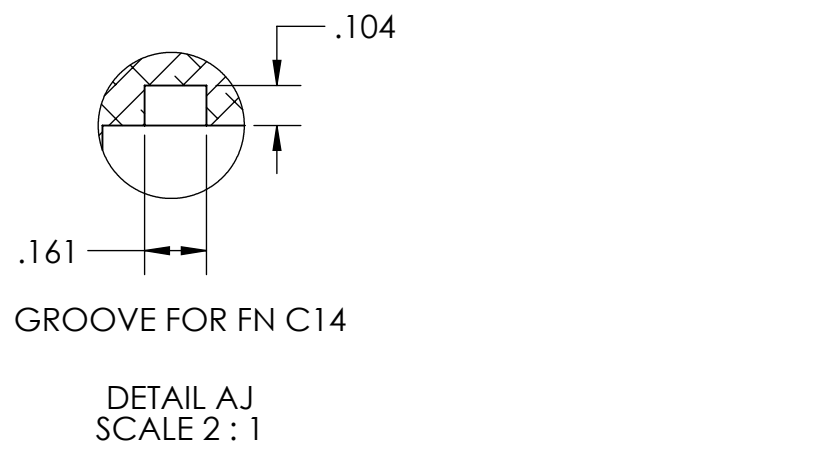
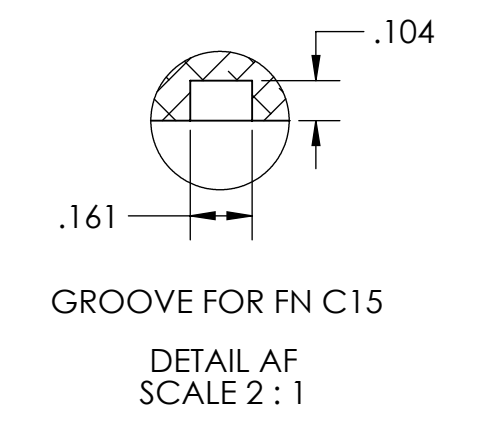
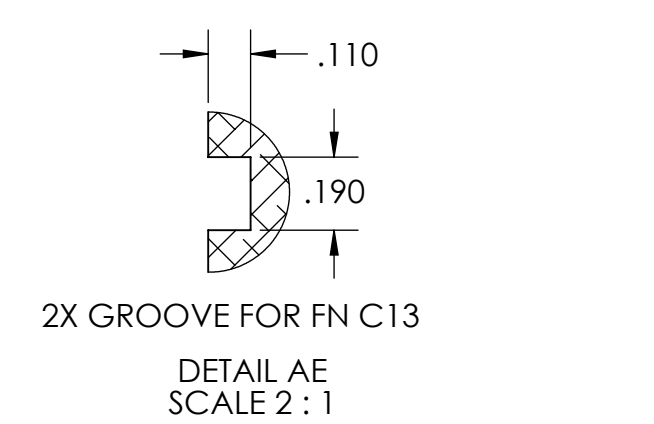
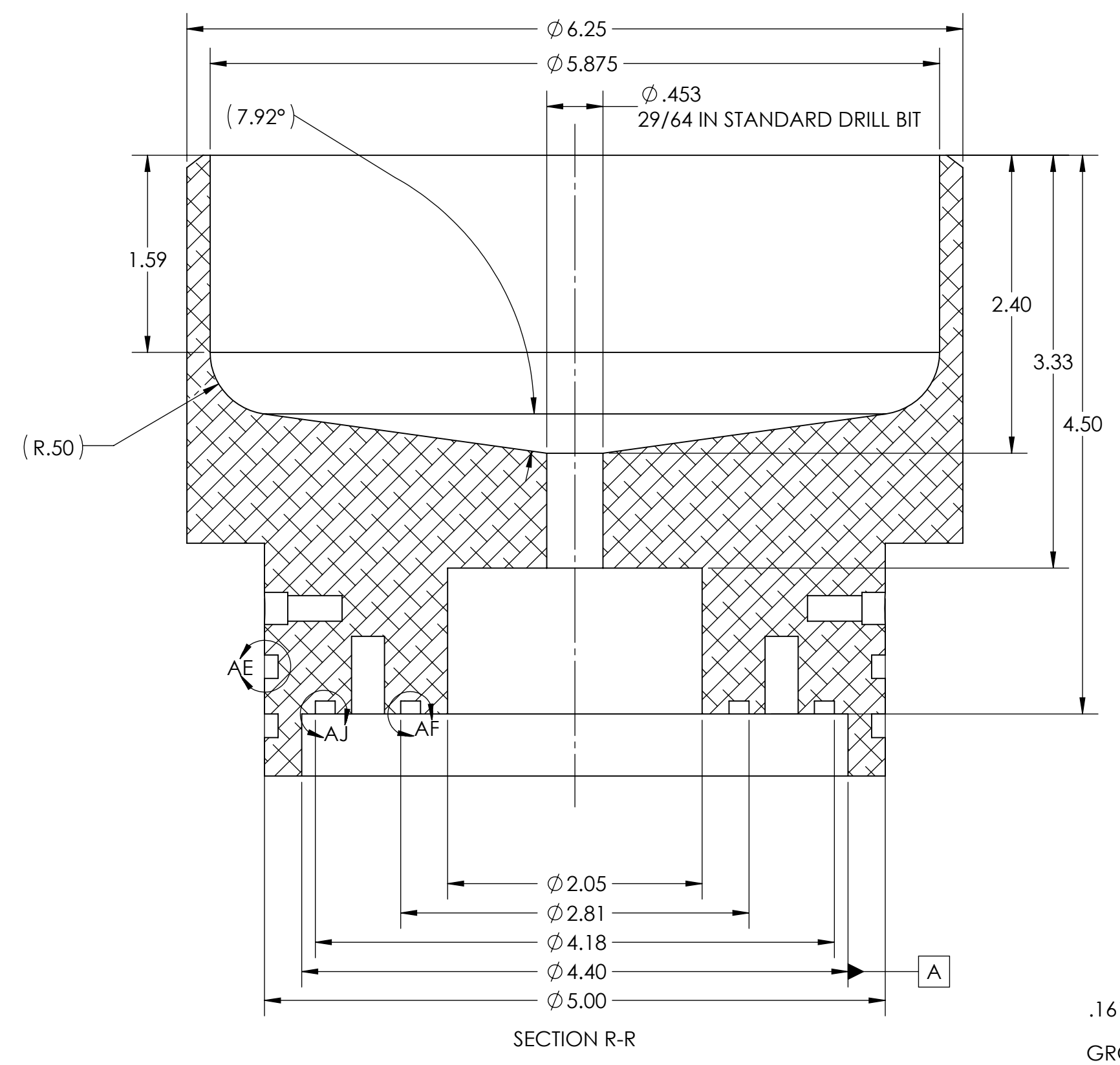
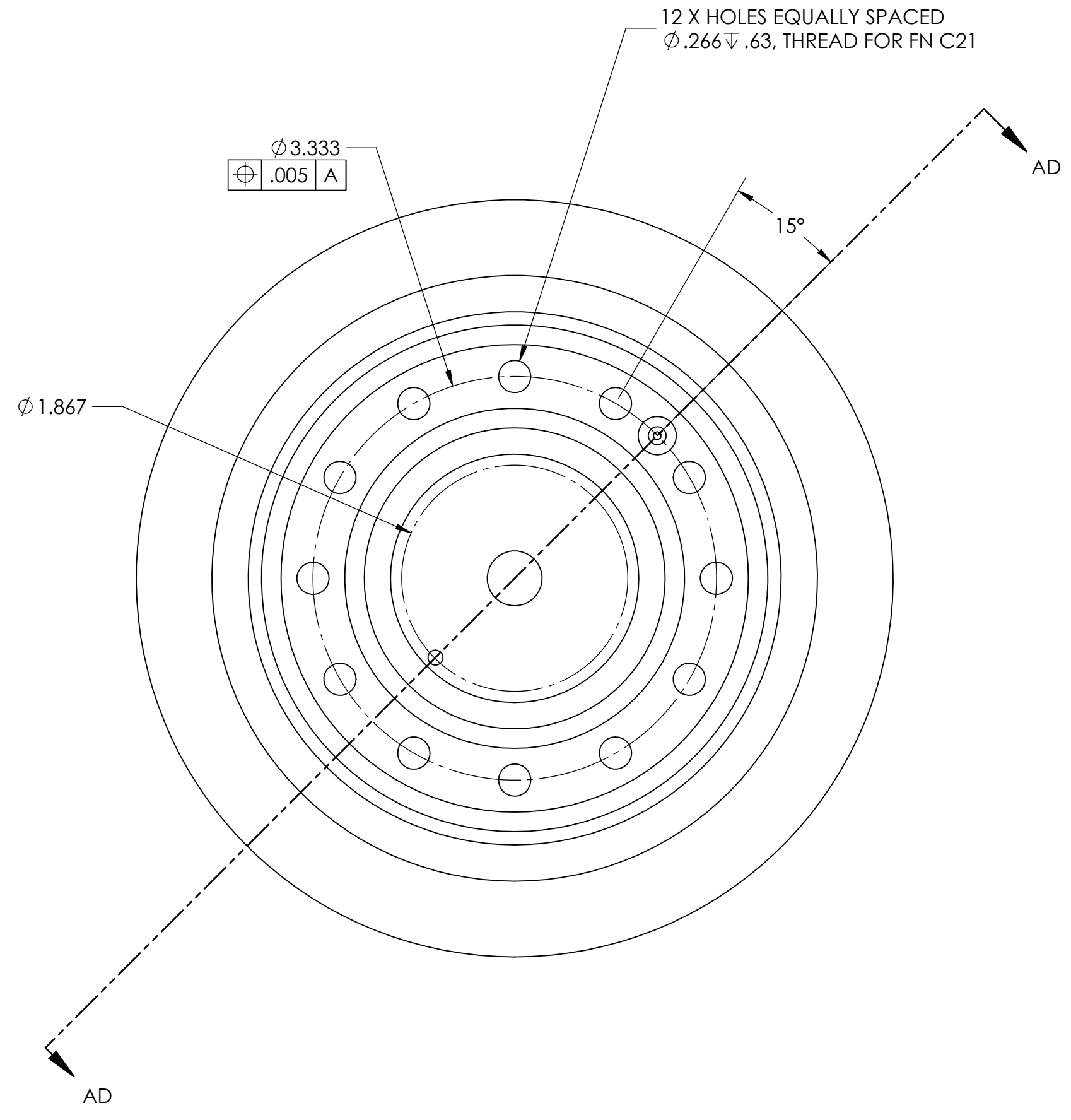
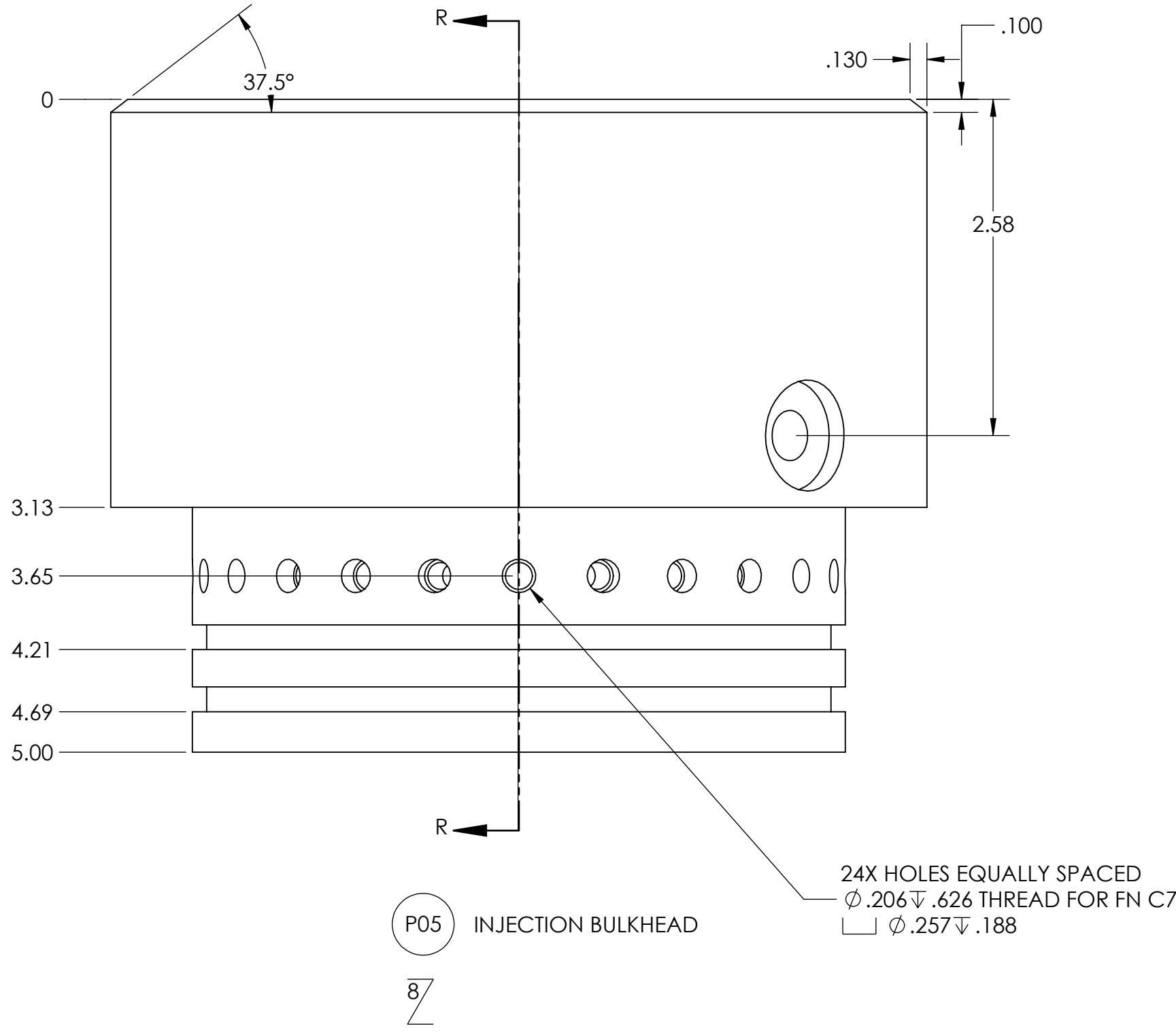
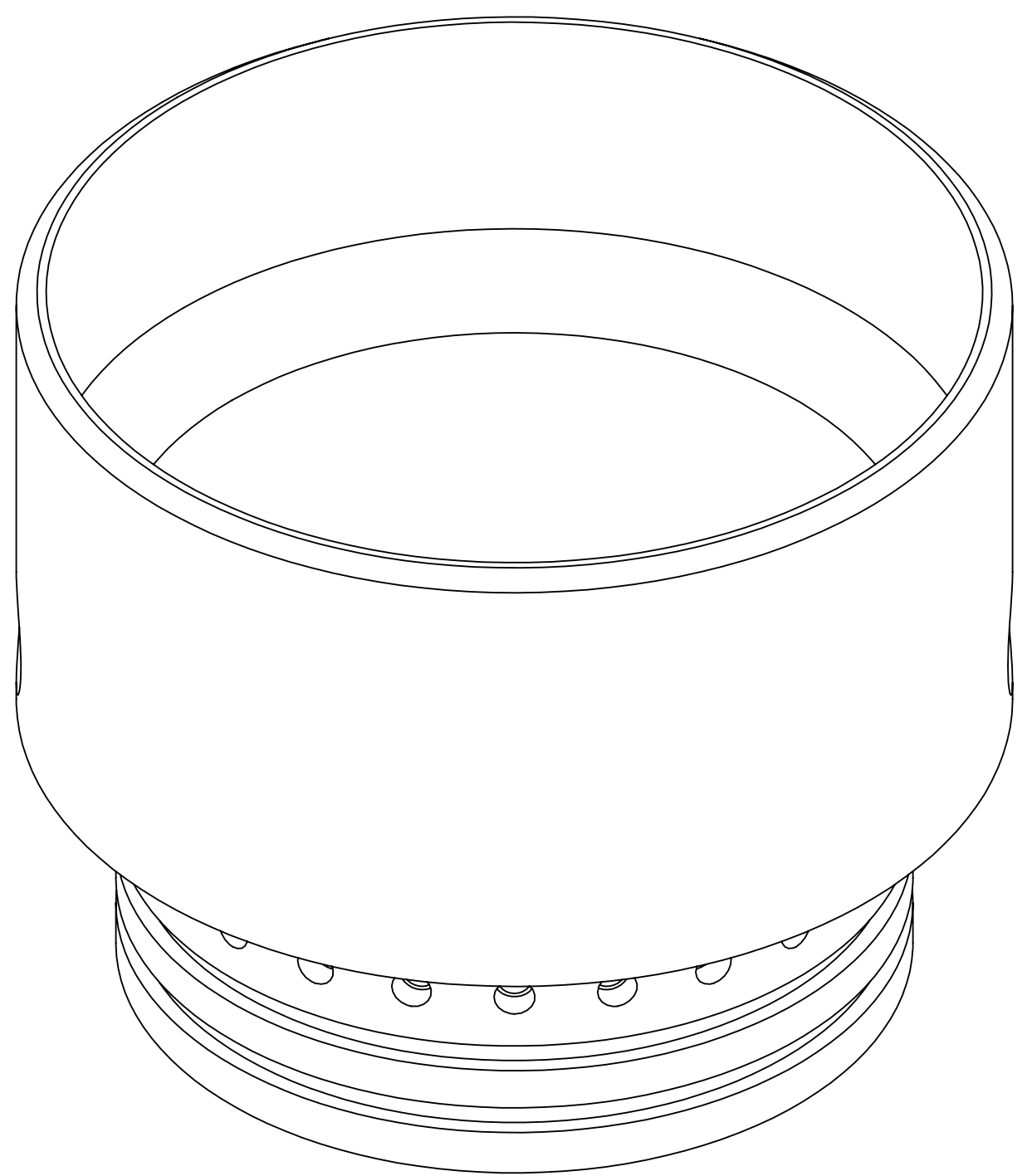
- PO4 ISOMETRIC VIEW FOR REFERENCE ONLY



Ø P04 BODY CYLINDER

REVISIONS				
ZONE	REV.	DESCRIPTION	DATE	APPROVED
	-	SEE SHEET 1	-	-

REVISIONS				
ZONE	REV.	DESCRIPTION	DATE	APPROVED
	-	SEE SHEET 1	-	-



8

7

6

5

4

3

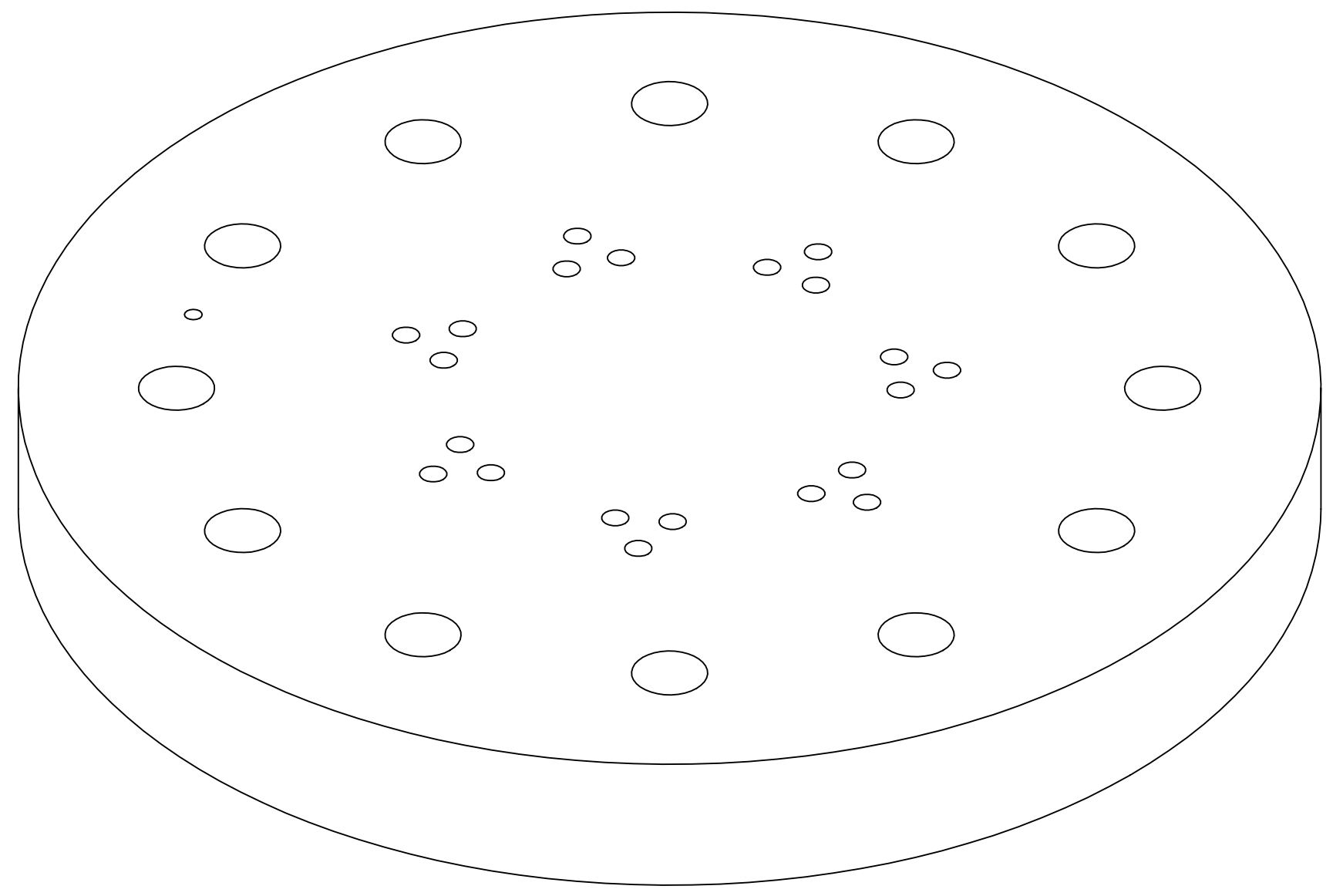
2

1

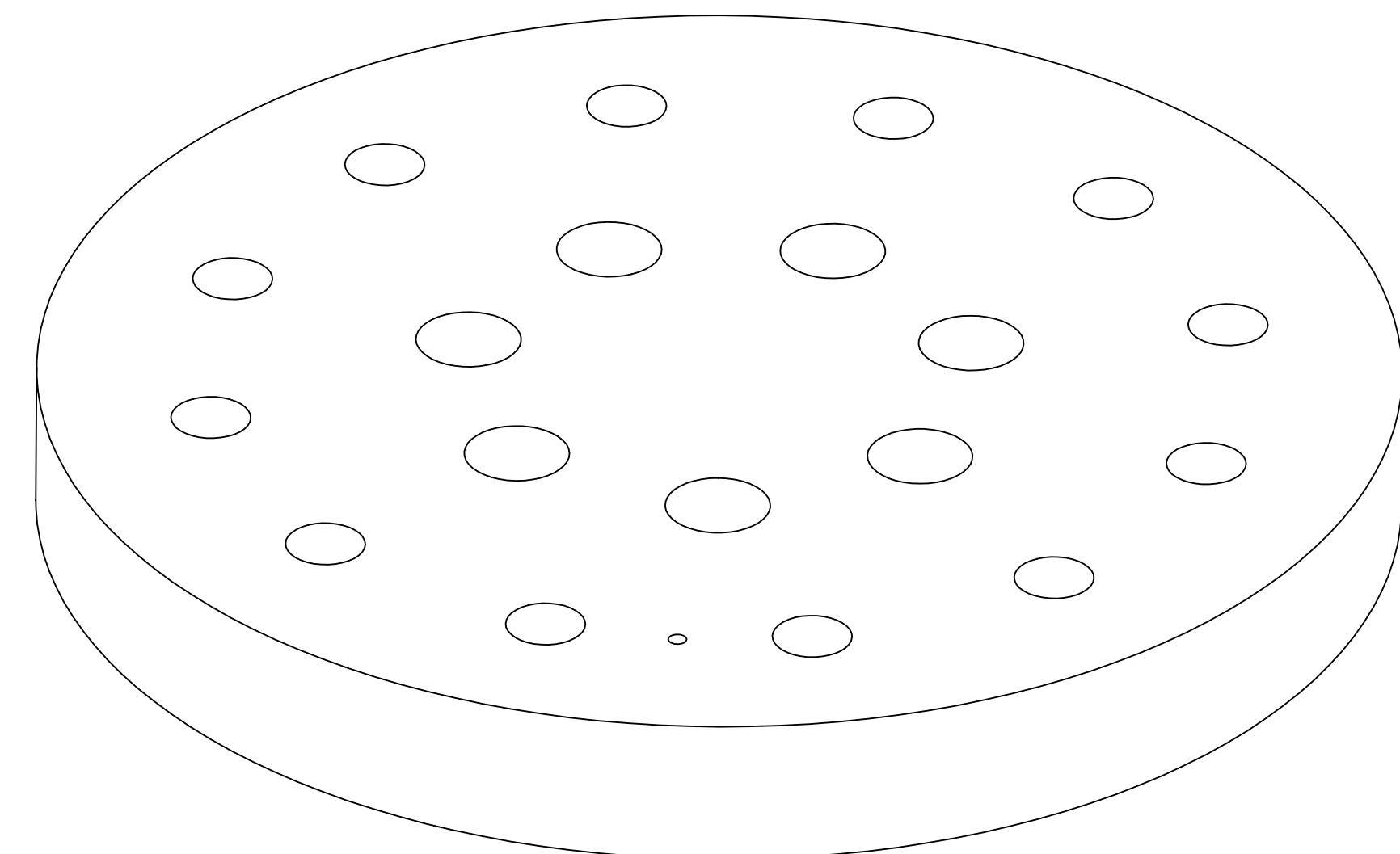
REVISIONS				
ZONE	REV.	DESCRIPTION	DATE	APPROVED
	-	SEE SHEET ONE	-	-



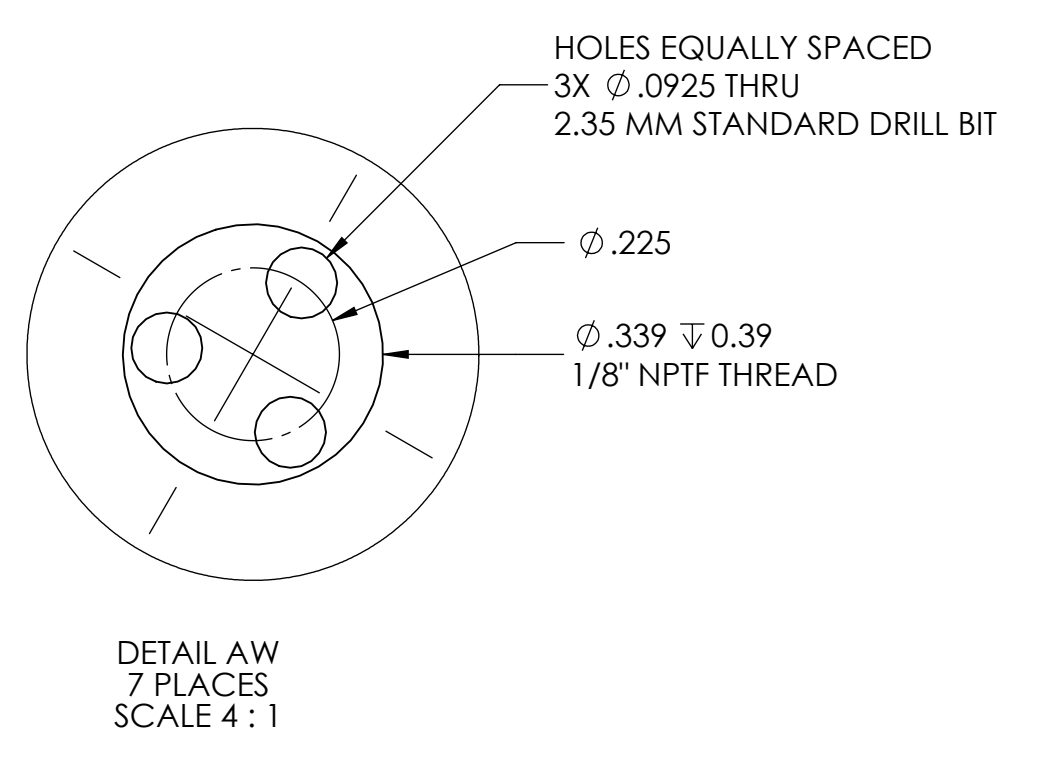
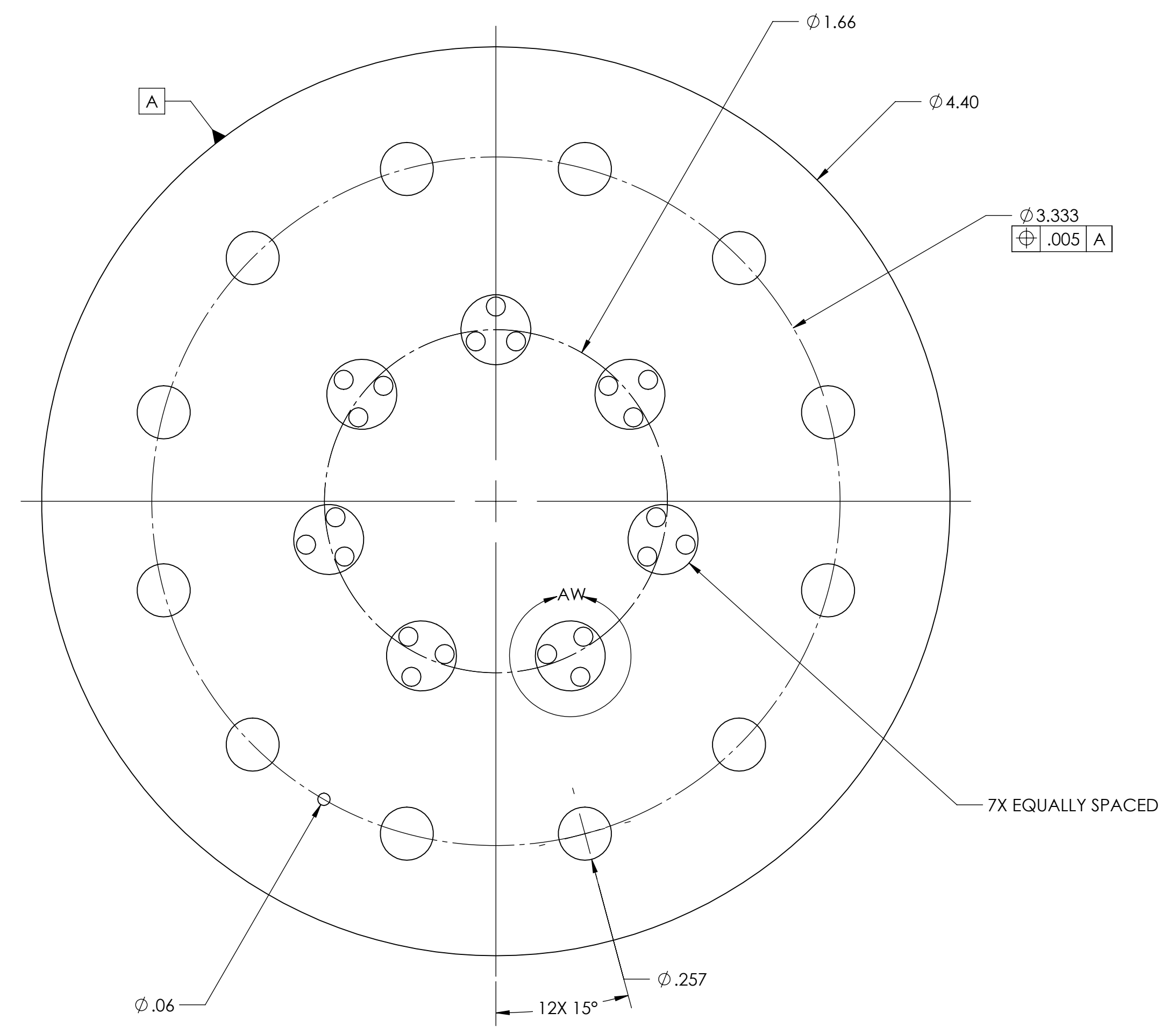
P06 INJECTOR PLATE



- P06 ISOMETRIC VIEW FOR REFERENCE ONLY



- P06 ISOMETRIC VIEW FOR REFERENCE ONLY



8

7

6

5

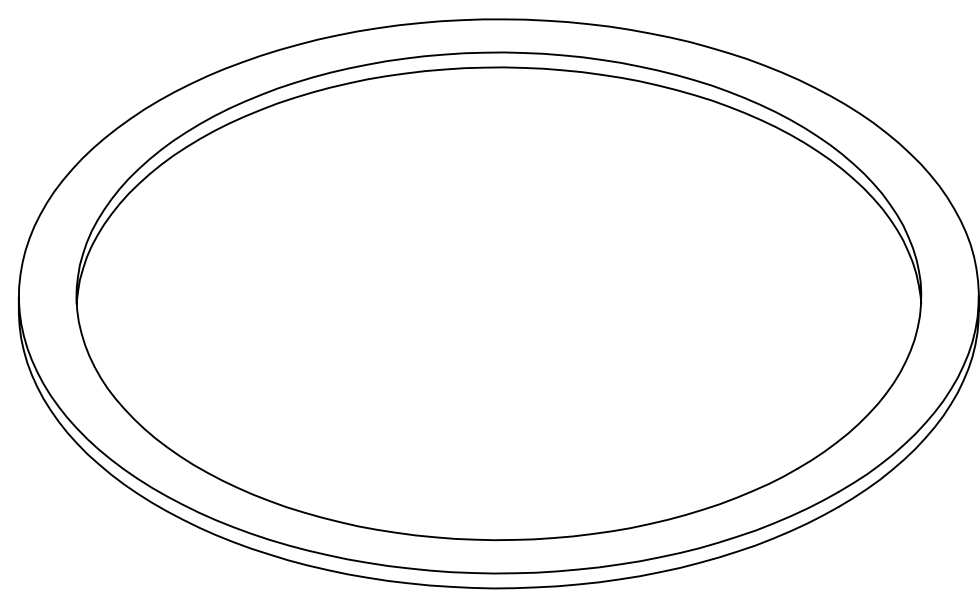
4

3

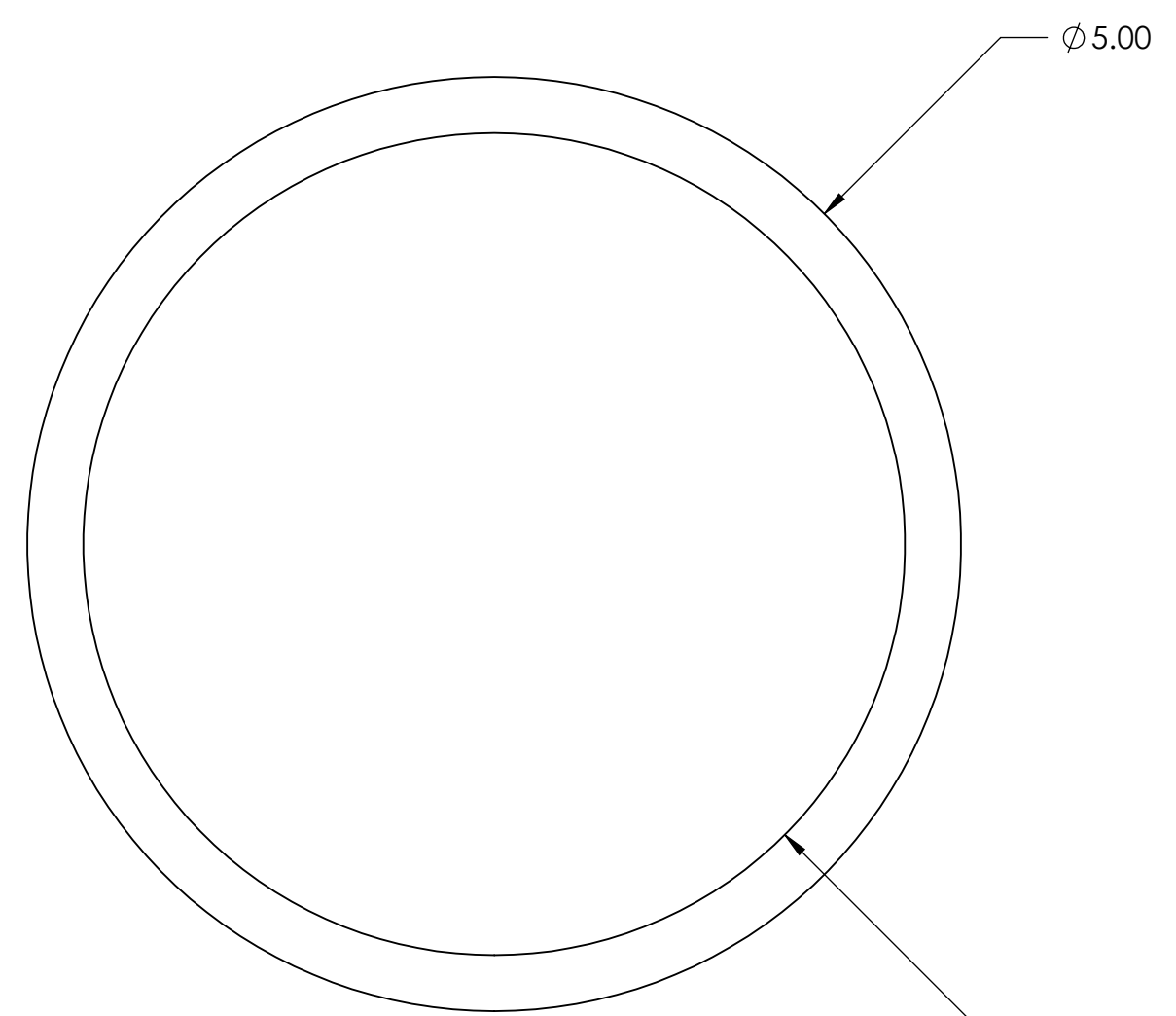
2

1

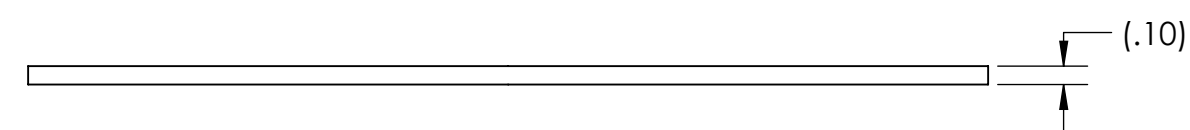
REVISIONS				
ZONE	REV.	DESCRIPTION	DATE	APPROVED
	-	SEE SHEET ONE	-	-



-P07 ISOMETRIC VIEW FOR REFERENCE ONLY



P07 FORWARD COMPRESSIBLE RING
SCALE 1:1



D

D

C

C

B

B

A

A

8

7

6

5

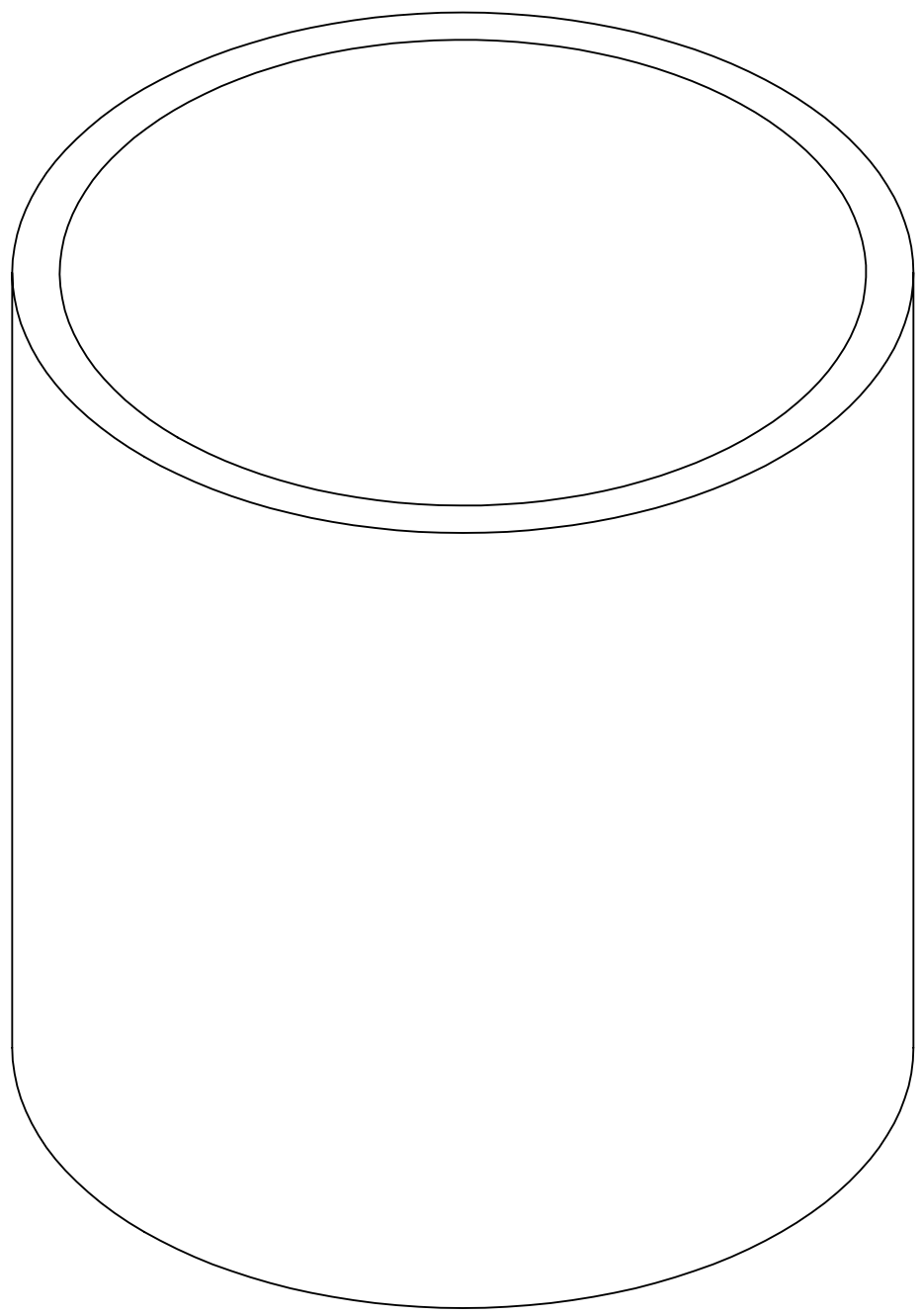
4

3

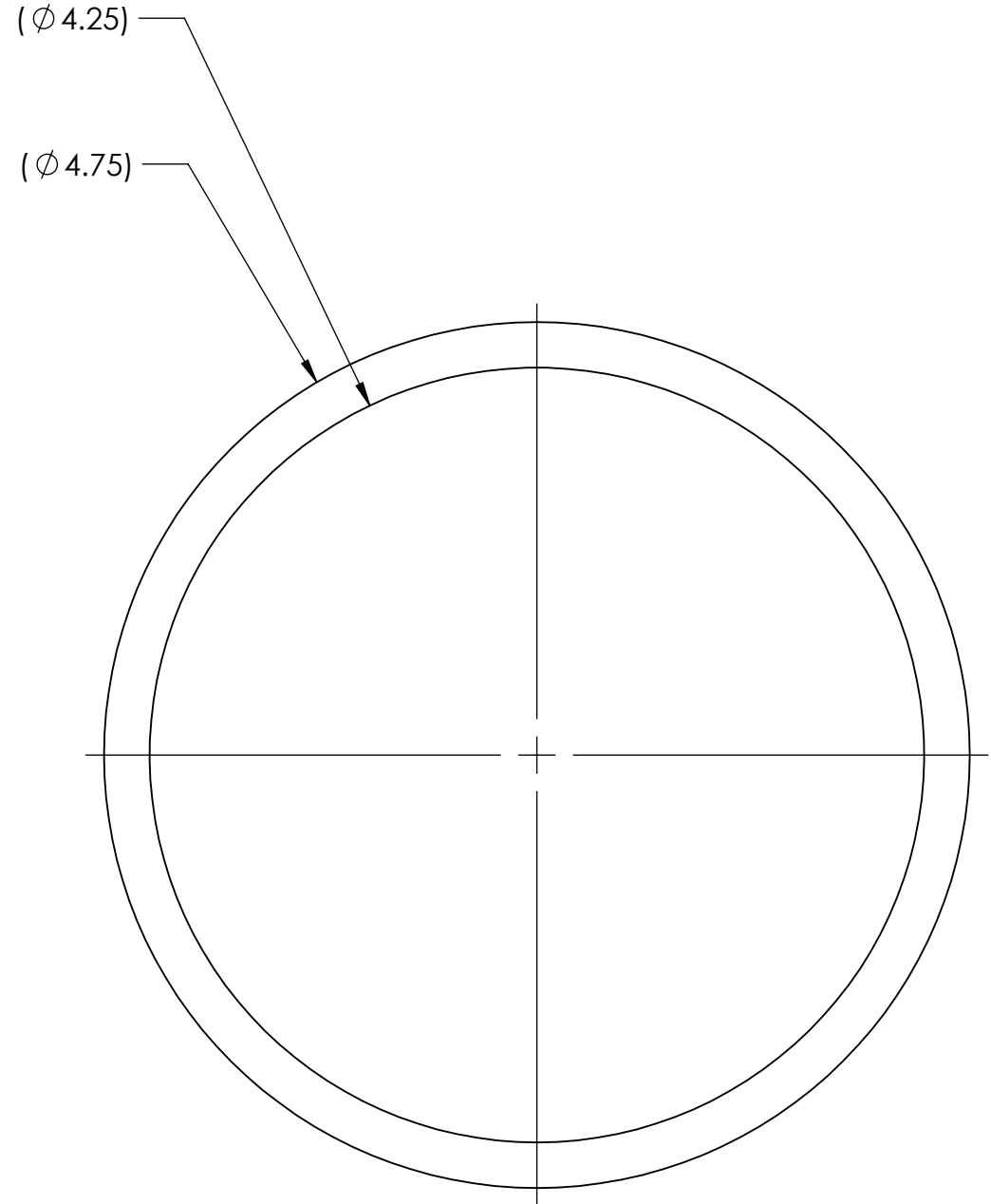
2


1

REVISIONS				
ZONE	REV.	DESCRIPTION	DATE	APPROVED
	-	SEE SHEET ONE	-	-



-P08 ISOMETRIC VIEW FOR REFERENCE ONLY



P08 PRE-COMBUSTION CHAMBER LINER


SIZE	DWG. NO.	REV
D	TII-2102-A	-
SCALE: 1:1	SHEET 18 OF 29	

5

4

3

2

1

D

D

C

C

B

B

A

A

8

7

6

5

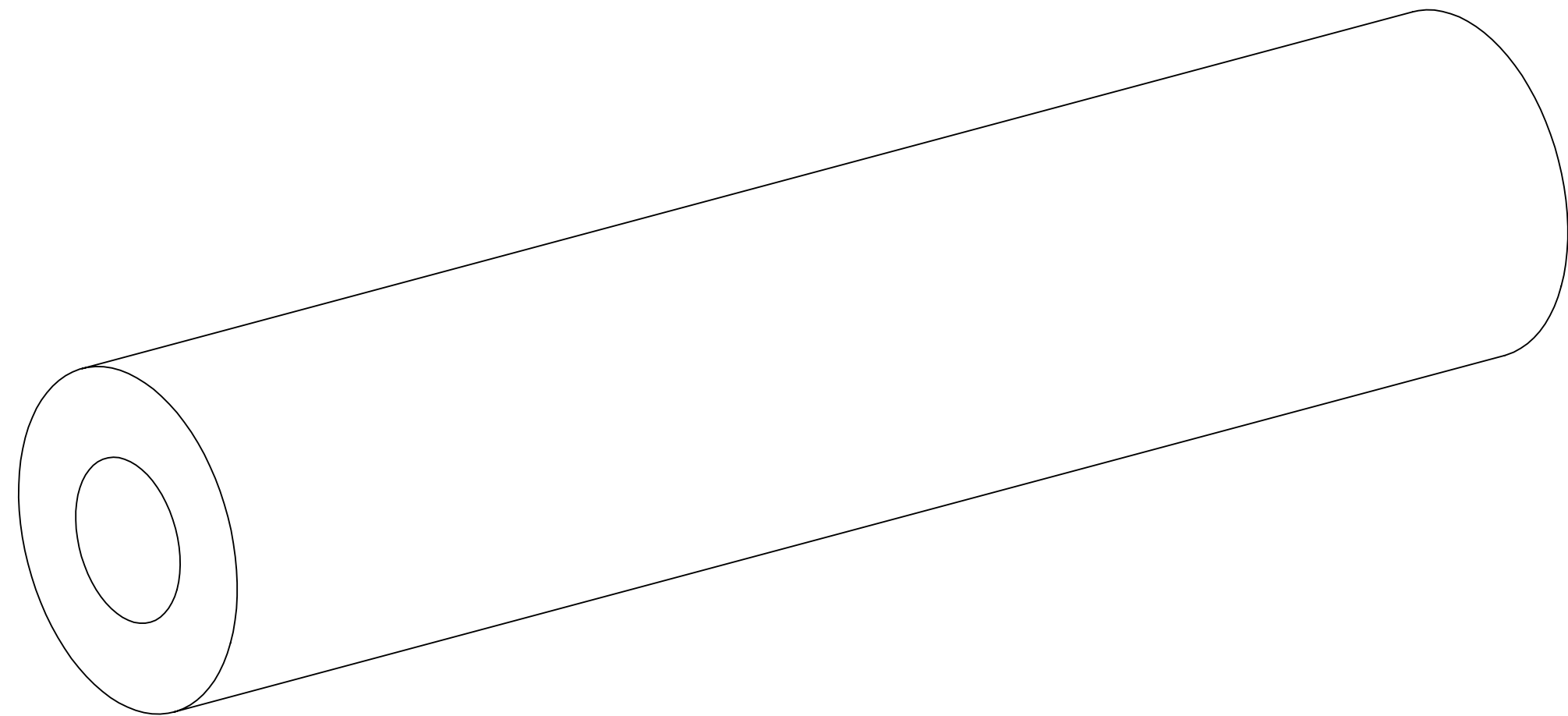
4

3

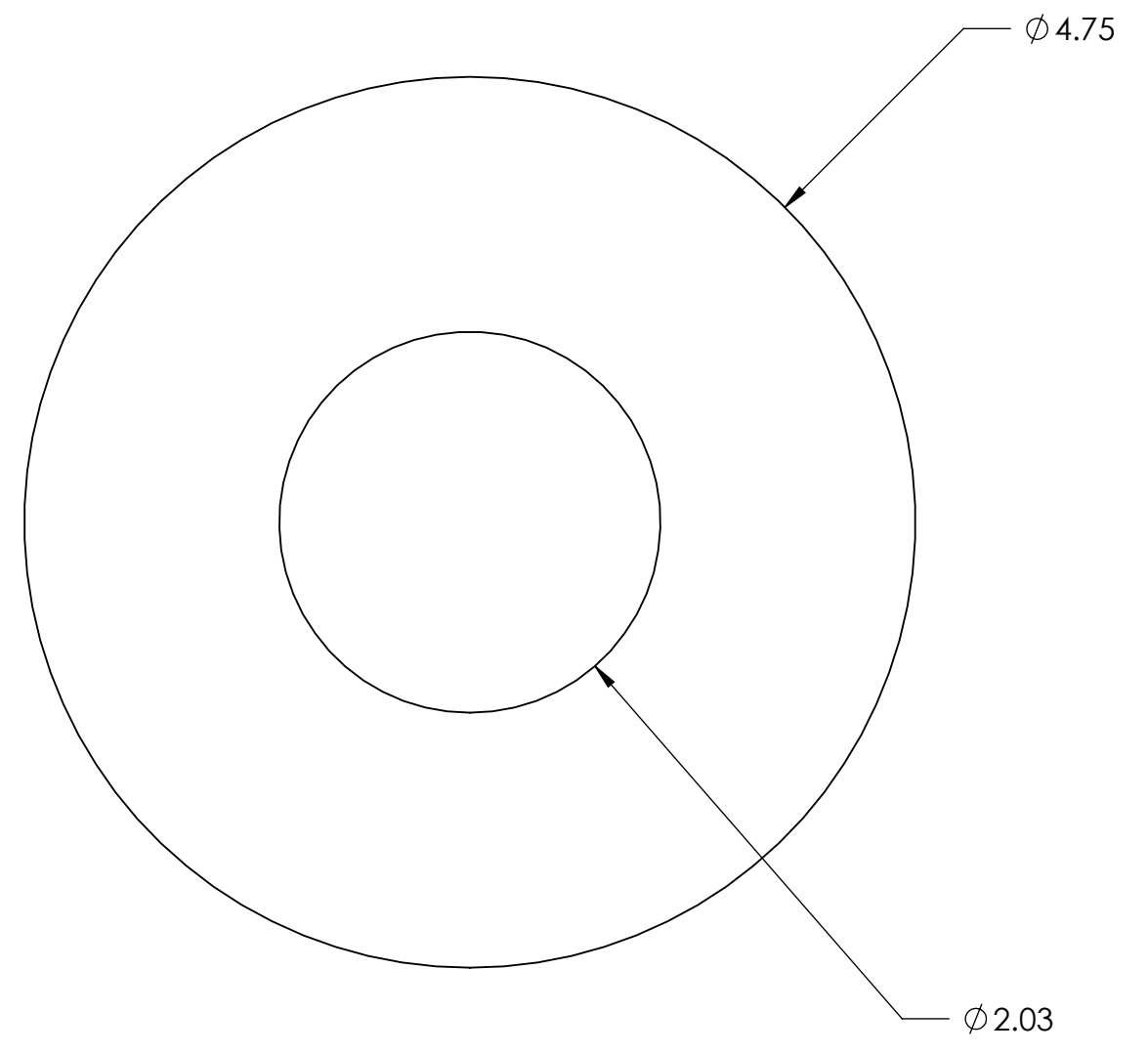
2

1

REVISIONS				
ZONE	REV.	DESCRIPTION	DATE	APPROVED
	-	SEE SHEET ONE	-	-



-P98 ISOMETRIC VIEW FOR REFERENCE ONLY



P09 FUEL GRAIN

SIZE	DWG. NO.	REV
D	TII-2103-A	-
SCALE: 1:1	SHEET 19 OF 29	

8

7

6

5

4

3

2

1

D

D

C

C

B

B

A

A

8

7

6

5

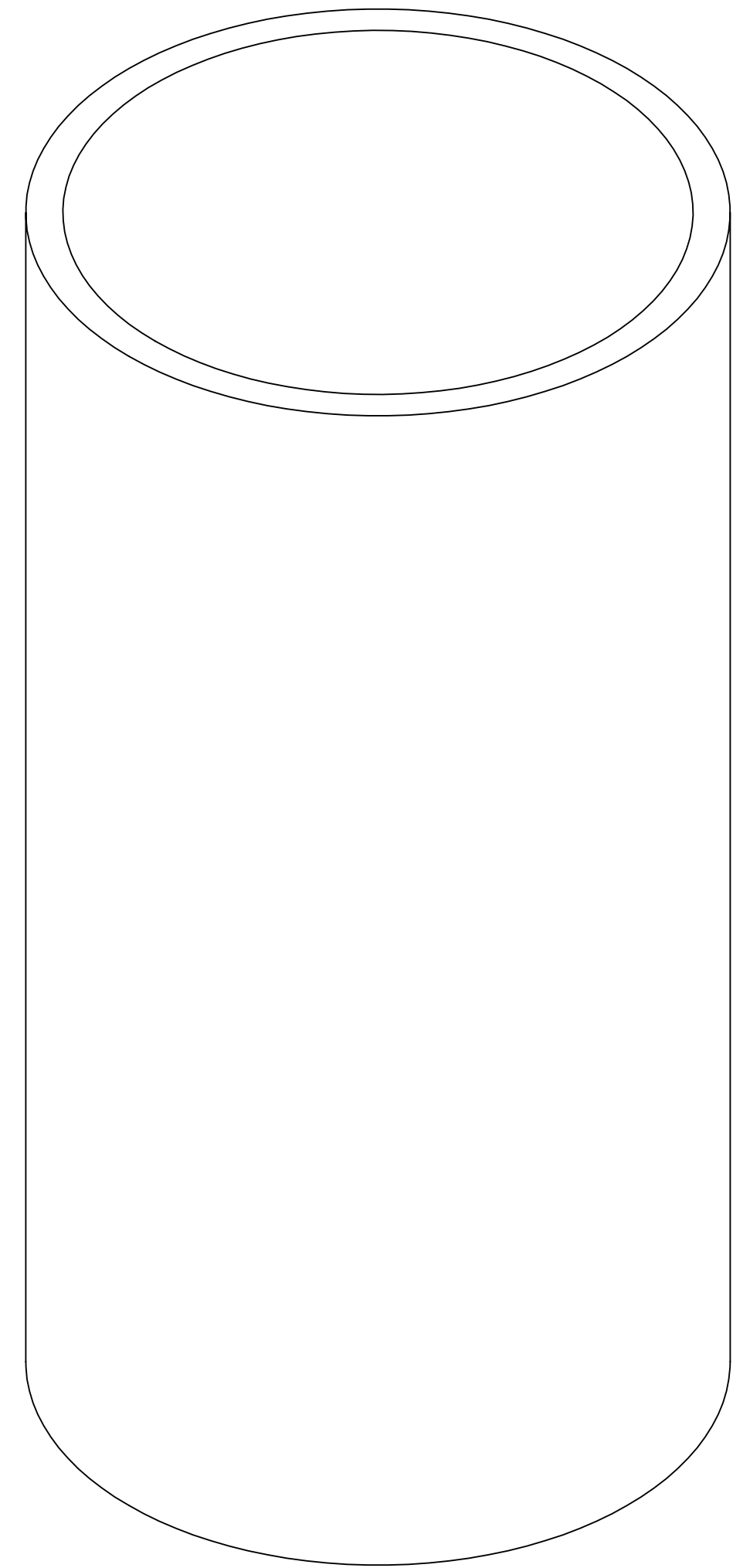
4

3

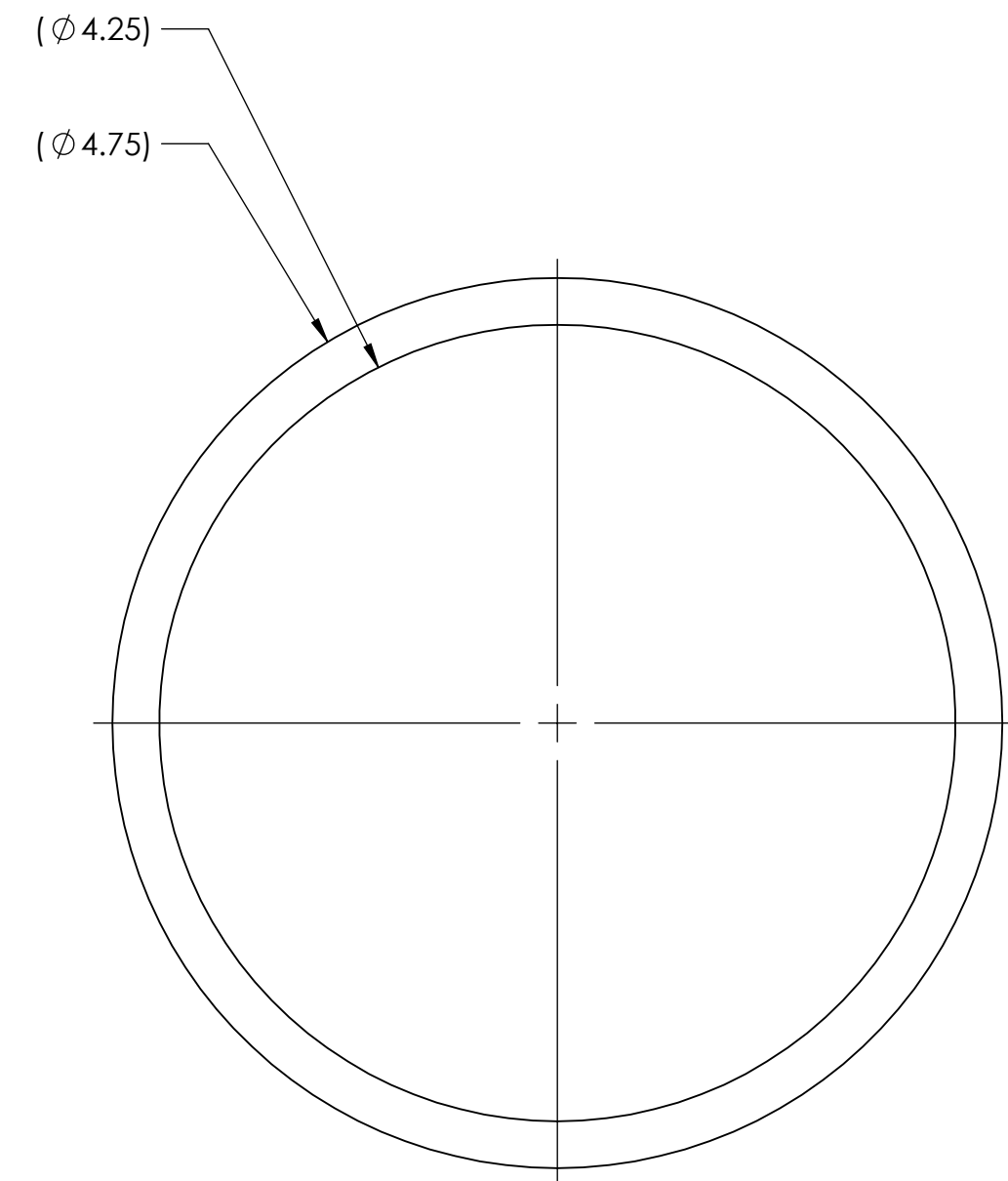
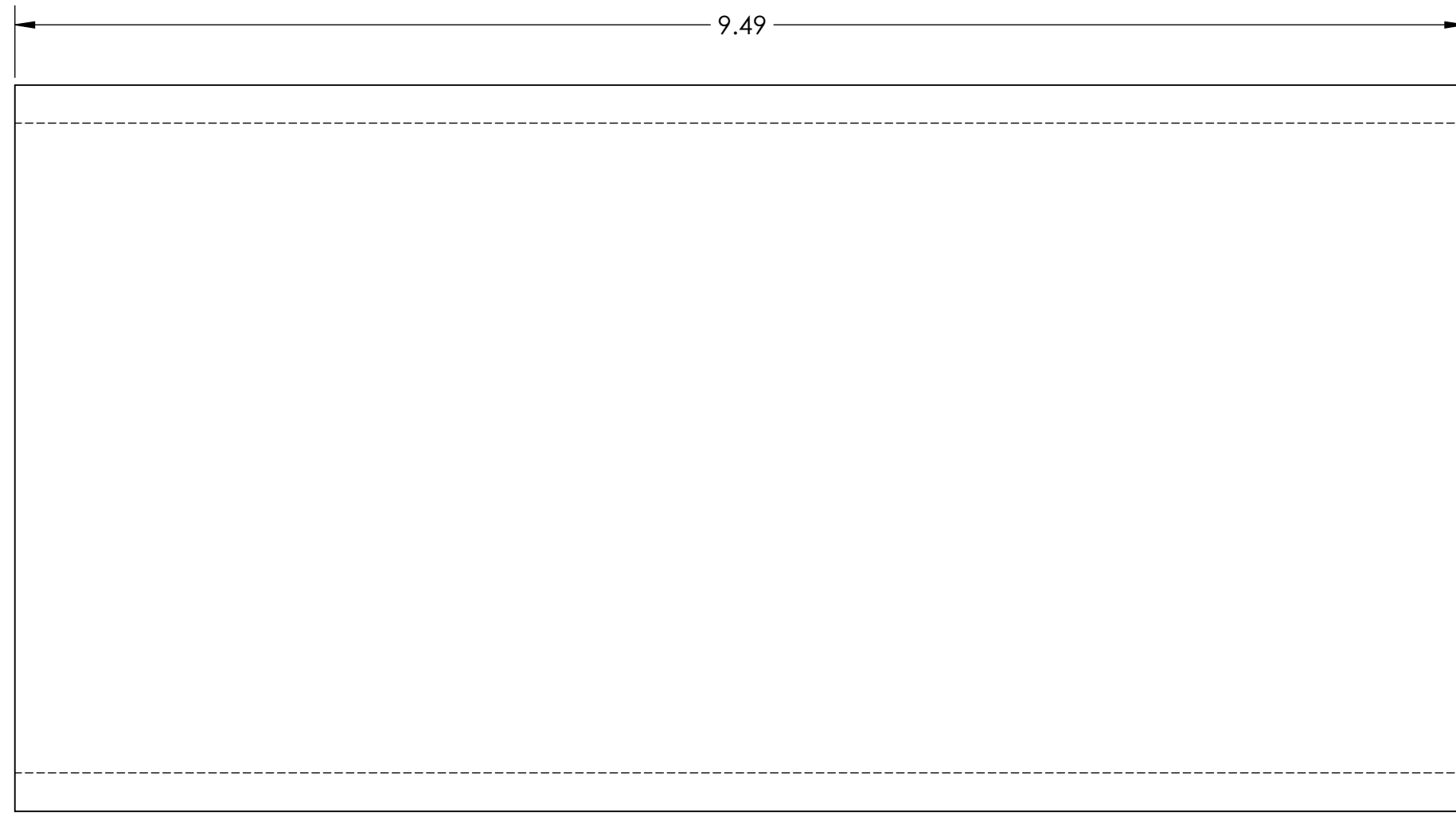
2

1

REVISIONS				
ZONE	REV.	DESCRIPTION	DATE	APPROVED
	-	SEE SHEET ONE	-	-



-P10 ISOMETRIC VIEW FOR REFERENCE ONLY



P10 POST-COMBUSTION CHAMBER LINER
 $\frac{9}{\Sigma}$

D

D

C

C

B

B

A

A

8

7

5

4

3

2

1

8

7

6

5

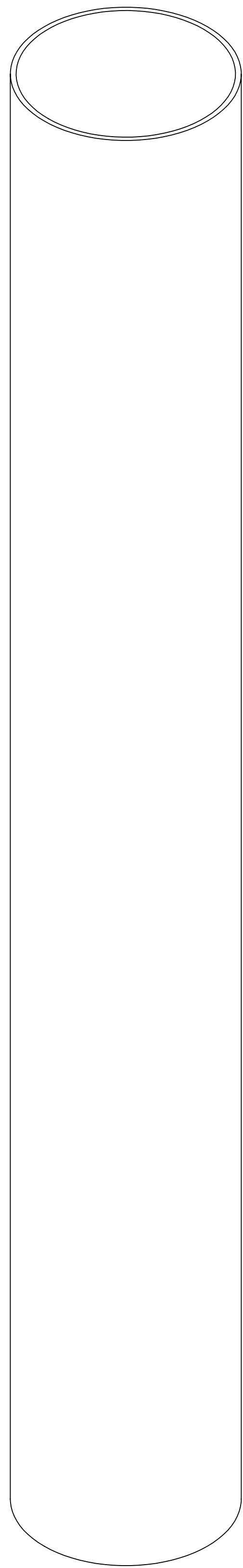
4

3

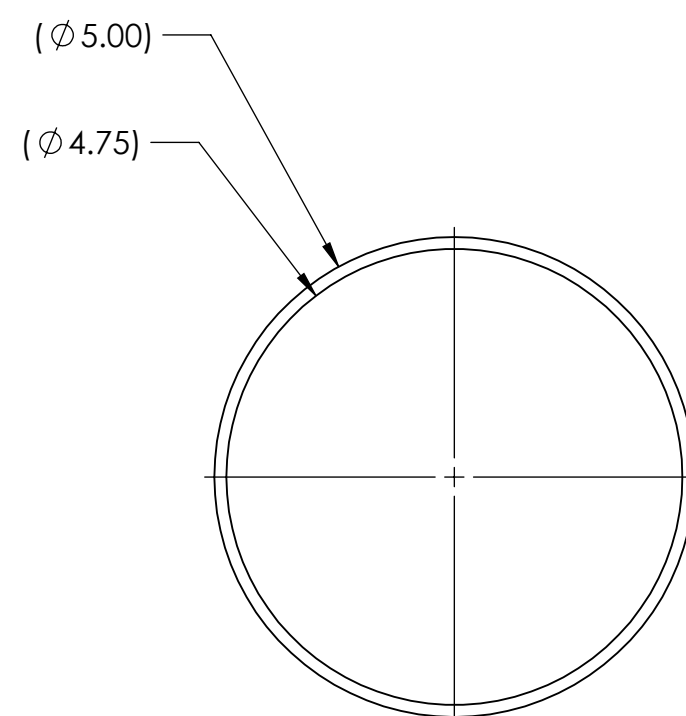
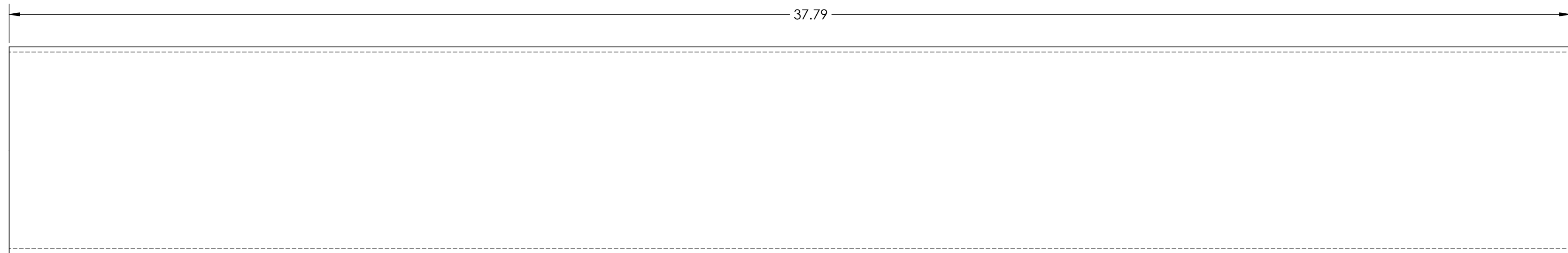
2

1

REVISIONS				
ZONE	REV.	DESCRIPTION	DATE	APPROVED
	-	SEE SHEET ONE	-	-



-P11 ISOMETRIC VIEW FOR REFERENCE ONLY



(P11) FUEL GRAIN LINER
 9/

8

7

6

5

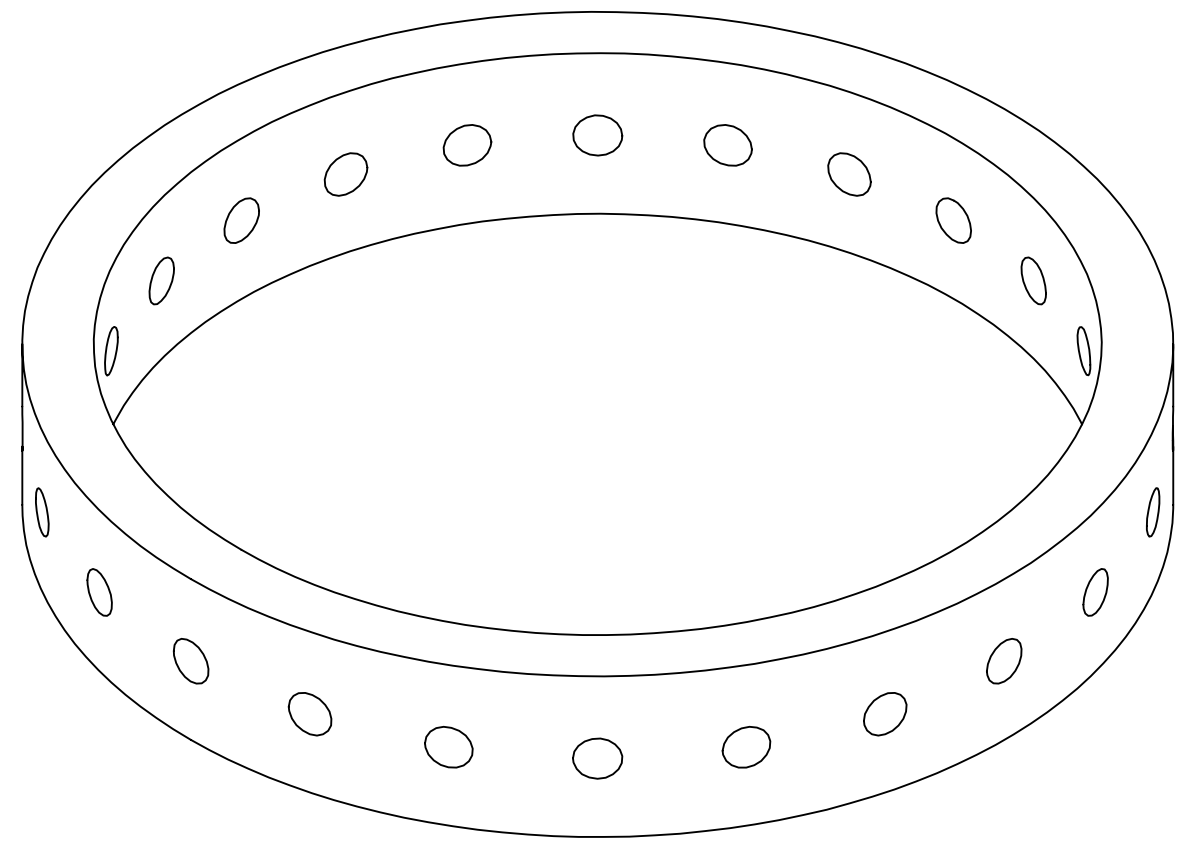
4

3

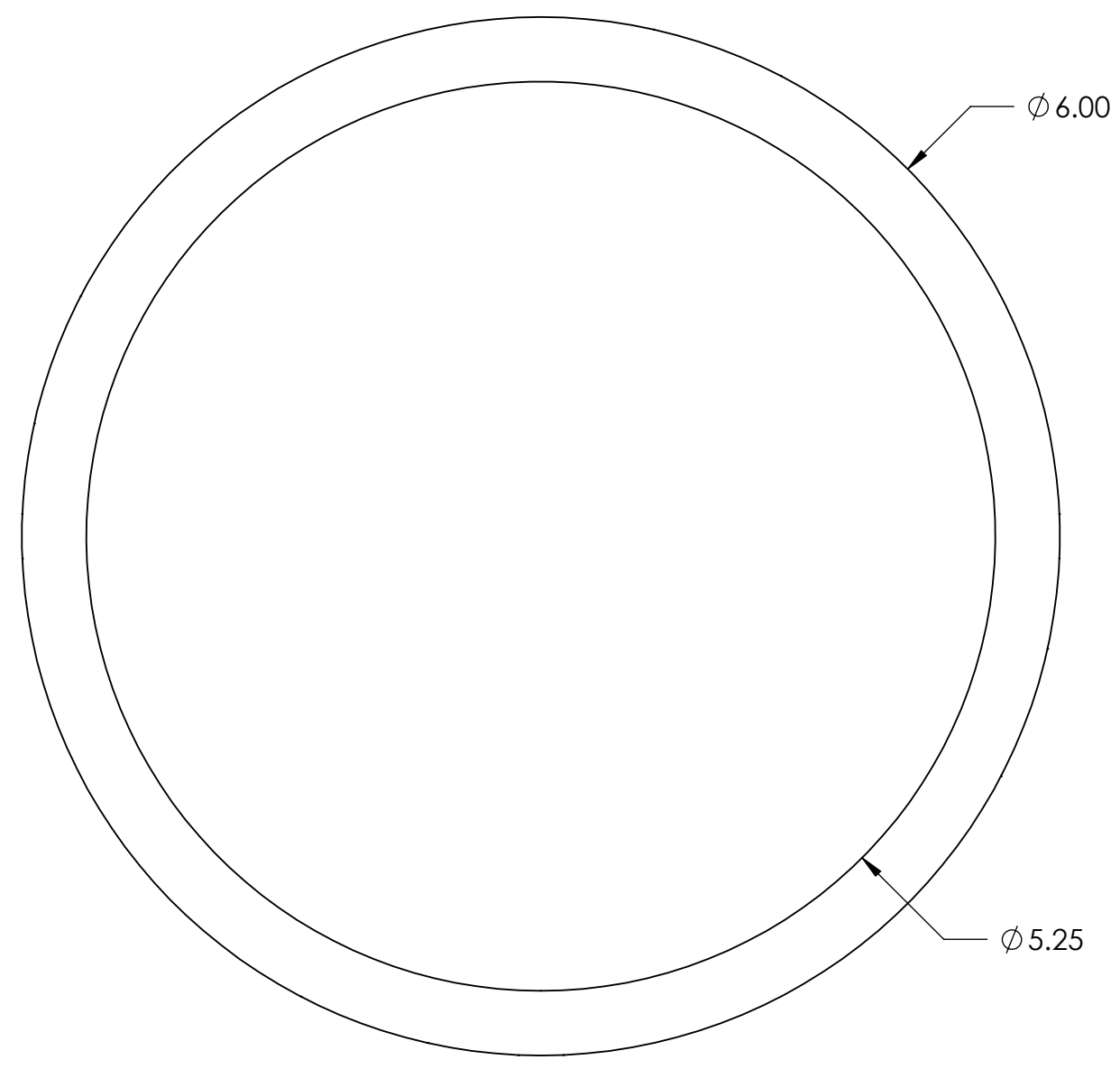
2

1

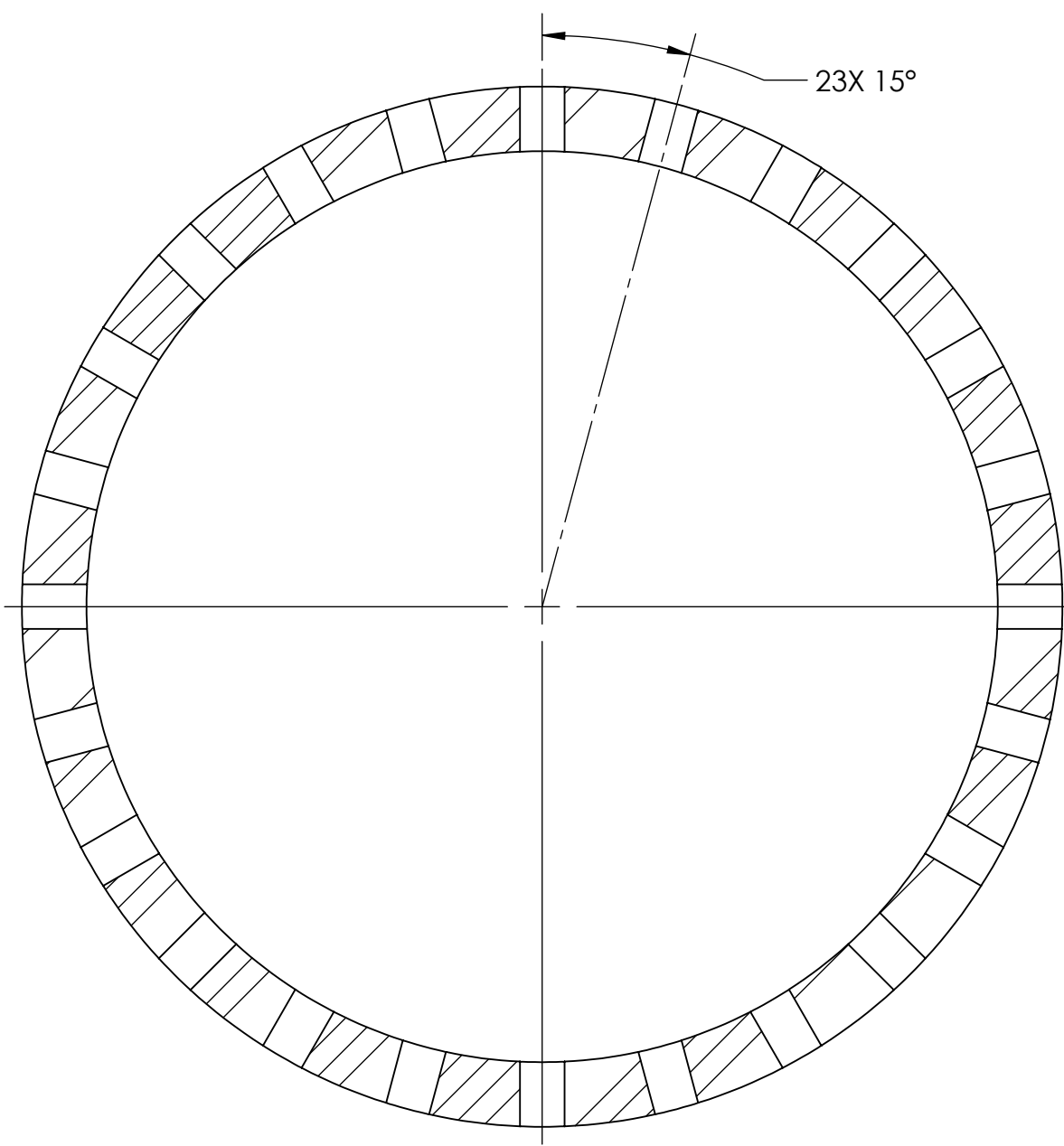
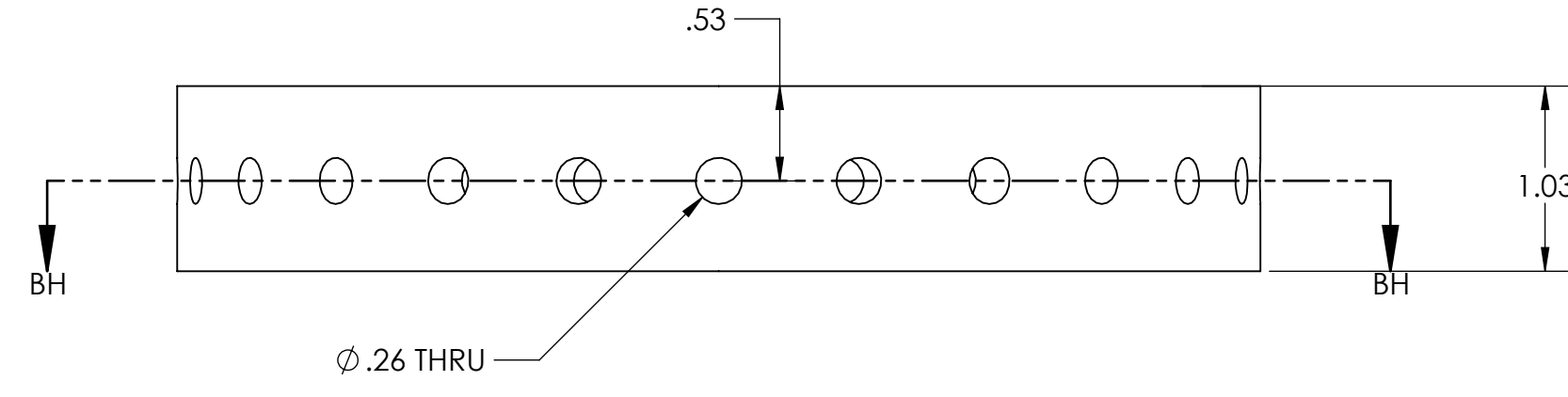
REVISIONS				
ZONE	REV.	DESCRIPTION	DATE	APPROVED
	-	SEE SHEET ONE	-	-



-P12 ISOMETRIC VIEW FOR REFERENCE ONLY



P12 FORWARD SPACER
 \sum 9



SECTION BH-BH

SIZE	DWG. NO.	REV
D	TII-2106-A	-
SCALE: 1:1	WEIGHT:	SHEET 22 OF 29

5

4

3

2

1

8

7

6

5

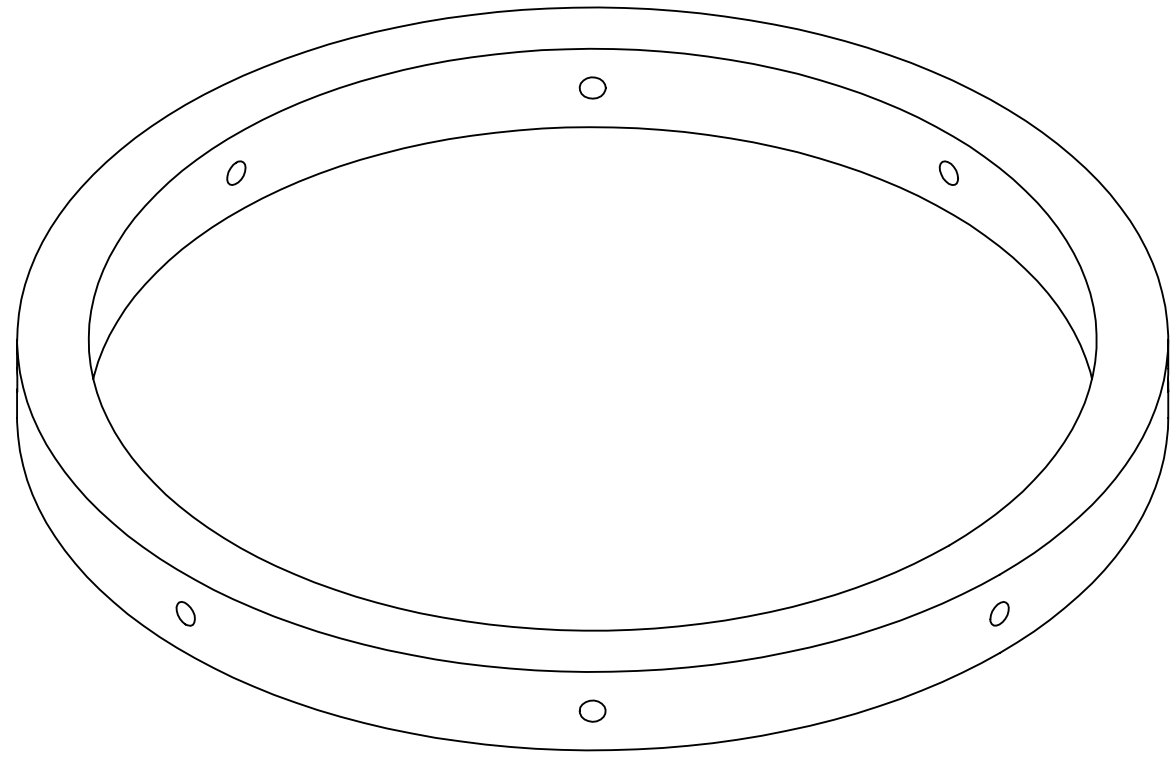
4

3

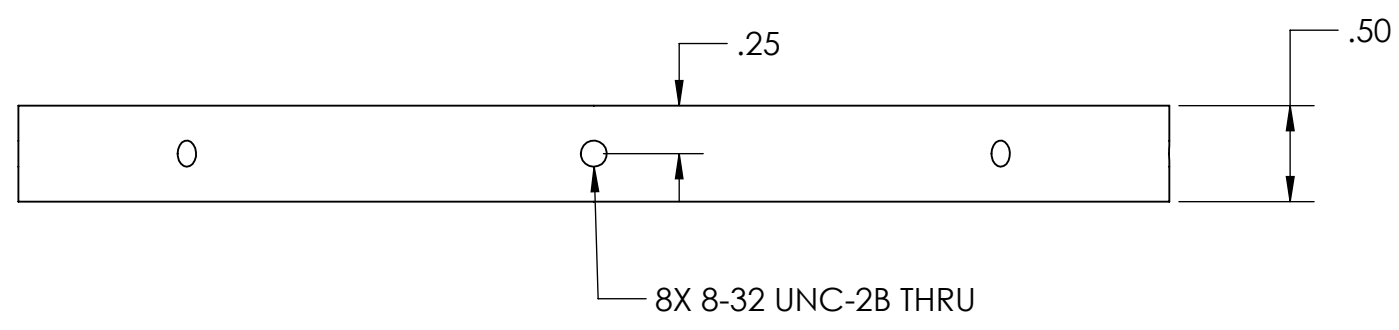
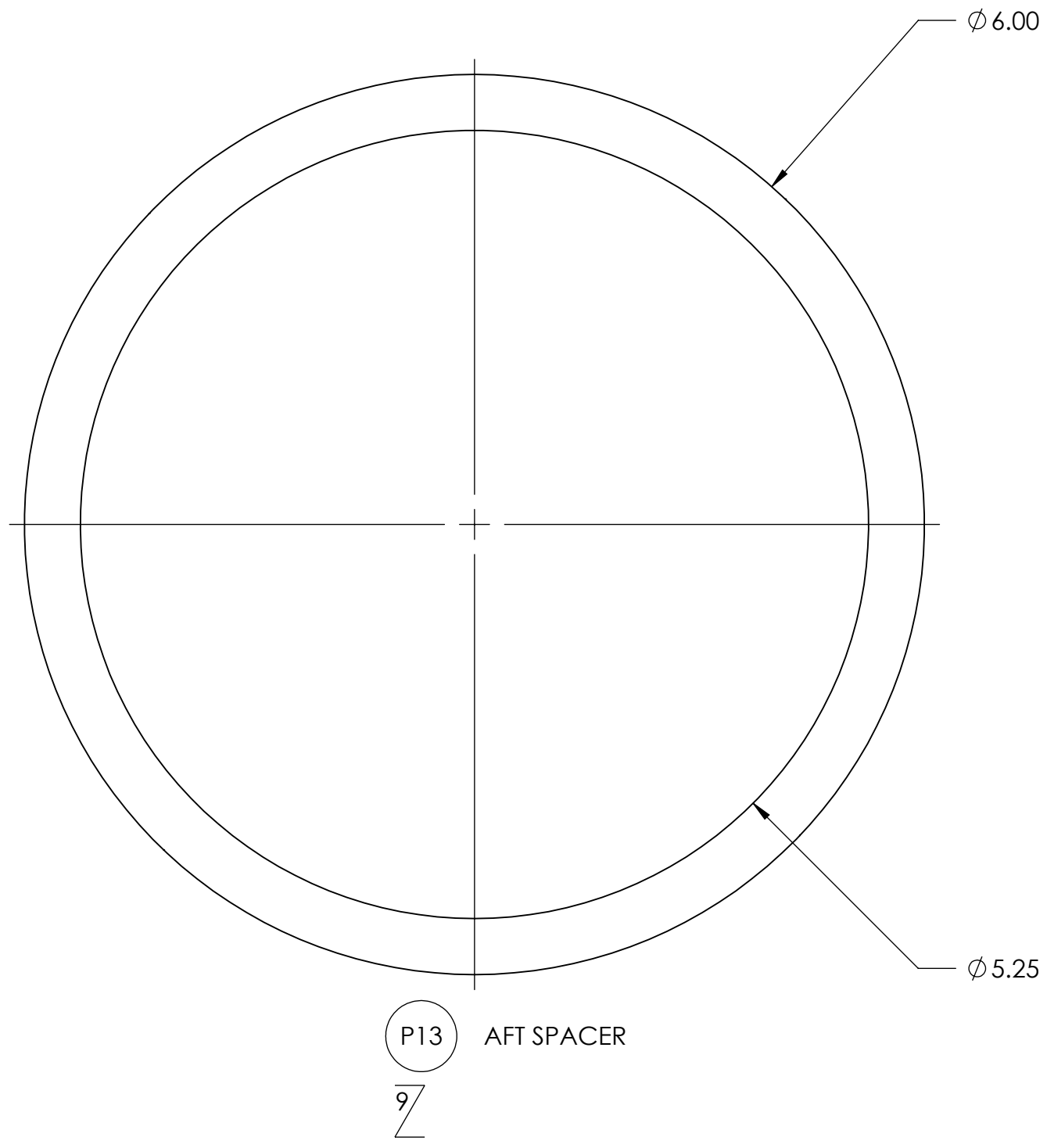
2

1

REVISIONS				
ZONE	REV.	DESCRIPTION	DATE	APPROVED
	-	SEE SHEET ONE	-	-



-P13 ISOMETRIC VIEW FOR REFERENCE ONLY



SIZE	DWG. NO.	REV
D	TII-2107-A	-
SCALE: 1:1	WEIGHT:	SHEET 23 OF 29

5

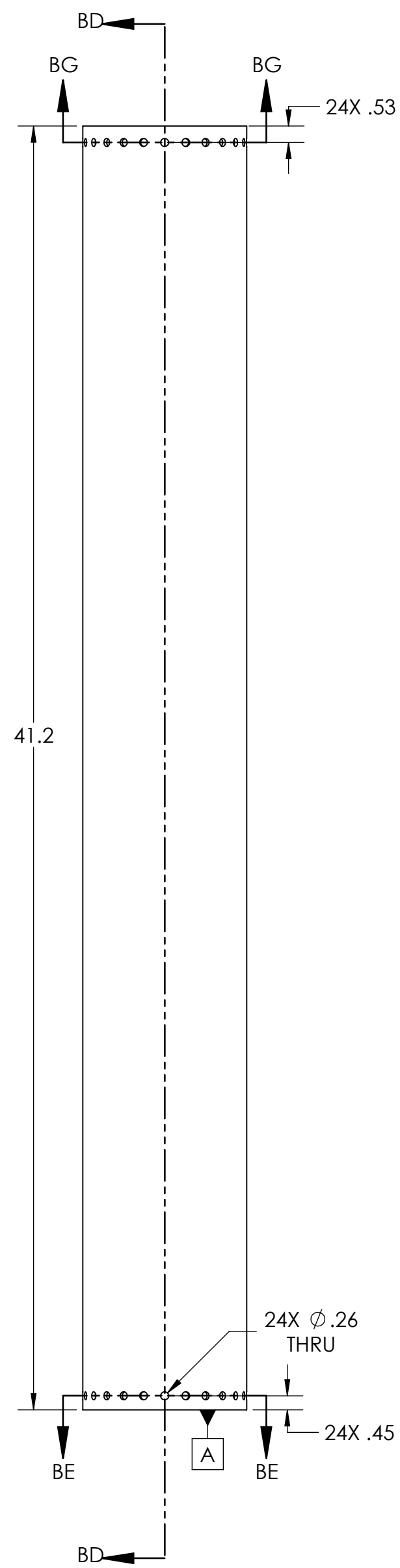
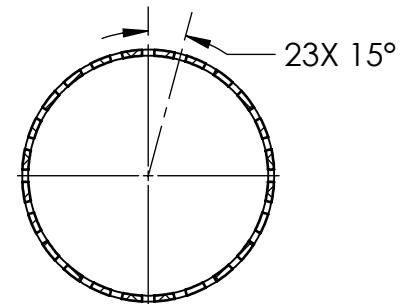
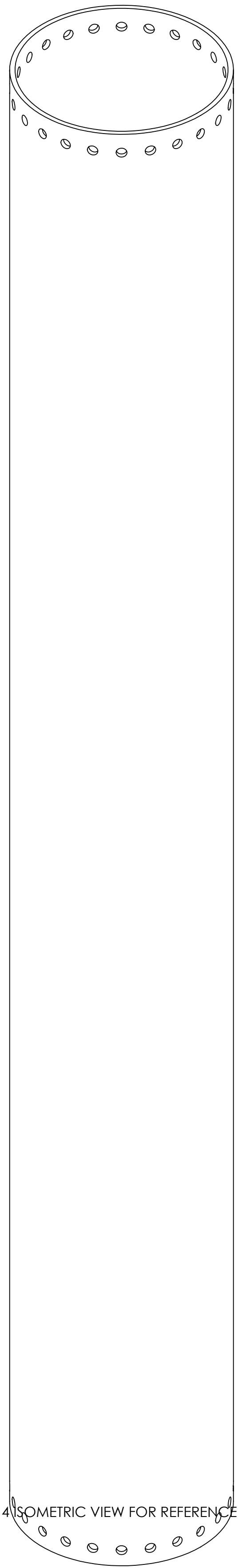
4

3

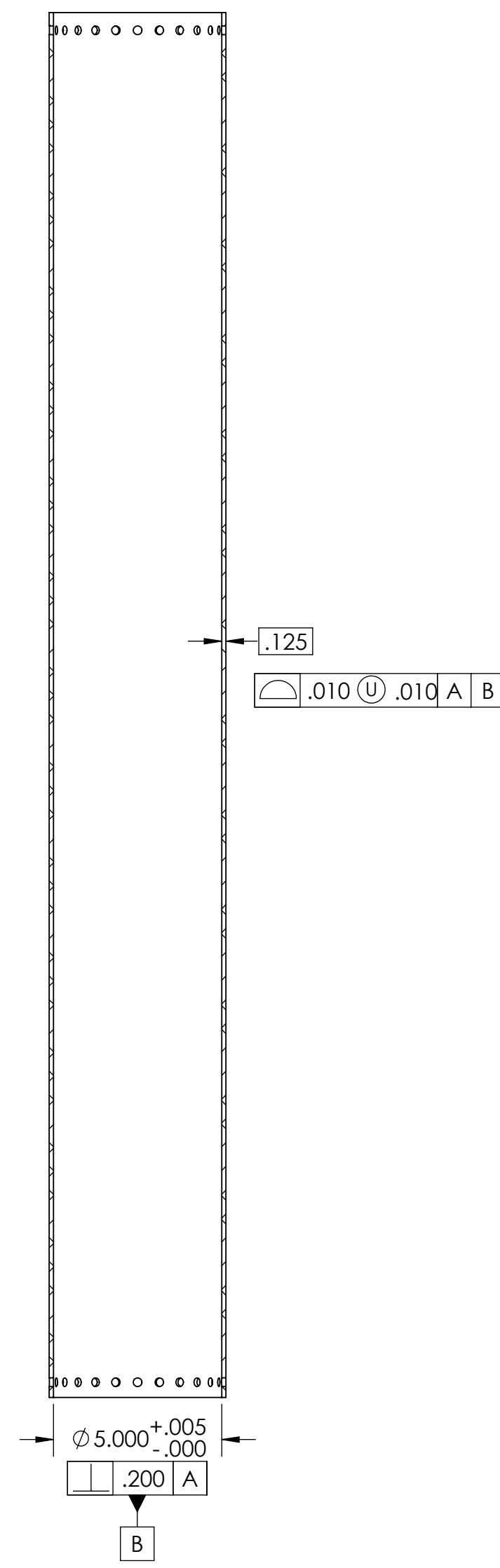
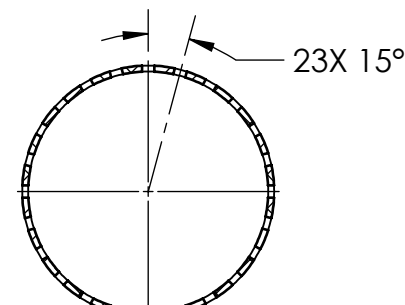
2

1

REVISIONS				
ZONE	REV.	DESCRIPTION	DATE	APPROVED
	-	SEE SHEET ONE	-	-



P14 COMBUSTION CHAMBER



8

7

6

5

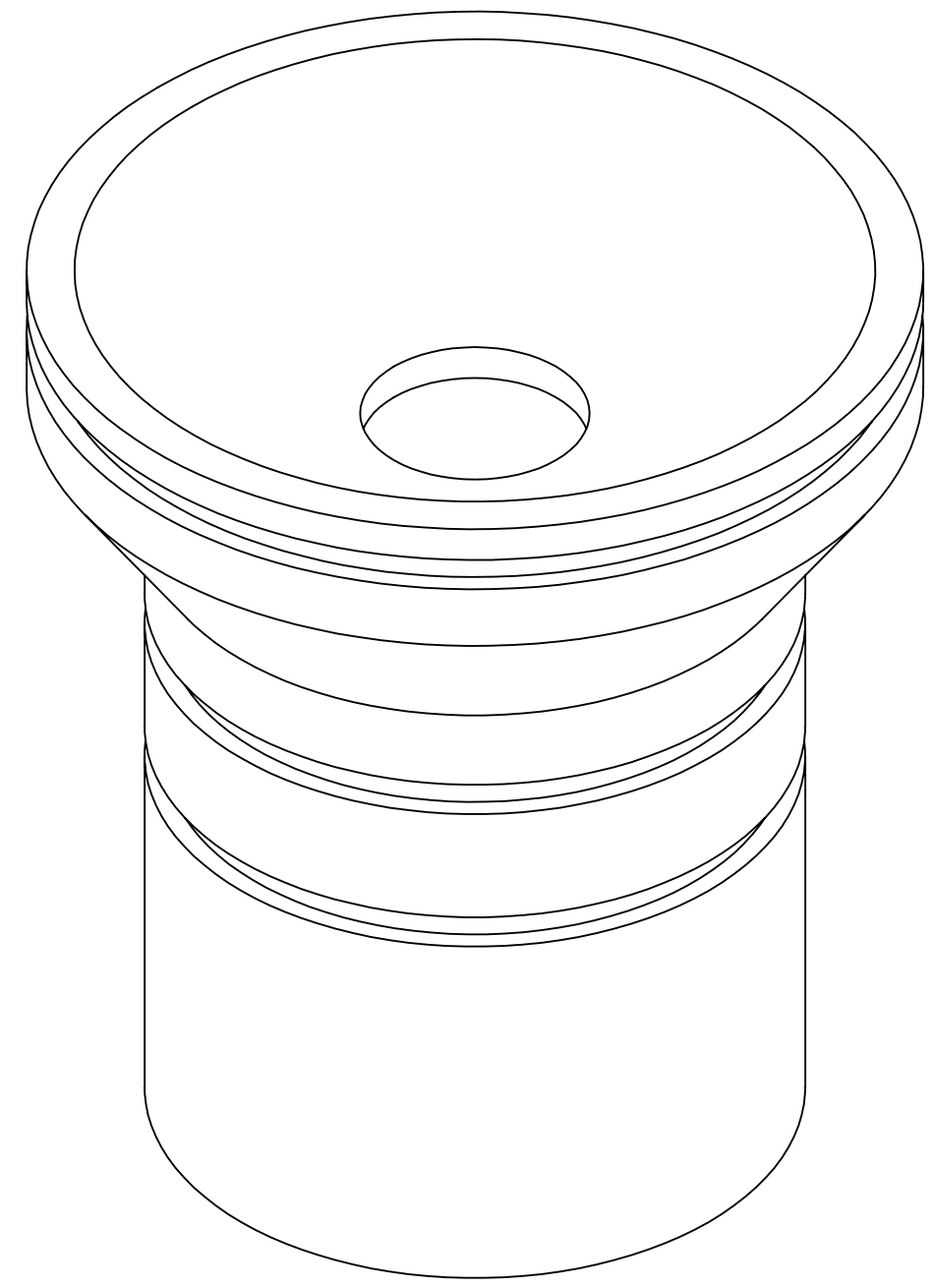
4

3

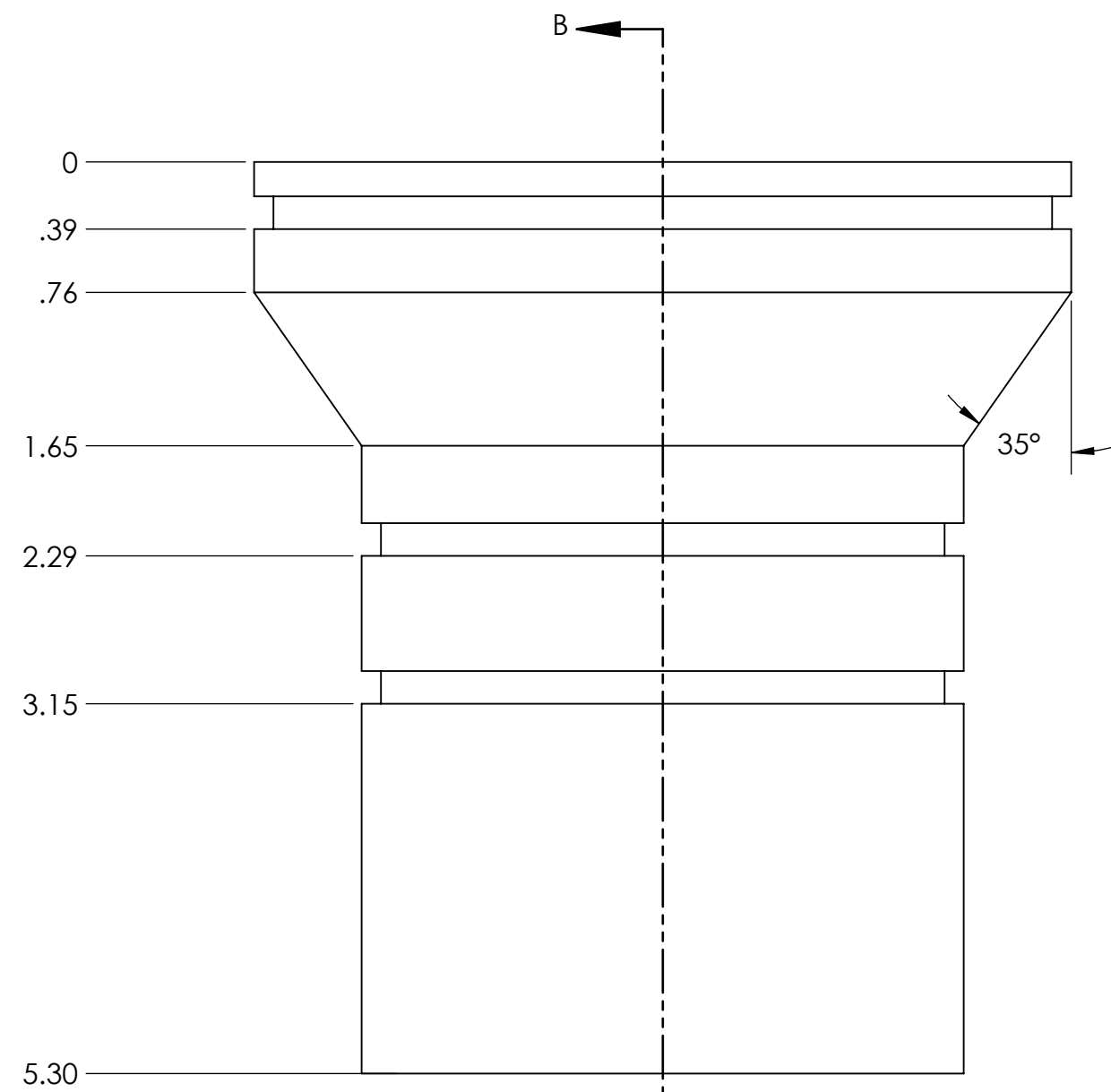
2

1

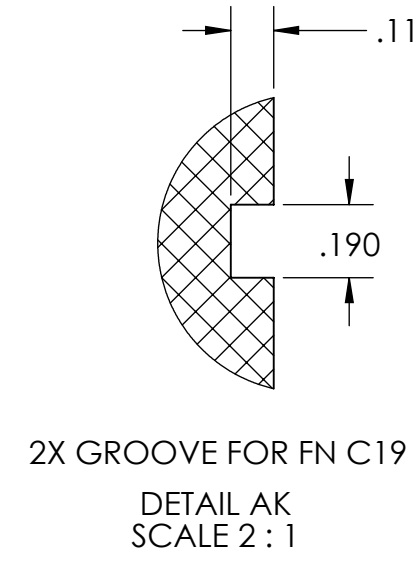
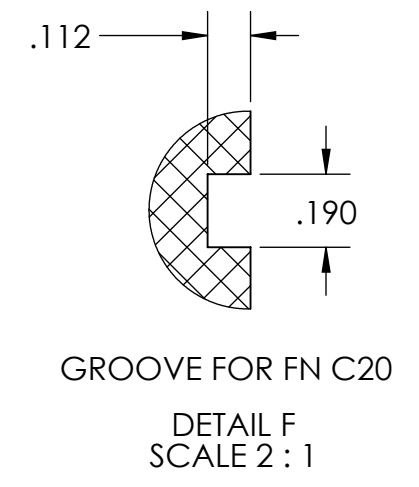
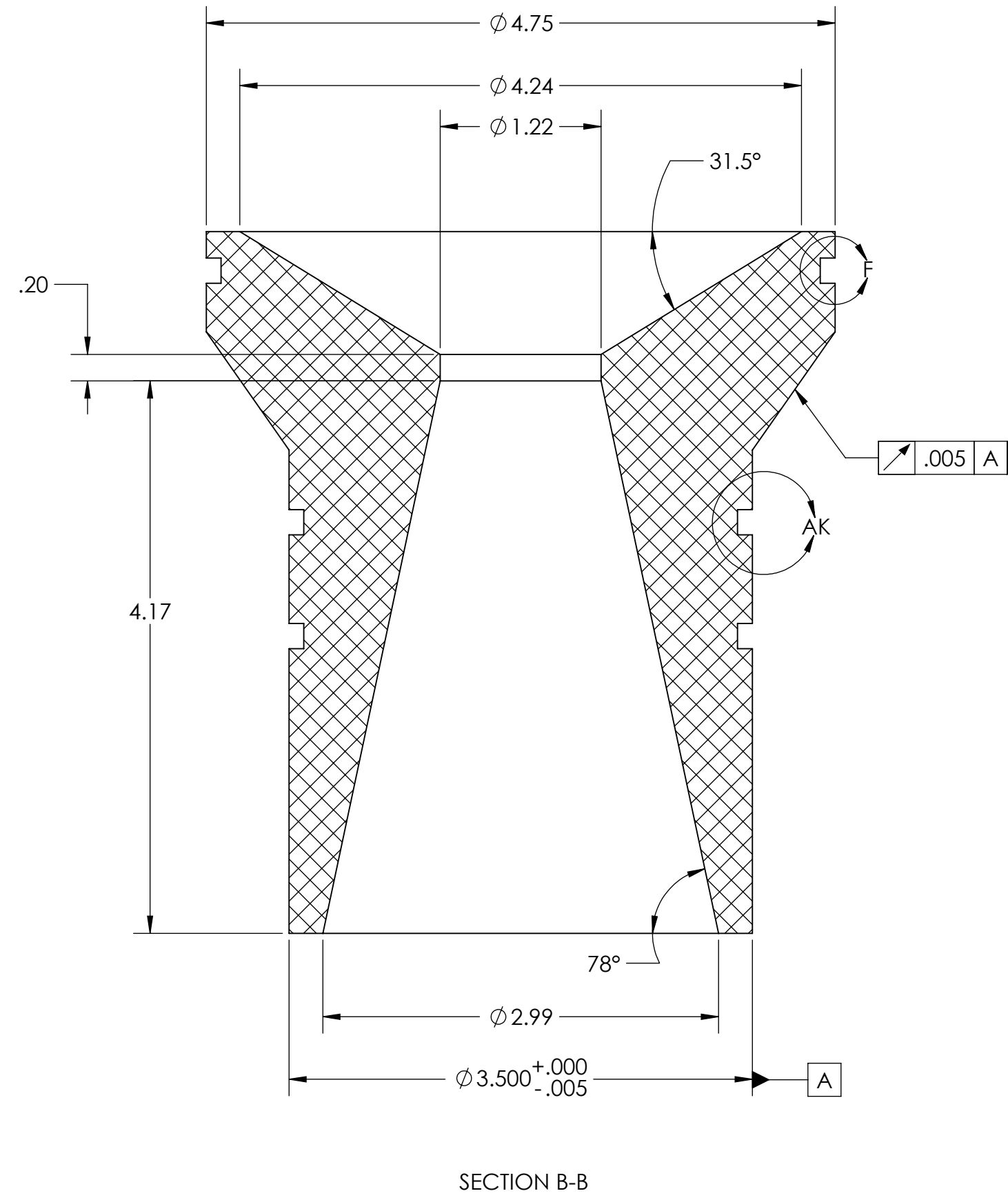
REVISIONS				
ZONE	REV.	DESCRIPTION	DATE	APPROVED
	-	SEE SHEET ONE	-	-



-P15 ISOMETRIC VIEW FOR REFERENCE ONLY



10/ P15 NOZZLE INSERT



∠.005 A

AK

A

5

4

3

2

1

8

7

6

5

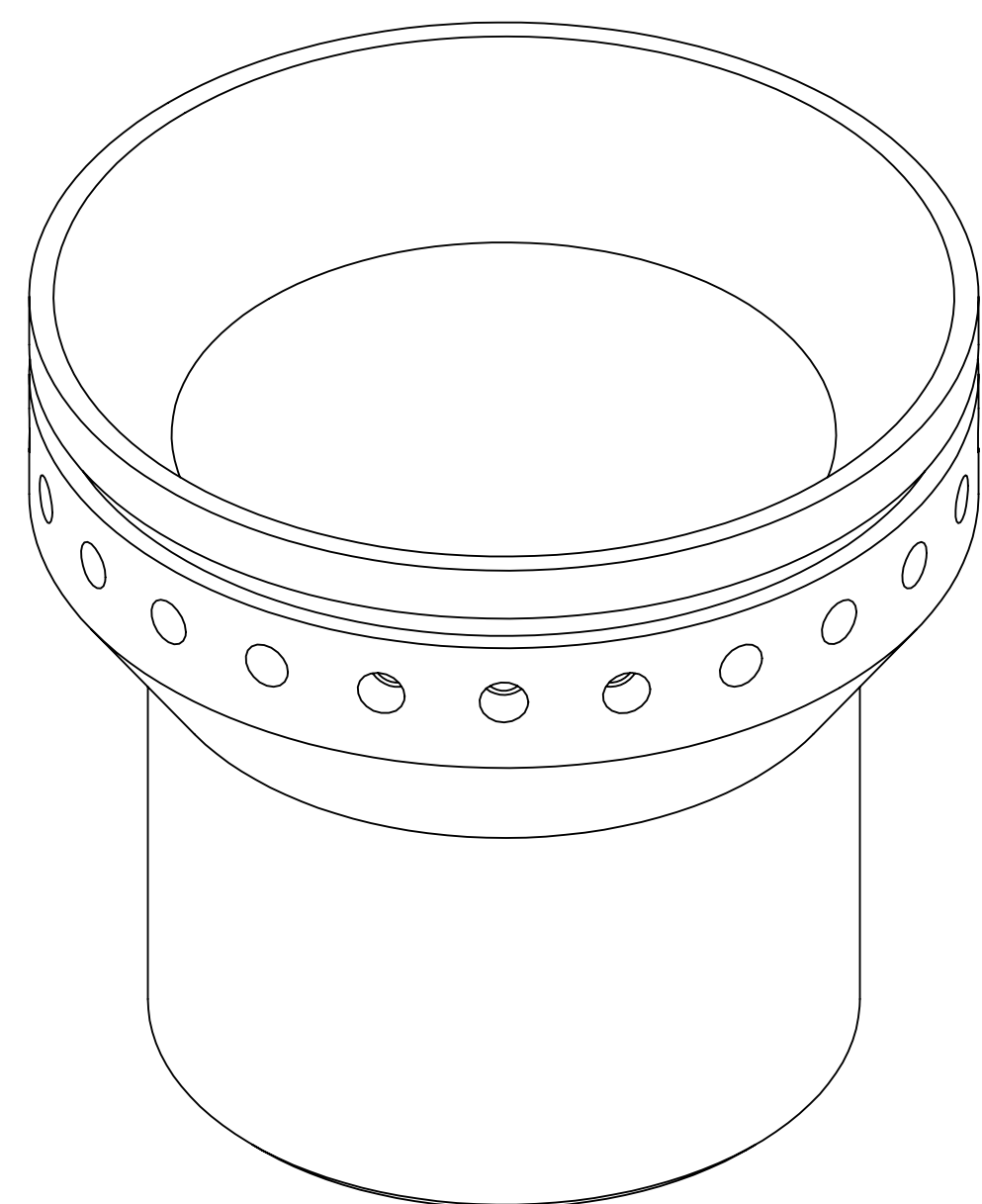
4

3

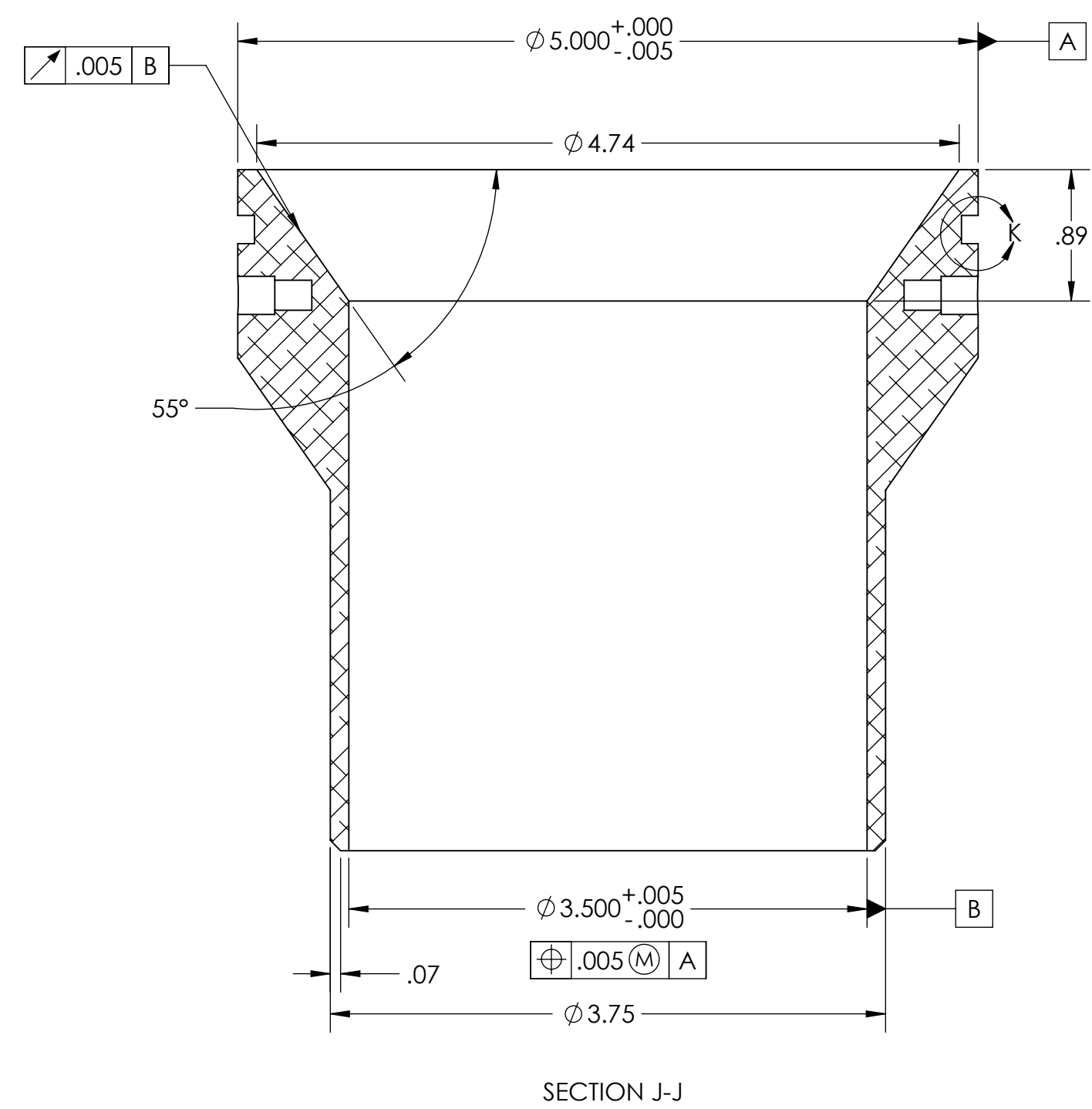
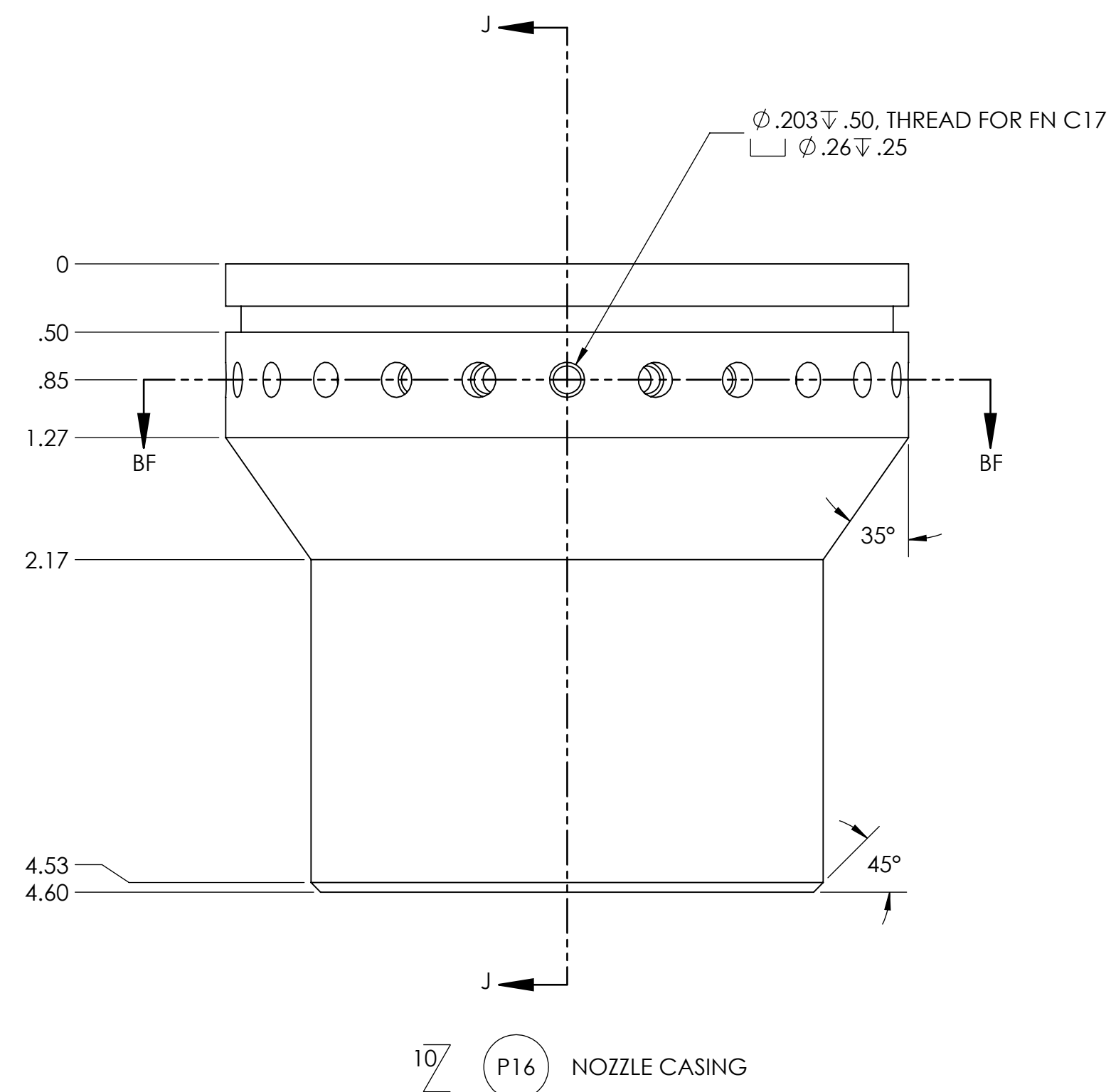
2

1

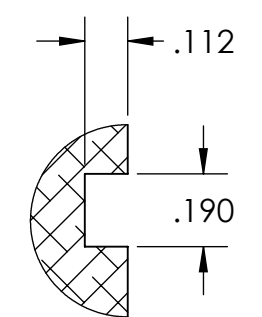
REVISIONS				
ZONE	REV.	DESCRIPTION	DATE	APPROVED
	-	see sheet one	-	-



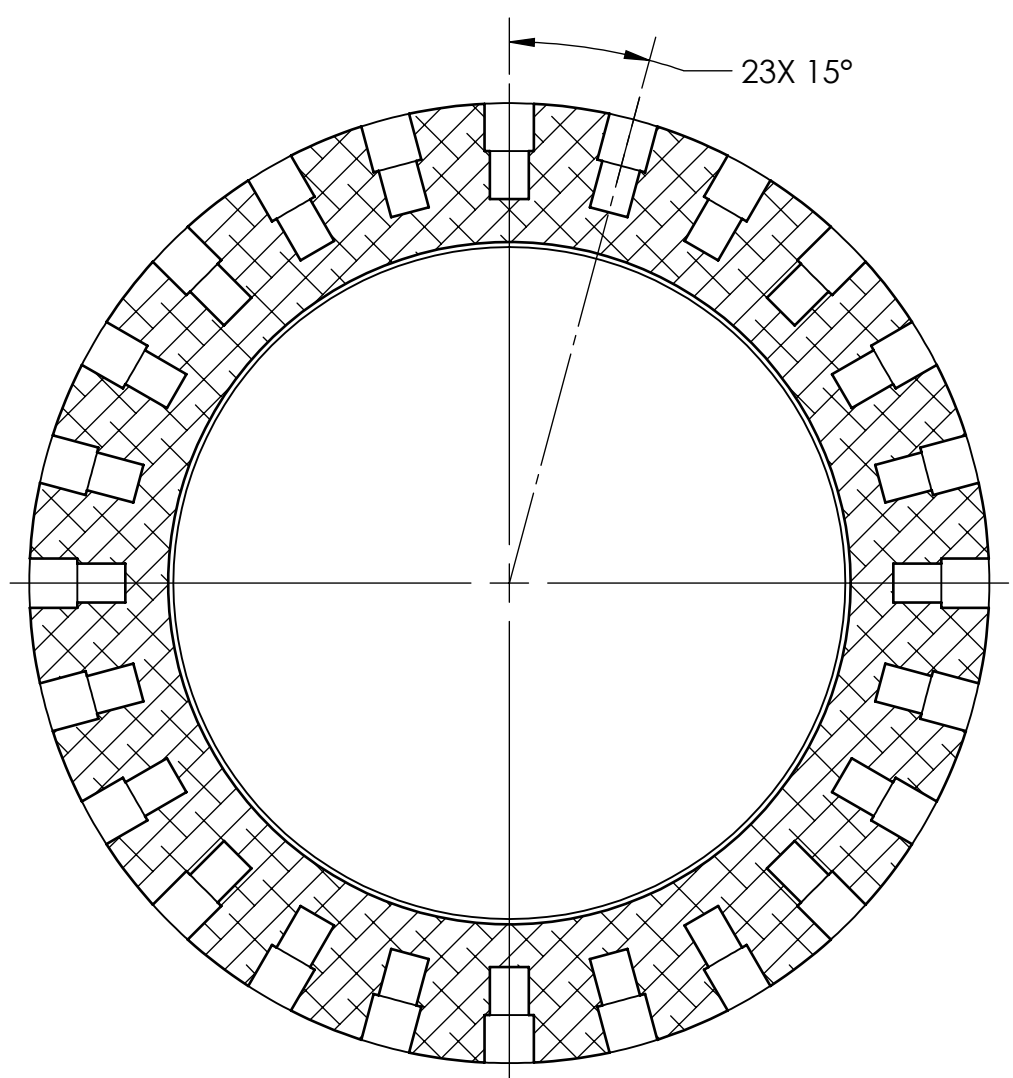
-P16 ISOMETRIC VIEW FOR REFERENCE ONLY



SECTION J-J



GROOVE FOR FN C13
DETAIL K
SCALE 2:1



SECTION BF-BF

8

7

6

5

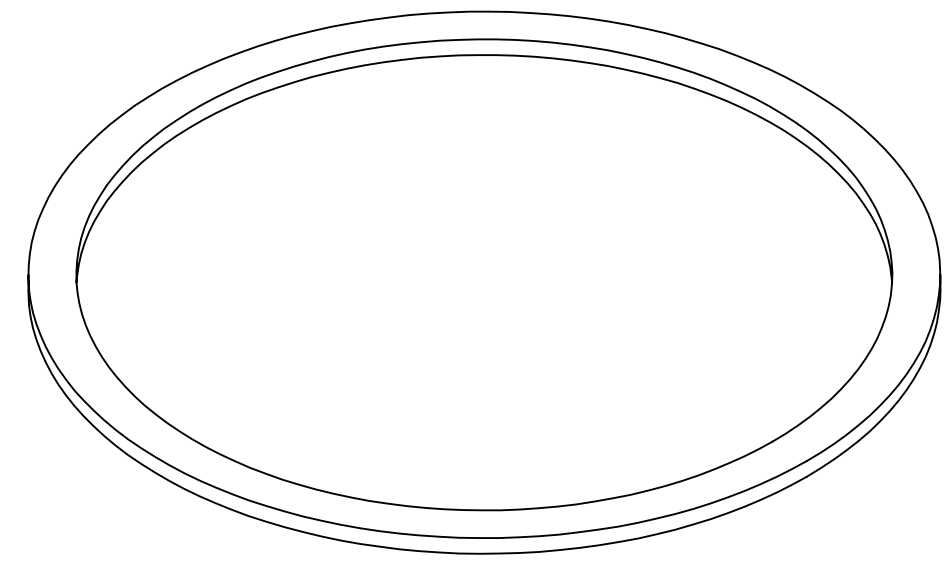
4

3

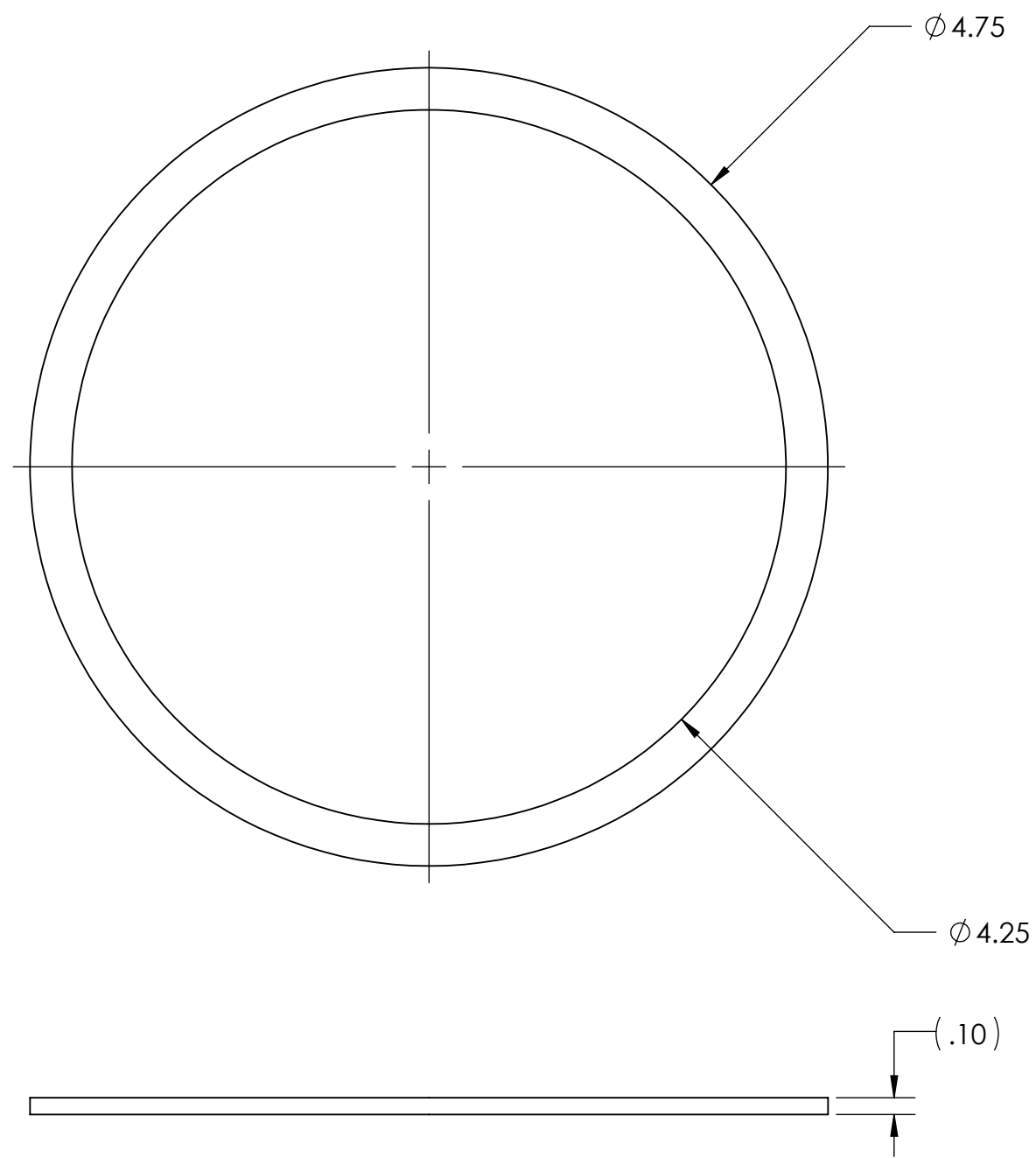
2

1

REVISIONS				
ZONE	REV.	DESCRIPTION	DATE	APPROVED
	-	SEE SHEET ONE	-	-



-P17 ISOMETRIC VIEW FOR REFERENCE ONLY



10 P17 MIDDLE COMPRESSIBLE RING

SIZE	DWG. NO.	REV
D	TII-2203-A	-
SCALE: 1:1	WEIGHT:	SHEET 27 OF 29

5

4

3

2

1

8

7

6

5

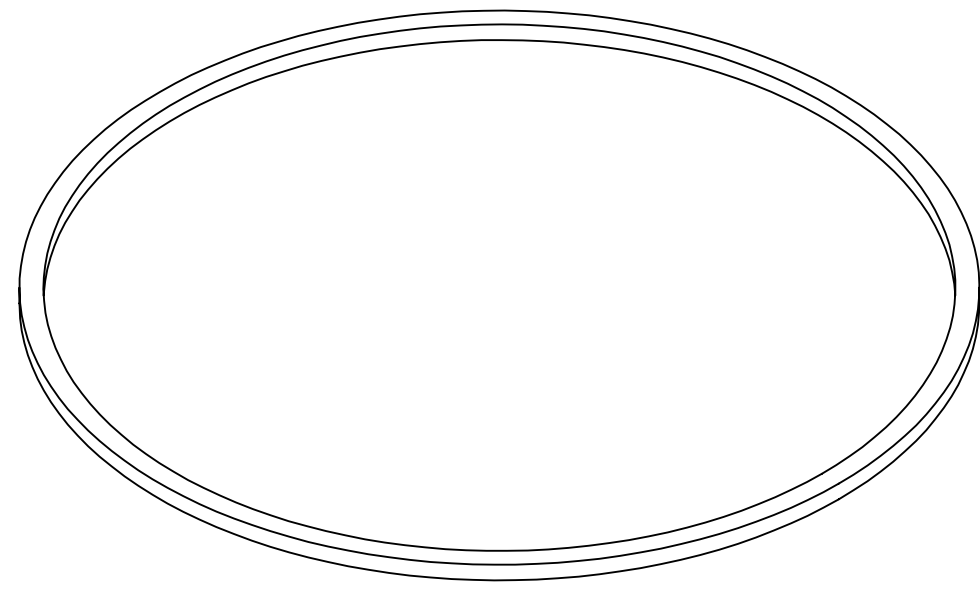
4

3

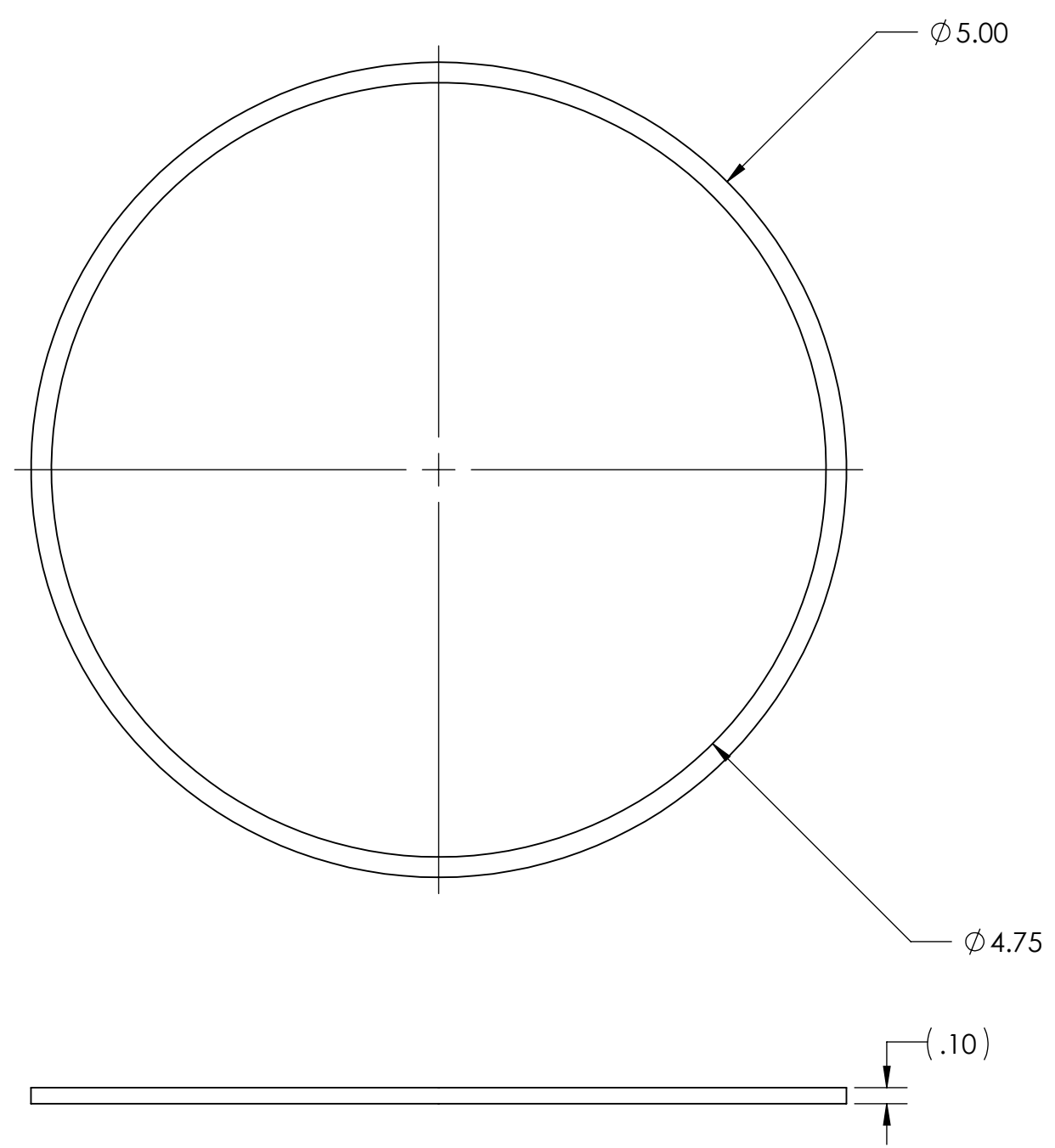
2

1

REVISIONS				
ZONE	REV.	DESCRIPTION	DATE	APPROVED
	-	SEE SHEET ONE	-	-



-P18 ISOMETRIC VIEW FOR REFERENCE ONLY



10 P18 AFT COMPRESSIBLE RING

D

D

C

C

B

B

A

A

8

7

6

5

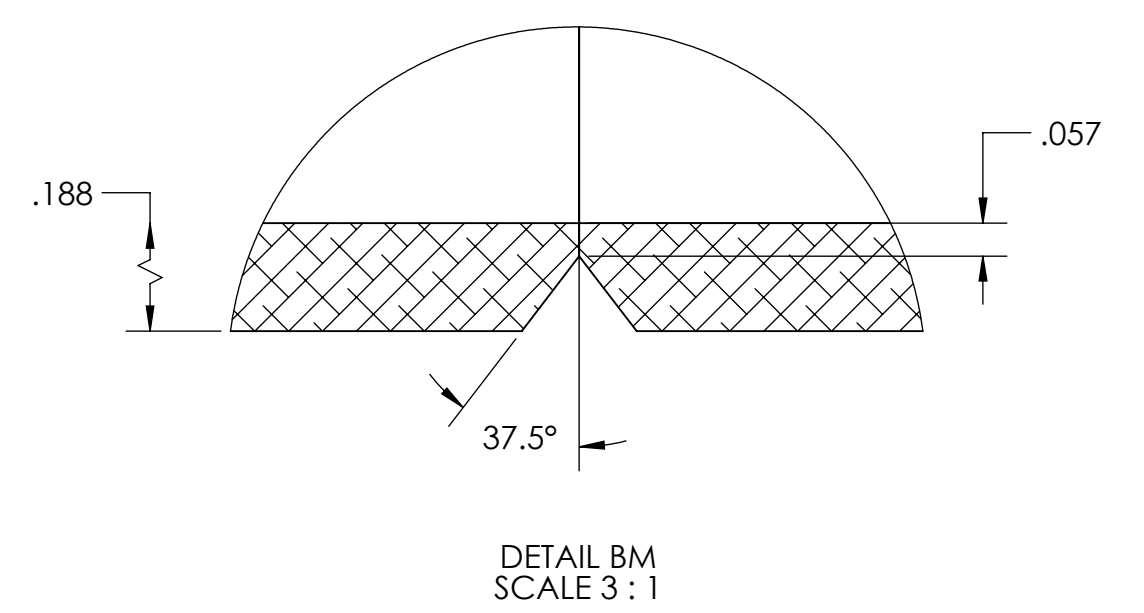
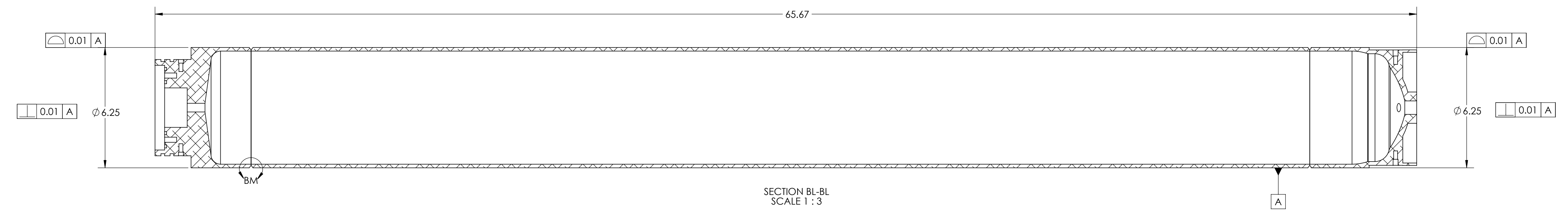
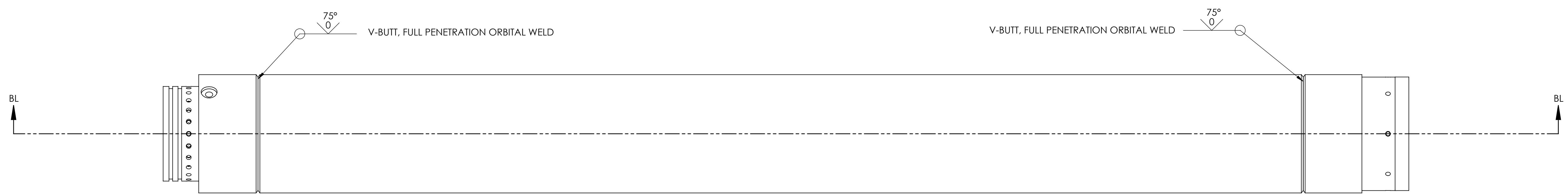
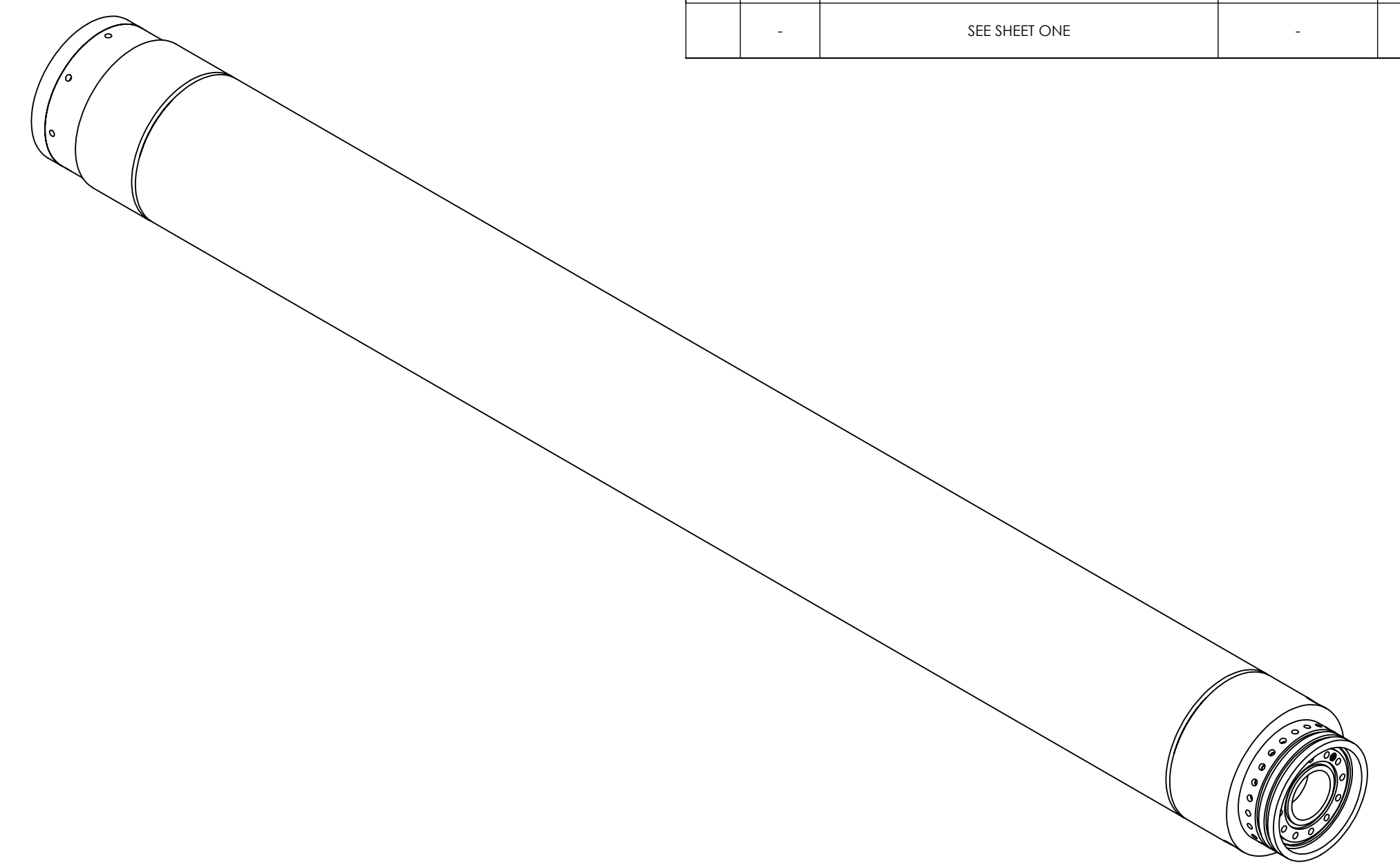
4

3

2

1

REVISIONS				
ZONE	REV.	DESCRIPTION	DATE	APPROVED
	-	SEE SHEET ONE	-	-



XIII. Appendix - Detailed Testing Logs

Every static test, data collected from pressure transducers, load cells, and thermal probe will be analyzed. The team is currently working on advanced statistical methods to extract information and predictions from the data the team receives from the small test engine, Luna. These methods will be applied to the Titan II engine once the team is ready for a hot fire. In addition to this analysis, a quick look at the maximum and average values for every sensor the team receives data from will give the team an easy, quantifiable estimate on the performance of the Titan II engine during the test. A sample of these summaries of logs for a single hot fire is shown in the table below.

Table 23. Logs Summaries Example		
Sensor	Maximum Value	Average Value
Axial Load Cell (lbf)		
Oxidizer Tank PT		
Pre-Injection Chamber PT		
Combustion Chamber PT		
Oxidizer Tank Thermal Probe		

XIV. References

- ¹Morris S. Clark BS, BDS, DDS, DSc, FACD, Ann L. Brunick RDH, MS, in Handbook of Nitrous Oxide and Oxygen Sedation (Sixth Edition), 2015 <https://www.sciencedirect.com/topics/nursing-and-health-professions/nitrous-oxide-cylinder>
- ²Lohner, Kevin, et al. "Fuel Regression Rate Characterization Using a Laboratory Scale Nitrous Oxide Hybrid Propulsion System." *AIAA/ASME/SAE/ASEE Joint Propulsion Conference & Exhibit*, 18 June 2012. *Aerospace Research Central*, doi:10.2514/6.2006-4671.
- ³Stanford University. "PDF." "Chapter 11: Hybrid Rockets." https://web.stanford.edu/~cantwell/AA283_Course_Material/AA283_Course_Notes/AA283_Aircraft_and_Rocket_Propulsion_Ch_11_BJ_Cantwell.pdf
- ⁴Sutton, George Paul, and Oscar Biblarz. "Rocket Propulsion Elements." 7th ed., Wiley., 2000. Walter, G H, et al. "Thermophysical properties of nitrous oxide." "PDF." 1991. <http://edge.rit.edu/edge/P07106/public/Nox.pdf>
- ⁵Walter, G H, et al. "Thermophysical properties of nitrous oxide." "PDF." 1991. <http://edge.rit.edu/edge/P07106/public/Nox.pdf>
- ⁶Rainer D., Joseph O. "Atomization and Dense Fluid Breakup Regimes in Liquid Rocket Engines" Combustion Research Facility, Sandia National Laboratories <https://www.osti.gov/servlets/purl/1237373>
- ⁷Waxman, Benjamin S., et al. "Mass Flow Rate and Isolation Characteristics of Injectors for Use with Self-Pressurizing Oxidizers in Hybrid Rockets." 49th AIAA/ASME/SAE/ASEE Joint Propulsion Conference, Dec. 2013, doi:10.2514/6.2013-3636.
- ⁸Yang, Pengze. "Numerical Study of Cavitation Within Orifice Flow" Texas A&M University. 2015.
- ⁹Inch and Metric Drill Bit Size Chart, https://www.engineersedge.com/drill_sizes.htm
- ¹⁰Pragya B., Shelly B., "Experimental Investigation on Combustion Characteristics of Hybrid Rocket Fuels with Multi-Angle Diverging Injector", 2020 <https://www.mdpi.com/2504-186X/5/2/12/pdf>
- ¹¹Polysoude Nantes France SAS. "The Orbital Welding Handbook." 2009. https://static1.squarespace.com/static/54becf2ae4b09fae314e6e56/t/57a89018c534a5bcfbe978da/1470664738648/Orbital_Welding_Handbook_EN_LR.PDF
- ¹²Pro-Fusion by Elderfield & Hall. "Fundamentals of Orbital Tube Welding" <https://www.pro-fusiononline.com/welding/applications/orbital.htm>
- ¹³"ASME B16.25-2012" 2012.
- ¹⁴Nakka, Richard. "Solid Rocket Motor Theory -- Propellant Grain." Richard Nakka's Experimental Rocketry Site, 5 July 2001, www.nakka-rocketry.net/th_grain.html.
- ¹⁵Cai G., Zhu H., Rao D., Tian H. "Optimal design of hybrid rocket motor powered vehicle for suborbital flight." *Aerospace Science and Technology* Volume 25, Issue 1, March 2013, Pages 114-124
- ¹⁶Budynas, Richard Gordon., and J. Keith. Nisbett. "Shigleys Mechanical Engineering Design." 9th ed., McGraw-Hill Higher Education, 2008.

- ¹⁷Humble, Ronald W., et al. *Space Propulsion Analysis and Design*. McGraw-Hill, 1995
- ¹⁸Cesaroni Technology Incorporated. “Pro98® Product Notes.” “PDF.” Aug. 2013
- ¹⁹Society for Advanced Rocket Propulsion. Kiefer Dundas, Aaron Goldfogel, et al. “Boundless 2018: Team 09 Project Technical Report to the 2018 Spaceport America Cup.” “PDF.” 2018.
http://www.soundingrocket.org/uploads/9/0/6/4/9064598/09_project_report.pdf
- ²⁰Spaceport America Cup. “Intercollegiate Rocket Engineering Competition Design, Test, & Evaluation Guide.” “PDF.” Nov. 2019.
- ²¹Suhang Chen, Yue Tang, et al. “Innovative Methods to Enhance the Combustion Properties of Solid Fuels for Hybrid Rocket Propulsion.” pg.16. *Aerospace*. March 2019.
- ²²MatWeb. “PDF.”. http://amet-me.mnsu.edu/UserFilesShared/DATA_ACQUISITION/mts/met277/9_13-12/MaterialData_9391_AI-6061.pdf
- ²³”Characterization of high-pressure cavitating flow through a thick orifice plate in a pipe of constant cross section” <https://www.sciencedirect.com/science/article/abs/pii/S129007291630809>
- ²⁴Arian Gas. “Nitrous Oxide Gas.” *Arian Gas*, Arian Gas Co. Web Design, 2017,
www.ariangas.com/en/product/nitrous-oxide-gas/.
- ²⁵Compressed Gas Association. “CGA E-4 - Standard For Gas Pressure Regulators - Seventh Edition.” “PDF.” 2016
- ²⁶ Volumetric Behavior of Nitrous Oxide. Pressure-Volume Isotherms at High Pressures. E. J. Couch and K. A. Kobe. *Journal of Chemical & Engineering Data* 1961 6 (2), 229-233. DOI: 10.1021/je60010a015,
<https://pubs.acs.org/doi/pdf/10.1021/je60010a015>.
- ²⁷Crowl, Daniel A, and Scott A Tipler. “Sizing Pressure-Relief Devices.” “PDF.” Oct. 2013. we
https://www.aiche.org/sites/default/files/cep/20131068_r.pdf
- ²⁸Young, W. C. (2002). Bodies in Contact Undergoing Direct Bearing and Shear Stress. In R. G. Budynas (Ed.), *Roark's Formulas for Stress and Strain* (7th ed., pp. 689-709). New York, NY: McGraw-Hill.
- ²⁹Brown, Kevin H., et al. Guideline for Bolted Join Design and Analysis: Version 1.0. *Sandia National Laboratories*. Jan 2008. <https://prod-ng.sandia.gov/techlib-noauth/access-control.cgi/2008/080371.pdf>
- ³⁰Stanley Engineering, “Heli-Coil Wire Insert System”, *Stanley Engineering*, pp. 12-20. “PDF”.
https://www.stanleyengineeredfastening.com/-/media/web/sef/resources/docs/heli-coil/hc-2000_rev11_web.pdf
- ³¹Engineers Edge “Shear Area Internal & External Thread Formula”, *Engineers Edge LLC*, Web, 2020
https://www.engineersedge.com/thread_strength/thread_bolt_stress.htm
- ³²MechaniCalc, “Bolted Joint Analysis”, MechaniCalc Inc, Web, <https://mechanicalcalc.com/reference/bolted-joint-analysis>

XV. Acknowledgments

The Eclipse team would first like to thank our generous sponsors whose continued support has enabled the team to work on the Titan II project and many others since the club's founding in 2014. Tripoli Houston, while not a sponsor on paper, has contributed abundant amounts of knowledge. We'd like to thank Rice University's Oshman Engineering Design Kitchen (OEDK) and the amazing OEDK faculty that supports the team both financially and through day-to-day interactions when designing and fabricating our projects. We would also like to thank all of the Eclipse alumni -- not only have their past contributions helped to bring the team where it is today, but their mentorship and advice continues to aid the team. Finally, we'd like to thank Chris Harris and Kaz Karwowski, the club sponsors. Without you, nothing we do would be possible.